8-17-2021 12:00 PM

Performance Assessment and Design Guidelines for RC Three-Sided Culverts

Safwat Hassan Ramadan, *The University of Western Ontario*

Supervisor: El Naggar, M. Hesham, *The University of Western Ontario*

A thesis submitted in partial fulfillment of the requirements for the Doctor of Philosophy degree in Civil and Environmental Engineering

Abstract

Reinforced concrete three-sided culverts (TSCs) are typically produced in large spans, up to 16.0 m, and low-rise profiles to handle heavy flows at sites with limited vertical clearance. Full-scale field studies and numerical analyses investigating TSCs do not exist to date. Accordingly, the current design practices specified in the Canadian Highway Bridge Design Code, CHBDC (CSA, 2014) and the American Association of State and Highway Transportation, AASHTO (AASHTO LRFD, 2014) do not distinguish between small-span box and large-span TSCs. A comprehensive study involving field monitoring and numerical analyses of TSCs is presented in this thesis. Three TSCs were instrumented to measure the soil-culvert interface pressures and the induced strains. The monitored TSCs covered intermediate to large spans, with spans of 7.3 m, 10.4 m, and 13.5 m. Each culvert had a unique geometry and installation method. Field data were collected for the three culverts during and after construction completion. These field measurements were analyzed, and then utilized to validate two-dimensional (2D) finite element (FE) models for the three culverts. The validated numerical models were employed to investigate the influence of many parameters on the applied earth pressures and the structural performance of TSCs at service and ultimate limit states (SLS and ULS). Moreover, three-dimensional (3D) FE models were developed to predict the ultimate capacity of the monitored TSCs precast units. In addition, parametric studies were conducted to investigate the influence of the precast unit width and sidewall height on its structural performance at ULS. The field measurements indicated that the CHBDC (CSA, 2014) overestimates the pressure along the top slab of TSCs for B1 installation. The results of the 2D models showed that the subsurface soil condition influenced the lateral earth pressure on the sidewall only. The sidewall and pedestal heights governed the deformation of the footing-culvert system. Equations have been proposed to estimate the applied earth pressures on large-span TSCs and limits to the midspan vertical deflection are proposed to satisfy the SLS requirements. Finally, the TSC precast units, without soil confinement, exhibited brittle failure.

Keywords: three-sided culverts; field monitoring; soil-culvert interaction, strip footing, precast units, finite element analysis, service limit state, ultimate limit state.

Summary for Lay Audience

Culverts are a vital part of the urban infrastructure for all societies. They are structures buried in the ground to convey water, utilities, or pedestrian on top of new roads. In general, earth weights on buried structures, which are used for their design, are affected by a phenomenon called soil arching. Simply, rigid buried structures attract more earth loads compared to relatively flexible structures. The current design guidelines included in the different codes in North America are for rigid concrete box culverts. Recently, concrete culverts with three sides and no bottom slab, also known as three-sided culverts, are gaining popularity. They are much wider than box culverts and are considered more flexible. However, the codes in North America do not differentiate between them and the same design guidelines are used to design large three-sided culverts. Accordingly, sensors were installed on three of these structures before their construction to measure the actual earth loads acting on them. Afterwards, an engineering software was used to simulate the monitored culverts. The results from the software simulation were similar to the sensors data. Accordingly, many scenarios were simulated to understand the behavior of three-sided culverts and to quantify the acting earth loads on their body in different cases. A clear understanding of the performance of large three-sided culverts is presented based on the sensors readings and the covered scenarios using the engineering software. Moreover, specific design guidelines for three-sided culverts have been presented that would lead to more cost-effective, yet reliable design.

Co-Authorship Statement

All the instrumentation field work, numerical modeling, interpretation of results and writing of the draft and the final thesis were carried out by the candidate himself, under the direct supervision of Prof. M. Hesham El Naggar. The supervisor's contribution consisted of providing advice throughout the research program and reviewing the draft and the final thesis and publication results from this research.

Publications resulted from this study were drafted by the author, reviewed and edited by Prof. El Naggar. The following is a list of publications accepted and submitted:

1- Ramadan, S. H., and El Naggar, M. H. (2021). Field monitoring and numerical analysis of a large span three-sided reinforced concrete culvert. *Journal of Geotechnical and Geoenvironmental Engineering*, 147 (4), 04021008. https://doi.org/10.1061/(ASCE)GT.1943-5606.0002489
Published.

2- Ramadan, S. H., and El Naggar, M. H. (2021). Structural performance of a medium-span RC three-sided culvert based on field measurements and numerical analyses. *Canadian Geotechnical Journal*. https://doi.org/10.1139/cgj-2020-0574
Published.

3- Ramadan, S. H., El Naggar, M. H., Drbe, O., and Embaby, K. (2021). Preliminary analysis and instrumentation of large-span three-sided reinforced concrete culverts. *Journal of Bridge Engineering*. https://doi.org/10.1061/(ASCE)BE.1943-5592.0001798
Accepted.

4- Ramadan, S. H., and El Naggar, M. H. (2021). Class-A prediction of three-sided reinforced concrete culverts and numerical investigation of the supporting strip footing geometry. *Structure and Infrastructure Engineering*.
Accepted.

1- Ramadan, S. H., and El Naggar, M. H. (2021). Effect of large-span three-sided culvert configuration on its performance at service and ultimate loading conditions. Submitted for possible publication in *Tunnelling and Underground Space Technology*.
Under Review.

2- Ramadan, S. H., and El Naggar, M. H. (2021). Design guidelines for reinforced concrete three-sided culverts. Submitted for possible publication in *Tunnelling and Underground Space Technology*.
Under Review.

Acknowledgments

First and foremost, I would like to thank God the Almighty for granting me the guidance, patience, and resilience to accomplish this thesis successfully.

I wish to express my sincere gratitude to my supervisor and mentor Prof. Hesham El Naggar, who has always been my role model on both academic and personal sides. His intellectual guidance, thoughtful ideas, continuous support, and most importantly, the confidence he gave me are the basis of any accomplished work. It is and will always be my honor to be your student. Thanks Professor for everything.

I would like to take this opportunity to acknowledge the fund provided by the Canadian Concrete Precast and Pipe Association (CCPPA), Natural Sciences and Engineering Research Council of Canada (NSERC), and Ministry of Transportation Ontario (MTO). I would also like to thank Mr. Enrico Stradiotto of CCPPA, Mr. Sammy Wong and Mr. James Malpass of Con Cast Pipe, Mr. George Poulias and Mr. Vince Ricciuti of ConDrain Company Ltd, Mr. Robert Pocrnic and Mr. Bruno Tucci of TACC Construction Ltd, Mr. Dan Haggerty of DECAST, and Mr. Paul Medeiros and Mr. Joe Medeiros of Performcrete Inc. for their contributions in facilitating the fieldwork and instruments installation.

I would like to express my deep appreciation to my friends and colleagues who helped me during my harsh field instrumentation work and spending days with me on-site: Osama Drbe, Kareem Embaby, Mohamed Alwalan, Denghui Dai, Juntao Wu, Jiujiang Wu, Abdalla Alhashmi, Jamal Assaf, Majid Touqan, and Zeid Abdelkhaliq. I would also like to thank Dr. Aiham Adawi, my friends Emad Abraik and Abdelrahman Fouad for their valuable advice and interesting discussions regarding the structural aspect of this work.

I hereby would like to express my love and deep appreciation to my wife, Esraa, who has been more than patient and exerted exceptional effort covering my responsibilities towards her and my lovely sons, Yaseen and Hassan, throughout the tough days of my Ph.D. journey. Finally, special thanks to my mother, sisters, and all family members for their prayers and support. I understand you can no longer wait for my return and for our regathering, so thanks for your patience.

Dedication

To my lovely father, Hassan El Rouby, who taught me to be thankful and to work hard to achieve my dreams. May ALLAH grant you peace and the highest level of Jannah.

Table of Contents

Chapter 3

Preliminary Analysis and Instrumentation of Large-Span Three-Sided RC Culverts

Chapter 4

Structural Performance of a Medium-Span RC Three-Sided Culvert Based on Field Measurements and Numerical Analyses

Chapter 5

Class-A Prediction of Three-sided Reinforced Concrete Culverts

Chapter 6

Field Monitoring and Numerical Analysis of a Large-Span Three-Sided RC Culvert

Chapter 7

Effect of Large-Span Three-Sided Culvert Configuration on its Performance at Service and Ultimate Loading Conditions

Chapter 8

Design Guidelines for Reinforced Concrete Three-Sided Culverts

Chapter 9

Summary, Conclusions, and Recommendations

List of Tables

List of Figures

List of Abbreviations, Symbols, and Nomenclature

1D	One-dimensional
2D	Two-dimensional
3D	Three-dimensional
A	Interface reduction factor
AASHTO	American Association of State and Highway Transportation
ASTM	American Society for Testing and Materials
ADAMS	Automated Data Acquisition Monitoring System
B_c	Outside width of the culvert
B_d	Trench width
B_f	Strip footing width
BF	Backfill
BM	Bending moment
c	Soil cohesion
C_c	Soil coefficient of curvature
C_d	Load coefficient
CF_c	Coefficient of thermal expansion of concrete

CF_{VW}	Coefficient of thermal expansion of the vibrating wire
CHBDC	Canadian Highway Bridge Design Code
CI	Culvert insertion
c_{int}	Interface adhesion
CL	Silty clay
CoV	Coefficient of variation
C_u	Soil uniformity coefficient
DC	Duncan-Chang
d	Cross-section depth
D_{nn}	Interface normal stiffness
D_{tt}	Interface tangential stiffness
E	Young's modulus
E_c	Concrete modulus of elasticity
E_s	Soil Young's modulus
E_{st}	Steel Young's modulus
f	Interface multiplication factor
f_{ct}	Concrete tensile strength
f'_c	28-day concrete compressive strength
F_e	Soil-structure interaction factor

FE	Finite element
FEA	Finite element analysis
F_{e-bot}	Vertical arching factor for the pressure on the bottom slab
FEM	Finite element model
F_{e-top}	Vertical arching factor for the pressure on the top slab
FL	Foundation level
f_r	Concrete modulus of rupture
F_t	Soil-structure interaction factor for trench installation
f_y	Steel yielding stress
G_f	Concrete fracture energy
GTA	Greater Toronto Area
H	Backfill height
HAF	Horizontal arching factor
H_B	Overall height of the culvert
HDPE	High-density polyethylene
H_{eq}	Equivalent backfill height
H_{max}	Backfill height at failure
I_g	Gross moment of inertia
IQR	Interquartile range

K	Modulus number in Duncan-Chang model
K_F	Footing rotational stiffness
K_o	At-rest earth pressure coefficient
LEA	Linear elastic model
LEP	Lateral earth pressure
MC	Mohr-Coulomb
ML	Sandy silt
n	Modulus exponent in Duncan-Chang model
NLA	Nonlinear model
P	Footing pedestal height
P_B	Pressure on the bottom slab
PC	Pressure cell
P_S	Lateral earth pressure on the sidewall
P_T	Earth pressure on the top slab
P_{ult}	Ultimate load capacity of the precast unit
Q_1	First quartile
Q_3	Third quartile
R	Culvert sidewall height
RC	Reinforced concrete

R_f	Failure ratio in Duncan-Chang model
S	The total height of footing pedestal and culvert sidewall
SD	Standard deviation
SF	Sidefill
SG	Strain gauge
SLS	Service limit state
SPT	Standard Penetration Test
SW	Well-graded sand
S/Δ	Culvert span to deflection ratios
T_0	Temperature at time of initial gauge reading
T_1	Temperature at time strain is measured
t	Virtual thickness of the interface
TSC	Three-sided culvert
ULS	Ultimate limit state
VAF	Vertical arching factor
VEP	Vertical earth pressure
VW	Vibrating wire
W	Precast unit width
W_E	Total earth load

W_m	Numerical model width
Δ_{ult}	Ultimate displacement
Δ_y	Yield displacement
ε_{cr}	Theoretical cracking strain of concrete
ε_e	External strain measured on the outer surface of the concrete structure
ε_i	Internal strain measured on the inner surface of the concrete structure
$\gamma_{backfill}$	Unit weight of the backfill soil
$\gamma_{max.\ compaction}$	Unit weight of the soil with the highest compaction in the same soil category (soil type)
γ_s	Soil unit weight
κ	Cross-section curvature
λ	modification factor to account for the reduced mechanical properties of lightweight concrete relative to normal weight concrete
λ and μ	Lame's parameters
μ	Ductility factor
μ_{int}	Interface friction coefficient
ν	Poisson's ratio
ϕ	Soil internal friction angle

ϕ_{int}	Interface friction angle
ψ	Soil angle of dilation
σ_v	Vertical earth pressure
θ	Footing rotation in radian

Chapter 1

Introduction

1.1 Overview

Culverts are buried structures used to convey water, utilities, or pedestrian through embankments. They are a vital part of the urban infrastructure for all societies and their failure can cause significant economic losses. Nowadays, culverts are manufactured using a variety of materials such as cast iron, aluminum, steel and reinforced concrete (RC). Concrete is the most commonly used in drainage systems among all the other materials due to its durability and approved strength. RC culverts are constructed as either cast-in-place or precast, with the latter becoming more common due to the improved quality control in their production, reduced construction cost and time, and road closure duration. Culverts are also produced in different sizes and shapes like pipes, boxes, and bottomless culverts.

The different stiffness of both the buried structure and surrounding soil mass results in redistribution of stresses in the surrounding soil mass, which in turn affects the applied loads on the structure. Many studies addressed the structural performance of RC box culverts and the factors affecting the soil arching mechanism through full-scale field tests, centrifuge tests, and numerical investigations (Tadros et al., 1989; Yang, 2000; Kim and Yoo, 2002; Bennett et al., 2005; Kim and Yoo, 2005; Yoo et al., 2005; Kang et al., 2008; Pimentel et al., 2009; Chen and Sun, 2014; Abuhajar et al., 2015). These studies identified the primary factors that influence the earth loads acting on RC box culverts to be the installation method, the subsurface soil condition, the backfill height, the compaction condition of the sidefill material, the soil type of the sidefill material, and the culvert span. Based on these studies on box culverts, different equations were proposed to estimate the earth loads on box culverts (Tadros et al., 1989; Bennett et al., 2005; Kim and Yoo, 2005; Yoo et al., 2005; Kang et al., 2008).

Recently, bottomless culverts are increasingly used as an economical alternative for short-span bridge replacement as opposed to multi-barrel box culverts in terms of materials cost, construction time, workforce, and future maintenance costs (Webb et al., 1999; Von

Handorf, 2004; Marshall et al., 2014). They are also more attractive from the environmental point of view compared to circular pipes, box, and multi-barrel box culverts as they allow water to flow in its natural course with minimal influence on the marine environment. Bottomless culverts are produced in different shapes, including: arch, three-sided with arched top slab, and three-sided with flat top slab. Flat top three-sided culverts (TSCs), which are the focus of this study, are typically produced in large spans, up to 16.0 m, and low-rise profiles to handle heavy flows at sites with limited vertical clearance. Meanwhile, with the absence of the bottom slab that restrains the lateral movement of the sidewalls, differential settlement may occur between the supporting strip footings and the large-span TSC deformation is expected to differ from that of the relatively rigid, short-span box culverts. These features would influence the soil-structure interaction mechanism of TSCs in the long and/or short terms.

Studies on large-span bottomless culverts are relatively scarce and limited to either arch culverts (Oswald, 1996; McGrath et al., 2002) or TSCs with arched top slab (Beach, 1988; McGrath et al., 1996; Zoghi and Farhey, 2006; Marshall et al., 2014). Based on field measurements and numerical analyses, McGrath et al. (2002) proposed non-uniform vertical earth pressure distribution on the top slab of large-span RC arch culverts with earth pressure magnitudes lower than that stipulated in the Canadian Highway Bridge Design Code, CHBDC (CSA, 2014). However, the current design practices specified in the CHBDC (CSA, 2014) and the American Association of State and Highway Transportation, AASHTO (AASHTO LRFD, 2014) do not distinguish between small-span box and large-span bottomless culverts. This can result in an overly conservative prediction of vertical earth pressures on the top slab and an unnecessary increase in the cost.

This study presents the first-ever research effort addressing the interaction of precast RC flat TSCs with the surrounding soil mass through full-scale field monitoring and advanced numerical analyses.

1.2 Research Objectives and Methodology

The main objective of this research is to enhance the knowledge on the structural performance of large-span TSCs with flat top slab at service and ultimate loading conditions based on full-scale field measurements and advanced numerical analyses. A particular emphasis is placed on evaluating the applied earth pressures on these structures to enhance their design criteria. The specific objectives of this study are:

1- Evaluating the real-time structural performance of TSCs at service loading conditions during and after construction completion.

2- Evaluating the actual earth loads acting on TSCs with different spans, as well as the induced transient loads from the equipment and materials during the common construction activities on site.

3- Investigating the effect of some governing factors on the applied earth pressures on TSCs, e.g., culvert dimensions, foundation soil condition, strip footing geometry, installation method, backfill height, backfill soil type, and compaction level of the backfill material surrounding the TSC.

4- Investigating the actual sidewall-footing connection behavior, considering the common construction practice.

5- Predicting the modes of failure of RC TSCs and the factors influencing their performance at ultimate limit state under earth loading conditions, e.g., subsurface soil condition, culvert configuration, footing geometry, backfill soil type, and compaction level of the sidefill and backfill materials.

6- Predicting the ultimate capacity of the precast units of TSCs under a specific experimental loading setup reported in the literature on an RC arched TSC, besides investigating the influence of the precast unit width as well as the sidewall height.

7- Providing recommendations for representative numerical modeling of the three-sided culvert-soil system at service and ultimate loading conditions.

8- Evaluating the applicability of the RC box culvert design guidelines stipulated in the codes and standards, e.g., CHBDC (CSA, 2014) and AASHTO (AASHTO LRFD, 2014), for the design of large-span TSCs.

9- Developing explicit design guidelines for large-span TSCs based on full-scale field measurements and advanced numerical analyses.

The followed approach to fulfill the key objectives of this study is to perform a comprehensive investigation program in the following order: preliminary analysis, full-scale field monitoring of three TSCs with different spans, two-dimensional (2D) finite element analyses (FEAs) for TSCs under earth loading conditions, and three-dimensional (3D) FEAs for modeling the precast units. The components of the investigation program are briefly described as follows:

- **Preliminary analysis**: Preliminary 3D FEAs were conducted to optimize the instrumentation plan and field tests for three TSCs. The results of the numerical models were utilized to predict the structural response, provide approximate magnitudes of parameters that would be measured during the field tests, and determine the critical locations where the instrumentation should be located for field measurements and data collection.

- **Full-scale field monitoring**: This part includes instrumentation and field monitoring of three TSCs with spans of 7.3 m, 10.4 m, and 13.5 m. The monitored culverts cover intermediate to large spans. Each culvert has a unique geometry, subsurface soil condition, and installation method.

- **Two-dimensional FEAs**: Two-dimensional (2D) plane-strain FE models were developed for the three culverts. The 2D FE models were validated against the field measurements. Afterwards, the validated models were employed to conduct comprehensive parametric studies.

- **Three-dimensional FEAs**: A nonlinear 3D FE model was developed to simulate the experimental loading test of an RC arched TSC precast unit reported by (Marshall et al., 2014). The 3D FE model was validated against the experimental

data. The same modeling approach was employed to investigate the structural performance of TSC precast units and the influencing parameters.

1.3 Thesis Organization

This thesis has been produced in accordance with the guidelines of the School of Graduate and Postdoctoral Studies. Substantial parts of this thesis have been published, accepted or submitted in peer-reviewed journals. The thesis consists of eight chapters that are briefly described as follows:

Chapter 1 describes the problem statement and the research motivation. It outlines the objectives and methodology of this research work. In addition, it presents the organization of the thesis.

Chapter 2 provides a critical review of previous studies conducted on reinforced concrete box and bottomless culverts. It discusses the CHBDC (CSA, 2014) and AASHTO (AASHTO LRFD, 2014) provisions regarding the design of RC box culvert. Moreover, the current approaches used to analyze and design large-span bottomless culverts are covered. Finally, gaps in the knowledge regarding the performance of large-span TSCs with flat top slab have been highlighted.

Chapter 3 presents the field instrumentation program of three functional precast RC TSCs in the Greater Toronto Area, Ontario, Canada. It includes details of the preliminary 3D finite element models developed to design the monitoring program. A brief description of the sensors' selection criteria and installation procedures has been presented. Moreover, all field measurements of a 7.3-m-span TSC up to the final backfill height are presented and analyzed.

Chapter 4 includes the collected field data from an instrumented 7.3-m-span TSC under 1.7 m of backfill and their analysis. The chapter presents details of the 2D FE models, which were validated against the field measurements and predicted the earth pressures at the final backfill height (3.2 m). The effects of nonlinear behavior of RC and foundation soil condition (yielding or non-yielding) on the culvert's structural performance and soil-structure interaction mechanism at service and ultimate loading conditions are investigated

using the validated 2D models. Moreover, details of the developed 3D nonlinear FE model used to predict the ultimate capacity of the TSC precast unit, and the influence of its width are provided.

Chapter 5 presents a comparison between the preliminary finite element analysis results and field measurements of a 10.4-m-span culvert. In addition, the predicted earth pressures at the final backfill height from the FE model presented in Chapter 4 were compared with the field monitoring results after reaching the final backfill height. Finally, the results of the parametric study conducted to investigate the effect of strip footing geometry for the cases of yielding and non-yielding foundation soil conditions are presented.

Chapter 6 presents a study investigating the soil-structure interaction mechanism and structural performance of a full-scale, 10.4-m-span, TSC under service and ultimate load levels. Field data up to the final backfill height are provided. The chapter also includes details of the 2D FE models developed to predict the failure mechanism and ultimate capacity of the TSC under soil loading condition. In addition, the ultimate capacity of the TSC precast unit under the experimental loading setup was predicted from the developed 3D FE model.

Chapter 7 provides a detailed study on the effect of large-span TSC configuration, more specifically the sidewall and footing pedestal heights, on its performance at service and ultimate loading conditions. The chapter includes the collected field data from an instrumented 13.5-m-span TSC under 3.0 m of backfill as well as the numerical results of the validated 2D FE model. At service loading condition, the effect of TSC configuration was discussed in terms of the applied earth pressures on the culvert body and footing pedestal, the contact earth pressure underneath the footing, the deformed shape of the footing-culvert system, and the crack pattern in the culvert body. At ultimate loading condition, the effect of TSC configuration was discussed in terms of the maximum backfill height at failure, the failure mechanism, the location of failure, the deformed shape of the footing-culvert system at failure, as well as the crack pattern in the culvert body at failure. Finally, the chapter presents an evaluation of the effect of culvert sidewall height on its structural capacity employing 3D nonlinear FE models.

Chapter 8 presents the results and analysis of a comprehensive parametric study conducted to investigate the influence of backfill height and soil type, installation method and compaction level, as well as the concrete compressive strength on the applied earth pressures and the structural performance of TSCs. The chapter includes a comparison between the estimated earth pressures and the CHBDC (CSA, 2014) and AASHTO (AASHTO LRFD, 2014) provisions. Equations are proposed to estimate the applied earth pressures on large-span TSCs. Finally, limits to the midspan vertical deflection are proposed to satisfy the serviceability limit state requirements in terms of flexural crack width limitations.

Chapter 9 provides a summary of the research work, main conclusions, and recommendations for future research.

1.4 Original Contributions

This study investigates the structural performance of RC TSCs at service and ultimate loading conditions as well as their interaction with the surrounding soil mass through full-scale field monitoring and advanced numerical analyses. The original contributions of this study are:

1- Presenting the first-ever field monitoring study addressing RC TSCs with flat top slab, including the largest RC culvert with flat top slab to be instrumented to date with a clear span of 13.5 m.

2- Revealing the influence of the subsurface soil condition (yielding vs. non-yielding) on the applied earth pressures on TSCs and their structural performance at service and ultimate loading conditions based on 2D nonlinear FEAs.

3- Studying the effect of strip footing geometry and culvert configuration on the earth pressures acting on the footing-culvert system.

4- Investigating the actual sidewall-footing connection behavior considering the common construction practice and elaborating the conditions when the assumption

of hinged connection at the sidewall base, typically assumed in the current design practice, would be suitable.

5- Conducting a comprehensive parametric study, based on validated 2D nonlinear FE models, to investigate the influence of backfill height, soil type, installation method and compaction level, as well as the concrete compressive strength on the applied earth pressures and the structural performance of TSCs.

6- Assessing the applicability of the RC box culvert design guidelines stipulated in CHBDC (CSA, 2014) and AASHTO (AASHTO LRFD, 2014) for the design of large-span TSCs.

7- Proposing equations to provide safe estimates of VAF for B1 and B2 installations for RC TSCs considering a wide range of culvert spans and backfill heights.

8- Proposing limits to the midspan vertical deflection to satisfy the serviceability limit state requirements in terms of flexural crack width limitations.

9- Evaluating the ultimate capacity of TSC precast units using 3D nonlinear FEAs and elaborating the influence of the precast unit width and sidewall height on its structural performance at ultimate limit state.

1.5 References

1. AASHTO (American Association of State Highway and Transportation Officials). (2014). *AASHTO LRFD bridge design specifications*. 7th ed. AASHTO, Washington, DC.

2. Abuhajar, O., El Naggar, H., and Newson, T. (2015). Static soil culvert interaction the effect of box culvert geometric configuration and soil properties. *Computers and Geotechnics Journal*, 69, 219-235. 10.1016/j.compgeo.2015.05.005

3. Beach, T. J. (1988). *Load test report and evaluation of a precast concrete arch culvert*. Transportation Research Record 1191, Transportation Research Board, Washington, DC, 12–21.

4. Bennett, R. M., Wood, S. M., Drumm, E. C., and Rainwater, N. R. (2005). Vertical loads on concrete box culverts under high embankments. *Journal of Bridge Engineering*, 10 (6), 643-649. 10.1061/(ASCE)1084-0702(2005)10:6(643)

5. Chen, B., and Sun, L. (2014). Performance of a reinforced concrete box culvert installed in trapezoidal trenches. *Journal of Bridge Engineering*, 19 (1), 120–130. https://doi.org/10.1061/(ASCE)BE.1943-5592.0000494.

6. CSA (Canadian Standards Association). 2014. *Canadian highway bridge design code*. CAN/CSA-S6-14. Mississauga, ON, Canada: CSA.

7. Kang, J., Parker, F., Kang, Y. J., and Yoo, C. H. (2008). Effects of frictional forces acting on sidewalls of buried box culverts. *International Journal for Numerical and Analytical Methods in Geomechanics*, 32 (3), 289-306.

8. Kim, K., and Yoo, C. H. (2005). Design loading for deeply buried box culverts. *Journal of Geotechnical and Geoenvironmental Engineering*, 131 (1), 20–27.

9. Kim, K., and Yoo, C. H. (2002). *Design loading for deeply buried box culverts*. IR-02-03, Highway Research Center, Auburn Uni., Auburn, AL.

10. Marshall, J. D., Anderson, J. B., Meadows, R. L., and Jensen, T. J. (2014). Full-scale testing of three-sided precast concrete arch sections. *Journal of Bridge Engineering*, 19 (12), 04014051. 10.1061/(ASCE)BE.1943-5592.0000630.

11. McGrath, T. J., Moore, I. D., Selig, E. T., Webb, M. C., and Taleb, B. (2002). *Recommend specifications for large-span culverts.* Report No. 473. Washington, DC: Transportation Research Board.

12. McGrath, T. J., Selig, E. T., and Beach, T. J. (1996). Structural behavior of three-sided arch span bridge. *Transportation Research Record 1541*, Transportation Research Record, Washington, DC, 112–119.

13. Oswald, C. J. (1996). Analysis of reinforced concrete culvert considering concrete creep and shrinkage. *Transportation Research Record 1541*, TRB. National Research Council. Washington, DC, 120–126.

14. Pimentel, M., Costa, P., Félix, C., and Figueiras, J. (2009). Behavior of reinforced concrete box culverts under high embankments. *Journal of Structural Engineering*, 135 (4), 366-375. 10.1061/(ASCE)0733-9445(2009)135:4(366), 366–375

15. Tadros, M. K., Benak, J. V., Abdel-Karim, A. M., and Bexten, K. A. (1989). *Field testing of a concrete box culvert*. Report No. 1231. Washington, DC: Transportation Research Board.

16. Von Handorf, J. J. (2004). Clear-span culverts: Economical designs. Better Roads, Feb. 2004.

17. Webb, M. C., Selig, E. T., and McGrath, T. J. (1999). Instrumentation for monitoring large-span culverts. *Field Instrumentation for Soil and Rock, Durham G. and Marr W.*, American Society for Testing and Materials, 66-86. 10.1520/STP14214S

18. Yang, M. Z. (2000). Evaluation of factors affecting earth pressures on buried box culverts. PhD dissertation, Uni. of Tennessee, Knoxville, TN.

19. Yoo, C. H., Parker, F., and Kang, J. (2005). *Bedding and fill heights for concrete roadway pipe and box culverts*. Final Report, ALDOT Project No. 930-592, Highway Research Center, Auburn Uni., AL.

20. Zoghi, M., and Farhey, D. N. (2006). Performance assessment of a precast concrete, buried, small arch bridge. *Journal of Performance of Constructed Facilities*, 20 (3), 244–252. 10.1061/(ASCE)0887 3828(2006)20:3(244).

Chapter 2

Literature Review

2.1 Introduction

Culverts are a vital part of the urban infrastructure for all societies, especially as a watercourse crossing on which roadways are constructed. Culverts are classified based on their material, construction method, shape, and geometry. Reinforced concrete (RC) culverts are widely used because of their durability and approved strength. They are constructed as either cast-in-place or precast, with the latter becoming more common due to the improved quality control in their production, reduced construction cost and time, and road closure duration. Recently, bottomless culverts, also known as three-sided culverts (TSCs), are increasingly used as an economical alternative for short-span bridge replacement (Webb et al., 1999; Marshall et al., 2014). They are more attractive from the environmental point of view compared to culverts with closed-bottom geometry, as they allow water to flow in its natural course with minimal influence on the marine environment. Bottomless culverts are produced in different shapes, including: arch, three-sided with arched top slab (arched TSC), and three-sided with flat top slab (TSC) as shown in **Figure 2-1** TSCs with flat top slab, which are the focus of this study, are produced in large spans reaching 16.0 m.

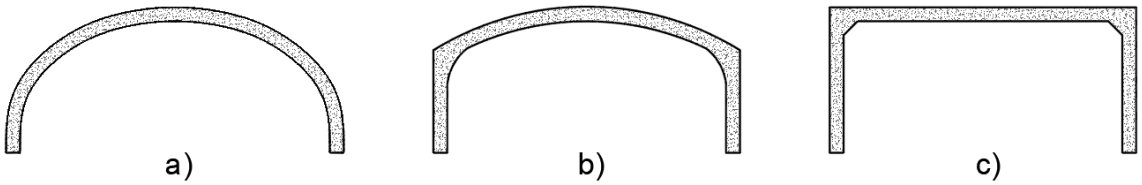

Figure 2-1. Different shapes of bottomless culverts: a) arch; b) three-sided with arched top slab; and c) three-sided with flat top alb.

TSCs with relatively large spans and without the bottom slab that restrains lateral leg movement under the applied loads may experience different earth and live load pressure distributions. In addition, they may experience deformations due to differential settlement of their footings, which would further complicate their soil-structure interaction behavior. Thus, their performance could be substantially different from the small-span rigid box

culverts. However, the current design practices specified in the Canadian Highway Bridge Design Code, CHBDC (CSA, 2014) and the American Association of State and Highway Transportation, AASHTO (AASHTO LRFD, 2014) do not distinguish between small-span box and large-span bottomless culverts. This can result in an overly conservative prediction of vertical earth pressures on the top slab and an unnecessary increase in the cost. Many field studies have been carried out on RC box culverts (Vaslestad et al., 1993; Yang, 2000; Bennett et al., 2005; Chen and Sun, 2014). On the other hand, studies on bottomless culverts are relatively scarce and limited to either arch culverts (McGrath et al., 2002) or TSCs with arched top slab (Beach, 1988; McGrath et al., 1996; Zoghi and Farhey, 2006; Marshall et al., 2014).

This chapter presents a critical review of the conducted research studies addressing the soil arching phenomenon, the factors affecting the earth pressures acting on RC box culverts and large-span bottomless culverts, the provisions of some codes and standards regarding the design of RC culverts, and discussion of the current approaches used to analyze and design large-span bottomless culverts, including frame analysis and finite element analysis. Finally, the existing gaps in the knowledge regarding RC TSCs with flat top slab have been highlighted.

2.2 Soil Arching

Soil arching is defined as the transfer of load to or away from the buried structure due to the relative stiffness of the structure to surrounding soil medium (Selig, 1964). When a structure is buried in a soil mass, incompatible stiffness between the structure and soil exists. Therefore, relative displacements occur between the central soil prism over the structure and the adjacent exterior soil prisms, resulting in the mobilization of shear stresses along these soil planes experiencing strain discontinuities. Arching can result in decreasing or increasing the stresses on buried structures, compared to the free-field stresses, depending on the direction of the mobilized shear stresses. Active arching, also termed positive arching, generates a reduction of the stresses on the structure and an increase on the adjacent soil. Active arching takes place when the buried structure is more flexible compared to the surrounding soil mass as presented in **Figure 2-2a**. Conversely, passive arching, also termed negative arching, results in increasing the stresses on the structure as

shown in **Figure 2-2b**. Passive arching occurs when the structure is more rigid than the soil (Evans, 1984).

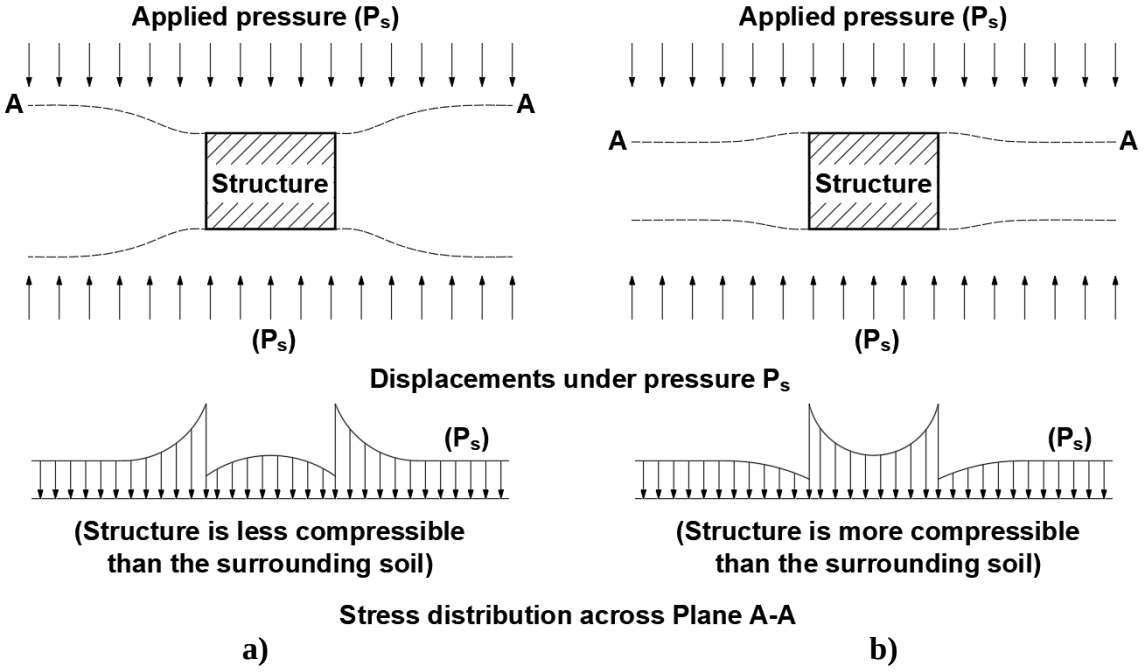

Figure 2-2. Soil arching mechanism and stress distribution: a) active arching; and b) passive arching. (After Evans, 1984)

Research studies addressing earth loads acting on buried structures have been ongoing since the pioneering contributions attributed to Marston (Marston and Anderson, 1913; Marston et al., 1917; Marston, 1930). The Marston theory demonstrated by mechanics principles that loads on buried structures are influenced by their installation conditions and backfill height over the structure. The installation condition controls the magnitude and direction of settlement of the soil prism on the culvert top slab relative to the settlement of the adjacent soil prisms as displayed in **Figure 2-3**. The relative settlement between these soil prisms results in the development of shearing stresses, as previously discussed. Depending upon the direction of the differential settlement between the above-mentioned soil prisms, the developed shearing stresses increase or decrease the applied earth pressures on the culvert top slab compared to the self-weight of the central soil prism ($\gamma_s \times H$, where γ_s is the soil unit weight and H is the backfill soil height above the culvert) as demonstrated in **Figure 2-3**. Accordingly, the vertical earth pressure on top of buried structures (σ_v) is not estimated as the free-field stress ($\gamma_s \times H$). Instead, a vertical arching factor (VAF), also

referred to as soil-structure interaction factor (F_e), is applied to account for the soil arching effect as follows:

$$\sigma_v = VAF \times \gamma_s \times H = F_e \times \gamma_s \times H \quad \textbf{(2-1)}$$

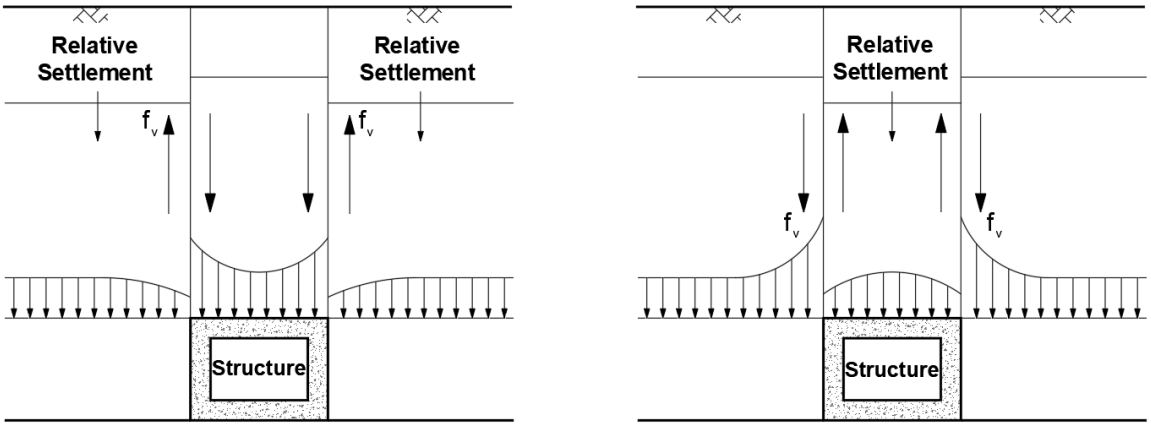

Figure 2-3. Pressure transfer mechanism within the soil-structure system: a) passive arching; and b) active arching. (After Kim and Yoo, 2005)

Many studies addressed the structural performance of RC box culverts and the factors affecting the soil arching mechanism through full-scale field tests, centrifuge tests, and numerical investigations (Tadros et al., 1989; Yang, 2000; Kim and Yoo, 2002; Bennett et al., 2005; Kim and Yoo, 2005; Yoo et al., 2005; Kang et al., 2008; Pimentel et al., 2009; Chen and Sun, 2014; Abuhajar et al., 2015). These studies identified the primary factors that influence the VAF to be the installation method, the subsurface soil condition, the backfill height (H), the compaction condition of the sidefill material, the soil type of the sidefill material, and the culvert span. Based on these studies on box culverts, different equations were proposed to estimate the VAF (Tadros et al., 1989; Bennett et al., 2005; Kim and Yoo, 2005; Yoo et al., 2005; Kang et al., 2008). Meanwhile, studies on large-span bottomless culverts are relatively scarce and limited to either arch culverts (Oswald, 1996; McGrath et al., 2002) or arched TSCs (Beach, 1988; McGrath et al., 1996; Zoghi and Farhey, 2006; Marshall et al., 2014). To date, studies investigating the soil-structure interaction of TSCs with flat top slab and the applied earth pressures on these structures do not exist. This section summarizes the findings of some studies on RC box culverts and large-span bottomless culverts.

2.2.1 Box Culverts

Tadros et al. (1989) conducted a finite element analysis (FEA) to evaluate the earth pressures on RC box culverts in embankment installation. They simulated 12 box culverts with inner dimensions between 1.2 × 1.2 m and 3.7 × 3.7 m. They considered two backfill soil types (silty sand and silty clay). They reported non-uniform distribution of the vertical earth pressure on the top slab and the contact pressure underneath the bottom slab. The lateral earth pressure distribution on the sidewalls was trapezoidal. The calculated average VAF increased from 1.00 to 1.15 as the H increased from 1.0 m to the largest backfill height considered. They proposed the following equations to estimate the earth loads on RC box culverts:

For silty-clay soil:

$$P_T = (0.984 + 0.0019H)\gamma_s H$$

$$F_e = \text{VAF} = (0.984 + 0.0019H)H$$

$$P_S = 0.6\gamma_s H \quad \textbf{(2-2)}$$

$$P_B = P_T + \frac{2H_B(57 + 26.3H_B)}{B_c}$$

For silty-sand soil:

$$P_T = (0.97 + 0.0020H)\gamma_s H$$

$$F_e = \text{VAF} = (0.97 + 0.0020H)H$$

$$P_S = 0.567\gamma_s H \quad \textbf{(2-3)}$$

$$P_B = P_T + \frac{2H_B(114 + 16.2H_B)}{B_c}$$

where: P_T is the pressure on the top slab (kPa); P_S is the pressure on the sidewall (kPa); P_B is the pressure on the bottom slab (kPa); H_B is the overall height of the box culvert (m); B_c is the outside width of the box culvert (m). It is worth noting that **Equation (2-2)** and **Equation (2-3)** consider the frictional drag forces resulting from the higher settlement of the sidefill material compared to the culvert sidewalls. However, these equations do not

account for the foundation soil condition and sidefill compaction level. Moreover, the numerical analysis was conducted for box culverts with spans up to 3.7 m only, which does not cover culverts with larger spans.

Yang (2000) reported the earth pressure measurements on a 9.9-m-wide × 3.7-m-high double box RC culvert covered with 11.7 m of backfill. The double box culvert was a replacement for a failed culvert. The backfill within 2.0 m of the culvert was not compacted in an attempt to reduce the vertical and lateral earth pressures acting on the culvert body. Based on the field measurements, an average VAF of 1.26 was estimated. Similarly, Bennett et al. (2005) monitored the response of an RC cast-in-place double box culvert with outside dimensions of 7.0-m-wide and 4.0-m-high at the two instrumented sections. The instrumented sections were located at the mid-length of the culvert and under a sloping side of the embankment. The total backfill height was 18.9 m at the mid-length of the culvert. The backfill consisted of gravel up to 0.6 m above the top slab, and silty clay was used for the rest of the embankment. Vibrating wire (VW) pressure cells and strain gauges were used to instrument the culvert. Bennett et al. (2005) reported non-uniform vertical earth pressure distribution on the culvert top slab, with higher pressures over the stiff sidewalls than those at the midspan. Based on the pressure cell measurements, they estimated VAFs of 1.64 and 1.04 at the mid-length and under the sloping side of the embankment, respectively. They presented equations to calculate the VAF based on typical values and design formulas developed by Clarke (1967) as follows:

$$F_e = \text{VAF} = \frac{e^{0.38\left(\frac{H}{B_c}\right)-1}}{0.38\left(\frac{H}{B_c}\right)}, \qquad \text{for } \frac{H}{B_c} \le 2.42$$

$$F_e = \text{VAF} = 1.69 - \frac{0.12}{\frac{H}{B_c}}, \qquad \text{for } \frac{H}{B_c} > 2.42 \qquad \textbf{(2-4)}$$

where H is the backfill height, and B_c is the outside width of the culvert. Three pressure cells were installed on the culvert sidewall at each instrumented section to measure the lateral earth pressures. However, Bennett et al. (2005) did not report their measurements or discuss the lateral earth pressure on the instrumented culvert.

Kim and Yoo (2005) simulated several RC box culvert configurations to investigate the influence of different parameters on the vertical earth pressures acting on the top slab in embankment and trench installations using different finite element (FE) programs. The box culvert dimensions were kept fixed at 2.4-m-wide × 2.4-m-high in all cases, while *H* was varied between 15.2 and 60.9 m. They concluded that the thicknesses of the culvert sidewalls and slabs within the range they investigated did not affect the calculated earth pressures. The numerical model results indicated higher vertical earth pressures for the case of non-yielding foundation soil (rock) compared to the case of yielding foundation soil (native soil). The following equations were proposed for embankment installation:

$$F_e = \text{VAF} = 1.047H^{0.055}, \quad \text{for yielding foundation soil}$$
$$F_e = \text{VAF} = 1.200H^{0.059}, \quad \text{for non-yielding foundation soil} \qquad \textbf{(2-5)}$$

Kim and Yoo (2005) reported that the vertical earth loads on the top slab were influenced by the foundation soil condition but were not affected by the compaction level of the sidefill material, which contradicts with other findings reported in the literature (Yoo et al., 2005; Kang et al., 2008; Pimentel et al., 2009). Moreover, the nonlinear behavior of the RC culvert and crack formation were ignored in their analysis, which might have influenced the obtained results (Pimentel et al., 2009).

Yoo et al. (2005) performed a comprehensive FEA to examine the soil-culvert interaction of box culverts and the influencing parameters, e.g., installation method, foundation soil condition, and soil type and compaction level of the sidefill material. Different FE programs (ABAQUS, NASTRAN, and CANDE) were used. They noted an increase in the magnitude of the contact earth pressure underneath the bottom slab over the predicted soil pressure on the top slab added to the self-weight of the culvert. This was attributed to the induced shear forces along the culvert sidewalls due to the relative settlement between the sidefill material and the relatively rigid culvert. These induced shear forces were higher in the case of uncompacted sidefill, reaching up to 27% of the total vertical load. They reported that the foundation soil condition (yielding vs. non-yielding) showed marginal influence on the calculated VAFs (<10%). For both yielding and non-yielding foundation soil conditions, the following equations were proposed to calculate the VAF:

$$F_{e-top} = -0.009\left(\frac{H}{B_c}\right)^2 + 0.109\left(\frac{H}{B_c}\right) + 1.131\,, \quad \text{for compacted sidefill}$$
$$F_{e-bot} = 1.823\left(\frac{H}{B_c}\right)^{-0.136}, \quad \text{for compacted sidefill} \qquad \textbf{(2-6)}$$

$$F_{e-top} = -0.007\left(\frac{H}{B_c}\right)^2 + 0.077\left(\frac{H}{B_c}\right) + 1.375\,, \quad \text{for uncompacted sidefill}$$
$$F_{e-bot} = 2.803\left(\frac{H}{B_c}\right)^{-0.169}, \quad \text{for uncompacted sidefill} \qquad \textbf{(2-7)}$$

where F_{e-top} is the VAF for the pressure on the top slab, F_{e-bot} is the VAF for the pressure on the bottom slab. The proposed equations were developed from the most critical case of vertical loading condition for rigid box culverts (positive projection embankment condition). Thus, the above-mentioned equations should be conservative for all other installation conditions (Yoo et al., 2005).

Kang et al. (2008) evaluate the influence of installation condition and compaction level of the sidefill material on the soil-structure interaction mechanism of box culverts employing different FE programs (ABAQUS, NASTRAN, and CANDE). They studied the effect of soil-culvert interface on the calculated earth pressures by considering two interface conditions: full bond and frictional slip between the soil and culvert during deformation. Interface frictional coefficients (μ_{int}) between 0.3 to 0.7 were considered in the frictional slip interface case. They reported significant shear forces developed along the culvert sidewall. For embankment installation, the soil-culvert interface condition did not affect the calculated contact pressures underneath the bottom slab. Kang et al. (2008) developed equations to estimate the vertical earth pressures on the top and bottom slabs accounting for the shear loads along the sidewalls, i.e.,

$$F_{e-top} = -0.005\left(\frac{H}{B_c}\right) + 1.304\,, \quad \text{for compacted sidefill}$$
$$F_{e-bot} = 0.004\left(\frac{H}{B_c}\right)^2 - 0.105\left(\frac{H}{B_c}\right) + 2.105\,, \quad \text{for compacted sidefill} \qquad \textbf{(2-8)}$$

$$F_{e-top} = -0.012\left(\frac{H}{B_c}\right) + 1.407, \qquad \text{for uncompacted sidefill}$$

$$F_{e-bot} = 0.006\left(\frac{H}{B_c}\right)^2 - 0.175\left(\frac{H}{B_c}\right) + 2.685\,, \qquad \text{for uncompacted sidefill} \qquad \textbf{(2-9)}$$

Pimentel et al. (2009) conducted experimental and numerical studies on an RC box culvert with a span and rise of 2.0 m and backfilled up to 9.5 m on its top slab. The backfill material was clayey sand compacted to 98% Standard Proctor, with an average unit weight of 20 kN/m^3. The culvert was instrumented with 10 embedded strain gauges and 4 VW pressure cells (one on the sidewall and 3 on the top slab). They validated a two-dimensional (2D) nonlinear FE model against the field measurements and employed it to investigate the culvert performance at service and ultimate loading conditions. The nonlinear behavior of the RC culvert and crack formation were considered in the numerical simulation. Moreover, they studied the influence of the sidefill material stiffness and the subsurface soil condition (yielding vs. nonyielding). The field measurements and numerical calculations indicated non-uniform vertical earth pressure distribution on the top slab. The two cases of non-yielding foundation soil (rock) and uncompacted sidefill (low stiffness) exhibited higher VAFs at all backfill heights compared to the cases of yielding foundation soil and compacted sidefill. Lower VAFs were calculated from the FEA results when the nonlinear behavior of the RC culvert was considered compared to the case of elastic behavior. Thus, Pimentel et al. (2009) emphasized the importance of considering the nonlinear behavior of the RC culvert for realistic simulation of the interaction mechanism. Although Pimentel et al. (2009) considered the nonlinear behavior of RC, the backfill soil was simulated using the elasto-plastic Mohr-Coulomb model, which does not account for the nonlinear behavior of soil and the stress-dependency of its stiffness. This might have influenced the obtained results (Katona, 2017).

Chen and Sun (2014) reported the field monitoring results of a large-span RC box culvert. They instrumented an 8-m-span and 6.8-m-rise cast-in-place RC box culvert installed in a natural trapezoidal trench in a mountainous area and covered by 18.0 m of backfill. Both top slab and sidewalls were 1.0-m-thick, while the bottom slab was 0.2 m thicker. The culvert was backfilled in layers; each was 0.5-m-thick. The backfill material consisted of well-graded crushed gravel and silty clay. Instruments were placed at two sections: one

approximately under the embankment shoulder and the other at the mid-length of the culvert. The instrumented section at the mid-length of the culvert was instrumented with 5 VW earth pressure cells distributed at the roof level of the culvert. They utilized the field measurements to validate a 2D FE model, which was used to investigate the influence of installation method (trench vs. embankment vs. induced trench), slope angle of the trench sides, bottom width of the trench, culvert dimensions, backfill height, and stiffness of the sidefill material. Chen and Sun (2014) reported that the vertical earth pressure distribution was non-uniform along the culvert top slab. The culvert installation method was found to affect the VAF and its changing trend with the increase of backfill height. The VAF increased from 1.13 to 1.25 as H increased from 3.0 to 18.0 m. The VAF decreased nonlinearly with the trench slope angle. The VAF increased nonlinearly with the increase of the trench width and increased with the increase of ratio of culvert outside height to outside width. The stiffness of the sidefill material significantly influenced the estimated VAFs at all backfill heights. The VAF decreased with increasing the stiffness of the sidefill material. Chen and Sun (2014) simulated the behavior of sidefill and backfill materials by using the elasto-plastic Mohr-Coulomb material model. Moreover, the nonlinear behavior of the RC culvert and crack formation were ignored in their analysis. These approximations might have influenced the results (Katona, 2017; Pimentel et al., 2009).

2.2.2 Bottomless Culverts

Oswald (1996) conducted a field study of a precast RC arch culvert characterized by a relatively large span-to-rise ratio (12.3-m-span × 2.9-m-rise). The culvert was instrumented with VW pressure cells and embedded strain gauges to monitor its long-term performance over a period of 2.5 years after construction completion. The arch culvert was covered by 7.3 m of compacted silty clay backfill with an average unit weight of 20.2 kN/m^3. Oswald (1996) also conducted an FEA considering the nonlinear behavior of both concrete and backfill soil using CANDE computer code. The compaction loads were considered by applying a temporary 35 kPa surface pressure to each backfill soil lift. An equal and opposite pressure was applied during the next load step. The code was modified to account for the concrete creep and shrinkage behaviors. Oswald (1996) reported that the measured stresses followed three different stages. At cover depths less than 1.2 m, the total stresses

were significantly higher than the free-field stresses, which were retained to the combined effect of soil loads, compaction effort, and the development of porewater pressure in the cohesive backfill material. Followed is the stage in which the induced pore pressures dissipated, and the rate of increase of measured pressures was the least among the three stages; this took place at backfill heights between 1.2 and 3.0 m. In the last stage, at *H* over 3.0 m, the rate of increase in total pressure was equivalent to the free-field stress rate with a pressure approximately equal to the theoretical free-field stress at the final cover depth. The measured soil pressure near the crown under 7.3 m of backfill exhibited vertical earth pressure of approximately 1.03 times the free-field stresses after construction completion. The long-term measurements showed that the postconstruction variations in the measured earth pressures were within 15% of the mean measured pressures. On the other hand, significant postconstruction increase in the culvert deflection (up to 50%) and culvert strains (up to 200%) were observed, which was attributed to the influence of concrete creep and shrinkage. This was supported by the numerical analysis results, where good agreement between the field measurements and numerical calculations was only obtained when concrete creep and shrinkage were considered. The number of soil pressure cells used in the arch culvert field monitoring program was not sufficient. Pressure cells were only located at the springline and crown of the arch culvert, hindering the ability to interpret the earth pressure distribution along the culvert's profile. Moreover, field measurements were recorded 11 times during the period of 2.5 years after construction completion. Such low frequency of readings cannot reflect the applied earth loads and the real influence of the seasonal variations.

McGrath et al. (2002) instrumented a 9.1-m-span × 3.5-m-rise precast RC arch culvert. The culvert was installed in a trench and was backfilled with well-graded sand with gravel to 1.5 m at the final stage. To study the influence of the sidefill compaction condition on the structural performance of the large-span concrete culvert, two different tests were conducted: one with the sidefill compacted to 92% Standard Proctor, and the other without compaction efforts, achieving approximately 85% Standard Proctor. The backfill soil on top of the culvert was compacted in both tests to sustain the live loads from the test truck, which was the focus of the conducted full-scale field testing. Field data were used to

calibrate 2D FE models. A limited parametric study was conducted using the validated models, which included modeling an 11.0-m-span arched TSC and a 9.0-m-span arch culvert. The backfill height was extended to 4.0 m in the conducted parametric study. The measured earth pressures at the crown were higher than the free-field stress for the compacted and uncompacted backfill soil conditions. The authors attributed this to an error in the field data as they expected the earth pressure to be equivalent to the geostatic pressure, which was supported by the numerical model predictions. Based on field observations and FEA results, McGrath et al. (2002) proposed that large-span RC culverts should be designed considering a non-uniform earth pressure distribution on the top slab with a VAF of 1.0 at the midspan and 1.2 at the stiffer edges as demonstrated in **Figure 2-4**. Lateral pressures on the sidewall were found to vary significantly with the backfill height and density of the backfill material. **Table 2-1** summarizes the proposed horizontal arching factors (HAFs) to calculate the lateral earth pressure on the culvert sidewall. The HAF is equivalent to the lateral earth pressure coefficient. It is worth noting that the field-testing program was designed to evaluate the live load transfer mechanism to the tested culvert, which is important at shallow cover depths. This justified the 1.5 m backfill height in the full-scale field testing. However, such shallow backfill height was not sufficient to elaborate the soil-structure interaction mechanism and soil arching effect from the field measurements. Moreover, McGrath et al. (2002) generalized the proposed design guidelines to all bottomless culverts, including TSCs with flat top slab, which were not considered in the full-scale field testing or the conducted numerical analyses, making such generalization questionable.

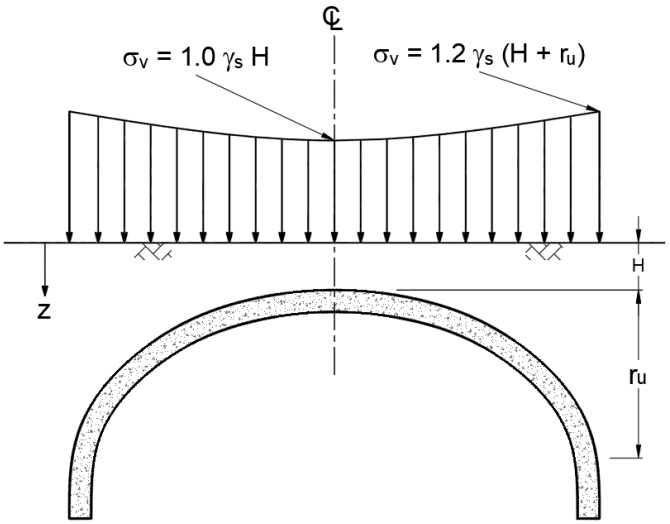

Figure 2-4. Proposed vertical earth pressure distribution on large-span RC culverts. (After McGrath et al., 2002)

Table 2-1. Proposed HAFs for large-span RC culverts. (After McGrath et al., 2002)

Soil type	Compaction level	HAF	
		Arched top slab	Flat top slab
SW	95	0.40 + 0.05 $H \leq 0.6$ (H in m) 0.40 + 0.16 $H \leq 0.6$ (H in ft)	0.40
SW ML	90 95	0.40 + 0.025 $H \leq 0.6$ (H in m) 0.40 + 0.08 $H \leq 0.6$ (H in ft)	0.40
SW ML CL	85 90 95	0.40	0.37
Other soils		0.30	0.30

Zoghi and Farhey (2006) investigated the ultimate load capacity of a 10.97-m-span × 2.74-m-rise arched TSC through field testing and FEA. The culvert was backfilled using well-graded granular soil material compacted to 95% Modified Proctor, with an average unit weight of 20 kN/m^3. The maximum backfill height on top of the culvert was 0.9 m. External loads were applied on the culvert using a hydraulic jack with a maximum capacity of 890 kN. The applied loading scheme imitated two truck axles positioned side-by-side at the

culvert midspan. The culvert was instrumented with 4 pressure cells installed on the culvert sidewalls. The structural performance was monitored using 16 dial gauges that measured the relative displacements at characteristic locations. The tested arch culvert sustained nearly 8 times the design live load without failure. It was concluded that the confinement provided by the surrounding soil mass enhanced the load-carrying capacity of the buried structure over a free-standing one. Additionally, Zoghi and Farhey (2006) pointed out that the measured horizontal displacements at the base of the sidewall were negligible at all load levels, justifying the assumption of hinged support at the sidewall base. However, pressure cells were installed only on the sidewalls, which is not sufficient to investigate the soil-structure interaction mechanism and hindered the quantification of the vertical earth pressures acting on the large-span culvert under the applied loads.

Marshall et al. (2014) conducted full-scale field and laboratory load testing studies on precast RC arched TSCs. The field test was conducted on a 12.8-m-span × 4.3-m-rise culvert, and the backfill height on top of the culvert was 0.6 m. The culvert was instrumented with strain gauges distributed along the precast unit and 4 pressure cells installed on the two sidewalls. Live-load testing was conducted using a three-axle dump truck with a total gross weight of 253 kN. The laboratory load tests were conducted on the RC precast units of a 6.1-m-span and an 11.0-m-span arched TSCs. The precast units were directly placed on the rigid laboratory floor and were laterally restrained at the base using HSS steel beams. Vertical loads were applied incrementally until failure was reached through three W8×35 beams spanning the width of the units. The field measurements indicated higher lateral earth pressures measured at the top than at the bottom of the sidewall. This was attributed to the higher restrain of the sidewall at the footing connection compared to its top. Marshall et al. (2014) suggested that these findings support the assumption of hinged connection at the sidewall-footing connection in the current design practice. The loaded precast units exhibited brittle failure under the experimental loading setup. No pressure cells were installed on the culvert top slab in the full-scale field test, which is not sufficient to investigate the soil-structure interaction mechanism and hindered the quantification of the vertical earth pressures acting on the large-span culvert under the applied loads. The structural performance of the arched TSCs precast units was

investigated at the ultimate loading condition. However, the study did not address the structural performance under soil loading conditions.

2.3 Codes and Standards Provisions

This section covers the provisions and design guidelines included in the CHBDC (CSA, 2014) and the AASHTO (AASHTO LRFD, 2014) regarding the design of RC culverts. It is worth mentioning that these guidelines are adopted for small-span box culverts. However, they are currently used for the design of large-span TSCs due to the absence of design guidelines specific to large-span TSCs.

2.3.1 CHBDC S6-14

The CHBDC (CSA, 2014) provides design guidelines for RC box culverts. In these guidelines, the backfill soils are categorized into three different groups (soil group I to III): sand and gravel, sandy silt (ML), and silty clay (CL) as listed in **Table 2-2**.

Table 2-2. Soil groups classification in the CHBDC (CSA 2014).

Soil group	Description	Unified Soil Classification symbols
I	Sand and Gravel	SW, SP, GW, GP
II	Sandy Silt	GM, SM, ML, GC, and SC with less than 20% passing #200 sieve
III	Silty clay	CL, MH, GC, and SC with more than 20% passing #200 sieve

The code does not distinguish between embankment and trench installations; instead, it defines two standard installations, namely, B1 and B2. The differences between B1 and B2 installations relate to the backfill soil type and compaction level in the sidefill and bedding zones as elaborated in **Figure 2-5** and summarized in **Table 2-3**. The code limits the compaction of the backfill material on top of the culvert, which shall not exceed the compaction or equivalent stiffness of the soils in the sidefill and bedding zones.

Table 2-3. Soils and compaction requirements for B1 and B2 standard installations. (CSA, 2014)

Installation type	Soil group	Equivalent minimum Standard Proctor compaction in sidefill and outer bedding zones
B1	I	90%
	II	95%
	III	Not permitted
B2	I	80%
	II	85%
	III	95%

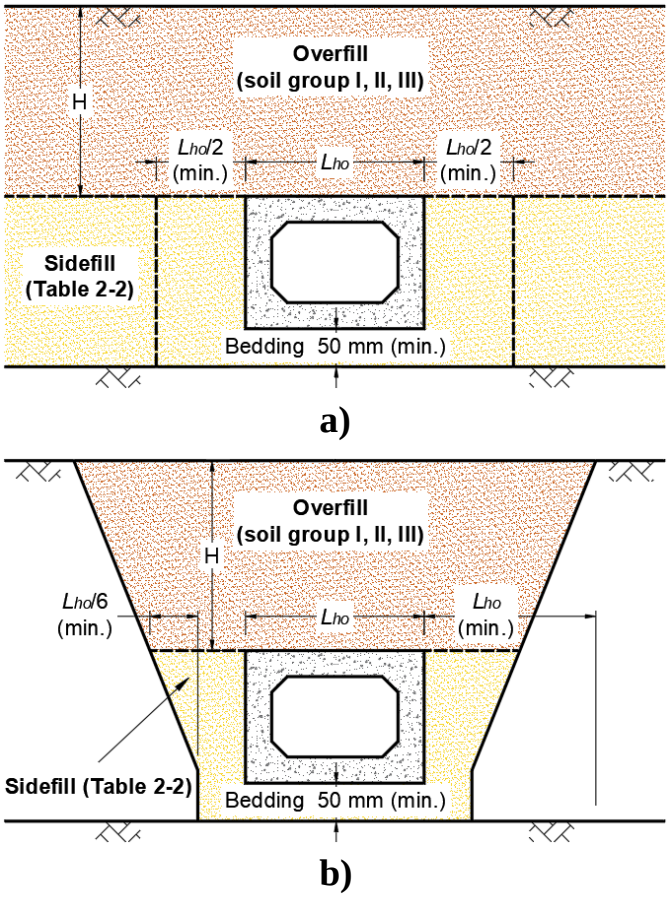

Figure 2-5. Standard installations for RC box culverts in the CHBDC (CSA, 2014): a) on embankments; and b) in trenches.

Based on previous practice and limited soil-structure interaction FEAs, the code stipulates VAFs to estimate the vertical earth pressure on the top slab and HAFs to estimate the lateral

earth pressure on the sidewall as summarized in **Table 2-4**. Higher VAF is specified for the case of B2 installation, which represents the case of moderately compacted sidefill compared to B1 installation. The higher VAF value accounts for the anticipated higher passive soil arching in case of loosely compacted sidefill material surrounding the RC box culvert. The code stipulates that both the minimum and maximum HAFs should be considered in the design to estimate the maximum negative and positive bending moments induced in the sidewalls. The CHBDC (CSA, 2014) allows for constructing RC box culverts in non-standard installations if their design is in accordance with approved methods based on soil-structure interaction, e.g., finite element analysis.

Table 2-4. Arching factors for box culverts in standard installations. (CSA, 2014)

Installation Type	Vertical Arching Factor, (VAF)	Horizontal Arching Factor, (HAF)	
		Minimum	Maximum
B1	1.20	0.30	0.50
B2	1.35	0.25	0.50

The CHBDC (CSA, 2014) includes limit states for large-span RC culverts that are similar to those adopted for RC box culverts. These limit states are consistent with those stipulated for most RC structures of all types. The limit states to be considered for RC culverts are as follows:

- Service limit state: the code specifies limits on the crack width of non-prestressed RC structures due to flexure depending on the exposure type as illustrated in **Table 2-5**.
- Ultimate limit state: the code specifies ultimate limit states for flexure, shear, and stability for RC culverts.

Table 2-5. Specified maximum crack width. (CSA, 2014)

Type of structural component	Type of exposure	Maximum crack width (mm)
Non-prestressed	De-icing chemicals; spray or surface runoff containing de-icing chemicals; marine spray; swamp; marsh; salt water; aggressive backfill	0.25
	Other environmental exposures	0.35

2.3.2 AASHTO LRFD

The AASHTO (AASHTO LRFD, 2014) differentiates between embankment and trench installations when determining the vertical earth pressure on the top slab of RC box culverts. The total earth load, W_E, on the top slab of box culverts is estimated by:

$$W_E = F_e \, \gamma_s \, B_c H \qquad \textbf{(2-10)}$$

The AASHTO estimates the soil-structure interaction factors (equivalent to the VAF) for embankment and trench installations based on the Marston-Spangler theory (Marston, 1930; Spangler, 1950). Meanwhile, the distribution of the total earth load on the top slab is not identified. The soil-structure interaction factor for embankment installation (F_e) is given by:

$$F_e = \text{VAF} = 1 + 0.20 \frac{H}{B_c} \qquad \textbf{(2-11)}$$

To account for the compaction condition of the sidefill material, the value of F_e shall not exceed 1.15 for compacted sidefill and 1.40 for uncompacted sidefill. However, the compaction requirements to classify the soil as compacted or uncompacted are not defined. The soil-structure interaction factor for trench installation (F_t) is given by:

$$F_t = \text{VAF} = \frac{C_d \, {B_d}^2}{H \, B_c} \leq F_e \qquad \textbf{(2-11)}$$

where C_d is a load coefficient to account for the type of backfill soil and the box culvert and embankment geometric properties, and B_d is the trench width. The earth loads in trench

installation shall not exceed those in embankment installation (AASHTO LRFD, 2014), which implies that embankment installation is relatively more critical for design purposes.

2.4 Design of Large-Span RC Culverts

The CHBDC (CSA, 2014) and AASHTO specification (AASHTO LRFD, 2014) do not distinguish between large-span RC TSCs and relatively small-span box culverts, and hence TSCs are designed employing the same guidelines adopted for small-span box culverts in accordance with the current design practice of RC. Analysis of large-span RC culverts is carried either using frame analysis with specified earth pressures or finite element analysis.

2.4.1 Frame Analysis

The common analysis method for RC TSCs in the current design practice is to conduct a rigid frame analysis assuming a linear RC structure with stiffness considering uncracked section. The structure is then loaded with the prescribed loads. Hinged connection is typically assumed at the sidewall footing base. This structural analysis approach requires design assumptions for the earth pressures and their distribution. Therefore, its use is justified for the standard installations specified in the applied code or standard. However, its application for other installation methods might be questionable. For instance, the equations included in the AASHTO specification (AASHTO LRFD, 2014) for estimating the soil-structure interaction factors are only applicable for either embankment or trench installation methods. For other installation methods, the AASHTO specification allows for the determination of the earth loads based on field tests, soil-structure interaction analyses, e.g., finite element analysis, or previous experience.

Studies on RC TSCs with flat top slab are limited to the experimental and analytical studies by Tarhini et al. (1997) and Fredrick and Tarhini (2000). Tarhini et al. (1997) designed two culverts with 7.2 and 8.0 m spans as elastic frames subjected to dead loads, live loads, and earth pressures in accordance with the American Society for Testing and Materials, ASTM, standards (ASTM C850, 1996) and AASHTO bridge specifications (AASHTO, 1996). Laboratory tests were performed on scaled models of the designed culverts (scale = 1/6), which were instrumented with strain gauges and dial indicators for deflection measurements. The scaled models were only subjected to live loads by means of a manual

screw jack and a proving ring; all the other loads, including earth loads, were ignored. They reported that failure of the models occurred at about four times the design load.

Fredrick and Tarhini (2000) conducted structural analysis of TSCs with spans between 4.2 and 11.0 m and considered two different approaches for their analysis and design. They initially used three-dimensional (3D) FEAs to evaluate straining actions in both the longitudinal and transverse directions and concluded that the straining actions in the transverse direction were minimal. Thus, it was concluded that the typical shrinkage crack reinforcement would be sufficient to withstand the computed bending moments and shear forces. Consequently, they conducted 2D plane frame analyses, and their results agreed well with testing data on 1/6-size scale models. Fredrick and Tarhini (2000) suggested that TSCs can be accurately analyzed using the 2D plane frame analysis. However, their study did neither address the soil-culvert interaction of TSCs nor the connection condition between the sidewall and the supporting strip footing.

In North America, the most common construction practice for precast RC bottomless culverts supported on keyed strip footings (arch or TSCs) is placing plastic shims along the footing keyway to guarantee the correct seating of the culvert's precast units. Once the unit is in its pre-specified position, plastic shims are placed between the keyway and the culvert leg to secure the unit in place and avoid any lateral spreading. Sequentially, the keyway is filled with non-shrink grout. Hinged connection at the sidewall-footing connection was suggested in previous studies (Beach, 1988; Zoghi and Farhey, 2006). Moreover, McGrath et al. (2002) reported that the strip footing supporting an arch culvert did not exhibit rotational or lateral movement at any of the testing stages. They recommended that the analysis of RC TSCs should be conducted assuming hinged connection at the sidewall base unless steel reinforcement is designed and detailed to provide fixity condition and to develop moment resistance.

2.4.2 Finite Element Analysis

Katona et al. (1976) pioneered the application of the FE method to analyze buried pipes by developing the FE software CANDE (Culvert ANalysis and DEsign). CANDE is a special-purpose FE program intended for the design and analysis of buried structures. The program has been used by a number of researchers (Katona and Vittes, 1982; Tadros et al., 1989; Kim and Yoo, 2002; Kim and Yoo, 2005; Katona, 2017). Other scholars developed FE codes specifically for the analysis of buried culverts, e.g., Byrne and Duncan (1979) developed NLSSIP for flexible culverts, and Heger et al. (1985) developed SPIDA for concrete culverts, which was modified from NLSSIP. These codes include the effect of construction procedure, culvert and soil geometry, material nonlinearity, and interface behavior (Leonards et al., 1982). Moreover, other general-purpose FE programs have been used to conduct nonlinear FE analysis of buried structures, e.g., ABAQUS (Kim and Yoo, 2002; Kim and Yoo, 2005), PLAXIS 2D (Chen and Sun, 2014; Ma et al., 2019), and DIANA (Pimentel et al., 2009).

The FE method provides a description of the stresses, strains, and deformations of the buried structure and surrounding soil mass, which facilitates the analysis and design of the soil-structure system. Meanwhile, realistic simulation of soil-structure systems using the FE method requires consideration of many details, including: the model extent and boundary conditions, material behavior (e.g., soil and concrete), construction process simulation, compaction loads, and interface properties.

2.4.2.1 Model Extent and Boundary Conditions

It is important to define boundary conditions at the model boundaries. The typical boundary conditions used in 2D models of RC culverts in the literature are fixity in vertical and lateral directions at the model bottom boundary and fixity in the lateral direction at the model side boundaries, e.g., Kim and Yoo (2005), Yoo et al. (2005), Pimentel et al. (2009), and Ma et al. (2019). However, these boundary conditions might affect the FE model results if the model boundaries were not sufficiently extended away from the buried culvert zone.

The width of the FE model affects the results of soil-structure models (Kim and Yoo, 2005) owing to the effect of the boundary conditions. Kim and Yoo (2002) conducted a sensitivity

analysis to evaluate the influence of the model width (W_m) to the culvert outside width (B_c) on the calculated VAFs. They reported that the calculated VAF increased gradually until W_m/B_c reached 12-14, after which no noticeable change occurred. For box culverts, Kim and Yoo (2005) reported no changes in the results as the foundation soil was extended more than four times the culvert height. It is believed that the extension of the foundation soil below the bottom slab should be related to its outside width, which affects the stresses transferred to the foundation soil as well as the influence zone below the bottom slab.

Yoo et al. (2005) suggested a W_m/B_c value of 6 to eliminate the influence of the side boundaries. They reported insignificant increase (0.5%) in the calculated vertical earth pressure on the top slab when the model width was extended to 11 times the culvert outside width compared to the model extended to 6 times B_c. In addition, the depth of the foundation soil below the bottom slab should be at least 1.5 times the culvert height (Yoo et al., 2005). For deep backfill heights exceeding 3 times the vertical height of the box culvert, the backfill layers can be replaced with additional surcharge loads equivalent to the remaining soil weight (Yoo et al., 2005). The same model extensions were found to be sufficient by Kang et al. (2008). Ma et al. (2019) extended the model boundaries to 10 times the culvert width and the vertical boundaries to 3 times the culvert width below the bottom slab.

In summary, a model width extended to 6 times the culvert width and extended vertically 3 times the culvert width below the bottom slab might seem to be sufficient to eliminate the effects of boundary conditions.

2.4.2.2 Soil Material Model

The stress-strain response of soil is very complex in nature due to its dependency on the soil's void ratio, stress history, and type of loading (Krizek and McQuade, 1978). Analytical and experimental studies have demonstrated that soil stiffness is a governing factor that influences the structural performance of buried structures (Katona, 2017). Many constitutive models were developed to represent the soil behavior ranging from simple linear elastic models to fully nonlinear plasticity and variable-modulus models. Vaslestad (1990) compared the general characteristics of some common soil models as follows:

- Bilinear model: A bilinear elastic model was introduced by McVay (1982) in which the soil behaves with a reduced stiffness following shear failure. McVay (1982) demonstrated that the use of this model yielded reasonable predictions of the deformation of a large-span steel culvert. However, Vaslestad (1990) reported that the predicted zone of yielded soil using this model was greater than that predicted using other models.

- Overburden-dependent modulus model: This model is a linear elastic model in which the soil stiffness is adjusted based on the soil stress state (Katona et al., 1976). Shear failure is not considered in this model. Thus, Vaslestad (1990) reported that this model is only suitable when the soil is in a state of confinement with no shear failure. Moreover, McVay (1982) and Leonards et al. (1982) concluded that the use of this model did not provide reasonable deformation predictions of buried structures.

- Elasto-plastic soil models: Most geotechnical FE programs include elasto-plastic soil models based on either the Mohr-Coulomb (MC) or Drucker Prager failure criteria, e.g., PLAXIS 2D, DIANA 10.1, CANDE. The flow rule in such models can be either associated or non-associated (Carter, 1992). Modifications have been made to the elasto-plastic models to consider the stress-dependent stiffness and improve predictions for granular soils (Brachman et al., 1996).

- Hyperbolic soil model: Duncan and Chang (1970) developed hyperbolic stress-strain relationships for the analysis of embankments and buried structures. This soil model has been extensively used in many studies and was incorporated in many FE programs, e.g., CANDE, DIANA 10.1.

- Extended Hardin model: This model employs shear stress-strain relationships instead of the nonlinear stiffness defined in the hyperbolic model. The use of the extended Hardin model overpredicted soil stiffness and caused convergence problems when it was used for the response analysis of a large-span steel culvert (Chang et al., 1980). Moreover, Leonards et al. (1982) reported that this model was not conservative at high shear strain levels.

Some studies in the literature investigated different models to simulate soil-structure interaction systems. Tadros et al. (1989) numerically simulated a box culvert with 1.5-m-span × 2.1-m-rise, backfilled with silty sand up to 8.2 m on the top slab using CANDE software. They considered the linear elastic model and Duncan hyperbolic soil model to simulate the behavior of the sidefill and backfill soils. Tadros et al. (1989) reported that the two soil models yielded comparable earth pressures on the studied box culvert. Zoghi and Farhey (2006) compared the results of FE models using five soil models with full-scale field measurements from an instrumented RC arched TSC. The investigated soil models were: the isotropic linear elastic, orthotropic linear elastic, overburden-dependent, Duncan, and Selig models. The two linear elastic models yielded poor correlation with field measurements as the soil does not behave linearly, and its stiffness is not constant. Similarly, poor correlation was obtained when the overburden-dependent soil model was used. The soil stiffness varies with overburden pressure in the overburden-dependent model in the case of one-dimensional (1D) compression. In case two-dimensional compression is prevalent, such as near culverts, the model does not yield accurate results (Katona et al., 1976). Better correlation between the field measurements and numerical model results was obtained with the hyperbolic models (Duncan and Selig models). Katona (2017) compared the performance of the linear elastic model, Mohr-Coulomb model, and hyperbolic Duncan-Selig model in replicating triaxial test data used to define the parameters of each soil model. In addition, Katona (2017) studied the influence of the three models on the estimated structural distress of typical culverts under loading conditions using CANDE software. The results indicated the superiority of the hyperbolic model over the other two models in replicating the triaxial tests. Moreover, the results indicated that the Duncan-Selig model provided more accurate and conservative predictions of distress in all pipe types. Thus, it was concluded that the hyperbolic model is more accurate and safer to use for the design of culverts backfilled with granular soils (Katona, 2017).

In conclusion, previous studies demonstrated that the hyperbolic model (Duncan-Chang or modified Duncan-Selig models) is more accurate and conservative than linear elastic or elasto-plastic material models in FE simulation of buried structures. One other advantage of the hyperbolic model is the availability of representative properties and input parameters

for typical backfill soil materials with different compaction levels (Duncan et al., 1980; Boscardin et al., 1990). Duncan et al. (1980) provided the model parameters for many soils tested under drained and undrained conditions. These values can be used as an approximation in case laboratory tests were not available on the actual backfill soils. **Figure 2-6** compares a typical deviator stress-axial strain curve from a triaxial test with the hyperbolic stress-strain relationship adopted in the Duncan-Chang model. Details on the formulation of the Duncan-Chang model can be found in Duncan and Chang (1970), Duncan et al. (1980), Boscardin et al. (1990), and Oswald and Furlong (1993).

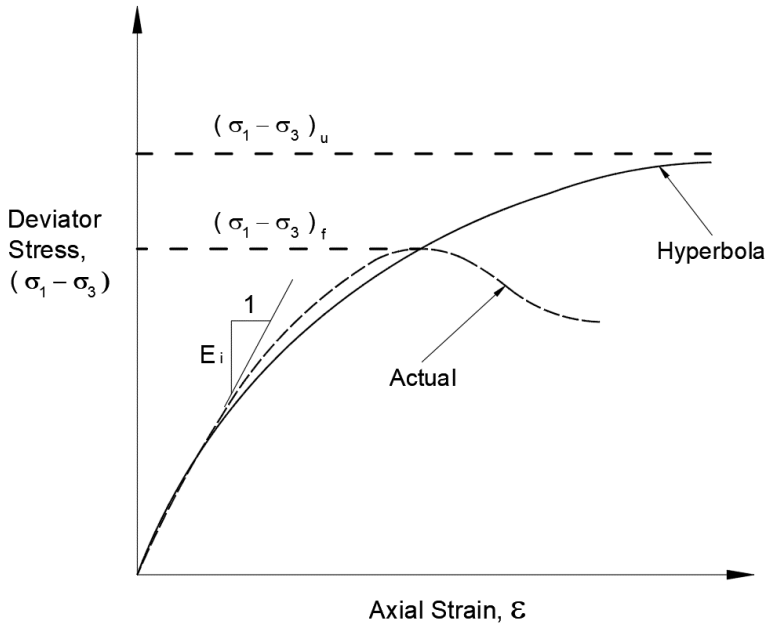

Figure 2-6. Comparison of actual stress-strain curve with hyperbola. (After Oswald and Furlong, 1993)

2.4.2.3 Reinforced Concrete Material Model

Reinforced concrete culverts can be represented in 2D FE models using 1D elements (e.g., beam-column elements) or using 2D elements (e.g., plane-strain and plane-stress elements). The use of 2D elements enables accurate representation of any culvert geometry and visualization of crack pattern when an appropriate material model is utilized.

RC culverts were modeled assuming linear elastic behavior employing 2D elements (e.g., McGrath et al., 2002; Kim and Yoo, 2005; Chen and Sun, 2014). An equivalent Young's modulus (E) and Poisson's ratio (ν) are used to represent the behavior of RC while

neglecting the simulation of the steel reinforcement. The assumption of linear elastic behavior of concrete is justified at service loading conditions prior to crack formation. On the other hand, the nonlinear behavior of RC should be considered for loading conditions beyond the service loading conditions. Pimentel et al. (2009) reported that it is necessary to account for the nonlinear behavior of the RC culvert for realistic simulation of the interaction mechanism. Moreover, Oswald (1996) observed significant postconstruction increase in the culvert deflection (up to 50%) and culvert strains (up to 200%). Accordingly, Oswald (1996) suggested that the simulation of concrete creep and shrinkage behaviors should be considered when modeling long-term performance of RC buried structures.

Pimentel et al. (2009) used the smeared crack model to simulate the nonlinear behavior of concrete in the analysis of RC box culvert at failure. The total strain-based smeared crack model is based on the Modified Compression-Field Theory, which assumes that cracks are formed normal to the direction of the principal tensile strain (Vecchio and Collins, 1986). Prior to crack formation, the stresses and strains are evaluated in the principal directions, and the material behaves as isotropic. Once cracks develop, the material behaves orthotropically with material axes aligned relative to the condition of crack initiation, and the stiffness is evaluated in the crack direction (Rots and Blaauwendraad, 1989). Different formulations exist for the smeared crack model, including the fixed crack and rotating crack models. The crack direction is fixed once the crack is formed in the fixed crack model. On the other hand, rotation of the principal axes is considered in the rotating crack model. Thus, a second crack is formed when the principal tensile stress exceeds the tensile strength, regardless of the stress direction. The fixed crack model is considered more accurate and recommended (Pettersen, 2014). More details about the smeared crack model are provided by Witte and Kikstra (2005). All the smeared crack model parameters can be correlated to the average 28-day concrete compressive strength f_c' following the guidelines of fib Model Code 2010 (2013).

The FE software DIANA 10.1 (2016) incorporates the total strain-based smeared crack model in its material library. The idealized uniaxial stress-strain curve under tensile and compressive loads for the model is displayed in **Figure 2-7**. Different hardening-softening

curves are available under compressive loading as shown in **Figure 2-8**. In addition, the tensile behavior of RC can be modeled using different approaches as presented in **Figure 2-9**.

The steel reinforcement should be simulated in case the nonlinear behavior and crack formation of RC are considered. The steel reinforcement behavior can be approximated by the von Mises plasticity model with no hardening behavior as shown in **Figure 2-10** (Pimentel et al., 2009).

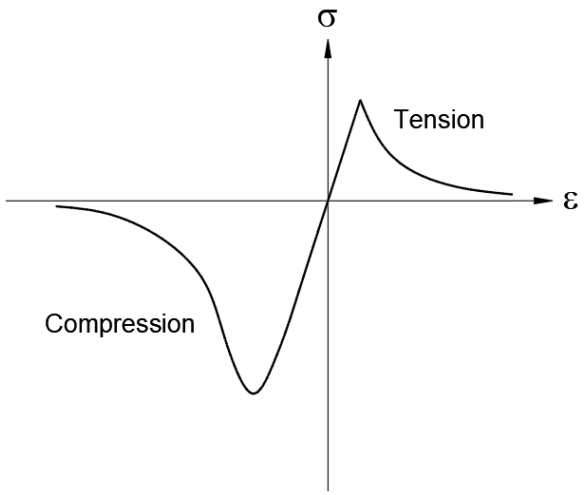

Figure 2-7. Idealized uniaxial compressive and tensile stress-strain curve in the smeared crack model. (TNO DIANA BV, 2016)

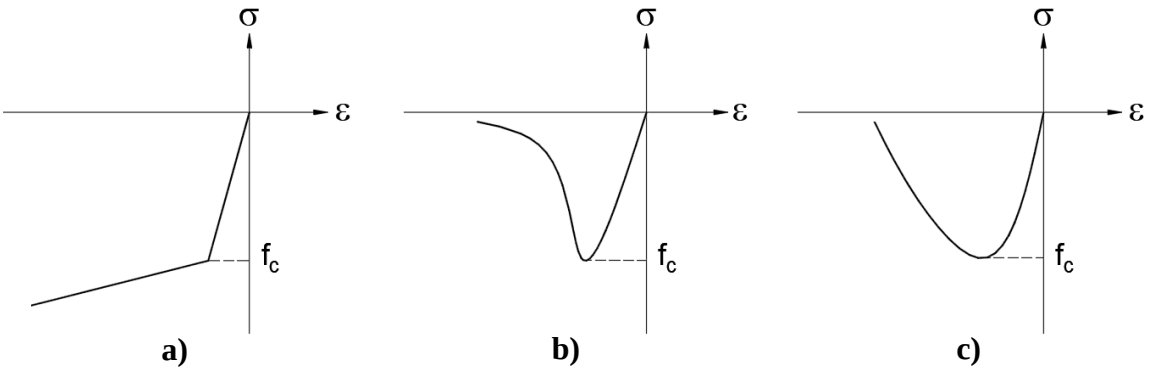

Figure 2-8. Samples of the predefined compression behavior for smeared crack model: a) linear; b) Thorenfeldt; and c) parabolic. (TNO DIANA BV, 2016)

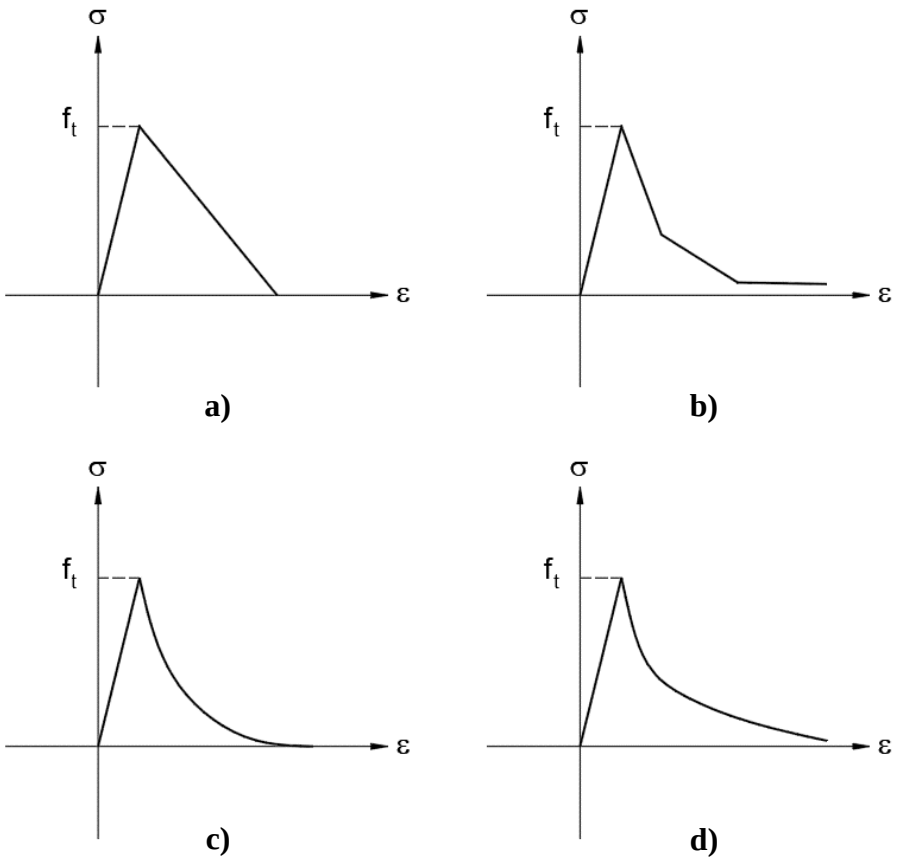

Figure 2-9. Samples of the predefined tension softening for smeared crack model: a) linear; b) multi-linear; c) exponential; and d) Hordijk. (TNO DIANABV, 2016)

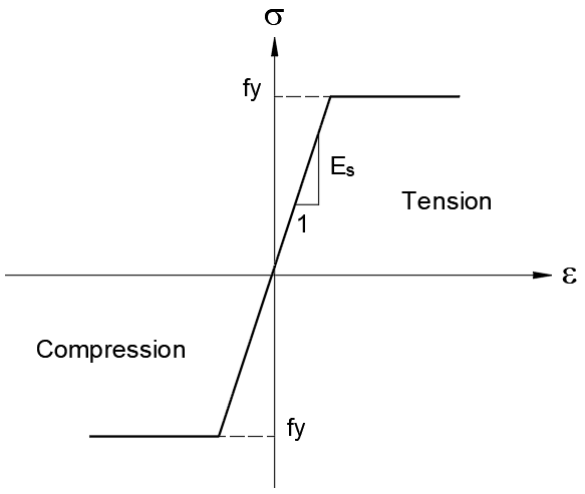

Figure 2-10. Idealized stress-strain curve for the steel reinforcement.

2.4.2.4 Staged Construction

Applying large load increments in FEA of soil-structure systems can lead to substantial errors in the estimation of stresses and strains within the soil mass due to the nonlinear stress-dependent behavior of soils (Yoo et al., 2005). Accordingly, nonlinear incremental analysis procedures should be considered in which the nonlinear soil behavior and incremental construction sequences are simulated. Appropriate simulation of the construction stages is essential for correct representation of the soil stress state, which affects the accuracy of the calculated soil pressures acting on the buried culvert (Pimentel et al., 2009).

2.4.2.5 Compaction Loads

Seed et al. (1991) investigated the compaction-induced stresses and proposed an analytical method to simulate the incremental placement and compaction of backfill, which is based on a hysteretic model for residual soil stresses induced by multiple cycles of loading and unloading. The method was calibrated and validated by comparing the results with full-scale field studies. They also developed FE models that considered the compaction effects, which demonstrated good agreement with the observed field measurements. They reported that neglecting the compaction-induced stresses resulted in underestimating the wall deflections, lateral earth pressures acting against the wall, the culvert deflections, and bending moments. However, they concluded that the magnitude of compaction-induced stresses is governed by the compaction equipment footprint geometry and weight as well as its closest proximity to the culvert body. For instance, a stiff metal culvert experienced twice the deflection of a more flexible metal culvert during backfill placement due to the difference in field compaction procedure, where large equipment operated in close proximity to the stiff culvert.

Elshimi and Moore (2013) investigated the behavior of five pipe products (two concrete pipes, two corrugated steel pipes, and one high-density polyethylene (HDPE) pipe), all had an inner diameter of 2.0 m. Elshimi and Moore (2013) studied the effect of compaction forces on the behavior of the different concrete pipes through a comprehensive FEA. Based on the measured values reported by McGrath et al. (1999) and the results of their numerical

models, Elshimi and Moore (2013) concluded that the effect of compaction-induced stresses can be ignored when vibratory plate compactor is used.

2.4.2.6 Interface

Relative movement occurs along the contact surface between the culvert and surrounding soil when the induced shear stresses tangent to the interface exceeds the interface frictional resistance. Accordingly, interface elements were developed to simulate the slippage that occurs between buried culverts and the surrounding soil. Two different modeling techniques of the interface can be found in the literature: the spring element model and the shear element model as displayed in **Figure 2-11** (Kim and Yoo, 2005).

Goodman et al. (1968) developed the spring interface element, shown in **Figure 2-11a**, to simulate the relative movement between rock joints. The element consists of two lines, each having two nodes with two translational degrees of freedom at each node. This enables the simulation of the tangential slippage across the interface and gap between the soil and culvert. One of the drawbacks of spring interface elements is the need to assign very high normal stiffness to prevent penetration of the two contacting bodies under compressive loads. High normal stiffness leads to errors in the calculated interface normal forces (Leonards and Wu, 1981).

The shear interface element is developed based on constraint equations introduced by Chan and Tuba (1971) to represent the interface behavior. Katona et al. (1976) developed a general theory for applying the constraint equations in the formulation of interface elements. The shear interface element (**Figure 2-11b**) is defined by a set of paired nodes, each having two translational degrees of freedom. One node belongs to the buried structure, and the other belongs to the surrounding soil in contact. A third node is included between the paired nodes to provide equation numbers for the normal and tangential interface forces, resulting in an element stiffness matrix in the order of 6×6. The concept of interface behavior by constraint equations is employed in many FE programs, e.g., CANDE. ABAQUS, DIANA 10.1, and PLAXIS 2D.

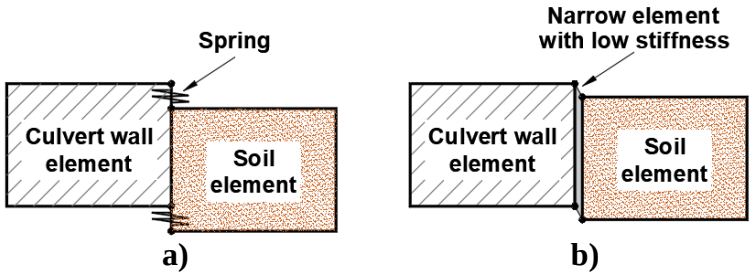

Figure 2-11. Interface models between soil and culvert elements: a) spring element model; and b) shear element model. (After Kim and Yoo, 2005)

There are some discrepancies in the literature regarding the importance of considering the interface between the soil and culvert when simulating soil-structure interaction systems. Kim and Yoo (2005) concluded that the effect of possible slippage between the sidefill material and the culvert sidewall on the calculated vertical earth pressures on the top slab of RC box culverts was insignificant. Thus, they neglected the interface simulation in their analysis. Kang et al. (2008) investigated the effect of soil-structure interface on the calculated earth pressures on box culverts. They reported that the soil-culvert interface did not influence the estimated earth pressures and can be neglected in the case of embankment installation. On the other hand, it significantly influenced the estimated earth pressures in the case of induced trench installation. Thus, the soil-culvert interface should be considered when simulating the induced trench installation method (Kang et al., 2008). Such contradictions need further investigation.

Moreover, the sidewall-footing interface was not previously considered in any of the previous numerical studies on bottomless culverts, e.g., Oswald (1996) and McGrath et al. (2002). This highlights the need to consider the sidewall-footing interface and to investigate its influence, which might elaborate the actual sidewall-footing connection behavior, considering the common construction practice.

2.5 Summary and Gaps in Knowledge

Soil arching occurs due to the relative stiffness of the structure to the surrounding soil medium, resulting in increasing or decreasing the earth pressures acting on buried structures. Many studies investigated the factors affecting the soil arching mechanism and the applied earth pressures through full-scale field tests, centrifuge tests, and numerical

investigations (Tadros et al. 1989; Yang, 2000; Kim and Yoo, 2002; Bennett et al., 2005; Kim and Yoo, 2005; Yoo et al., 2005; Kang et al., 2008; Pimentel et al., 2009; Chen and Sun, 2014; Abuhajar et al., 2015). On the other hand, studies on large-span bottomless culverts are relatively scarce and limited to either arch culverts (Oswald, 1996; McGrath et al., 2002) or arched TSCs (Beach, 1988; McGrath et al., 1996; Zoghi and Farhey, 2006; Marshall et al., 2014). Some contradictions were found in the literature regarding the effect of some parameters on the applied earth pressures on box culverts, i.e., the effect of culvert span, backfill height, foundation soil condition, and compaction level of the sidefill material. Many gaps in the knowledge about the performance of large-span TSCs with flat top slab can be interpreted from the presented literature review. These gaps in the knowledge were the basis of the main objectives of this study and are listed as follows:

1. Full-scale field studies monitoring the structural performance and acting earth pressures on RC TSCs do not exist.

2. The structural performance of TSCs with flat top slab under service and ultimate soil loading conditions was not investigated.

3. The effect of some governing factors on the applied earth pressures on TSCs with flat top slab was not investigated, e.g., culvert dimensions, foundation soil condition, strip footing geometry, installation method, backfill height, backfill soil type, and compaction level of the backfill material surrounding the TSC.

4. Many studies did not account for the nonlinear behavior of RC culverts in their FEAs (e.g., McGrath et al., 2002; Kim and Yoo, 2005; Chen and Sun, 2014). Accordingly, more studies are required to evaluate the influence of considering such behavior on the structural performance of large-span TSCs under service and ultimate loading conditions.

5. The current design practice is to design TSCs assuming hinged connection at the sidewall base. However, no efforts were directed to evaluate the actual connection behavior considering the common construction practice and how it might affect the deformation and induced straining actions (bending moment and shear forces) in

the culvert sidewall as well as the contact pressure distribution underneath the footing.

6. The applicability of the design guidelines stipulated in the codes and standards, e.g., CHBDC (CSA, 2014) and AASHTO (AASHTO LRFD, 2014), has not been validated for the design of large-span TSCs.

2.6 References

1. AASHTO (American Association of State Highway and Transportation Officials). (2014). *AASHTO LRFD bridge design specifications*. 7th ed. AASHTO, Washington, DC.

2. AASHTO (American Association of State Highway and Transportation Officials). (1996). *Standard Specifications for Highway Bridges*. 16th Edition, AASHTO, Washington, DC.

3. Abuhajar, O., El Naggar, H., and Newson, T. (2015). Static soil culvert interaction the effect of box culvert geometric configuration and soil properties. *Computers and Geotechnics Journal*, 69, 219-235. 10.1016/j.compgeo.2015.05.005

4. ASTM (American Society for Testing and Materials). (1996). *Standard Specification for Precast Concrete Box Sections for Culverts. Storm Drains and Sewers with less than 2 ft (0.6 m) of Cover Subjected to Highway Loadings*. Standard C 850-95, 1996 Annual Book of Standards, Vol. 04.05, Philadelphia.

5. Beach, T. J. (1988). *Load test report and evaluation of a precast concrete arch culvert*. Transportation Research Record 1191, Transportation Research Board, Washington, DC, 12–21.

6. Bennett, R. M., Wood, S.M., Drumm, E. C., and Rainwater, N.R. (2005). Vertical loads on concrete box culverts under high embankments. *Journal of Bridge Engineering*, 10 (6), 643-649. 10.1061/(ASCE)1084-0702(2005)10:6(643).

7. Boscardin, M. D., Selig, E. T., Lin, R. S., and Yang, G. R. (1990). Hyperbolic parameters for compacted soils. *Journal of Geotechnical Engineering*, 116 (1), 88-104.

8. Brachman, R. W. I., Moore, I. D., and Rowe, R. K. (1996). Interpretation of buried pipe test: small diameter pipe in Ohio University Facility. *Transportation Research Record 1541*, 64-70.

9. Byrne, P. M., and Duncan. (1979). Nlssip: A computer program for nonlinear analysis of soil-structure interaction problems. *Soil Mechanics*, Series No. 41, University of British Columbia, BC.

10. Carter, J. P., (1992). Program AFENA: A general finite element algorithm, User Manual, Sydney, NS 2006, Australia, Centre for Geotechnical Research, The University of Sydney.

11. Chan, S. H., and Tuba, I. S. (1971). A finite element method for contact problems of solid bodies. *International Journal of Mechanical Science*, 13 (7), 615-639.

12. Chang, C. S., Espinoza, J. M., and Selig, E. T. (1980). Computer analysis of Newtown Creek culvert. *Journal of Geotechnical Engineering*, 106 (GT5), 531-556.

13. Chen, B., and Sun, L. (2014). Performance of a reinforced concrete box culvert installed in trapezoidal trenches. *Journal of Bridge Engineering*, 19 (1), 120–130. https://doi.org/10.1061/(ASCE)BE.1943-5592.0000494.

14. Clarke, N. W. B. (1967). The loads imposed on conduits laid under embankments or valley fills. *In Proc., of the Institution of Civil Engineers*, 36, 63–98.

15. CSA (Canadian Standards Association). 2014. *Canadian highway bridge design code*. CAN/CSA-S6-14. Mississauga, ON, Canada: CSA.

16. Duncan, J. M., Byrne, P., Wong, K. S., and Mabry, P. (1980). *Strength, stress-strain and bulk modulus parameters for finite element analysis of stresses and movements in soil masses*. Report No. UCB/GT/80-01, University of California at Berkeley.

17. Duncan, J. M., and Chang. C. Y. (1970). Nonlinear analysis of stress and strain in soils. *Journal of Soil Mechanics and Foundations Division*, 96 (5),1629–1653.

18. Elshimi, T. M., and Moore, I. D. (2013). Modeling the effects of backfilling and soil compaction beside shallow buried pipes. *Journal of Pipeline Systems Engineering and Practice*, 4 (4), 04013004.

19. Evans, C. H. (1984). An examination of arching in granular soils. M.Sc. Thesis, MIT.

20. Frederick, G. R., and Tarhini, K. M. (2000). *Structural evaluation of three-sided concrete culverts. Concrete piper for the new millenium*. ASTM STP 1368, I.I Kaspar and J. I. Enyart, Eds., American Society of Testing and Materials, West Conshohocken, PA.

21. Goodman, R. E., Taylor, R. L., and Brekke, T. (1968). A model for the mechanics of jointed rock. *Journal of the Soil Mechanics and Foundations Division*, 94 (SM3), 473-496.

22. Heger, F. J., Liepins, A. A., and Selig, E. T. (1985). SPIDA: An analysis and design system for buried concrete pipe. *In Proc., Advances in Underground Pipeline Engineering*, ASCE, 143-154.

23. International Federation for Structural Concrete. (2013). *Fib model code for concrete structures 2010*. Berlin: Verlag Ernst & Sohn.

24. Kang, J., Parker, F., Kang, Y. J., and Yoo, C. H. (2008). Effects of frictional forces acting on sidewalls of buried box culverts. *International Journal for Numerical and Analytical Methods in Geomechanics*, 32 (3), 289-306.

25. Katona, M. G. (2017). Influence of soil models on structural performance of buried culverts. *International Journal of Geomechanics*, 17 (1), 04016031.

26. Katona, M. G., Smith, J. M., Odello, R. S., and Allgood, J. R. (1976). *CANDE: A modern approach for the structural design & analysis of buried culverts*. Rep. FHWA-RD-77-5, FHWA, U.S. Department of Transportation, Washington, D.C.

27. Katona, M. G., and Vittes, P. D. (1982). "Soil-Structure Analysis and Evaluation of Buried Box-Culvert Designs," Transportation Research Record 878, Washington, DC, TRB, National Research Council, pp. 1-7.

28. Kim, K., and Yoo, C. H. (2005). Design loading for deeply buried box culverts. *Journal of Geotechnical and Geoenvironmental Engineering*, 131 (1), 20–27.

29. Kim, K., and Yoo, C. H. (2002). *Design loading for deeply buried box culverts*. IR-02-03, Highway Research Center, Auburn Uni., Auburn, AL.

30. Krizek, R. J. and McQuade, P. V. (1978). Behavior of buried concrete pipe. *Journal of the Geotechnical Engineering Division*, ASCE, 99 (GT7), 815-836.

31. Leonards, G. A., and Wu, T. H. (1981). *Predicting performance of Buried Conduits*. Report No. 6-36-62F, Final Report to Indiana State Highway Commission and FHWA, Engineering Experiment Station, Purdue University, W. Lafayette, Indiana.

32. Leonards, G. A., Wu, T. H., and Juang, C. H. (1982). *Predicting Performance of Buried Conduits*. Report No. FHWAlINIJHRP-8113, West Lafayette, IN, School of Civil Engineering, Purdue University.

33. Ma, Q., Ku, Z., Xiao, H., and Hu, B. (2019). Calculation of earth pressure on culvert underlying flexible subgrade. *Results in Physics Journal*, 12, 535-542. https://doi.org/10.1016/j.rinp.2018.11.100

34. Marshall, J. D., Anderson, J. B., Meadows, R. L., and Jensen, T. J. (2014). Full-scale testing of three-sided precast concrete arch sections. *Journal of Bridge Engineering*, 19 (12), 04014051. 10.1061/(ASCE)BE.1943-5592.0000630.

35. Marston, A. (1930). *The theory of external loads on closed conduits in the light of the latest experiments*. Bulletin 96, Iowa Engineering Experiment Station.

36. Marston, A., and Anderson, A. O. (1913). *The theory of loads on pipes in ditches and tests of cement and clay drain tile and sewer pipes*. Bulletin 31, Iowa Engineering Experiment Station, Ames, Iowa.

37. Marston, A., Schlick, W. J., and Clemmer, H. F. (1917). *The Supporting strength of sewer pipe in ditches and methods of testing sewer pipe in laboratories to determine their ordinary supporting strength*. Bulletin 47, Iowa State College.

38. McGrath, T. J., Moore, I. D., Selig, E. T., Webb, M. C., and Taleb, B. (2002). *Recommend specifications for large-span culverts.* Report No. 473. Washington, DC: Transportation Research Board.

39. McGrath, T. J., Selig, E. T., and Beach, T. J. (1996). Structural behavior of three-sided arch span bridge. *Transportation Research Record 1541*, Transportation Research Record, Washington, DC, 112–119.

40. McGrath, T. J., Selig, E. T., Webb, M. C., and Zoladz, G. V. (1999). *Pipe interaction with the backfill envelope*. FHWA-RD-98-191.

41. McVay, M. C. (1982). Evaluation of Numerical Modeling of Buried Conduits. Ph.D. Dissertation, Dept of Civil Engineering, University of Massachusetts, Amherst, Massachusetts.

42. Oswald, C. J. (1996). Analysis of reinforced concrete culvert considering concrete creep and shrinkage. *Transportation Research Record 1541*, TRB. National Research Council. Washington, DC, 120–126.

43. Oswald, C., and Furlong, R. W. (1993). *Observed behavior of a concrete arch culvert*. Center for Transportation Research Burau of Engineering Research, the University of Texas at Austin. Research Report Number 932-1F.

44. Pettersen, J. S. (2014). *Non-linear finite element analyses of reinforced concrete with large scale elements: including a case study of a structural wall*. Norwegian University of Science and Technology 85 p.

45. Pimentel, M., Costa, P., Félix, C., and Figueiras, J. (2009). Behavior of reinforced concrete box culverts under high embankments. *Journal of Structural Engineering*, 135 (4), 366-375. 10.1061/(ASCE)0733-9445(2009)135:4(366), 366–375

46. Rots, J. G., Blaauwendraad, J. (1989). Crack models for concrete: discrete or smeared? Fixed, multi-directional or rotating? *Heron*, 34 (1), 5–55.

47. Seed, R. B., Duncan, J. M., and Ou, C. Y. (1991). Finite element analysis of compaction problems. *Advanced Geotechnical Analysis-Development in Soil Mechanics and Foundation Engineering-4, Ed*. Banerjee, P. K. and Butterfield, R. Elsevier Applied Science.

48. Selig, E. T. (1964). Subsurface soil-structure interaction: a synopsis. *In Proc., Symp. on Soil Structure Interaction*, Uni. of Arizona.

49. Spangler, M.G. (1950). A theory on loads on negative projecting conduits. *In Proc., Highway Research Board*, 30, 153-161.

50. Tadros, M. K., Benak, J. V., Abdel-Karim, A. M., and Bexten, K. A. (1989). *Field testing of a concrete box culvert*. Report No. 1231. Washington, DC: Transportation Research Board.

51. Tarhini, K.M., Frederick, G. R., Mabsout, M. E., and Faraj, C. (1997). Experimental and analytical evaluation of three-sided concrete box culverts. *Post Conference Proceedings of the 1997 SEM Spring Conference on Experimental Mechanics, Bellevue*, WA, 209-213.

52. TNO Diana BV. 2016. *DIANA—User's manual: Material library*. Delft, Netherlands: TNO Diana BV.

53. Vaslestad, J. (1990). Soil structure interaction of buried culverts. Ph.D. Dissertation, Department of Civil Engineering, Norwegian Institute of Technology.

54. Vaslestad, J., Johansen, T. H., and Holm, W. (1993). *Load reduction on rigid culverts beneath high fills: long-term behavior*. Report No. 1415. Washington, DC: Transportation Research Board.

55. Vecchio, F. J., and Collins, M. P. (1986). The modified compression-field theory for reinforced concrete elements subjected to shear. *ACI Journal*, 22, 219–231.

56. Webb, M. C., Selig, E. T., and McGrath, T. J. (1999). Instrumentation for monitoring large-span culverts. Field Instrumentation for Soil and Rock, Durham G. and Marr W., American Society for Testing and Materials, 66-86. 10.1520/STP14214S

57. Witte, F. C., and Kikstra, W. P. (2005). DIANA user's manual, Material Library, TNO DIANA, BV, Delft, The Netherlands.

58. Yang, M. Z. (2000). Evaluation of factors affecting earth pressures on buried box culverts. PhD dissertation, Uni. of Tennessee, Knoxville, TN.

59. Yoo, C. H., Parker, F., and Kang, J. (2005). *Bedding and fill heights for concrete roadway pipe and box culverts*. Final Report, ALDOT Project No. 930-592, Highway Research Center, Auburn Uni., AL.

60. Zoghi, M., and Farhey, D. N. (2006). Performance assessment of a precast concrete, buried, small arch bridge. *Journal of Performance of Constructed Facilities*, 20 (3), 244–252. 10.1061/(ASCE)0887 3828(2006)20:3(244).

Chapter 3

* Preliminary Analysis and Instrumentation of Large-Span Three-Sided RC Culverts

3.1 Introduction

Culverts are a vital part of the urban infrastructure for all societies, especially as a watercourse crossing on which roadways are constructed. Culverts are classified based on their material, construction method, shape, and geometry. Reinforced concrete (RC) culverts are widely used because of their durability and approved strength. They are constructed as either cast-in-place or precast, with the latter becoming more common due to the improved quality control in their production, economical construction cost, and reduced construction time and road closure duration. Recently, bottomless culverts, also known as three-sided culverts (TSCs), are increasingly used as an economical alternative for short-span bridge replacement (Marshall et al., 2014; Webb et al., 1999). They are more attractive from the environmental point of view compared to culverts with closed-bottom geometry, as they allow water to flow in its natural course with minimal influence on the marine environment. Bottomless culverts are produced in different shapes, including: arch, three-sided with arched top slab, and three-sided with flat top slab. TSCs with flat top slab, which are the focus of this study, are produced in large spans reaching 16.0 m.

TSCs with relatively large spans and without the bottom slab that restrains lateral leg movement under the applied loads may experience different earth and live load pressure distributions. In addition, they may experience deformations due to the differential settlement of their footings, which would further complicate their soil-structure interaction behavior. Thus, their performance could be substantially different than the small-span rigid box culverts. However, the current design practice specified in the Canadian Highway Bridge Design Code, CHBDC (CSA, 2014), does not distinguish between small-span box and large-span bottomless culverts. This can result in an overly conservative prediction of

---

* A version of this chapter is under review in Journal of Bridge Engineering.

vertical earth pressures on the top slab and an unnecessary increase in the cost. Many field studies have been carried out on RC box culverts (Chen and Sun, 2014; Bennett et al., 2005; Yang, 2000; Vaslestad et al., 1993). On the other hand, studies on bottomless culverts are relatively scarce and limited to either arch culverts (McGrath et al., 2002) or TSCs with arched top slab (Marshall et al., 2014; Zoghi and Farhey, 2006; McGrath et al., 1996; Beach, 1988).

This research effort involved the first-ever field monitoring study addressing bottomless RC culverts with flat top slab, referred to herein as TSCs. It attempts to evaluate the structural behavior and performance related to the interaction of precast RC TSCs with the surrounding soil mass and investigate the boundary conditions at the bottom of the sidewalls. A particular emphasis is placed on evaluating the applied earth pressures on these structures to enhance their design criteria. In order to achieve these objectives, a field-monitoring program is carried out. This chapter is part of a comprehensive study involving field monitoring and numerical analysis of TSCs with different spans, foundation types, and ground conditions. Advanced finite element modeling supported by field measurements has proven to be a robust approach for facilitating the management of large infrastructures and prediction of their performance in the long term (Sousa, 2020). The current chapter presents the field instrumentation program of three functional precast RC TSCs in the Greater Toronto Area (GTA), Ontario, Canada. Continuous monitoring of these structures is undertaken during the construction activities, and long-term monitoring will extend up to 3 years from construction completion. Moreover, all field measurements of a 7.3-m-span TSC up to the final backfill height are presented.

3.2 Projects Description

This study involves the instrumentation and field monitoring of three TSCs with spans of 7.3 m, 10.4 m, and 13.5 m, which are designated as Remembrance, Pickering, and Oshawa culverts, respectively. The monitored culverts cover intermediate to large spans. Each culvert has a unique geometry and installation method, as detailed in the following subsections.

3.2.1 Remembrance Culvert

The Remembrance culvert is part of the infrastructure of a new subdivision extension. The culvert is constructed to convey the creek water through the road embankment. It is assembled using 11 precast units, each is 2.44 m-wide and weighing approximately 278 kN, with a total length of 26.9 m. The culvert span is 7.3 m, and its rise is 2.4 m with sidewalls and slab thicknesses of 0.36 m. The final backfill cover from the culvert's top slab to the final road grade is 3.2 m.

Subsurface boreholes data at the site indicate that the native soil consists mainly of silty clay to clayey silt till with occasional boulder and cobble sizes. The measured SPT N-value at the foundation level (FL) was 26 and increased to 55 at 3.5 m below that level. The measured SPT N-values reflect stiff to hard consistency of the foundation soil. The Remembrance culvert is founded on a 0.6-m-thick × 3.6 m-wide strip footing with a 0.7 m-thick pedestal. The culvert is constructed in a trench with sloped edges as shown in **Figure 3-1a**.

3.2.2 Pickering Culvert

The Pickering culvert is part of the Enterprise Gateway project in Pickering, Ontario, which includes the construction of a 1,660 m long by-pass, parallel to Highway 407. The culvert is 45.97 m long, constructed utilizing 25 precast concrete units, each is 1.83-m-wide, and weighs 372 kN. The clear opening dimensions of the culvert are 10.36 × 1. 50 m (span × rise), and both sidewalls and slab are 0.46-m-thick. The pavement grade level is almost 3.1 m above the culvert's top slab.

Based on the geotechnical investigation conducted at the culvert location, the soil profile is mainly composed of sandy silt till to the end of the boreholes at 8.0 m below the ground surface. The measured SPT N-value at the FL was 25 and increased to 100 at 4.0 m below the FL, indicating a dense to very dense sandy silt till layers. The culvert foundation is a 3.8-m-wide × 0.9-m-thick strip footing. The natural ground surface is almost at the same elevation as the top slab, reflecting the case of zero projection culvert installation as displayed in **Figure 3-1b**.

3.2.3 Oshawa Culvert

The Oshawa culvert is part of the Courtice Trunk Sanitary Sewer Extension in the city of the Oshawa, Ontario. It is the largest RC culvert with flat top slab to be instrumented with a clear span of 13.5 m and a shallow rise of 1.29 m. This culvert will be covered by 3.8 m of backfill upon completion of the embankment construction. The culvert is 49.4-m-long and is assembled from 1.3-m-wide precast segments, each weighing around 390 kN. The thicknesses of the sidewall and top slab are 0.66 m and 0.61 m, respectively.

According to the boreholes drilled in the vicinity of the culvert, the soil profile is composed of silty sand and sandy silt tills from the ground surface, extending to a depth of 8.0 m. The SPT N-value at the FL located 2.7 m from the ground surface was 63 and reached refusal just below that level. These SPT N-values indicate that the soil is very dense at the culvert's FL. The precast units are founded on a 3.8-m-wide keyed strip footing with a 1.9-m-high pedestal such that the FL is 1.44 m below the streambed elevation, which is below the frost depth of 1.2 m (OPSD, 2010). The Oshawa culvert is being constructed following the embankment installation method, with the ground surface being at the crest of the footing pedestal as presented in **Figure 3-1c**. **Table 3-1** provides the main features and relevant information of the three test culverts.

Table 3-1. Comparison between the features of the three instrumented culverts.

Project	Span (m)	Backfill height (m)	Foundation type	Installation configuration	Current project status*
Remembrance	7.3	3.2	Strip footing with pedestal	Trench	Completed
Pickering	10.4	3.1	Strip footing	Zero projection conduit	Completed
Oshawa	13.5	3.8	Strip footing with pedestal	Embankment	H = 3.0 m

* As of November 2020

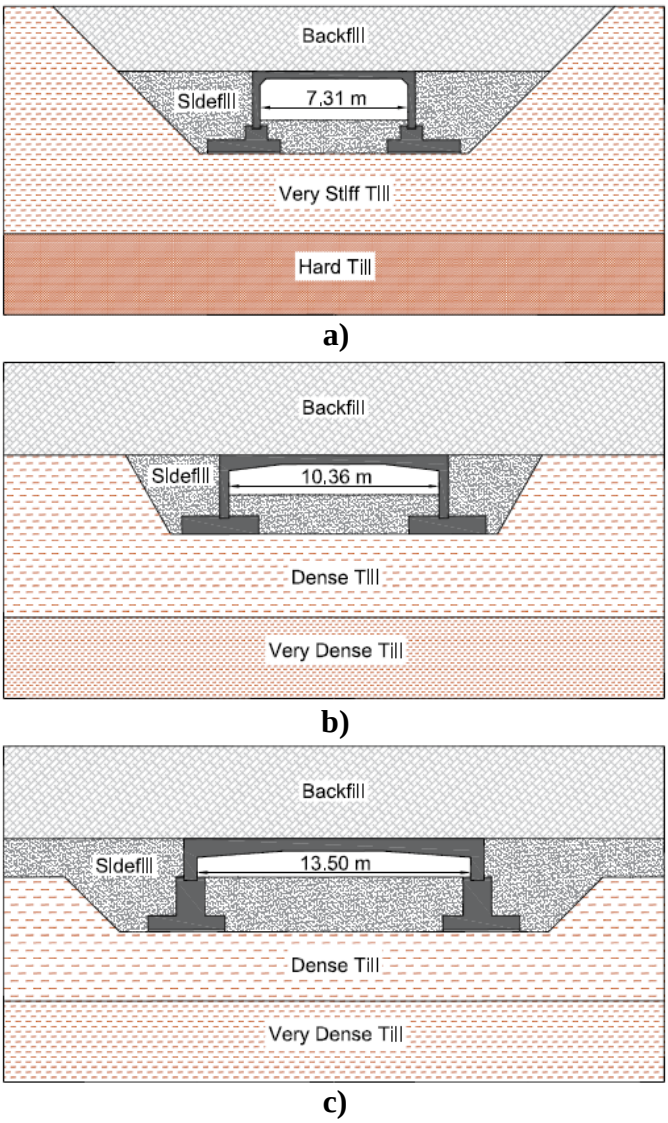

Figure 3-1 Geometry and installation method of the instrumented culverts: a) Remembrance culvert; b) Pickering culvert; and c) Oshawa culvert.

3.3 Preliminary Numerical Simulation

Preliminary three-dimensional (3D) finite element analyses (FEAs) were conducted to evaluate the soil-culvert interaction in order to optimize the instrumentation plan and field tests for the three culverts. The results of the numerical models were utilized to predict the structure response, provide approximate magnitudes of parameters that would be measured during the field tests, and determine the critical locations where the instrumentation should be located for field measurements and data collection.

The preliminary analysis was conducted before instrumenting the TSCs, thus field monitoring data were not available. Therefore, the preliminary analysis was initiated by simulating a large-span RC box culvert and comparing the numerical model results with the field measurements reported in the literature by Chen and Sun (2014). The same modeling approach used in the validated box culvert model was used for the TSC numerical models.

3.3.1 Validated Model

Chen and Sun (2014) instrumented a large cast-in-place RC box culvert, 8-m-span and 6.8-m-rise, installed in a natural trapezoidal trench in a mountainous area and covered by 18.0 m of backfill. Chen and Sun (2014) conducted a two-dimensional (2D) plane-strain analysis to model the instrumented box culvert. The general-purpose finite element (FE) software package ABAQUS v.6.13.3 (Abaqus, 2013) was used to reproduce the 2D plane-strain model in the same geometry of the field test, with 18 m of backfill as shown in **Figure 3-2a**. The RC culvert and fresh rock layer were simulated as linear elastic materials. The backfill, cushion, and weathered mudstone were simulated using the elastic-plastic Mohr-Coulomb (MC) model. The contact interaction between the culvert and surrounding soil was considered using the contact pair algorithm. The concrete surface of contact was defined as the master surface, and the soil surface of contact was the slave surface. The normal and tangential behaviors characterized the interface properties. The normal behavior was defined as “hard” contact to avoid penetration of the contact surfaces with each other. The tangential behavior was simulated using the Coulomb friction model with an assumed friction coefficient of 0.8. The assigned material properties, summarized in **Table 3-2**, were adopted from Chen and Sun (2014). The results of the developed numerical model exhibited excellent agreement with the field measurements reported by Chen and Sun (2014) as presented in **Figure 3-2b**, which demonstrate the ability of the developed modeling approach to simulate the culvert construction process and to reasonably predict the imposed earth pressures on the buried structure body. The results indicate higher earth pressures at the top slab edges than at the mid-span for backfill heights over 2.0 m. Such distribution clarifies the effect of soil arching and buried structure rigidity on the redistribution of earth pressures.

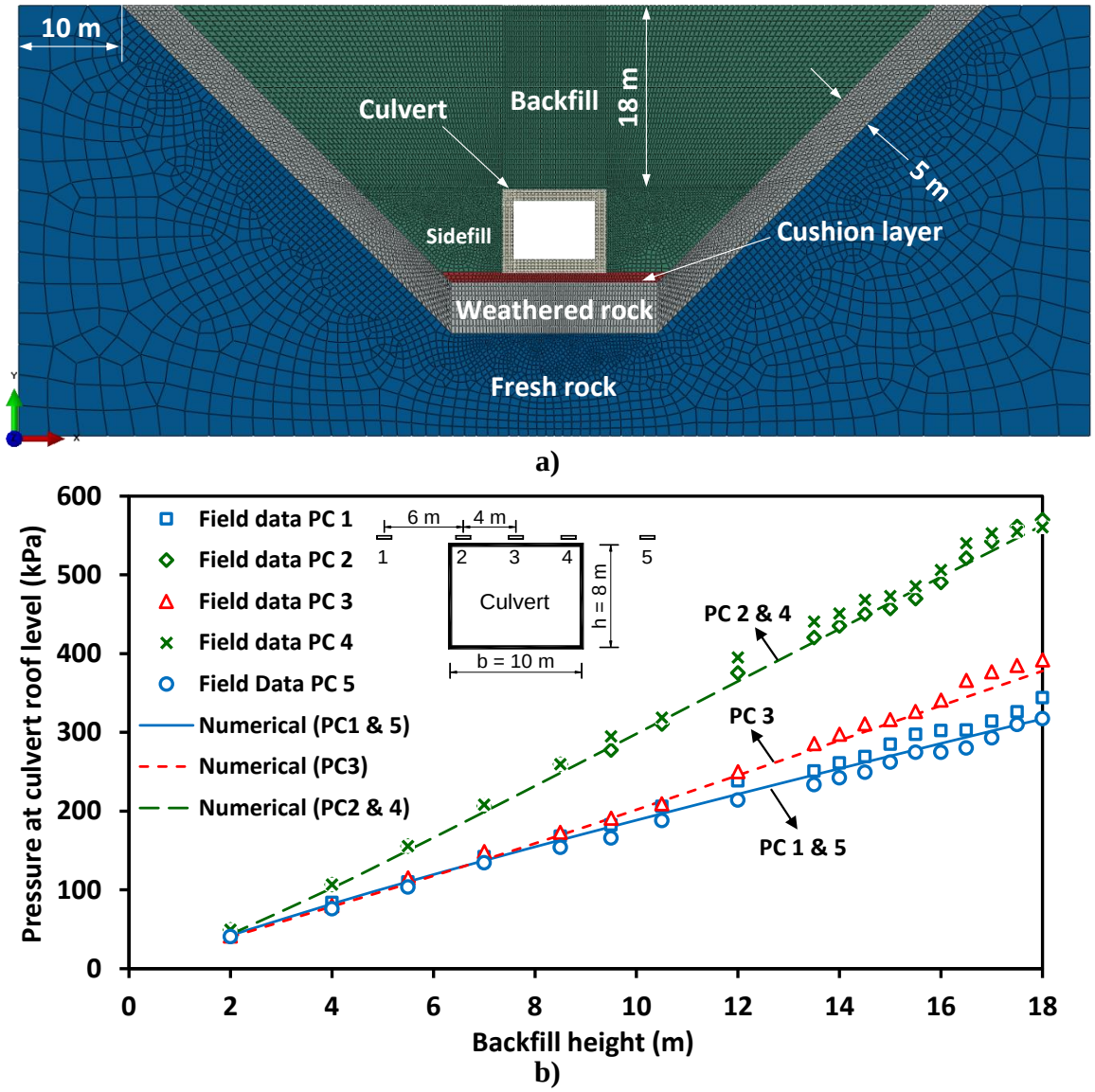

Figure 3-2. Details of the validated model: a) geometry and meshing details of the box culvert model; and b) measured and calculated earth pressures at different backfill heights.

Table 3-2. Input parameters in the box culvert model. (After Chen and Sun, 2014)

Parameter	Culvert	Backfill	Cushion	Weathered rock	Fresh rock
Material model	Elastic	MC	MC	MC	Elastic
Unit weight (kN/m^3)	25.0	21.4	22.5	26.05	27.2
Young's modulus (MPa)	30,000	60	300	15,000	26,000
Poisson's ratio	0.20	0.30	0.25	0.23	0.20
Cohesion (kPa)	-	0	50	600	-
Friction angle (°)	-	30	32	29	-

3.3.2 Preliminary Analysis

The culvert geometry, structural data, in-situ soil conditions, and backfill height were used to develop FE models for the three test culverts. The field-testing program incorporates performing static live load tests at different backfill heights. Therefore, 3D models were developed to account for the 3D feature of the live load transfer mechanism through soil. The same modeling approach and assumptions were employed in the three models. Thus, details of the Oshawa culvert model will be discussed herein.

The 3D model of the Oshawa culvert consisted of two parts: the concrete culvert and the soil block as shown in **Figure 3-3**. The culvert body and soil block were modeled using 3-dimensional 8-noded, first-order (linear), reduced integration, hourglass control elements (C3D8R). A sensitivity analysis was conducted for the model mesh density until no changes in the calculated results were observed with further refinement of the model. The installation method and excavation geometry were unknown at the preliminary analysis stage. Therefore, embankment installation was assumed, and the sidefill and backfill soils were discretized into 0.3-m-thick layers to mimic the incremental construction procedure as depicted in **Figure 3-3b**. The overburden stresses of each layer were activated in a separate stage up to the final backfill height. The contact pair algorithm was used to define the contact interaction between the TSC and the surrounding backfill soil, following the same procedure used in the validated model. **Table 3-3** summarizes the input parameters assigned for the different soil layers and the RC culvert. The Mohr-Coulomb plastic model

was used to simulate the behavior of both the native and backfill soils. The elastic moduli (E) of the dense and very dense till layers were correlated to the measured SPT N-values using the equation proposed by Balachandran et al. (2015), i.e., $E = 1.33 \times N$. Manzari et al. (2014) reported an internal friction angle (ϕ) in the range of 31° to 45° for cohesionless till materials in the Toronto area based on triaxial tests on undisturbed samples. Accordingly, internal friction angles of 35° and 40° were selected for the dense and very dense till layers, respectively. To meet the CHBDC (CSA, 2014) requirements for B1 standard installation, cohesionless soil compacted to 90% relative compaction has been assumed as the backfilling material. The linear elastic model was assigned to the RC culvert part, in which equivalent stiffness (E) and Poisson's ratio (ν) were selected to represent the behavior of RC, which does not consider concrete cracking.

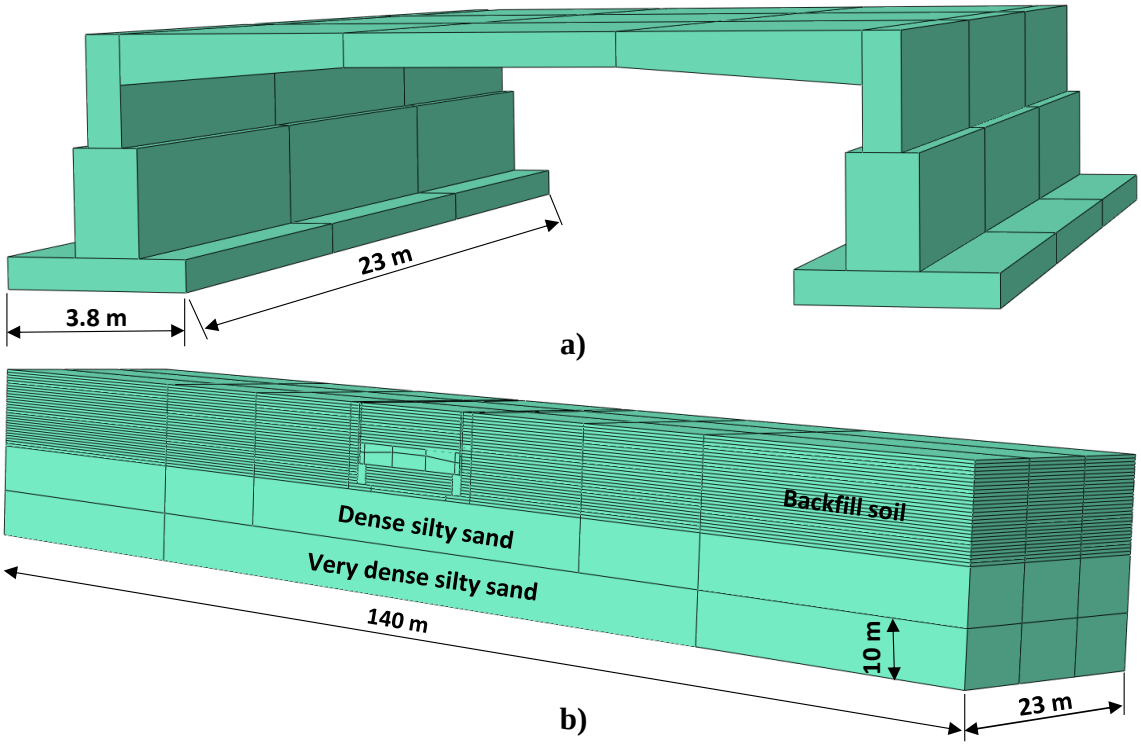

Figure 3-3. Schematic of the Oshawa culvert model parts: a) culvert part; and b) soil block part.

Table 3-3. Summary of the material properties in the Oshawa culvert model.

Part	Material model	Density (kN/m^3)	E (MPa)	ν	Friction angle (°)
Backfill soil	MC	20.0	30	0.25	36
Dense silty sand	MC	20.0	40	0.25	35
V. dense silty sand			160		40
Culvert	Elastic	24.0	3x10^4	0.2	-

3.3.3 Results of the Finite Element Analysis

This section presents preliminary numerical analysis results considered in the design of the instrumentation layout. The presented results include the soil pressure distribution on the top slab, the contact stresses underneath the culvert footing, and the induced internal strains in the culvert body. All the displayed results were calculated considering the final cover depth.

Figure 3-4 displays the normalized soil pressure distribution, denoted as the vertical arching factor (VAF), which is obtained by:

$$\text{VAF} = \frac{\sigma_v}{\gamma_s H} \quad \textbf{(3-1)}$$

where: σ_v is the vertical earth pressure on the top slab; γ_s is the backfill soil unit weight; H is the backfill height over the top slab. The estimated soil pressure distribution along the culvert top slab for the three culverts exhibited similar trends as observed in **Figure 3-4**, with non-uniform earth pressure distribution along the culvert span. The earth pressures are concentrated at the relatively rigid edges as opposed to the more flexible mid-span. The calculated pressures for the Oshawa culvert were higher than both Remembrance and Pickering culverts primarily due to the difference in backfill height (3.8 m versus 3.2 and 3.1 m). However, the calculated normalized VAF curves of the three culverts are very comparable owing to the equivalent mechanical properties assigned for the backfill material in the three models. This soil pressure distribution is consistent with field

measurements and numerical analyses reported in the literature on box culverts (Chen and Sun, 2014; Tadros et al., 1989; Yang et al., 1999) and arch culverts (McGrath et al., 2002). **Figure 3-4** compares the calculated VAF with the values stipulated in the CHBDC (CSA, 2014). The comparison indicates that the CHBDC overestimates the vertical soil pressure by specifying a VAF of 1.2 for the B1 standard installation, which represents the case of compacted sidefill.

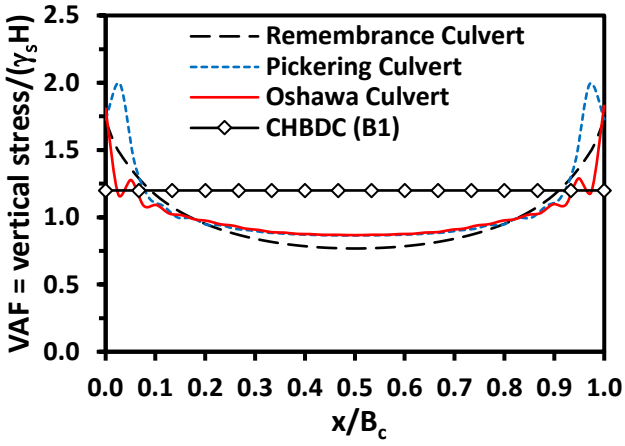

Figure 3-4. Normalized vertical earth pressure distribution along the top slab.

The internal strain contours in the concrete culvert body are presented in **Figure 3-5**. The locations of maximum tensile strains (+ve strain value) are depicted in red, and the locations of maximum compressive strains (-ve strain value) are depicted in blue. The maximum values of the anticipated stresses and strains are presented in **Table 3-4**. It can be observed that the highest pressure and strain magnitudes were calculated for the Oshawa culvert, which has the longest span (13.5 m) and highest backfill height (H = 3.8 m) compared to the other culverts.

Table 3-4. Summary of the maximum stresses and strains from the numerical models.

Numerical models output	Remembrance culvert	Pickering culvert	Oshawa culvert
Max. vertical soil pressure on top slab (kPa)	110.3	129.5	181.2
Max. stress underneath the footing (kPa)	234.6	272.5	443.8
Max. tensile strain (με)	171.0	203.0	272.7
Max. compressive strain (με)	180.0	219.3	302.0

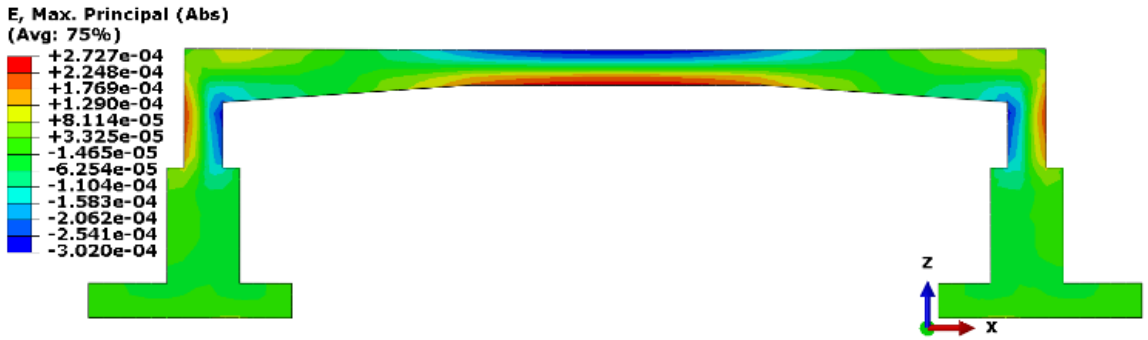

Figure 3-5. Maximum principal strains in the concrete culvert body of the Oshawa culvert.

3.4 Instrumentation Plan

The available literature on case studies of instrumented RC culverts was carefully reviewed to establish best practices. This section presents the selection criteria of the sensors used for instrumenting the investigated culverts. The final instrumentation layouts that were implemented on-site for the three culverts are also presented.

3.4.1 Selection of Instrumentation Sensors

In order to investigate the earth pressures imposed on large-span TSCs and their structural performance during and after construction, the culverts were instrumented with earth pressure cells (PCs) and strain gauges (SGs). PCs are used to measure the interface pressure and the loads imparted onto the structure from the surrounding soil as well as wheel loads during stationary live load tests. The SGs measure the induced strains and reflect the structural behavior of the buried culvert. Thus, the combination of these sensors would guarantee that the structural behavior of TSCs is monitored under quantified loads.

One of the main criteria used for sensors selection was the durability and stability for long-term monitoring purposes. The sensors should be able to withstand the installation, construction, and backfilling operations, besides the repeated traffic loading under normal operating conditions of the culvert. Furthermore, the three projects are located in Southern Ontario, which has a humid continental climate characterized by warm summers and severe winters. Thus, the sensors should be able to withstand the harsh seasonal temperature variations while operating within the manufacturer's specified accuracy.

Vibrating wire (VW) sensors are suitable for long-term static measurements (Perkins and Lapeyre, 1997). The VW transducers, including PCs and SGs, are widely used in different measurement applications (Dunnicliff, 1988). The signal cable length has a minimal effect on the performance of VW sensors because the output signal is in the form of frequency. This was particularly useful in the current study, given that the required length of signal cables reached up to 40 m for some sensors. Piezoresistive transducers were evaluated for possible use; however, it was found that the measurements from these sensors tend to drift with time. Thus, they are not suitable for long-term measurements (Marr, 1999). Moreover, errors in their measurements were observed due to voltage losses in the cable extensions, which affects the sensor's calibration (Marr, 1999). Accordingly, piezoresistive transducers were excluded.

The total contact pressure on buried structures can be measured with high accuracy using PCs (Dunnicliff, 1988). Seed et al. (1991) recommended the use of non-displacement type PCs with their faces flush with the wall face for accurate measurements of earth pressures. However, the subject TSCs are precast RC culverts, and all the precast segments were already cast prior to commencing the instrumentation plan. Thus, the use of embedded sensors was excluded. Model 4810 VW PCs (Geokon, Lebanon, New Hampshire) were selected for measuring the soil-culvert interface pressure. Model 4810 VW PC is 230 mm in diameter, which is large enough to reduce the influence of local non-uniform stresses on the cell surface (Dunnicliff, 1988). Based on the pressure values calculated from the FEAs summarized in **Table 3-4**, PCs with 700 kPa range were installed underneath the footing for both Pickering and Oshawa culverts, and PCs with 350 kPa were used elsewhere. The selected PCs have an over-range capacity of 150% full-scale, which means that the 350 kPa PC can measure up to 525 kPa. This capacity should cover any additional pressure that might be experienced from the construction equipment or during the live load testing, which is part of the field-testing plan. The VW PCs, and specifically model 4810, were successfully used for instrumenting several buried structures (Sama et al., 2015; Marshall et al., 2014; Wood, 2000; Yang, 2000; Yang et al., 1999).

The structural performance of the test TSCs is monitored by means of SGs. The bending moments and induced thrusts can be determined from the measured strains in the

instrumented precast segment. Surface-mounted VW SG model 4000 (Geokon, Lebanon, New Hampshire) was used in the current study. A VW SG consists of a steel wire clamped at each end and is attached to the concrete structure using mounting blocks. With the induced strains in the concrete structure, a relative movement occurs between the mounting blocks changing the tension in the steel wire, which changes its natural frequency. Such change in the natural frequency is directly calibrated to strain measurements (Dunnicliff, 1988). To obtain the average strain of a concrete section and avoid measuring the undesirable strains at the macro level, the length of the used SG should be several times longer than the largest aggregate size in the concrete mix (Wood, 2000). Accordingly, model 4000 SG with a 150 mm active gauge length was selected for the current application. The SG range was chosen based on the calculated maximum strains presented in **Table 3-4**. With a maximum anticipated strain value of 302.0 με, the SG with the lowest strain range (3000 με) was employed for the three culverts. Model 4000 SG has been used successfully in different field-testing applications (Marshall et al., 2014; Perkins and Lapeyre, 1997). Electrical resistance foil strain gauges were evaluated for possible use in this project. However, they were excluded due to their limitations, i.e., low electrical output, lead wire effects, and possible errors due to moisture, temperature, and electrical connections (Dunnicliff, 1988).

All used sensors were calibrated and certified by the manufacturer, which was demonstrated to be accurate (McGrath et al., 1999; Webb et al., 1999; McGrath and Selig, 1996) and can be directly implemented in calibrating the field measurements. The calibration factors of similar VW PCs were found to be within 3% of the calibration factors supplied by the manufacturer (McGrath and Selig, 1996). The operating temperature range, -20 to +80° C, was considered adequate for the expected seasonal temperature variations at the three site locations. Furthermore, each sensor is equipped with a thermistor, which permits recording the temperature while simultaneously measuring strains or pressures and correcting the measurements against temperature variations. **Table 3-5** summarizes the technical specifications of the used sensors.

Table 3-5. Summary of the technical specifications of the used VW sensors.

Sensor	Model	Range	Accuracy	Temperature range	Sampling frequency*
Strain gauge	4000	3000 με	9.7	-20 to +80° C	one reading/2 minute
PC below the footing	4810	700 kPa	7.9		
PC on the structure	4810	350 kPa	5.1		

* Controlled by the number of VW sensors and the data logger speed.

3.4.2 Instrumentation Layout

The three culverts were instrumented to provide sufficient data to better understand the performance of large-span TSCs, and to validate advanced FE models that can be used for further analysis of the soil-culvert interaction considering varying culvert geometries and soil conditions. The layouts of the sensors installed in the three culverts are depicted in **Figure 3-6**. Due to budget limitations, the distribution of sensors was unsymmetrical; however, the final layouts ensure an acceptable level of redundancy for the measurements, especially at the critical locations, to guard against the possibility of instrument failures during the construction process. In each culvert, one segment was instrumented. The instrumented segment was approximately in the middle of the closest lane to the data logger's location. At the selected location, the precast segment will experience the full backfill depth as well as the highest live load (in the middle of the lane) during the future road operation.

As the FEA results predicted non-uniform stress distribution on the top slab, the PCs were distributed along the top slab to quantify the actual soil pressure applied to the top slab. Accordingly, 4, 5, and 7 PCs were distributed along the top slab of the Remembrance, Pickering, and Oshawa culverts, respectively. In addition, 3 PCs were placed underneath each strip footing of the Pickering and Oshawa culverts to measure the total stresses transferred to the bedding soil and their distribution. Installing PCs underneath the strip footing of the Remembrance culvert was not possible as the strip footings were already constructed. Six PCs were distributed along the span of the Remembrance culvert, while 11 and 13 PCs were used for the Pickering and Oshawa culverts, respectively.

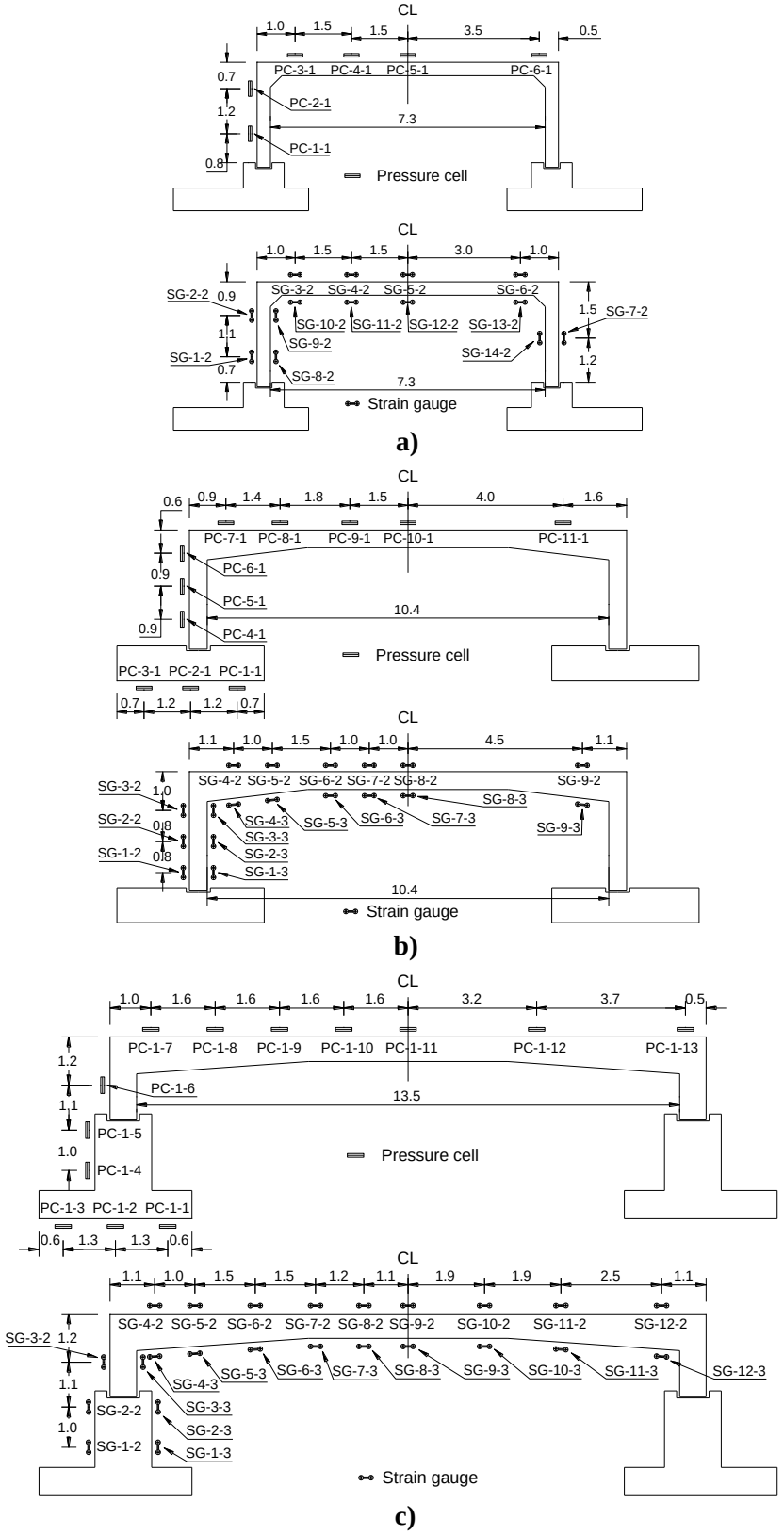

Figure 3-6. Culverts' instrumentation layout: a) Remembrance culvert; b) Pickering culvert; and c) Oshawa culvert. (All dimensions are in m)

At each assigned location, SGs were installed in pairs on the inner and outer surfaces of the culvert. The gauges were oriented along the profile of the culvert to register both tensile and compressive strains. This arrangement enables the determination of the axial force and bending moment across the structure. The total number of SGs installed in each project are: 14 for the Remembrance culvert, 18 for the Pickering culvert, and 24 for the Oshawa culvert.

Each sensor was uniquely identified by labeling its signal cable. The labeling scheme incorporated, in the following order: sensor type, channel, and multiplexer numbers. For example, PC 3-1 indicates the PC installed in the third channel of the first multiplexer.

3.5 Instrument Installation

The installation work commenced with Remembrance culvert, followed by Pickering culvert and finally Oshawa culvert. All the sensors were installed according to the manufacturer's recommendations while applying some modifications when necessary. A detailed description of the installation procedures is reported herein.

3.5.1 Pressure Cells Underneath the Footing

Three VW PCs were installed underneath one cast-in-place strip footing of the Pickering and Oshawa culverts. To accommodate the PCs installation, a 0.6 m strip of the mud slab was not cast at their specified locations as shown in **Figure 3-7**. At the marked locations of the PCs, an approximately 0.4-m-wide hole was excavated to a depth of 50 mm, which was then filled with compacted sand as shown in **Figure 3-7b**. The PC was then placed on the sand and leveled to ensure its horizontal alignment. The PC was fixed into the ground using four 100 mm long nails through the 4 PCs mounting lugs of the PC plate. The signal cable was then fed into a 12.7 mm (0.5″) flexible polyethylene pipe for protection, which was tied to the steel bars and routed through the footing. Finally, Initial readings were recorded using the VW readout unit, model GK-404 (Geokon, Lebanon, New Hampshire). The PCs were covered with fast-setting mortar, as displayed in **Figure 3-7c**, to protect them during the casting of footing concrete.

Leveling the PC and ensuring its horizontal alignment is essential for accurate measurements of the contact pressure underneath the footing. The PC reads the total stress perpendicular to its surface. Thus, vertical contact pressure would not be recorded in case the PC was inclined. Moreover, the sand underneath the PC should be well compacted to avoid the change in orientation of the PC with the increase of the applied loads.

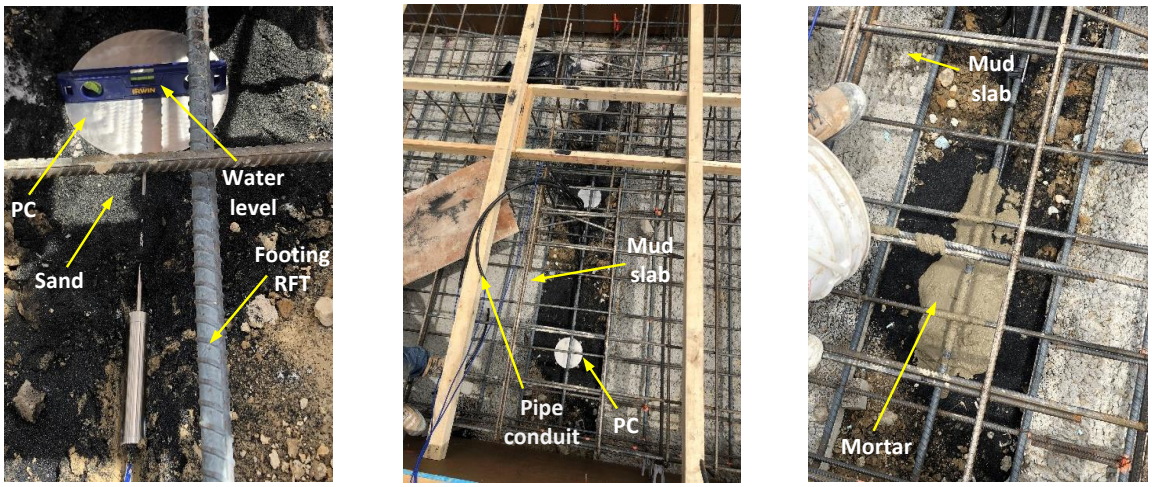

a) **b)** **c)**

Figure 3-7. Footing pressure cells installation for the Pickering culvert: a) pressure cell leveling; b) cables routing; and c) mortar pouring.

3.5.2 Pressure Cells on the Structure

PCs were placed on the culvert top slab and one sidewall. After positioning the PCs at their specified location, four holes were drilled at the mounting lugs locations for the Tapcon screws. In order to ensure full contact between the PC and culvert surface, fast-setting cement mortar was poured on the surface, and the PC was pushed till excess mortar extrudes out of the sides of the PC as presented in **Figure 3-8**. The PC was then leveled and fixed in place using Tapcon screws. Unrealistic measurements occur in case gaps existed between the PC and the RC surface.

The PC transducer and exposed portion of the signal cable were covered with mortar. Moreover, all sensors and cables were backfilled with clean sand free of any large particles having grain size over 10 mm. This ensured that the PC would not be exposed to direct contact with large aggregates in the backfilling material, which might cause stress

concentration or distortion of the PC measurements. Finally, the center coordinate of each PC was surveyed, and initial readings were recorded.

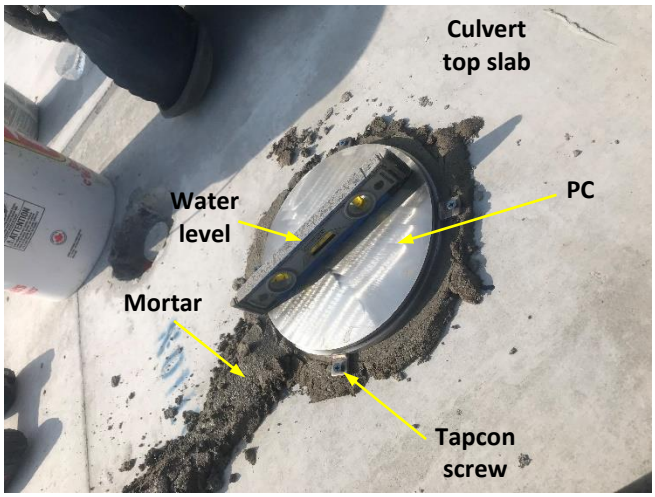

Figure 3-8. Pressure cells installation on the top slab of the Remembrance culvert.

3.5.3 Strain Gauges

VW SGs were installed on the inner and outer sides of the culverts to determine the thrust and bending moment across particular sections along the culvert span. For each SG, two 12.7 mm (0.5″) diameter holes were drilled to a depth of 63.5 mm (2.5″) to fix the mounting blocks in place. The mounting blocks were anchored using high-strength epoxy to assure adequate mechanical coupling to the RC culvert. Otherwise, erroneous strain measurements would be obtained if the mounting blocks are not totally fixed because strains would be measured due to the movement of the loose mounting blocks. The mounting blocks were oriented in the direction of strain measurement as depicted in **Figure 3-9**. After securing the SG into the holes of the mounting blocks, it was connected to the readout unit to adjust the initial reading to the desired level within its useable range (1000 - 4000 με). The adjusted initial reading depended on whether compressive or tensile strains were anticipated as per the FE analysis results. The SG that would be backfilled was covered using cover plates, as shown in **Figure 3-9b**, to protect it during backfilling. Initial readings of all SGs were measured several times after installation. It was observed that the utilized VW SG readings stabilized after six hours from installation on average.

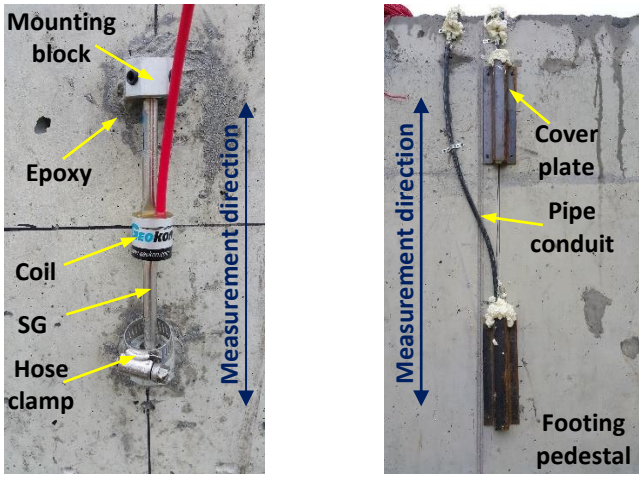

Figure 3-9. Strain gauges installation on the footing pedestal of the Oshawa culvert: a) installed SG; and b) cover plates.

3.5.4 Signal Cables

All signal cables were clearly labeled to uniquely identify the connected sensor. The signal cables of sensors placed on the top slab were fed into a 25.4 mm (1″) diameter flexible polyethylene pipe. The cables were grouped at a collection point on the sidewall, from which they were routed to the data logger location in the main conduit as shown in **Figure 3-10**. The percentage of conduit area occupied by the cables was approximately 25% to ensure unrestricted feeding of the long cables. The pipes' connections and elbows were sprayed with protective foam to mitigate direct loads during backfilling. It is highly recommended to determine the location of the data logger on-site to estimate the required signal cable length for each instrument. Such practice saves the time and effort required for splicing the cables on-site.

3.5.5 Data Acquisition System

An Automated Data Acquisition Monitoring System (ADAMS) was utilized to allow for automated real-time remote monitoring. The data logger had interface modules, cellular modem, and a solar panel with charge controller along with an external battery to power the system. The data logger was supplemented by multiplexers, with each adding 16 signal channels to the system to accommodate the quantity of VW sensors utilized in each project. The ADAMS was enclosed in a waterproof fiberglass housing to conceal it from adverse

weather conditions. The data acquisition program was coded to operate the modem and collect the data for only 4 hours/day to conserve power and ensure that the solar panel would provide sufficient power throughout the gloomy winter.

Data is remotely collected through software that connects to the data logger using a static IP address. The maximum sampling frequency is controlled by the number of VW sensors and the data logger speed. Therefore, it was necessary to run a test for each project with all cables connected to the data logger in order to determine the maximum sampling frequency that will be set during the live load testing. The maximum achievable sampling frequency was found to be one reading/2 minute. The ADAMS is programmed with different sampling frequencies corresponding to different stages of the project; a sampling rate of one reading/5 minute is assigned during construction, and one reading/hour will be used for the long-term measurements after construction completion. The post-construction sampling rate could be changed in the future depending on the trend of measurements and range of variation.

A grounding system was used to protect the data logger from lightning strikes. The grounding system comprised a 2.0 m copper rod pushed into the ground and connected to the data logger through a copper wire as shown in **Figure 3-10**.

Figure 3-10. Overview of the final instrumentation: a) Remembrance culvert; Oshawa culvert; c) data logger and grounding system; and d) data logger components.

3.5.6 Installation Enhancement Measures

Full-scale field tests on real-life buried structures are always confronted with short notices, unforeseen obstacles, and time constraints. Impeding the contractor's construction operations is not permitted and fitting the sensors installation work within the contractor's schedule is necessary. Consequently, the installation technique was modified in some cases to facilitate and accelerate the installation process. For example, the PCs were installed underneath the footing of the Oshawa culvert directly after finalizing the bottom reinforcement mesh. This was done after the experience with installing the PCs underneath the footing of the Pickering culvert and realizing that placing the top reinforcement mesh limited the working zone and obstructed the accessibility. At the same time, the placement of the PCs before commencing the reinforcement work might expose the PCs to higher risks of damage during the installation of reinforcing bars. Similarly, the SGs of the Remembrance culvert were installed on-site after assembling the culvert. However, the holes of the mounting blocks were drilled at the manufacturing plant for the Pickering culvert while the installation was accomplished on-site, and for the Oshawa culvert, the holes were drilled, and the mounting blocks were attached to the culvert segment at the manufacturing plant. This saved at least 60 person-hours of on-site work. Lastly, during the instrumentation of the Remembrance culvert, it was difficult to feed the long signal cables through the main conduit (ABS pipe of 50.8 mm (2″) diameter, see **Figure 3-10a**). For the other two projects, galvanized steel channels (shown in **Figure 3-10b**) were utilized as the main conduits, which facilitated routing the signal cables to the data logger. Overall, the modifications discussed above resulted in reducing the average working person-hours per sensor as illustrated in **Table 3-6**.

Table 3-6. Summary of the average working person-hours on-site for the three projects.

Site	Total working person-hours	Number of sensors	Person-hours/sensor
Remembrance culvert	194	20	9.7
Pickering culvert	228	29	7.9
Oshawa culvert	189	37	5.1

3.6 Monitoring Results and Analysis

So far, all the installed sensors are functioning properly. This section presents the monitoring data and analysis of the measurements obtained from Remembrance culvert up to date. Construction of the Remembrance culvert was recently completed with a total backfill height of 3.2 m as illustrated in **Table 3-1**. The culvert was backfilled with well-graded sand (SW), compacted to 90-100% of the Standard Proctor density reflecting B1 standard installation of the CHBDC (CSA, 2014). Nuclear density test data suggested an average dry density of 22.2 kN/m^3 and a moisture content of 3.6%, resulting in an average wet density of 23.0 kN/m^3. The presented results provide useful insights into the field data and aid in assessing the stability and reliability of the installed sensors.

3.6.1 Pressure Cells Data

The recorded PC readings since the start of backfilling on the sidewalls up to the final backfill condition (3.2 m) are displayed in **Figure 3-11**. Backfilling of the culvert was carried out in stages, where a backfill height (H) of 1.7 m was reached on day 105 and increased to 3.0 m on day 167 when the winter season started. The top 0.5 m of the backfill, which was exposed to frost, was removed as a common construction practice on day 270. This explains the reduction in the measured earth pressures in **Figure 3-11** between days 270 and 415 before the final backfill height (H = 3.2 m) was reached. The four wing walls of the Remembrance culvert were cast-in-place. Construction of these wing walls commenced after day 19 of construction when the backfill height reached 0.6 m on top of the culvert. Thus, the measured spikes in **Figure 3-11b** and **Figure 3-11c** during the construction period that reached up to 165 kPa are transient loads from the equipment and materials used in constructing the wing walls. Continuous changes in the earth pressure measurements are recognized in **Figure 3-11** since the start of backfilling for two main reasons: 1) the construction activities did not stop for the subdivision extension project and the culvert was continuously exposed to transient loads; and 2) season and rain accumulations, which increase the total loads applied on the culvert. However, the PCs' readings stabilized after the road work was completed and the final backfill height was reached.

The CHBDC (CSA, 2014) designates different VAFs and horizontal arching factors (HAFs) for earth pressure calculations on RC culverts based on the soil type and compaction level in the sidefill and bedding zones. The HAF is equivalent to the lateral earth pressure coefficient used to estimate the lateral earth pressure on the culvert sidewall. The code identifies B1 and B2 standard installations, with higher compaction requirements for B1 installation compared to B2 installation for the same type of backfill material. Based on previous practice and limited soil-structure interaction FE analyses, the CHBDC stipulates a VAF of 1.20 and 1.35 for B1 and B2 installations, respectively. The code specifies minimum and maximum HAF values of 0.3 and 0.5 for B1 installation, which was considered while constructing the subject TSC.

Figure 3-12 shows the measured earth pressures on the culvert body at 3.2 m of backfill, which was estimated for each PC as the average readings in the past 10 days when the readings were stable. The measured vertical earth pressures on the top slab in **Figure 3-12a** indicate non-uniform earth pressure on the top slab with the highest pressure measured by PC 6-1 located near the edge. The lowest pressure was measured by PC 5-1 installed at the mid-span, while PC 3-1 and PC 4-1 exhibited almost the same pressures. These results are in good agreement with the distribution obtained from the preliminary FEAs as depicted in **Figure 3-12a**. An average VAF of 1.05 was estimated from the PCs distributed on the top slab, which is 12.5% lower than the 1.2 VAF stipulated in the CHBDC for B1 standard installation. The 1.05 VAF from the field measurements agrees well with the 1.04 VAF reported by Ramadan and El Naggar (2021) for the 10.4-m-span TSC, as will be discussed in Chapter 6. This may indicate that the CHBDC overestimates the pressure along the top slab of TSCs for B1 installation.

The measured lateral earth pressures on the sidewall are presented in **Figure 3-12b**. The actual earth pressure distribution along the sidewall cannot be determined with only two pressure cells; however, the measurements of PC 1-1 and PC 2-1 almost fall on the maximum bound of the code (HAF = 0.5). Ramadan and El Naggar (2021) reported parabolic distribution of the lateral earth pressure on the sidewall of the 10.4-m-span TSC based on field and numerical results, as will be elaborated in Chapter 6.

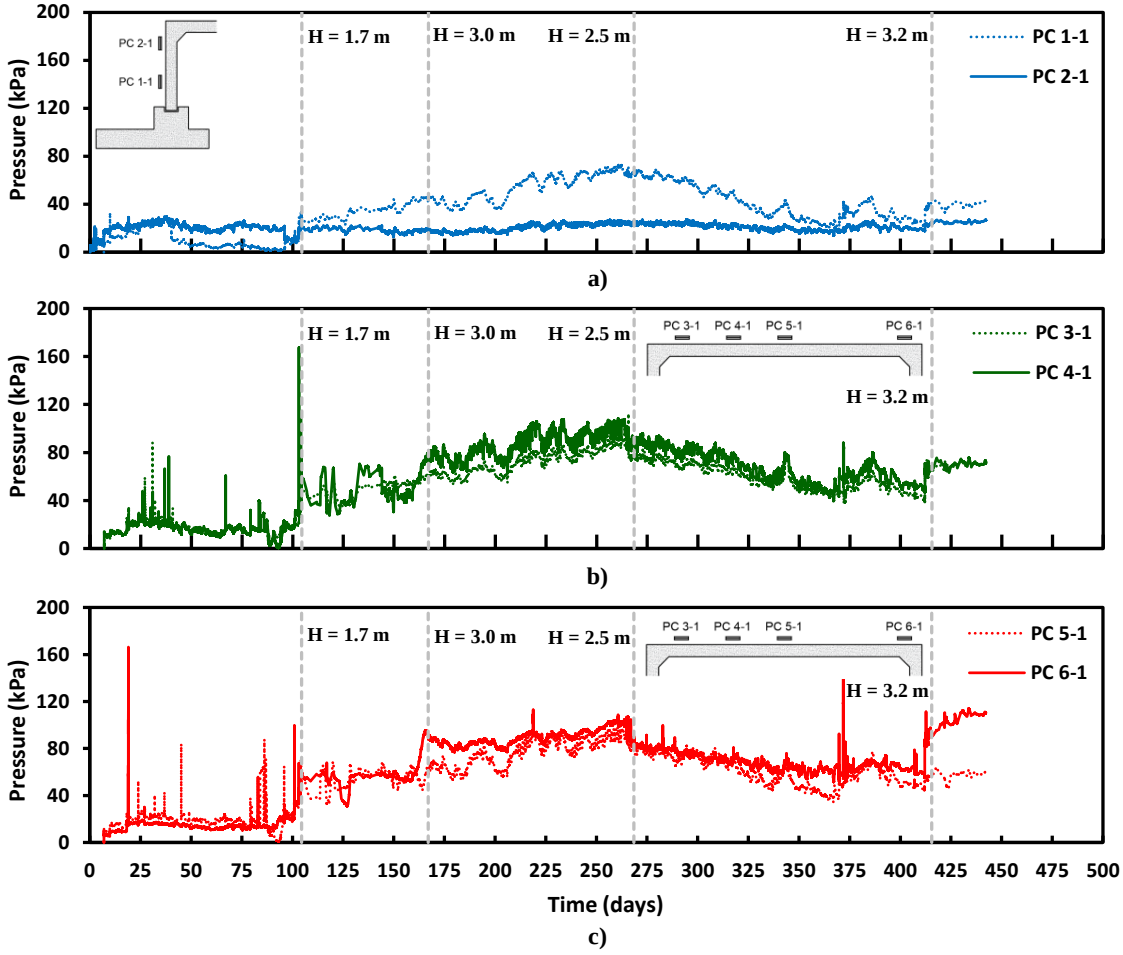

Figure 3-11. PC measurements of the Remembrance culvert at different backfill heights: a) lateral pressure on the sidewall; b) vertical pressure on the top slab (PC 3-1 and PC 4-1); and c) vertical pressure on the top slab (PC 5-1 and PC 6-1).

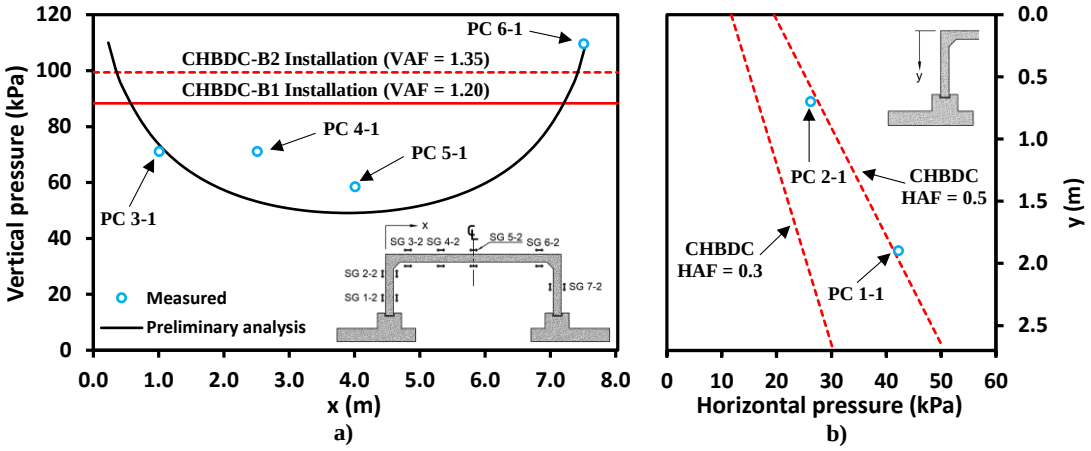

Figure 3-12. Comparison of the measured earth pressures on Remembrance culvert with the CHBDC (CSA, 2014) pressures: a) pressures on the top slab; and b) lateral pressure on the sidewall.

3.6.2 Strain Gauges Data

SGs were installed in pairs at each section to measure the strain on the two extreme fibers, enabling the measurement of tensile (+ve strain value) and compressive (-ve strain value) strains as demonstrated in **Figure 3-13**. The coefficient of thermal expansion of the vibrating wire in the surface-mounted VW SG model 4000 is different from that of concrete, resulting in some temperature-induced no-stress readings due to temperature variations. Accordingly. temperature correction was applied for the presented strain measurements following the manufacturer's recommendations as follows:

$$strain_{corrected} = strain_{measured} - (T_1 - T_0) \times (CF_{VW} - CF_c) \quad \textbf{(3-2)}$$

where T_1 is the temperature at time strain is measured; T_0 is the temperature at time of initial gauge reading; CF_{VW} is the coefficient of thermal expansion of the VW (+12.2 με/°C); and CF_c is the coefficient of thermal expansion of concrete (+10.4 με/°C). It should be noted that temperature was measured using the thermistor included in each strain gauge. Analysis of the SG data is discussed herein at two backfill height of 1.7 m (between day 105 and 125) and 3.2 m (after day 270).

The average measured earth pressures from the PCs and strains from the SGs at 1.7 m of backfill are summarized in **Table 3-7**. The strain measurements indicate that the majority of the cross-sections experienced a net compression (compressive strain higher than tensile strain) except for the two cross-sections at both edges of the top slab. It should be noted that SG 3-2 and SG 6-2, placed at these two cross-sections, were damaged at separate periods due to the construction loads between the 0.6 m and 1.7 m backfilling phases. The damaged SGs were replaced, and the missing data were interpreted from the other functioning SG as they were symmetrically located. The authors attribute the net tension measured at these cross-sections to the potential error in interpreting the missing data during the malfunctioning period of each SG.

Visual inspection demonstrated that no cracks were developed on the inner surface of the culvert at 1.7 m of backfill. Also, excluding SG 2-2 located below the haunch, the maximum tensile strain measured at all cross-sections did not exceed the theoretical

cracking strain (133 με) as illustrated in **Table 3-7**. The theoretical cracking strain is calculated as the ratio between the modulus of rupture (f_r) and modulus of elasticity (E_c) of the concrete. Both f_r and E_c were estimated for concrete with normal weight aggregate according to CSA A23.3-14 (CSA, 2014), i.e.,

$$f_r = 0.6\lambda\sqrt{f_c'}\ ,MPa$$
$$E_c = 4500\sqrt{f_c'}\ ,MPa \quad \textbf{(3-3)}$$

in which f_c' is the 28-day compressive strength of concrete (57 MPa for the subject culvert), and λ is the modification factor to account for the reduced mechanical properties of lightweight concrete relative to normal weight concrete of the same f_c' (λ = 1.0 for normal weight concrete (CSA, 2014), which reflects the case in the present study). Accordingly, the bending moment (BM) can be evaluated from the recorded strain readings assuming plane sections remain plane after loading and linear elastic behavior of the RC material. Both the external strain (ε_e) measured on the outer surface and the internal strain (ε_i) measured on the inner surface were employed to calculate the BM, which was assumed to be positive when the tensile stress was on the inner surface of the culvert and calculated as,

$$BM = \frac{E_c . I_g . (\varepsilon_i - \varepsilon_e)}{d} \quad \textbf{(3-4)}$$

where I_g is the gross moment of inertia; and d is the section depth. Moreover, a plane frame analysis was conducted using the FE program, SAP 2000 (CSI, 2020) in order to estimate the BM distribution on Remembrance culvert under service earth loads. The TSC was analyzed as a rigid frame structure whose base is pin-supported at the strip footing, which is the common practice in designing these structures. Two different loading conditions were considered in the frame analysis: one considering the measured earth loads from the PCs with non-uniform earth pressure distribution on the top slab and considering a constant average horizontal stress (22 kPa) on the sidewalls based on the average values in **Table 3-7**; the other represents the specified earth loads in the CHBDC (CSA, 2014) for B1 installation, with a VAF of 1.2 and a HAF of 0.5.

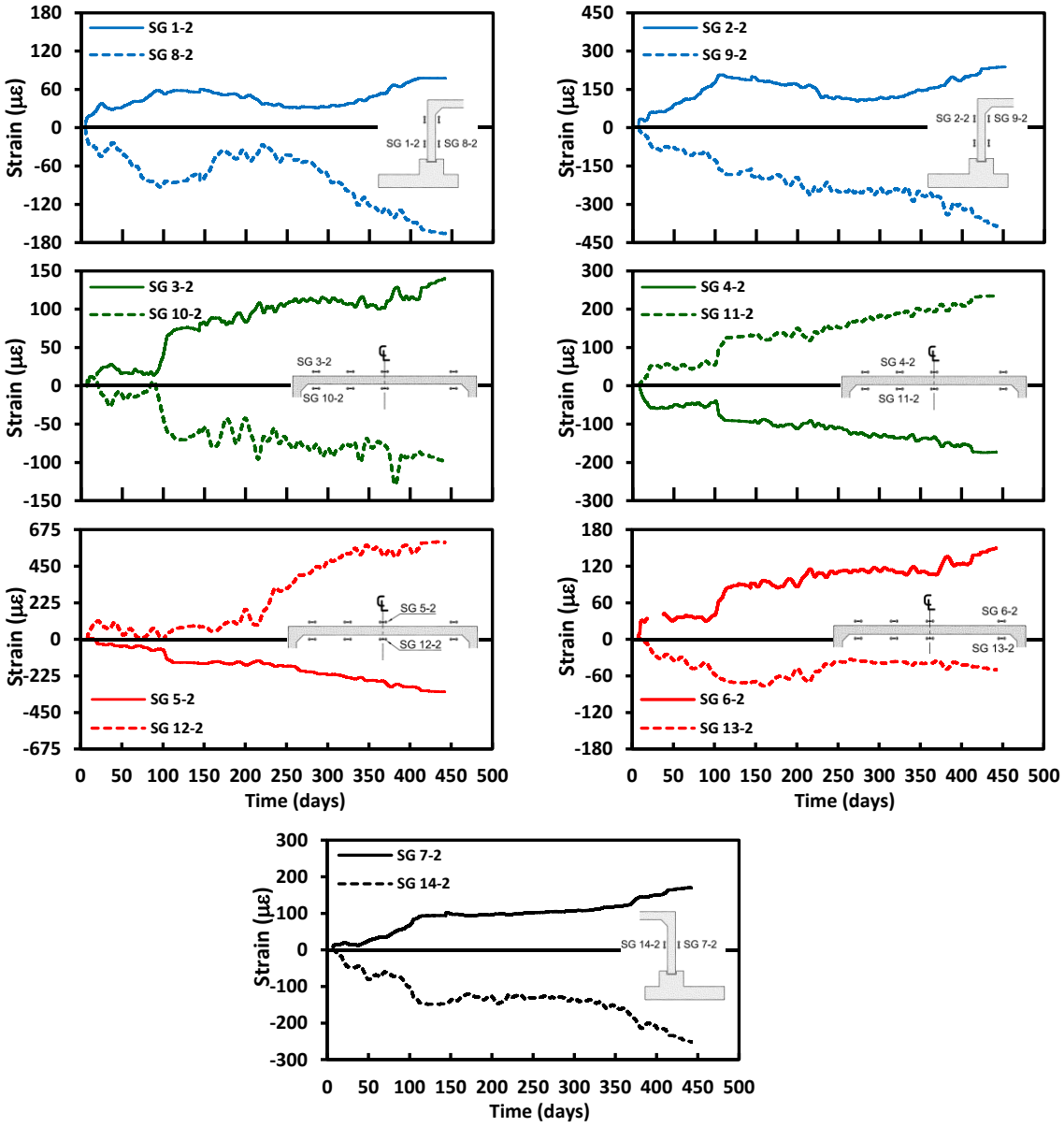

Figure 3-13. Strain gauge measurements of the Remembrance culvert.

Figure 3-14 compares the bending moments estimated from the SGs measurements and those obtained from the frame analyses. For the *BM* distribution on the top slab, the comparison shows excellent agreement between the values estimated from the SGs measurements and those from the PCs measurements, with a maximum difference of 10%. On the other hand, the CHBDC exhibited higher values. The maximum positive moment at the mid-span of the top slab using the code arching factors is 31% and 19% higher than the estimated values from the SGs and PCs, respectively. For the *BM* on the sidewall,

higher moments were estimated from the SGs near the base compared to the other two cases. Ramadan and El Naggar (2021) reported the development of BM at the sidewall base of the 10.4-m-span TSC, which was attributed to the rotation of the footing combined with the connection condition at the base. At the base, the culvert sidewalls were secured in the keyways of the strip footing; then, the keyways were filled with nonshrink grout. The results of the preliminary FEA for the Remembrance culvert anticipated the rotation of the strip footing as shown in the deformed shape presented in **Figure 3-15**. Therefore, the results from the preliminary analysis support the hypothesis that the rotation of the footing resulted in additional induced stresses, which leads to the development of BM at the base. Accordingly, it can be predicted that the connection condition at the base of the sidewall is not a pure hinged connection, at least for the soil condition on which the subject culvert was constructed.

Table 3-7. Summary of the measured average stresses and strains at 1.7 m of backfill.

Average stresses					
Sensor	Average stress (kPa)	Sensor	Average stress (kPa)	Sensor	Average stress (kPa)
PC 1-1	24.3	PC 3-1	45.8	PC 5-1	38.1
PC 2-1	21.0	PC 4-1	38.5	PC 6-1	58.2
Average strains					
Sensor	Average strain (με)	Sensor	Average strain (με)	Sensor	Average strain (με)
SG 1-2	57.0	SG 6-2	80.7	SG 11-2	82.5
SG 2-2	141.2	SG 7-2	92.1	SG 12-2	132.5
SG 3-2	71.6	SG 8-2	-86.1	SG 13-2	-67.7
SG 4-2	-93.2	SG 9-2	-177.1	SG 14-2	-139.6
SG 5-2	-153.0	SG 10-2	-68.3		

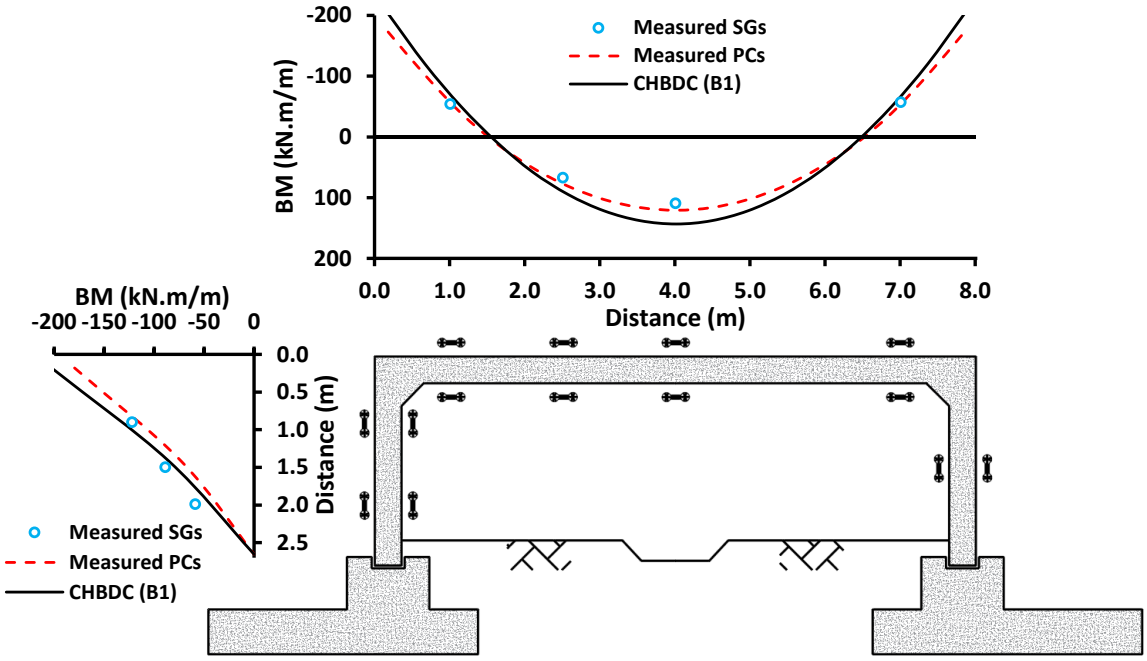

Figure 3-14. Comparison between the bending moment (*BM*) estimated from the strain gauges reading; the frame analysis results using pressure cell readings; and the frame analysis results using the CHBDC (CSA, 2014) loads at 1.7 m of backfill.

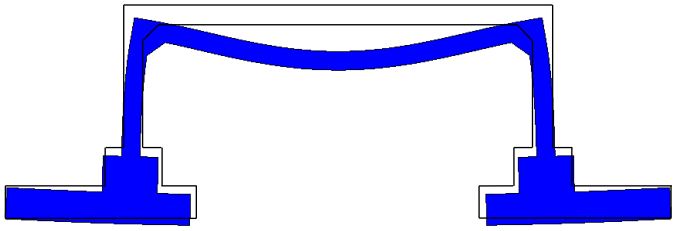

Figure 3-15. Deformed shape and footing rotation from the preliminary finite element model. (Magnification × 100)

At the final backfill height (3.2 m), the SG measurements presented in **Figure 3-13** indicate the development of cracks at SG 2-2 and SG 7-2 on the outer surface of the sidewall, where the measured tensile strains are higher than the theoretical cracking strain (133 με). Similarly, flexural cracks are predicted at the bottom surface of the top slab from SG 11-2 and SG 12-2 measurements. **Figure 3-13** shows that the first cracks developed at SG 2-2 when the backfill height reached 1.7 m. Cracks then developed at the midspan (SG 12-2) when the backfill increased to 3.0 m on day 167, which evolved, reaching the location of SG 11-2 on day 200. The final cracks developed at the location of SG 7-2 when the final backfill height (3.2 m) was reached on day 415. Visual inspection confirmed the formation

of cracks on the bottom surface of the top slab within its middle 3.1 m as shown in **Figure 3-16**. This consistency indicates the reliability of the field measurements. Cracks on the outer surfaces of the sidewall could not be inspected due to the surrounding sidefill material.

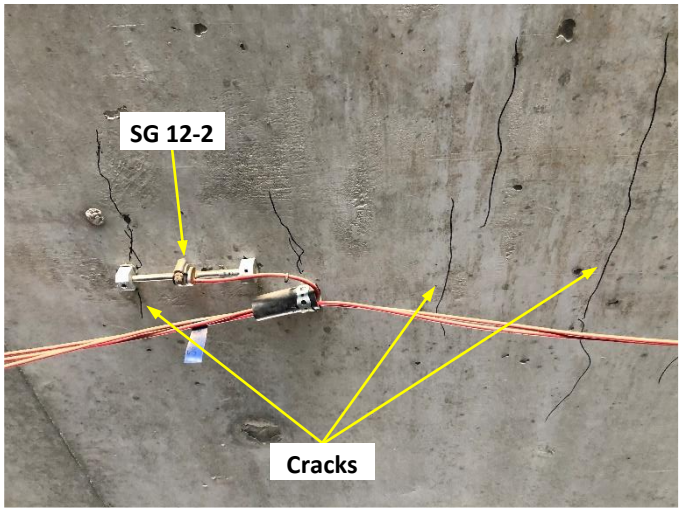

Figure 3-16. Observed cracks at the midspan (H = 3.2 m).

3.7 Summary and Conclusions

Full-scale field monitoring of three RC three-sided culverts is undertaken to help characterize the culvert behavior under earth and live loads. The instrumented culverts vary in span from 7.3 m to 13.5 m. To design and execute an efficient and optimized field monitoring plan, preliminary finite element analyses were conducted for the investigated culverts. The FE analyses quantified the target measurements, which is essential for selecting the instruments' ranges. Moreover, the results were employed to specify the optimal instrument quantities required to capture the structural performance of each culvert.

The subject culverts were instrumented with a total of 30 pressure cells and 56 strain gauges to measure the soil-culvert interface pressures and the developed strains in the buried concrete structure, respectively. Vibrating wire sensors were selected for their durability and stability for long-term monitoring purposes. A brief description of the sensors' selection criteria and installation procedures has been presented. Based on the experience

gained from the instrumentation of the first culvert, modified installation procedures were adopted to reduce in-situ work effort and time. As a result, the average working person-hours were reduced from 9.7 to 5.1 hours/sensor. All installed sensors in the three projects have survived the construction activities and are functioning properly to date. Building on the experience gained from these projects, some recommendations for future instrumentation of similar projects are as follows:

a. The location of the data logger on-site should be determined to estimate the required signal cable length for each instrument. This saves the time and effort required for splicing the cables on-site.

b. The vibrating wire strain gauge used in this study requires 6 hours on average for the initial reading to stabilize after installation.

c. The main conduit for signal cables should be sized such that the percent occupancy does not exceed 25%, especially for long cables.

d. Galvanized steel channels provide good protection for signal cables.

e. The maximum sampling rate for vibrating wire transducers is controlled by both the number of instruments and speed of the data logger. Thus, the data logger should be tested with all cables connected to determine the maximum sampling rate.

Monitoring data from both pressure cells and strain gauges were presented for the 7.3-m-span TSC which was completed to a final backfill height of 3.2 m. Field observations and data analysis confirmed the reliability and consistency of the installed monitoring system as follows: 1) stability of measurements after reaching the final road grade level, where no noticeable changes in the readings occurred under constant loading condition; 2) both strain gauge and pressure cell measurements retain comparable bending moments on the top slab at 1.7 m of backfill; and 3) visual inspection demonstrated the reliability of using the SGs data to indicate cracks formation in the culvert body at two backfill heights (1.7 and 3.2 m). The presented field measurements enhance the knowledge on the structural performance of TSCs. The data were used to evaluate the current design practice and

CHBDC (CSA, 2014) provisions regarding earth loads on RC TSCs. The following conclusions can be drawn from the measured field data:

1. The earth pressure distribution on the top slab is non-uniform, with an average VAF of 1.05 at a backfill height of 3.2 m, indicating that the CHBDC (CSA, 2014) provisions tend to overestimate the vertical earth pressure on the top slab of TSCs by specifying a VAF of 1.2 for the case of B1 standard installation. However, more studies are still required to validate such findings.

2. The measured lateral earth pressure on the sidewall mostly falls on the upper bound of the CHBDC (CSA, 2014) for B1 installation with a HAF of 0.5.

3. Strain measurements on the sidewall indicated that the strip footing might have rotated, resulting in imposing additional stresses to the sidewalls of the culvert and the development of bending moment at the base. Thus, the base connection does not behave as a pure hinge, at least for the soil condition on which the subject culvert was constructed.

3.8 References

1. Balachandran, K., Liu, J., Cao, L., and Peaker, S. (2015). Statistical correlations between pressuremeter modulus and SPT N-value for glacial tills. In *Proc., 68th Canadian Geotechnical Conf. and 7th Canadian Permafrost Conf*. Richmond, BC, Canada: Canadian Geotechnical Society.

2. Beach, T. J. 1988. Load test report and evaluation of a precast concrete arch culvert. Rep. No. 1191. Washington, DC: Transportation Research Board.

3. Bennett, R. M., Wood, S.M., Drumm, E. C., and Rainwater, N.R. (2005). Vertical loads on concrete box culverts under high embankments. *Journal of Bridge Engineering*, 10 (6), 643-649. 10.1061/(ASCE)1084-0702(2005)10:6(643).

4. Chen, B., and Sun, L. (2014). Performance of a reinforced concrete box culvert installed in trapezoidal trenches. *Journal of Bridge Engineering*, 19 (1), 120–130. https://doi.org/10.1061/(ASCE)BE.1943-5592.0000494.

5. CSA (Canadian Standards Association). 2014. *Canadian highway bridge design code*. CAN/CSA-S6-14. Mississauga, ON, Canada: CSA.

6. CSA (Canadian Standards Association). 2014. *Design of concrete structures (A23.3-14)*. CSA Group, Mississauga, Ontario.

7. CSI (Computers and Structures, Inc.). 2020. *SAP2000 integrated software for structural analysis and design*. Berkeley, California: CSI.

8. Dassault Systems Simulia. 2013. *Abaqus-Version 6.13 Documentation*. Providence, RI: Dassault Systems Simulia Corp.

9. Dunnicliff, J. (1988). *Geotechnical instrumentation for monitoring field performance*. John Wiley and Sons, New York.

10. Manzari, M., Drevininkas, A., Olshansky, D., and Galaa, A. (2014). Behavioral modeling of Toronto glacial soils and implementation in numerical modeling. In *Proc., 67th Canadian Geotechnical Conf*. Richmond, BC, Canada: Canadian Geotechnical Society.

11. Marr, W. A. (1999). Uses of automated geotechnical instrumentation systems. *Field Instrumentation for Soil and Rock, ASTM STP 1358, G. N. Durham and W.A. Marr, Eds.*, American Society for Testing and Materials, West Conshohocken, PA.

12. Marshall, J. D., Anderson, J. B., Meadows, R. L., and Jensen, T. J. (2014). Full-scale testing of three-sided precast concrete arch sections. *Journal of Bridge Engineering*, 19 (12), 04014051. 10.1061/(ASCE)BE.1943-5592.0000630.

13. McGrath, T. J., Moore, I. D., Selig, E. T., Webb, M. C., and Taleb, B. (2002). *Recommend specifications for large-span culverts.* Report No. 473. Washington, DC: Transportation Research Board.

14. McGrath, T. J., and Selig, E. T. (1996). *Instrumentation for investigating the behavior of pipe and soil during backfilling*. Rep. No. NSF96-442P. Amherst, MA: Department of Civil and Environmental Engineering, University of Massachusetts.

15. McGrath, T. J., Selig, E. T., and Beach, T. J. (1996). Structural behavior of three-sided arch span bridge. *Transportation Research Record 1541*, Transportation Research Record, Washington, DC, 112–119.

16. McGrath, T. J., Selig, E. T., and Webb, M. C. (1999). Instrumentation for monitoring buried pipe behavior during backfilling. *Field Instrumentation for Soil and Rock, Durham G. and Marr, W.*, American Society for Testing and Materials. https://doi.org/10.1520/STP14216S

17. MTO (Ministry of Transportation of Ontario). 2010. *Frost Penetration Depths for Southern Ontario*. Ontario Provincial Standard Drawing OPSD 3090. ON, Canada: MTO.

18. Perkins, S. W., and Lapeyre, J. A. (1997). *Instrumentation of a geosynthetic-reinforced flexible pavement system*. Report No. 1596. Washington, DC: Transportation Research Board. https://doi.org/10.3141%2F1596-05.

19. Ramadan, S. H., and El Naggar, M. H. (2021). Field monitoring and numerical analysis of a large-span three-sided reinforced concrete culvert. *Journal of Geotechnical and Geoenvironmental Engineering*, 147 (4), 04021008. 10.1061/(ASCE)GT.1943-5606.0002489

20. Sama, M., Sykora, D. W., and Vytiniotis, A. (2015). Vertical pressures produced by controlled low strength material (CLSM) poured into pipe trenches. *IsnowEE*, ASCE, 429-441. https://doi.org/10.1061/9780784479087.043.

21. Seed, R. B., Duncan, J. M., and Ou, C. Y. (1991). Finite element analysis of compaction problems. *Advanced Geotechnical Analysis-Development in Soil Mechanics and Foundation Engineering-4, Ed*. Banerjee, P. K. and Butterfield, R. Elsevier Applied Science.

22. Sousa, H. (2020). Advanced FE modeling supported by monitoring toward management of large civil infrastructures: The case study of Lezíria Bridge. *Structural Concrete Journal*, 21, 1309-1320. 10.1002/suco.201900382

23. Tadros, M. K., Benak, J. V., Abdel-Karim, A. M., and Bexten, K. A. (1989). *Field testing of a concrete box culvert*. Report No. 1231. Washington, DC: Transportation Research Board.

24. Vaslestad, J., Johansen, T. H., and Holm, W. (1993). *Load reduction on rigid culverts beneath high fills: long-term behavior*. Report No. 1415. Washington, DC: Transportation Research Board.

25. Webb, M. C., Selig, E. T., and McGrath, T. J. (1999). Instrumentation for monitoring large-span culverts. *Field Instrumentation for Soil and Rock, Durham G. and Marr W.*, American Society for Testing and Materials, 66-86. 10.1520/STP14214S

26. Wood, S. M. (2000). Internal forces in a reinforced concrete box culvert. Master's dissertation, Dep. of Civil Engineering. Uni. of Tennessee.

27. Yang, M. Z. (2000). Evaluation of factors affecting earth pressures on buried box culverts. PhD dissertation, Uni. of Tennessee, Knoxville, TN.

28. Yang, M. Z., Drumm, E. C., Bennett, R. M., and Mauldon, M. (1999). Measurement of earth pressures on concrete box culverts under highway embankments. *Field Instrumentation for Soil and Rock, Durham G. and Marr W.,* American Society for Testing and Materials, 87-100. https://doi.org/10.1520/STP14215S

29. Zoghi, M., and Farhey, D. N. (2006). Performance assessment of a precast concrete, buried, small arch bridge. *Journal of Performance of Constructed Facilities*, 20 (3), 244–252. 10.1061/(ASCE)0887 3828(2006)20:3(244).

Chapter 4

* Structural Performance of a Medium-Span RC Three-Sided Culvert Based on Field Measurements and Numerical Analyses

4.1 Introduction

Flat top three-sided culverts (TSCs) are bottomless reinforced concrete (RC) culverts typically produced in large spans, up to 16.0 m, and low-rise profiles to handle heavy flows at sites with limited vertical clearance. TSCs are gaining popularity as a sustainable and economical alternative for short span bridge replacement as opposed to multi-barrel box culverts in terms of materials cost, construction time, workforce, and future maintenance costs (Von Handorf, 2004). TSCs are also more attractive from the environmental point of view compared to circular pipes, box, and multi-barrel box culverts. Meanwhile, with the absence of the bottom slab that restrains the lateral movement of the sidewalls, differential settlement may occur between the supporting strip footings and the large-span TSC deformation is expected to differ from that of the relatively rigid, short-span box culverts. These features would eventually influence the soil-structure interaction mechanism of TSCs. However, the current design practice treats TSCs same as box culverts in the Canadian Highway Bridge Design Code, CHBDC, (CSA, 2014).

Field monitoring and numerical analyses of large-span arch culverts and TSCs with arched top slab, also known as Con/Spans, were discussed in previous studies. Oswald (1996) monitored a 12.3-m-span arch culvert with 7.3 m of silty clay backfill cover. Oswald (1996) also conducted a two-dimensional (2D) finite element analysis (FEA) using CANDE software, in which the nonlinear behavior of both backfill soil and concrete were considered. The results demonstrated the importance of simulating concrete creep and shrinkage in the numerical analysis to reasonably simulate the culvert's long-term behavior. McGrath et al. (2002) instrumented a RC 9.1-m-span arch culvert with 1.5 m of

---

* A version of this chapter has been accepted for publication in the Canadian Geotechnical Journal.

backfill over its crown. They performed stationary live load tests at various backfill heights to investigate the transferred loads to the buried structure. McGrath et al. (2002) also developed 2D and three-dimensional (3D) FEAs in which the soil behavior was simulated using the Mohr-Coulomb elastic-plastic model with a linear increase of the elastic modulus with depth. A linear-elastic behavior was assumed for the concrete material. Based on the obtained results, they proposed a non-uniform earth pressure distribution on the top slab of the arch culvert. For Con/Spans, Beach (1988) performed a full-scale load test on a 5.8-m-span arched top culvert, where the tested precast unit was covered with 0.3 m (1 ft) of backfill and then loaded to failure using a hand-operated hydraulic jack. It was reported that the Con/Span exhibited a capacity that exceeded five times the design service live loads. Beach (1988) assumed a hinged connection at the base of the sidewall considering the lateral restraint provided by the surrounding soil. McGrath et al. (1996) instrumented an 11.0-m-span Con/Span, on which live loads were conducted at different backfill heights, up to 0.9 m. They reported excellent performance of the tested culvert under the applied loads in terms of the measured deflections and crack formations. Zoghi and Farhey (2006) load tested an 11.0-m-span Con/Span, covered with 0.9 m of soil when loaded, but could not reach its ultimate capacity. They concluded that the passive resistance provided by the backfill soil surrounding the culvert enhanced the culvert's ultimate capacity. They also reported negligible lateral displacement at the base of the sidewall, which they argued it justified the assumption of hinged connection.

More studies are still required to enhance the understanding of the soil-structure interaction mechanism of TSCs and evaluate the need for developing specific guidelines for their design. Consequently, this chapter contributes to the literature of TSC through the following: 1) collection and analysis of field data obtained from an instrumented 7.3-m-span TSC under 1.7 m of backfill; 2) 2D finite element analysis to evaluate the nonlinear behavior of the concrete material at service limit state (SLS); 3) the analysis of the structural behavior and soil-structure interaction mechanism considering the influence of foundation soil condition (yielding or non-yielding) at SLS; 4) a validated 3D FEA model to predict the ultimate capacity of the precast unit of the subject TSC under a specific experimental loading configuration reported in the literature; 5) evaluating the effect of the precast unit width on its load capacity and failure mechanism; and 6) predicting the

maximum backfill height at failure of the test TSC for yielding and non-yielding foundations. In this study, the term yielding foundation refers to the case of TSC constructed on the native soil, while non-yielding foundation refers to the case of TSC constructed on rock.

4.2 Full-Scale Tests

A precast RC TSC was constructed to provide a watercourse crossing through a road embankment in the Greater Toronto Area, Ontario. The culvert was 26.9 m in length, assembled using 11 precast RC units with span of 7.3 m, and total rise of 2.4 m. The geometry and reinforcement details of the used precast units are presented in **Figure 4-1**.

The native soil at the site consisted of silty clay to clayey silt till with very stiff to hard consistency below the foundation level (FL), which was approximately 6.3 m from the ground surface. The average SPT N-value of the silty clay layer extending from the ground surface and up to 3.9 m below the FL was 25, while a stiffer layer was encountered below that layer with an SPT N-value of 55 as shown in **Figure 4-2**. The TSC was supported on a 3.6-m-wide keyed cast-in-place strip footing with a total thickness of 1.3 m, including a 0.7 m thick pedestal as shown in **Figure 4-3**. The FL was 1.5 m below the streambed elevation due to the presence of the pedestal, which was below the 1.2 m frost depth at the construction site (OPSD, 2010).

The subject TSC was instrumented along one section, where the full backfill height, 3.2 m, would be covering the culvert top slab and the highest live loads would be experienced during the future road operation. The contact earth pressure imposed on the buried structure was measured using Geokon Model 4810 vibrating wire pressure cells (PCs) and the structural behavior was monitored using Geokon Model 4000 vibrating wire strain gauges (SGs). Model 4810 PC provides an accuracy of 0.1 % of its full-scale range when using the polynomial expression in the data reduction of its measurements (i.e., 0.35 kPa for the used PC with 350 kPa full-scale range). The utilized Model 4000 SG accuracy is 0.5% of its full-scale range (3000 με). The monitoring system was planned based on a preliminary numerical analysis, and the details of the instruments selection criteria and field installation

procedure are presented in Chapter 3. The culvert was instrumented with 6 PCs and 14 SGs distributed along its span as illustrated in **Figure 4-3**.

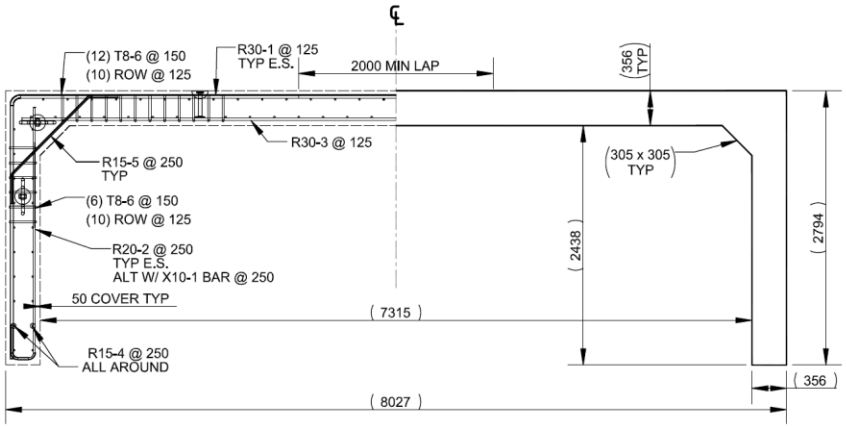

REINFORCING LIST				
MARK	SIZE	QTY	SPACING	LENGTH
R30-1	30M	38	125	7647
R20-2	20M	20	250	3172
R30-3	30M	19	125	7687
R15-4	15M	101	250	2338
R15-5	15M	20	250	1726
T8-6	D8	360	150/125	1400
X10-1	10M	18	250	1200

Figure 4-1. Geometry and reinforcement details of the Remembrance culvert. (All dimensions are in mm)

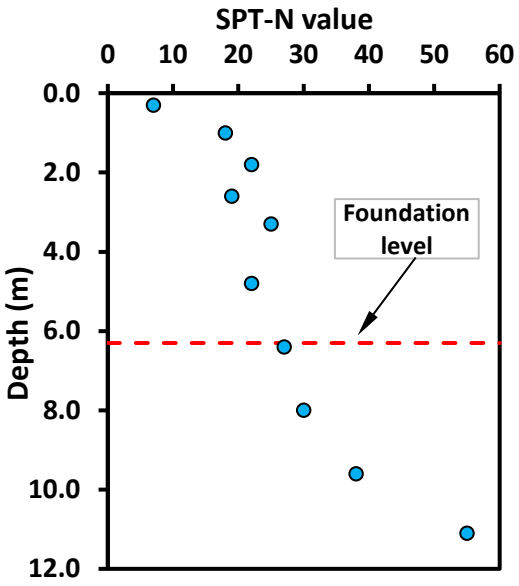

Figure 4-2. Variation of SPT N-value with depth.

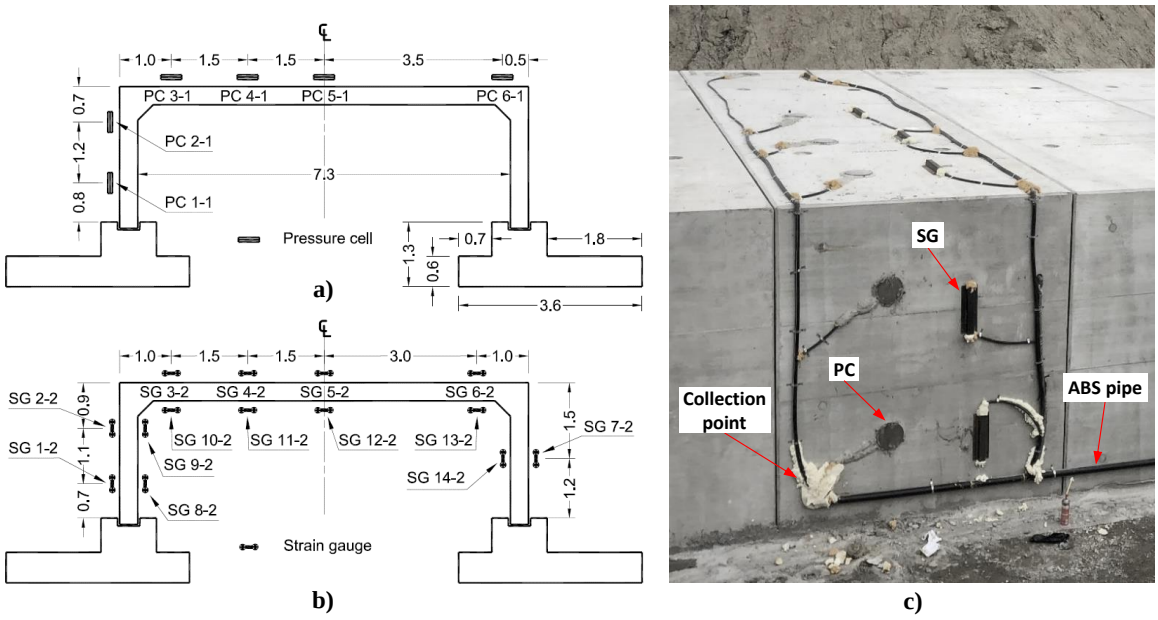

Figure 4-3. Remembrance culvert instrumentation layout: a) pressure cells; b) strain gauges; and c) instrumented segment.

4.2.1 Culvert Construction Sequence

Construction of the precast RC TSC started with the watercourse diversion to dry the construction work area. Excavation works then commenced to prepare the culvert trench and cast the keyed cast-in-place strip footings, which was underlain by a 0.1 m thick concrete levelling slab. The footing concrete was allowed sufficient time for curing to achieve at least 70% of its design strength (OPSS, 2010) before being backfilled. Levelling shims (plastic shims) were placed along each strip footing keyway to guarantee the correct seating of the culvert units, as depicted in **Figure 4-4**. Once the precast unit was in place, leg shims (plastic shims) were placed between the culvert sidewall and the keyway sides to secure the precast unit and avoid any lateral spreading. After installing all the precast units, non-shrink grout was poured to fill in the voids between the keyway and the culvert sidewall.

The CHBDC (CSA, 2014) specifies different VAFs for vertical earth pressure calculations on RC box culverts based on the soil type and compaction level of the backfill material in the sidefill and bedding zones. The code specifies two standard installations, named B1 and B2, with higher compaction requirements for B1 installation compared to B2

installation for the same type of backfill material. Based on previous practice and limited soil-structure interaction FEAs, the code stipulates a VAF of 1.20 for B1 installation and 1.35 for B2 installation. Backfill against the subject TSC was completed in lifts of well-graded sand (SW) compacted to 90-100% Standard Proctor, which complies with the construction requirements for B1 installation (CSA, 2014). Each backfill lift was less than 300 mm, and the difference in backfill elevation on both sides of the culvert did not exceed 0.6 m at any stage of backfilling to prevent exposing the culvert to excessive lateral deflection. A hand-operated vibrating plate compactor was utilized adjacent to the culvert body until reaching 0.6 m of backfill over the top slab to avoid distressing the culvert body by heavy compaction equipment. The four wing walls of the subject TSC were cast-in-place.

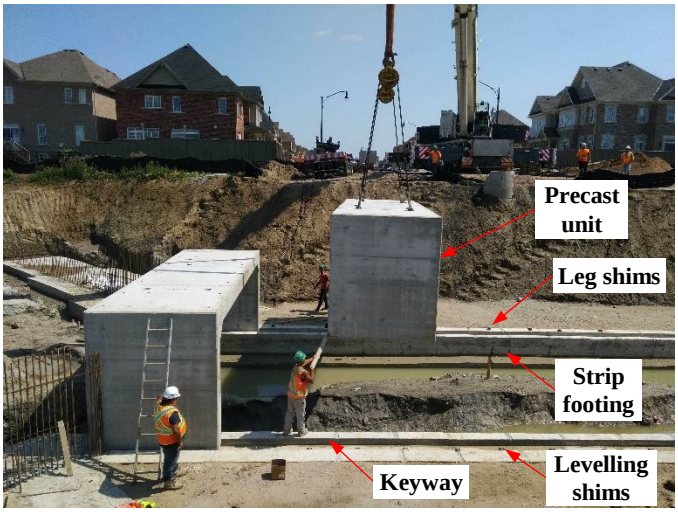

Figure 4-4. Installation of the Remembrance culvert precast units.

4.2.2 Field Data

The full height of backfill up to the finished road grade level is 3.2 m and is not expected to be reached during this construction season. Accordingly, field measurements were recorded during the backfilling process and up to the final reached cover depth of 1.7 m. All the installed sensors survived the construction activities and the collected measurements from PCs and SGs with construction time to date are presented in **Figure 4-5** and **Figure 4-6**, respectively.

Construction of the cast-in-place wing walls started upon reaching a 0.6 m backfill cover on top of the culvert. Accordingly, the culvert was exposed to transient loads due to the wing walls construction activity between days 18 and 105 of construction as shown in **Figure 4-5**. These construction activities resulted in damaging SG 6-2 on day 19, which was replaced on day 41. Replacing SG 6-2 required exposing the culvert and removing the soil cover over the SG and near the culvert edge to check the sensors cables, which resulted in sudden drop of the lateral earth pressure measured by the upper pressure cell (PC 2-1) on day 41 of construction as displayed in **Figure 4-5a**. The culvert edge was not backfilled until day 96, when the lower pressure cell (PC 1-1) exhibited a sudden drop and PC 2-1 measured an increase in the lateral earth pressure. The sudden drop in PC 1-1 readings is attributed to the relaxation of the compaction-induced locked-in-stresses in the sidefill material. **Figure 4-5a** demonstrates that PC 2-1 exhibited higher magnitudes than PC 1-1 after reaching a backfill height of 1.7 m. The imposed lateral pressure depends on the sidewall deflection relative to the surrounding soil. In the current study, the exact pressure distribution along the sidewall cannot be determined with only two PCs; however, the collected data indicates that the linear increase of lateral earth pressure with depth stipulated in the CHBDC (CSA, 2014) does not represent the actual loading case on the TSC.

Figure 4-5b and **c** show the vertical earth pressure measurements at four locations on the top slab. During the backfilling from 0.6 m to 1.7 m high, the earth pressure measurements at the top slab exhibited frequent spikes. These spikes resulted from transient loads applied to the culvert while constructing the wing walls as previously discussed. Both PCs located near the far edges of the slab (PC 3-1 and PC 6-1) recorded higher values than the other two PCs, reflecting non-uniform earth pressure distribution on the top slab. Similar studies on arch culverts (McGrath et al., 2002) have reported similar findings.

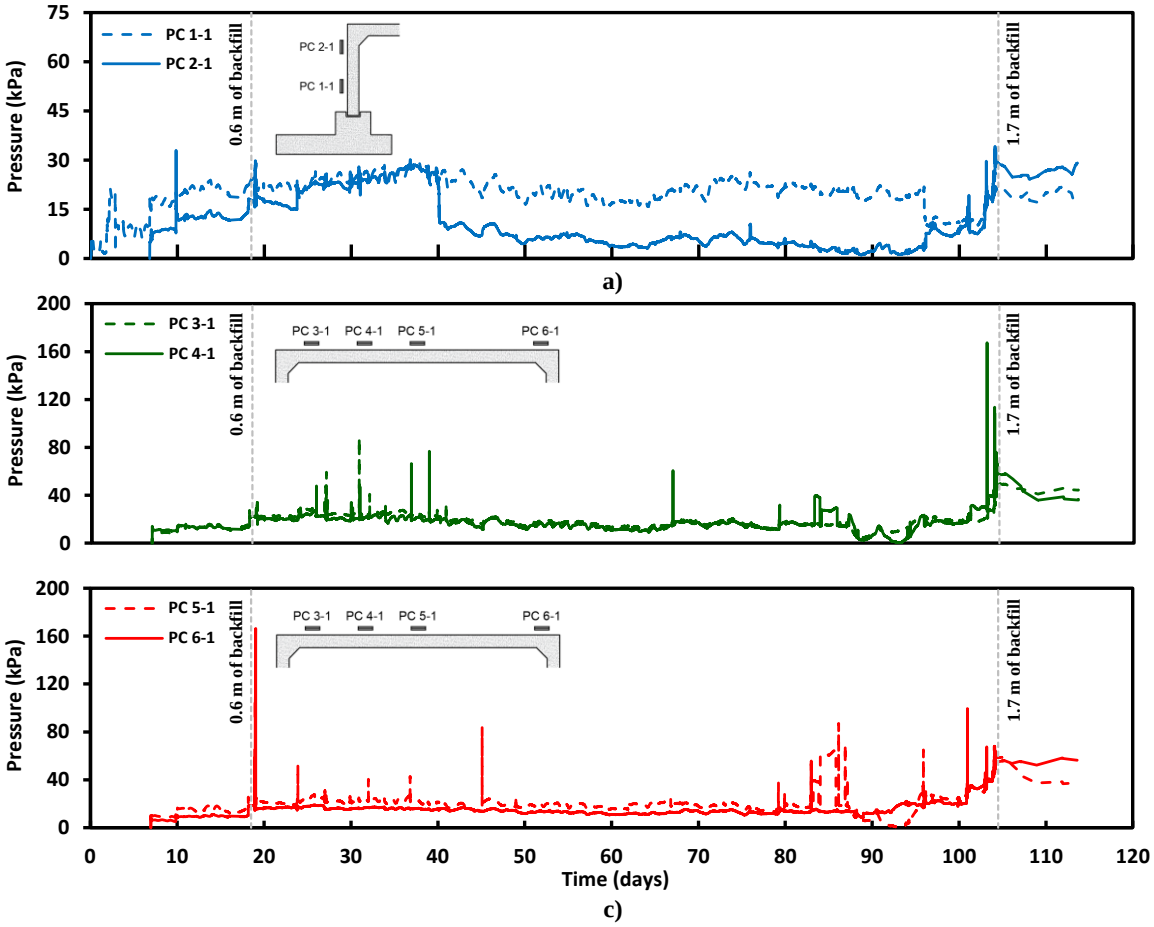

Figure 4-5. Sample pressure cell measurements: a) pressures on the sidewall; b) pressures on the top slab (PC 3-1 & PC 4-1); and c) pressures on the top slab (PC 5-1 & PC 6-1).

The measured strains at the culvert's inner and outer surfaces at the instrumented sections are presented in **Figure 4-6**. Tensile strains are denoted positive and compressive strains are denoted negative. Visual inspection of the test culvert did not reveal any cracks development on the inner surface of the top slab, which is supported by the measured tensile strains that fall below the theoretical cracking strain (ε_{cr} = 133 με) calculated according to CSA A23.3-14 (CSA, 2014) for an average 28-day concrete compressive strength (f_c') of 57 MPa. Only the tensile strain measured on the top corner of the sidewall by SG 2-2 slightly exceeded ε_{cr}; however, cracks development at this zone can not be visually confirmed due to the surrounding sidefill.

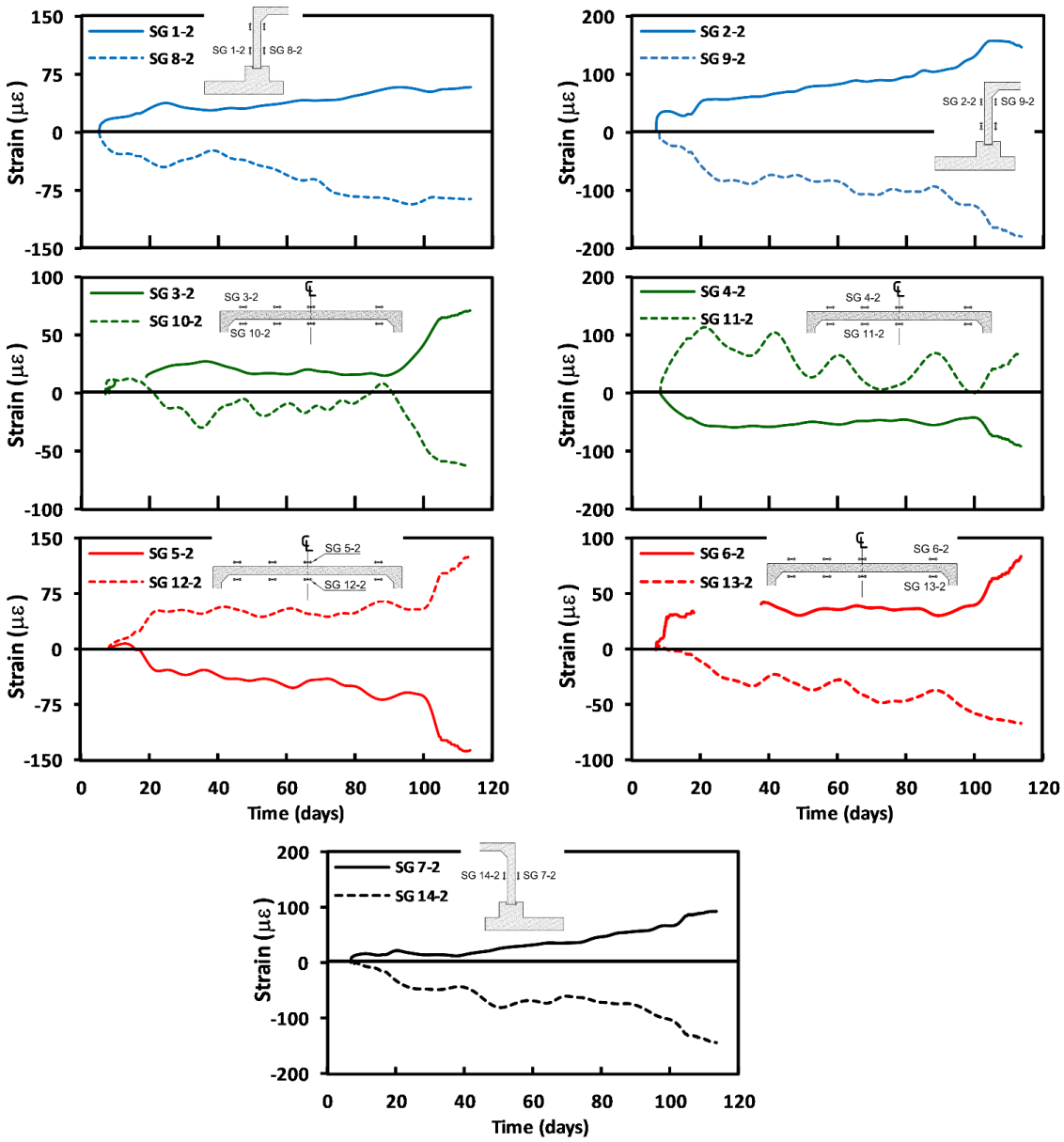

Figure 4-6. Sample strain gauge measurements.

4.3 Numerical Model – Serviceability Limit State (SLS)

According to the site topography, the finished road elevation is approximately at the ground level. Thus, the subject TSC was installed in a trench with sloping sides (1:1). Backfilling against the structure was completed in lifts no greater than 300 mm and compacted to 90-100% Standard Proctor in compliance with the construction requirements stipulated by the CHBDC (CSA, 2014) for B1 standard installation. The culvert was backfilled with well-

graded sand (SW), which consisted of 25% gravel, 73% sand, and 2% fines. The estimated uniformity coefficient ($C_u = D_{60}/D_{10}$) and coefficient of curvature ($C_c = D_{30}^2/(D_{60}\times D_{10})$) were 10.67 and 1.04, respectively. Backfill adjacent to the culvert was compacted using hand-operated vibrating plate compactor and the conducted nuclear density tests indicated an average wet unit weight of 23.0 kN/m^3.

Two-dimensional plane-strain FE models have been created for the monitored culvert using the computer program DIANA 10.1 (2016). The 2D models comprised the native soil, backfill soil, culvert body, and supporting strip footing as illustrated in **Figure 4-7**. The native soil, backfill soil, and strip footings were discretized using eight-node quadrilateral plane-strain elements, whilst the culvert body was discretized using plane-stress elements to account for the absence of structural connectivity between the adjacent precast units forming the buried culvert (Pimentel et al., 2009). The model was composed of 1870 plane-stress elements and 23559 plane-strain elements, with the mesh being refined within the vicinity of the culvert body to ensure high accuracy within the studied area.

Figure 4-7 shows the geometry and boundary conditions of the 2D model. Based on a conducted sensitivity analysis, the model width was 11 times the TSC span to eliminate the influence of the boundaries on the zone of interest. The model was extended vertically 8.0 m below the strip footing to represent the native soil, which was divided into two equal layers to account for the increase in strength and stiffness of the till layer reflected in the measured SPT N-values. The model was fixed at its bottom boundary and the side boundaries were restrained from lateral movement. The sidefill and backfill soils were divided into 8 and 7 layers, respectively, to mimic the incremental phases of installation. The overburden stresses of each layer were introduced in a separate phase. Each loading increment was solved iteratively using the Quasi-Newton (Secant) iteration method. Convergence was achieved once the computed out-of-balance force norm and displacement norm ratios were below 0.01 for each loading increment. To date, the backfill height has reached 1.7 m on top of the culvert; however, the full backfill height (3.2 m) was considered in the 2D models.

The effect of simulating the nonlinearity of RC was evaluated by developing two different sets of 2D models: a) linear elastic model (LEA) in which the RC culvert body was simulated using a linear-elastic material model, and b) nonlinear model (NLA) in which a nonlinear material model with crack formation predictions was applied. It is worth mentioning that backfill soil's nonlinear behavior was considered in both sets of models.

The backfill material adjacent to the culvert body was compacted using a hand-operated vibrating plate compactor up to a backfill height of 0.6 m over the top slab. Elshimi and Moore (2013) evaluated the influence of compaction effort on the behavior of two concrete pipes. They concluded that the compaction-induced stresses can be neglected when vibratory plate compactors are used. Accordingly, the effect of compaction during the backfill placement was not considered in the developed models.

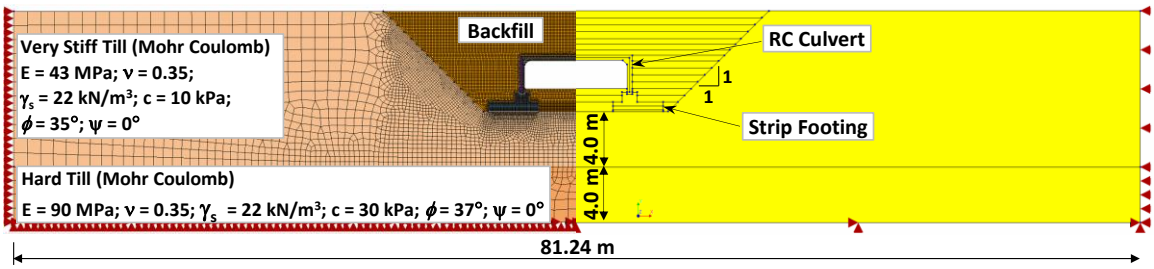

Figure 4-7. Geometry, boundary conditions, and meshing details of the 2D FE model.

4.3.1 Native and Backfill Soils

The behavior of the native clayey silt till was approximated by the elastic perfectly plastic Mohr-Coulomb material model. The empirical correlation proposed by Balachandran et al. (2015) to estimate the elastic modulus (E_s) of clayey silt till using SPT N-values, i.e., E_s = 1.67×N, was employed for both the very stiff and hard till layers, resulting in E_s values of 43 MPa and 90 MPa, respectively. The Mohr-Coulomb strength parameters (angle of internal friction, ϕ, and cohesion, c) were adopted from the ranges provided by Cao et al. (2015) for silty clay and clayey silt tills; ϕ ranges between 31° and 41°, and c ranges between 0 and 50 kPa. In accordance, ϕ of 35° and c of 10 kPa were assigned for the very stiff till layer, while ϕ of 37° and c of 30 kPa were assumed for the hard till layer as depicted in **Figure 4-7**.

It is important to account for the nonlinear stress-dependent stiffness of the backfill soil to ensure realistic prediction of applied earth pressures on buried structures. Thus, the hyperbolic model developed by Duncan and Chang (1970) was implemented to simulate the backfill soil behavior. Boscardin et al. (1990) performed an extensive laboratory testing on different backfill materials, e.g., well-graded sand. The particle size distributions of the SW used in backfilling the subject culvert and that tested by Boscardin et al. (1990) were very similar. Accordingly, the Duncan-Chang parameters reported by Boscardin et al. (1990) for SW compacted to 90% of the Standard Proctor density (SW-90) were assigned for the backfill material. The assigned parameters are as follow: modulus number (K) = 640, modulus exponent (n) = 0.43, failure ratio (R_f) = 0.75, Poisson's ratio (ν) = 0.3, angle of internal friction (ϕ) = 42°, cohesion (c) = 0.1 kPa, and unit weight (γ_s) = 23 kN/m^3.

4.3.2 Reinforced Concrete

The 2D FE models comprised two different RC parts, i.e., the strip footing and the culvert body. The strip footing is designed to remain in the elastic range, and nonlinearity of RC is not expected. Accordingly, the strip footing was assigned linear-elastic behavior in all developed models with an average 28-day compressive strength (f_c') of 40 MPa, elastic modulus (E_c) of 29.7 GPa (fib Model Code, 2010), and ν of 0.15.

The precast RC culvert had an average f_c' of 57 MPa. Linear-elastic behavior was assumed for the RC culvert in LEA model. An equivalent E_c of 35.5 GPa and ν of 0.15 were assigned. On the other hand, the total strain-based smeared crack model with fixed crack criteria was adopted in NLA model to simulate the culvert's nonlinear behavior and predict the formation of cracks. The compressive strain-softening behavior was simulated using the Thorenfeldt model (1987), and the Hordijk nonlinear model (1991) was used to represent the strain-softening behavior under tension loading. The smeared crack model parameters were estimated based on the formulae stipulated in the fib Model Code 2010 (2013) for normal weight concrete and are summarized in **Table 4-1**.

Table 4-1. Input parameters for the concrete smeared crack model in NLA model.

f_c' (MPa)	E_c (GPa)	Tensile strength f_{ct} (MPa)	Fracture energy G_f (Nmm/mm^2)	ν -
57.0	40.1	5.9	0.202	0.15

Embedded bar elements, which are fully bonded to the host elements, were utilized in NLA model to represent the steel reinforcement detailed in **Figure 4-1**. The mechanical behavior of the steel reinforcement was simulated using the von Mises plasticity model with yielding stress (f_y) of 450 MPa and Young's modulus (E_{st}) of 200 GPa. The steel hardening behavior was ignored in the analysis.

4.3.3 Interfaces

Line interface elements were introduced at the soil-footing, soil-culvert, and culvert-footing interfaces. The soil-footing interface comprised contact surfaces between the foundation soil and footing base (footing base interface) and the footing sides and sidefill material (footing sides interface). At the culvert-footing interface, the sidewall was secured in the strip footing keyway, then non-shrink grout was poured to fill in the voids between the keyway and sidewall. The friction behavior of the interface elements followed the Mohr-Coulomb yielding criterion and the displacement across the interface was governed by the defined normal and tangential stiffnesses, D_{nn} and D_{tt}, respectively. The interface properties were estimated according to the following formulae (TNO DIANA BV, 2016):

$$D_{tt} = \frac{A^2}{t}\frac{E_s}{2(1+\nu_s)} \quad ; \quad D_{nn} = f \times D_{tt}$$
$$c_{int} = A \times c \quad ; \quad \phi_{int} = A \times \phi \qquad \textbf{(4-1)}$$

where A is a reduction factor (0.67), f is a multiplication factor (50), t is the virtual thickness of the interface (10 mm), E_s is the soil Young's modulus, ν_s is the soil Poisson's ratio, c_{int} is the interface cohesion, and ϕ_{int} is the interface friction angle. The backfill soil properties were employed to estimate the interface properties at the soil-culvert and footing sides interfaces. The interface properties at the footing base interface were estimated using

the foundation soil properties, either very stiff till in the case of yielding foundation or rock in the case of non-yielding foundation. The grout properties reported by Samaiklang and Fuenkajorn (2013) for a cement grout with a compressive strength of 27.64 MPa, which is comparable with the 30 MPa of the grout used during construction, were used to determine the culvert-footing interface properties. The reported grout properties were: E = 3.56 GPa, ϕ = 40°, and c = 5.42 MPa (Samaiklang and Fuenkajorn, 2013).

4.3.4 Model Validation

The field data recorded by the SGs and PCs were utilized to validate the developed FE models (LEA and NLA). Representative values of contact earth pressures and strain values at 1.7 m of backfill were selected after the readings stabilized. The field measurements stabilized 2 days after reaching the 1.7 m of backfill, day 107, as presented in **Figure 4-5** and **Figure 4-6**. Accordingly, the average readings of pressure cells and strain gauges after day 107 were used in the comparison with the numerical results. **Figure 4-8** compares the measured and calculated earth pressures acting on the culvert surfaces as well as the values estimated based on the CHBDC (CSA, 2014) provisions for the two standard installations (B1 and B2 installations). The predicted vertical earth pressures on the top slab from LEA and NLA FE models almost coincided. The numerical models slightly underestimated the earth pressures on the top slab compared to the field measurements with a maximum difference of 12% at the far-right edge of the culvert; however, they demonstrated the same trend of the measured values. The earth pressure on the top slab was non-uniformly distributed with higher magnitudes at the stiffer edges compared to the relatively flexible mid-span. Similar findings were reported in previous studies on box culverts (Chen and Sun, 2014), arched culverts (McGrath et al., 2002), and TSCs (Chapter 6). The installation of the subject TSC followed the specifications listed in the CHBDC (CSA, 2014) for B1 installation, even though both the field measurements and analytical results in **Figure 4-8a** indicated that almost 80% of the top slab experienced earth pressures lower than the code values.

The calculated lateral earth pressures on the culvert sidewall agree well with the field measurements as presented in **Figure 4-8b**. There are some differences between the measured and calculated values due to the simplifications and assumptions in the numerical

analysis compared to the exact field conditions. The numerical results exhibited a parabolic distribution of the lateral earth pressure, which has been reported in previous studies on box culverts (Chen and Sun, 2014; Oshati et al., 2012). The differences between the estimated pressures from LEA and NLA models are trivial. Thus, it can be claimed that the consideration of RC nonlinear behavior for estimating the applied earth pressures on the buried structure at SLS is not essential and simplifying the analysis by defining a linear elastic behavior is sufficient at such level of loading. It can be recognized from **Figure 4-8b** that the measured and computed values of the lateral earth pressure almost lie within the bounds stipulated in the CHBDC (CSA, 2014) with minimum and maximum horizontal arching factors of 0.3 and 0.5 for B1 installation, respectively. Therefore, the load combinations considered in the design of these structures, which include the minimum and maximum values at separate combinations, are expected to cover the actual applied lateral earth loads experienced by the buried structure.

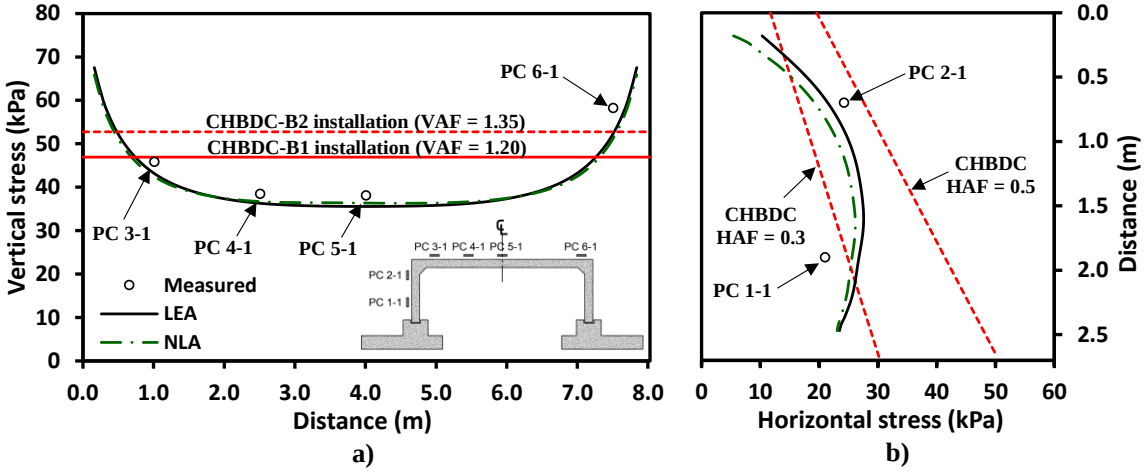

Figure 4-8. Comparison between measured and estimated pressures on the culvert surfaces at 1.7 m of backfill: a) vertical earth pressure on the top slab; and b) lateral earth pressure on the sidewall.

The measured tensile and compressive strains at each instrumented cross-section were utilized to further validate the FE models. Visual inspection of the culvert's inner surfaces did not show any signs of cracks, which was corroborated by the predictions of NLA model and the SG measurements that did not exceed the theoretical cracking strain (ε_{cr} = 133 με). Consequently, the analysis proceeded with the assumption of uncracked sections and the

bending moment (BM) at each cross-section was calculated using **Equation (4-2)** as follows:

$$BM = \frac{E_c . I_g . (\varepsilon_i - \varepsilon_e)}{d} \quad \textbf{(4-2)}$$

where I_g is the gross moment of inertia; ε_i and ε_e are the strains measured on the culvert's inner and outer surfaces, respectively; and d is the section depth. As per **Equation (4-2)**, the BM is considered positive when tensile stresses are located on the culvert's inner surface.

BM is not a direct output of either plane-stress or plane-strain elements. Consequently, composed line elements were implemented in LEA and NLA models to estimate the BM by integrating the induced internal stresses in the plane-stress elements of the culvert body in post-processing of analysis results (TNO DIANA BV, 2016).

Figure 4-9 displays the computed BMs from the SGs measurements and those numerically computed from LEA and NLA models. Additionally, a FE plane frame analysis was conducted using SAP 2000 (2020) in which the measured earth pressures presented in **Figure 4-8** were utilized. The base connection of the sidewall was assumed to be hinged in the plane frame analysis, as typically assumed in the current design practice. The results indicated excellent match between the BMs estimated from the SGs and PCs measurements, which confirm the integrity of the monitoring system. **Figure 4-9a** shows that the computed BMs across the top slab from NLA model were in better agreement with that estimated from the field measurements compared to LEA model, which slightly overpredicted the BM at the mid-span. On the other hand, LEA model results better matched the estimated BM from the SGs data along the sidewall as depicted in **Figure 4-9b**. Consequently, it can be interpreted that the BM magnitudes from LEA would lead to a conservative design.

The BM distribution along the sidewall obtained from the plane frame analysis exhibited zero BM at the base of the sidewall as depicted in **Figure 4-9b**. This output is attributed to the definition of a hinged condition at the base of the sidewall. Conversely, the SGs

measurements and numerical results indicated non-zero BM at the sidewall base. Similar observations were reported by Ramadan and El Naggar (2021) as will be discussed in Chapter 6. They attributed this BM at the base to the rotation of the strip footing along with the connection condition at the base, which results in additional stresses in the enclosed depth of the sidewall in the strip footing keyway, thus, the development of BM at the base. This explanation will be furtherly inspected in the following subsection.

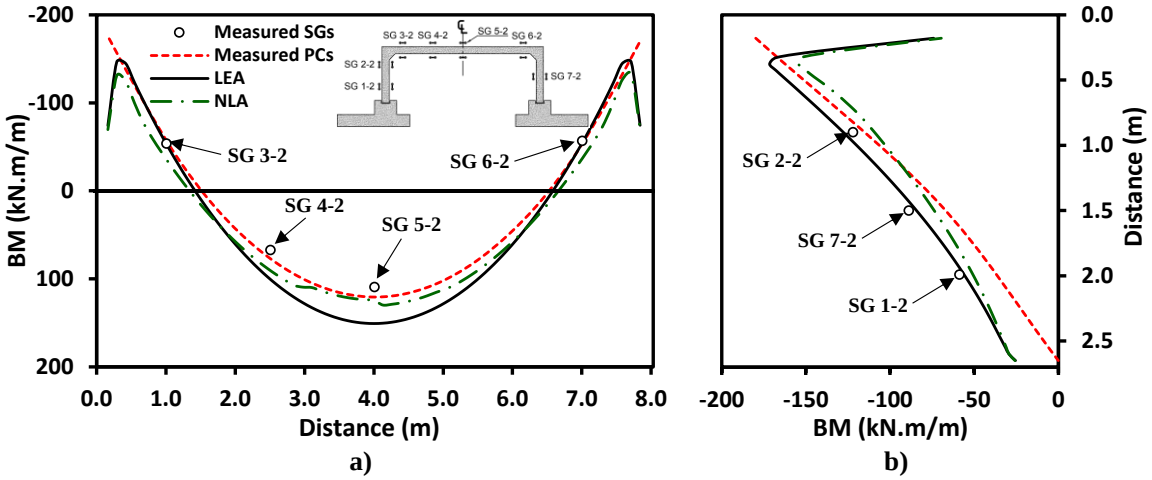

Figure 4-9. Comparison between measured and estimated bending moments at 1.7 m of backfill: a) top slab; and b) sidewall.

4.3.5 Effect of Foundation Soil Condition

The LEA numerical model, which was validated for the analysis at service loading conditions, was utilized to conduct a parametric study to elaborate on the influence of the foundation soil condition, either yielding or non-yielding, on the applied earth pressures on TSCs, stress distribution underneath the strip footing, and the induced straining actions in the culvert body. The FE model for yielding foundation was denoted LEA-Y and that for non-yielding foundation was denoted LEA-NY. The existing native till layer represented the case of yielding foundation, while rock was assumed for the non-yielding foundation case. The behavior of the competent rock was simulated using the Mohr-Coulomb material model and the assigned properties were adopted from Yoo et al. (2005); listed as follows: E_s = 34.3 GPa, $\nu = 0.25$, ϕ = 0°, and c = 6.9 MPa.

Figure 4-10 shows the applied earth pressures on the culvert surface and the lateral deflections of the sidewall for both conditions of yielding and non-yielding foundation soils at 3.2 m of cover depth. The computed earth pressure distributions on the top slab displayed in **Figure 4-10a** show insignificant influence of the subsurface condition, where both LEA-Y and LEA-NY models almost exhibited similar earth pressures. This contradicts with the findings of Kim and Yoo (2005) in their study on box culverts, which stated that the applied earth pressures on the top slab were much higher for the case of non-yielding foundation compared to the case of yielding foundation. Similar to the results obtained at 1.7 m of backfill, the majority of the top slab is expected to experience earth pressures lower than the code value for B1 installation as shown in **Figure 4-10a**. The effect of the foundation soil properties on the lateral earth pressure applied on the sidewall is shown to be significant in **Figure 4-10b**. Although the sidewall lateral deflection towards the sidefill material was much higher in the case of yielding foundation soil compared to the case of non-yielding foundation as elaborated in **Figure 4-10c**, higher lateral earth pressures were computed for the case of non-yielding foundation with values at the base of the sidewall being the only exception. This is attributed to the higher confinement of the compacted sidefill material when surrounded by rock as opposed to the yielding native soil. It can also be noticed from **Figure 4-10b** that the computed lateral earth pressures in LEA-Y and LEA-NY models almost fall within the bounding values of the CHBDC (CSA, 2014). The stress distributions underneath the strip footing for the cases of yielding and non-yielding foundations are presented in **Figure 4-11a**. The results show that the stresses are almost uniform in the case of non-yielding foundation, where it varies between 170 kPa at the backfill side and 203 kPa at the waterside. On the other hand, the stresses are almost uniform over 70% of the strip footing in the case of yielding foundation, with an average value of 181 kPa, then significantly increases to a maximum value of 273 kPa over the remaining 30% on the waterside. Generally, higher stresses are expected at the waterside for both cases of yielding and non-yielding foundations.

Figure 4-11b shows the BM distribution along the sidewall. The results of the developed BM at the sidewall base indicate that BM develops due to the rotation of the strip footing; the BM developed at the sidewall base for the case of yielding foundation but did not develop for the case of non-yielding foundation, in which the rotation of the footing is

restrained. Therefore, the assumption of pure hinged condition, usually considered in the current design practice of TSCs, is realistic for the case non-yielding foundation. However, for yielding foundation, *BM* develops due to the rotation of the strip footing and should be accounted for in the design.

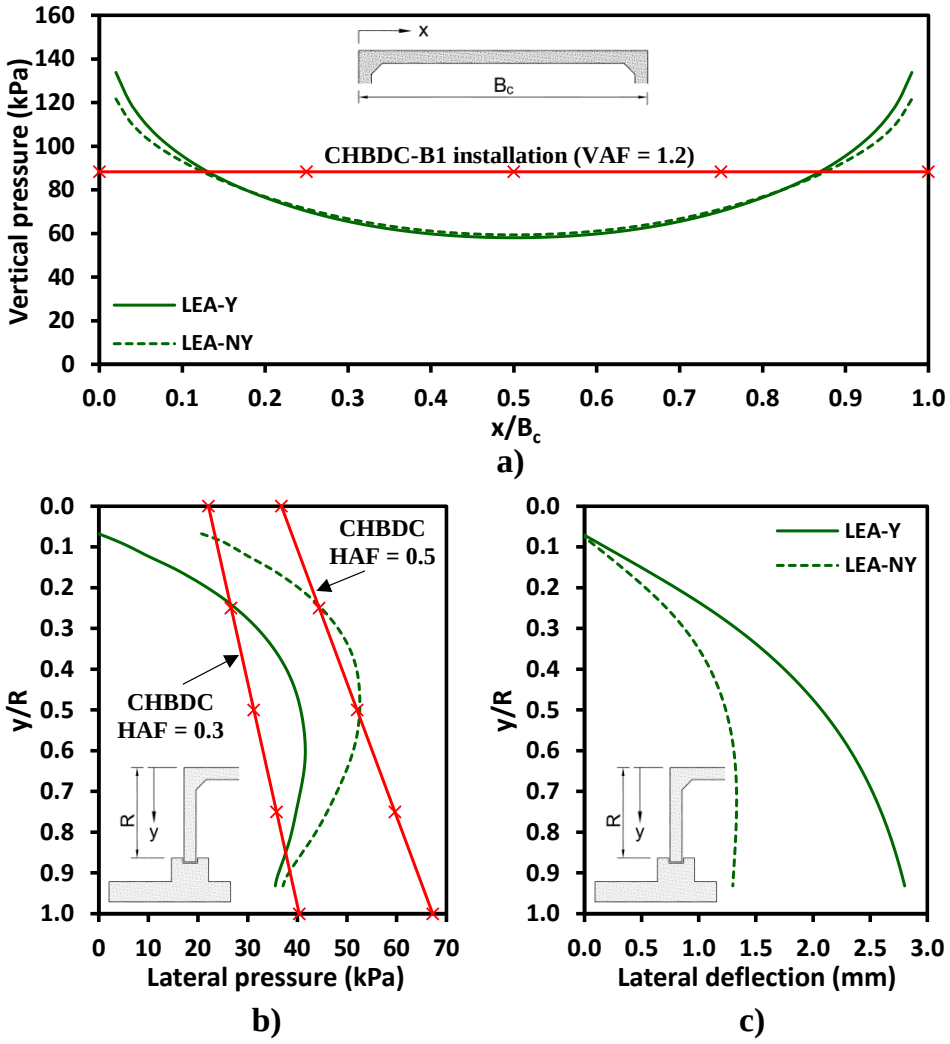

Figure 4-10. Effect of foundation soil condition on the applied earth pressure and sidewall deflection at 3.2 m of backfill: a) vertical pressure on the top slab; b) lateral pressure on the sidewall; and c) lateral deflection of the sidewall.

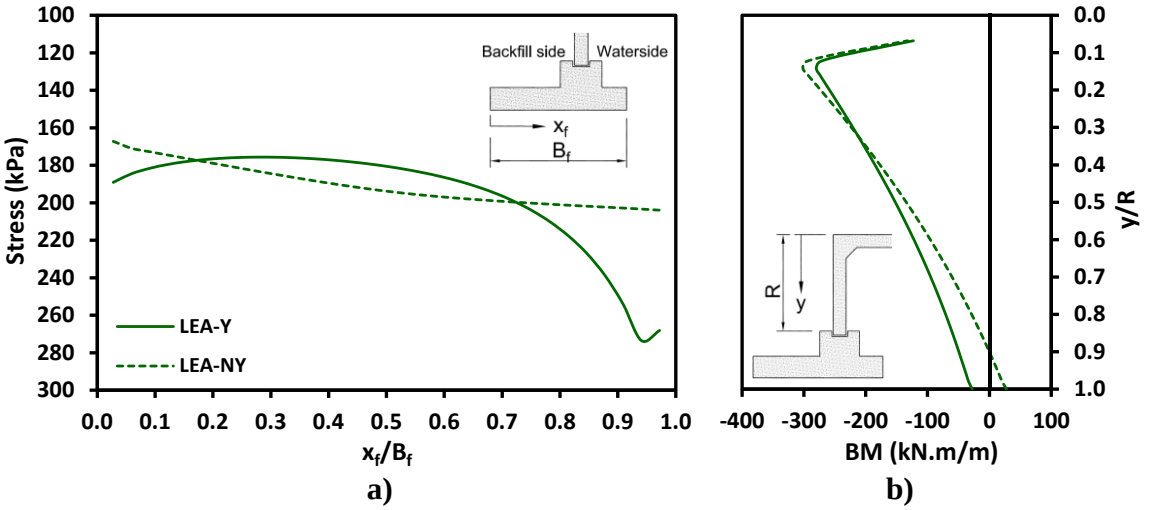

Figure 4-11. Effect of foundation soil condition at 3.2 m of backfill: a) stresses underneath the footing; and b) bending moment along the sidewall.

4.4 Numerical Model – Ultimate Limit State (ULS)

The ultimate capacity of an 11.0-m-span RC Con/Span has been experimentally measured through load testing one precast unit to failure by Marshall et al. (2014). The results of the load test were utilized to validate a three-dimensional (3D) FE model, which was then used to predict the ultimate capacity of the precast units used in constructing the TSC analyzed in this study. Moreover, the 2D numerical models discussed above were modified to evaluate the structural performance and soil-structure interaction mechanism at the ultimate limit state (ULS) for yielding and non-yielding foundations.

4.4.1 Capacity of Precast Units

Marshall et al. (2014) load tested an 11.0-m-span precast unit with a mid-span height of 2.7 m and 1.2 m in width. The precast unit rested on rigid floor and was restrained from lateral movement at the base of its sidewalls. Loading was applied incrementally on the top slab of the Con/Span through three W8×35 beams spanning the width of the precast unit as shown in **Figure 4-12a**. Each load increment was 17.8 kN/beam until the maximum load was reached. The concrete compressive strength, f_c', was 48.5 MPa and the elastic modulus, E_c, was 28.3 GPa. The yielding strength of steel rebars, f_y, was 507 and 642 MPa depending on the size of bars, and their elastic modulus, E_{st}, was 182.7 GPa (Marshall et al., 2014).

A 3D FE model was developed for the Con/Span with the same reported geometry, concrete and steel properties, steel reinforcement, and loading configuration. The precast unit was discretized using 20-node soil brick elements and the steel rebars were simulated using embedded elements. Similar to NLA model previously described, smeared crack material model was used for the concrete and von Mises plasticity model was used for the reinforcing steel. The precast unit was fixed from vertical movement at its base and horizontal movement at the outer edge of the sidewall base as shown in **Figure 4-12a**. Vertical stresses were applied at the loading beams locations along the precast unit width in increments of 71.7 kPa (i.e., corresponding to 17.8 kN load increment applied to the contact surface of loading beams, 1.2 x 0.204 m^2). The same analysis procedure was repeated on the precast unit of the subject TSC, as shown in **Figure 4-12b**, with the same geometry and reinforcement details as in **Figure 4-1**. Moreover, the material properties of concrete and steel reinforcement were the same as in the 2D NLA model.

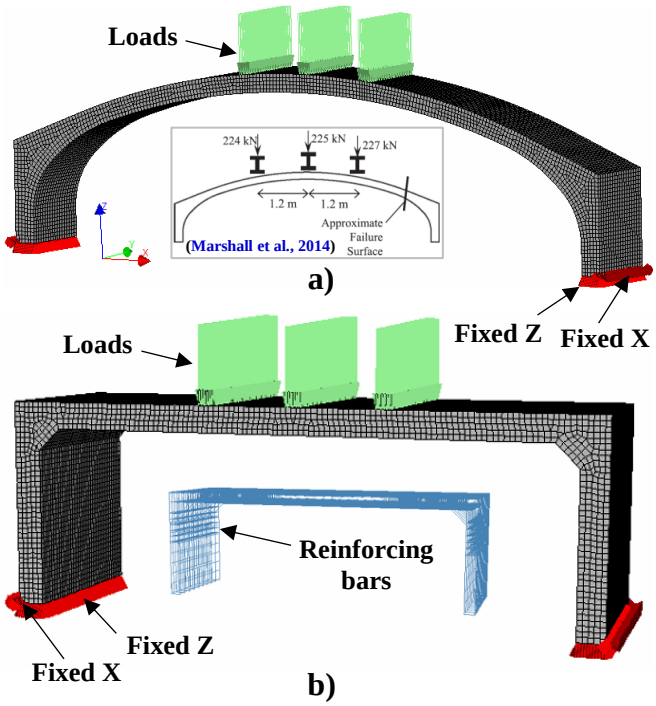

Figure 4-12. Overview of the 3D FE models: a) TSC with arched top slab; and b) Remembrance TSC.

The 3D model of the Con/Span precast unit was validated by comparing its predictions with the measured load-deflection curves at the mid-span and the top corner of the sidewall

as shown in **Figure 4-13a**. Downward vertical deflection at the mid-span and outward lateral deflection at the corner are considered positive. As can be observed from **Figure 4-13a**, the measured and calculated ultimate load capacity of the precast unit agree well, where a value of 675.7 kN was measured and 673.0 kN was predicted by the FE model. Nevertheless, the computed vertical deflection at the mid-span that corresponds to the ultimate load (90.5 mm) was much lower than the measured 150 mm. Assuming full bond between the concrete and steel bars as well as the stress-locking behavior that occurs in displacement-based FE analyses with smeared softening approach (Rots and Blaauwendraad, 1989) might explain the calculated stiffer behavior. The computed outward lateral deflection at the top corner of the sidewall matched well with the measured values throughout the whole loading stages.

The ductility factor (μ) was evaluated from the load-deflection curves at the mid-span as the ratio between the ultimate displacement (Δ_{ult}), corresponding to the ultimate load, and the yield displacement (Δ_y), corresponding to the development of 75% of the ultimate capacity. The μ values obtained from the experiment data and FE model are 1.71 and 1.89, respectively.

Figure 4-13b shows the deformed shape and cracks pattern predicted by the 3D model. The numerical model predicted yielding of the steel reinforcement at three different locations leading to the formation of plastic hinges as presented in **Figure 4-13b**. This explains the increase of vertical deflection at the mid-span without remarkable increase in the load prior to failure. Interestingly, Marshall et al. (2014) reported yielding of the steel reinforcement at the failure surface, almost located at plastic hinge-A shown in **Figure 4-13b**, before the concrete crushed. Additionally, Beach (1988) reported the formation of three-plastic hinges in his testing program of a Con/Span culvert. The three plastic hinges occurred at the same locations predicted by the 3D numerical model presented in **Figure 4-13b**.

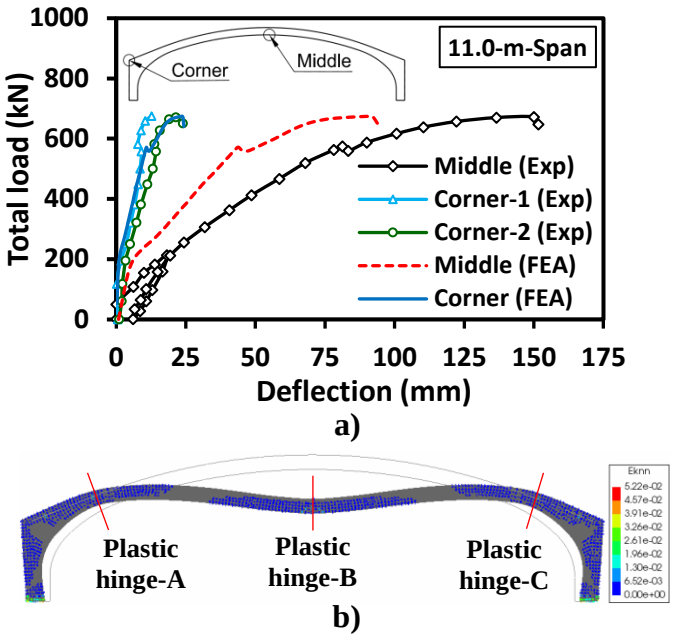

Figure 4-13. Arched TSC results: a) load-deflection curves; and b) deformed shape and crack pattern. (Magnification × 10)

The load-deflection curve, deformed shape, and crack pattern of the test TSC are displayed in **Figure 4-14**. A brittle behavior can be noted from the load-deflection curve at the mid-span; **Figure 4-14a** shows that crushing of concrete occurred at failure while steel reinforcement did not reach its yield strength. This results in a low vertical deflection at the ultimate load; 20.9 mm. Moreover, the estimated μ is 1.38, which is 37% lower than the estimated value for the Con/Span indicating the lower ductility of the subject TSC compared to arched top culvert. The top corner of the sidewall experienced negligible lateral movement up to failure as shown in **Figure 4-14a**. Failure of the subject TSC is predicted just below the culvert haunch at the top corner of the sidewall, where the highest concrete crack strain is anticipated as depicted in **Figure 4-14b**. Such findings agree with the predicted failure surface of a box culvert under high embankment by Pimentel et al. (2009).

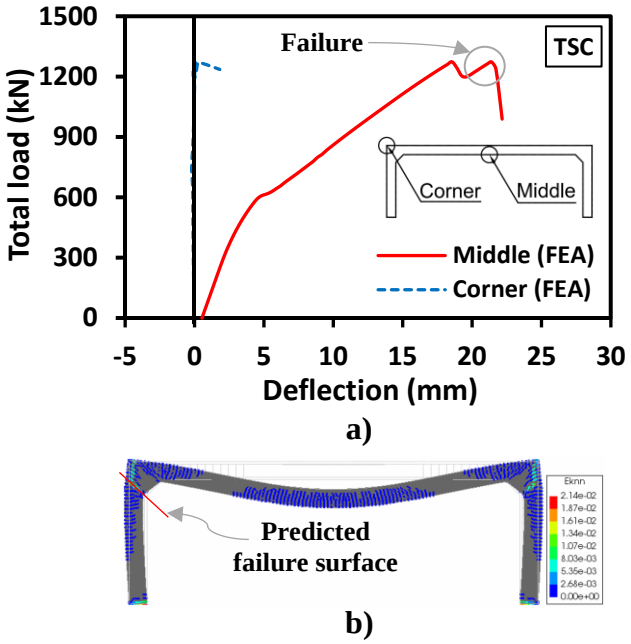

Figure 4-14. Remembrance culvert results: a) load-deflection curves; and b) deformed shape and crack pattern. (Magnification × 25)

4.4.2 Effect of Precast Unit Width

Precast RC units are produced in widths varying between 1.0 and 2.4 m. The width (W) of the precast unit is governed by many factors, including: 1) total length of the culvert, 2) size and delivery vehicle payloads restrictions on major roads, and 3) handling loads and lifting equipment limits. This section discusses the influence of the precast unit width on its ultimate capacity, ductility, and failure mechanism. A parametric study was conducted employing 3D nonlinear FE models considering four different precast unit widths: 1.0, 1.5, 2.0, and 2.4 m. The four FE models had the same boundary conditions and loading configuration as that presented in **Figure 4-12**. Additionally, the steel reinforcement per meter width was kept the same in the longitudinal and transversal directions.

Figure 4-15a displays the calculated vertical load-deflection relations at the mid-span. The results demonstrate the expected increase of ultimate capacity as the unit width increases. However, the peak load seems to occur at higher deflection levels for smaller unit widths as summarized in **Table 4-2**. To benchmark the results against each other, the total load was normalized by the corresponding unit width. The normalized load-deflection curves are presented in **Figure 4-15b**. It is noted from **Figure 4-15b** that the initial linear behavior

is identical for the four cases up to a load of 180 kN/m, beyond which stiffness degrades due to the formation of cracks. **Figure 4-15b** demonstrates that the ultimate load capacity per unit width and the corresponding deflection increase as the precast unit width decreases. In terms of ductility, **Table 4-2** provides a summary of the results for all four cases. The results suggest minimal influence of the precast unit width on the ductility with a maximum variation of 5% between the considered widths. Eventually, the precast unit width has no influence on either the failure mechanism or the predicted failure surface.

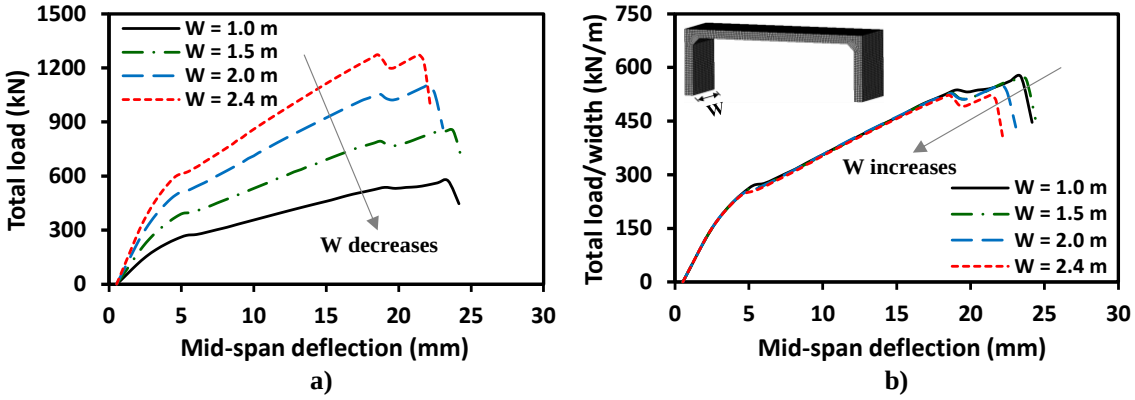

Figure 4-15. Effect of precast unit width: a) total load; and b) total load/unit width.

Table 4-2. Results summary of the 3D nonlinear models.

Precast unit	Ultimate load (kN)	Ultimate load/unit width (kN/m)	Δ_{ult} (mm)	Δ_y (mm)	Ductility, μ
Arched TSC (Exp)	675.7	563.1	150.0	87.8	1.71
Arched TSC (FEA)	672.0	560.0	91.1	48.1	1.89
TSC (W = 2.4 m)	1273.0	530.4	20.9	15.2	1.38
TSC (W = 2.0 m)	1104.5	552.3	21.6	16.1	1.34
TSC (W = 1.5 m)	858.0	572.0	23.1	17.3	1.34
TSC (W = 1.0 m)	581.0	581.0	22.9	17.5	1.31

4.4.3 Backfill Height at Failure

The investigated TSC was designed for a total backfill height of 3.2 m. The maximum backfill height at which the TSC would fail has been predicted employing the validated

numerical models and extending the backfill height to 10.0 m. The influence of the concrete nonlinear behavior and the subsurface condition (yielding and non-yielding) on the maximum height at failure were investigated.

Figure 4-16 displays the vertical load-deflection curve at the mid-span and the lateral load-deflection curves at the corner and mid-height of the sidewall (denoted as Side-M). As expected, the linear-elastic model, LEA model, exhibited linear load-deflection curves up to 10.0 m of backfill. Conversely, NLA model demonstrated stiffness degradation and higher deflections at the mid-span beyond 3.6 m of backfill height due to the formation of cracks. For the case of yielding foundation, presented in **Figure 4-16a**, failure is expected to occur at a backfill height of 9.2 m, which is 2.8 times the design backfill height. Ductile failure is expected for the TSC at the 9.2 m of backfill, where yielding of the steel reinforcement occurred prior to failure resulting in noticeable increase in the culvert deflection with minimal increase in the backfill height. This failure mechanism is an inverse of the predicted brittle mode of failure under the laboratory loading configuration previously discussed. Such improvement in the structural performance of the RC culvert can be attributed to the confinement provided by the surrounding soil, which agrees with previous findings on box culverts (Moradi et al., 2016; Marshall et al., 2014; Zoghi and Farhey, 2006).

Similar observations can be interpreted for the case of non-yielding foundation from **Figure 4-16b**. However, failure is expected to occur at a lower backfill height, 8.6 m, and lower vertical and lateral deflections are estimated compared to the case of yielding foundation. For instance, the maximum mid-span vertical deflections at failure are 27.6 and 21.6 mm for yielding and non-yielding foundations, respectively.

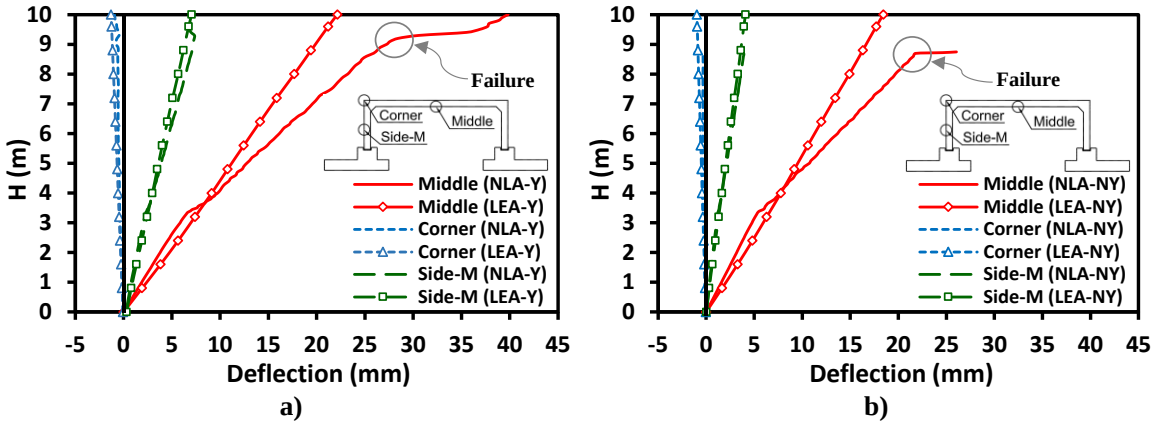

Figure 4-16. Deflection of the TSC at different backfill heights: a) yielding soil; and b) non-yielding soil.

4.5 Conclusions

Field data obtained from an instrumented 7.3-m-span TSC covered with 1.7 m of well-graded sand were presented and discussed. The recorded pressure cells' and strain gauges' measurements were employed to validate 2D FE models, which were then utilized to evaluate the effect of nonlinear behavior of RC on the culvert's structural performance and soil-structure interaction mechanism. The validated models were used to investigate the effect of foundation soil condition (yielding or non-yielding) on the culvert behavior. Moreover, experimental data of a Con/Span precast unit loaded to failure was utilized to validate a 3D finite element model and investigate the structural performance of the subject TSC at ultimate limit state. The 3D model was replicated for the test TSC and the influence of the precast unit width was investigated. Eventually, the 2D FE analysis was extended to predict the maximum backfill height at which failure of the TSC is expected for the cases of yielding and non-yielding foundations. The following conclusions can be drawn from the conducted analyses:

1. For the studied TSC, the vertical earth pressure is non-uniformly distributed along the top slab with 80% of the top slab experiencing earth pressures lower than the value specified in the CHBDC (CSA, 2014) for B1 standard installation. On the other hand, the measured and estimated lateral earth pressures along the sidewall fell within the minimum and maximum bounds of the code for the same standard installation method.

2. Bending moment was developed at the base of the sidewall due to the footing rotation for yielding foundation, while negligible bending moment was estimated at the base for the case of non-yielding foundation. Thus, the assumption of hinged support at the base is suitable for the case of non-yielding foundation. However, bending moment develops at the sidewall base for yielding foundation condition and should be considered in design.

3. The concrete behavior can be simulated by the linear-elastic material model to reasonably estimate the applied earth pressures on TSCs at service loading conditions.

4. The foundation soil condition has negligible effect on the estimated vertical earth pressure on the top slab. However, the estimated lateral earth pressure on the sidewall was much higher for the case of non-yielding foundation compared to the case of yielding foundation.

5. The precast unit width has no influence on the ductility, failure mechanism, or predicted failure surface. However, the ultimate load capacity per unit width and the corresponding mid-span vertical deflection increase as the unit width decreases.

6. The subject TSC is expected to exhibit ductile failure as the backfill height increases to 9.2 m in case of yielding foundation and backfill height of 8.6 m in case of non-yielding foundation. Moreover, the estimated maximum mid-span deflection at failure is higher in case of yielding foundation as opposed to the non-yielding foundation.

4.6 References

1. Balachandran, K., Liu, J., Cao, L., and Peaker, S. (2015). Statistical correlations between pressuremeter modulus and SPT N-value for glacial tills. In *Proc., 68th Canadian Geotechnical Conf. and 7th Canadian Permafrost Conf*. Richmond, BC, Canada: Canadian Geotechnical Society.

2. Beach, T. J. (1988). *Load test report and evaluation of a precast concrete arch culvert*. Transportation Research Record 1191, Transportation Research Board, Washington, DC, 12–21.

3. Boscardin, M. D., Selig, E. T., Lin, R. S., and Yang, G. R. (1990). Hyperbolic parameters for compacted soils. *Journal of Geotechnical Engineering*, 116 (1), 88-104.

4. Cao, L., Liu, J., Peaker, S. and Ahmad, S. (2015). Engineering characteristics of glacial tills in GTA. In *Proc., 68th Canadian Geotechnical Conference and 7th Canadian Permafrost Conference*, Quebec.

5. Chen, B., and Sun, L. (2014). Performance of a reinforced concrete box culvert installed in trapezoidal trenches. *Journal of Bridge Engineering,* 19 (1), 120–130. https://doi.org/10.1061/(ASCE)BE.1943-5592.0000494.

6. CSA (Canadian Standards Association). 2014. *Canadian highway bridge design code*. CAN/CSA-S6-14. Mississauga, ON, Canada: CSA.

7. CSA (Canadian Standards Association). 2014. *Design of concrete structures (A23.3-14)*. CSA Group, Mississauga, Ontario.

8. CSI (Computers and Structures, Inc.). 2020. *SAP2000 integrated software for structural analysis and design*. Berkeley, California: CSI.

9. Dasgupta, A., and Sengupta, B. (1991). Large scale model test on square box culvert backfilled with sand. *Journal of Geotechnical and Geoenvironmental Engineering*, 117 (1), 156–161. 10.1061/(ASCE)0733-9410 (1991) 117:1(156)

10. Duncan, J. M., and Chang. C. Y. (1970). Nonlinear analysis of stress and strain in soils. *Journal of Soil Mechanics and Foundations Division*, 96 (5),1629–1653.

11. Hordijk, D. A. (1991). Local approach to fatigue of concrete. Doctor of Philosophy, Ph.D. dissertation, Delft University of Technology, Delft, The Netherlands.

12. International Federation for Structural Concrete. (2013). "Fib model code for concrete structures 2010." Berlin: Verlag Ernst & Sohn.

13. Kim, K., and Yoo, C. H. (2005). Design loading for deeply buried box culverts. *Journal of Geotechnical and Geoenvironmental Engineering*, 131 (1), 20–27.

14. Marshall, J. D., Anderson, J. B., Meadows, R. L., and Jensen, T. J. (2014). Full-scale testing of three-sided precast concrete arch sections. *Journal of Bridge Engineering*, 19 (12), 04014051. 10.1061/(ASCE)BE.1943-5592.0000630.

15. McGrath, T. J., Moore, I. D., Selig, E. T., Webb, M. C., and Taleb, B. (2002). *Recommend specifications for large-span culverts.* Report No. 473. Washington, DC: Transportation Research Board.

16. McGrath, T. J., Selig, E. T., and Beach, T. J. (1996). Structural behavior of three-sided arch span bridge. *Transportation Research Record 1541*, Transportation Research Record, Washington, DC, 112–119.

17. Moradi, M., Valipour, H., and Foster, S. (2016). Reserve of strength in inverted u-shaped RC culverts: effect of backfill on ultimate load capacity and fatigue life. *Journal of Bridge Engineering*, 21 (2), 04015051. 10.1061/(ASCE)BE.1943-5592.0000800

18. MTO (Ministry of Transportation of Ontario). 2010. Construction Specification for Excavating and Backfilling-Structures. Ontario Provincial Standard Specification OPSS 902. ON, Canada: MTO.

19. MTO (Ministry of Transportation of Ontario). 2010. *Frost Penetration Depths for Southern Ontario*. Ontario Provincial Standard Drawing OPSD 3090. ON, Canada: MTO.

20. Oshati, O.S., Valsangkar, A.J., and Schriver, A.B. (2012). Performance of two cast-in-place box culverts under high embankments. *Canadian Geotechnical Journal*, 49 (12), 1331–1346. 10.1139/t2012-094

21. Oswald, C. J. (1996). Analysis of reinforced concrete culvert considering concrete creep and shrinkage. *Transportation Research Record 1541*, TRB. National Research Council. Washington, DC, 120–126.

22. Pimentel, M., Costa, P., Félix, C., and Figueiras, J. (2009). Behavior of reinforced concrete box culverts under high embankments. *Journal of Structural Engineering*, 135 (4), 366-375. 10.1061/(ASCE)0733-9445(2009)135:4(366), 366–375

23. Ramadan, S. H., and El Naggar, M. H. (2021). Field monitoring and numerical analysis of a large-span three-sided reinforced concrete culvert. *Journal of Geotechnical and Geoenvironmental Engineering*, 147 (4), 04021008. 10.1061/(ASCE)GT.1943-5606.0002489

24. Rots, J. G., Blaauwendraad, J. (1989). Crack models for concrete: discrete or smeared? Fixed, multi-directional or rotating? *Heron*, 34 (1), 5–55.

25. Samaiklang, W., and Fuenkajorn, K. (2013). Mechanical and hydraulic performance of cement grouts from 5 suppliers in Thailand. In *Proc., of the Second Thailand Symposium on Rock Mechanics* (ThaiRock 2013), Im Poo Hill Resort, Nakhonratchasima, 333–342.

26. Thorenfeldt, E., Thomaszewic, A., and Jensen, J. J. (1987). 'Mechanical properties of high-strength concrete and applications in design. In *Proc., Symp. on Utilization of High-Strength Concrete*, Tapir Publishers, Stavanger, Norway, 149–159.

27. TNO Diana BV. 2016. *DIANA—User's manual: Material library*. Delft, Netherlands: TNO Diana BV.

28. Von Handorf, J. J. (2004). Clear-span culverts: Economical designs. Better Roads, Feb. 2004.

29. Yoo, C. H., Parker, F., and Kang, J. (2005). *Bedding and fill heights for concrete roadway pipe and box culverts*. Final Report, ALDOT Project No. 930-592, Highway Research Center, Auburn Uni., AL.

30. Zoghi, M., and Farhey, D. N. (2006). Performance assessment of a precast concrete, buried, small arch bridge. *Journal of Performance of Constructed Facilities*, 20 (3), 244–252. 10.1061/(ASCE)0887 3828(2006)20:3(244).

Chapter 5

* Class-A Prediction of Three-sided Reinforced Concrete Culverts

5.1 Introduction

Reinforced concrete (RC) three-sided culverts (TSCs) with flat top slab provide an economical alternative for short-span bridges (Marshall et al., 2014). They are produced in large spans up to 16.0 m to provide large hydraulic openings for watercourse crossings under roadways. Water flows in TSCs in its natural course, hence, has minimal impact on the marine environment. Thus, TSCs are more attractive from the environmental perspective than culverts with closed-bottom geometries, like box and pipe culverts. However, the structural performance of RC TSCs has not been investigated sufficiently to date.

The Canadian Highway Bridge Design Code, CHBDC, (CSA, 2014) defines two standard installation methods (B1 and B2) for RC box culverts. For the same type of backfill material in the sidefill and bedding zones, higher compaction requirements are specified for B1 standard installation compared to B2 standard installation. Moreover, some low quality backfill materials with more than 20% of fine grained soils, e.g., silty clay, are allowed to be used in B2 standard installation but not in B1 standard installation.

Numerous field studies on RC box culverts can be found in the literature (Bennett et al., 2005; Chen and Sun, 2014; Chen et al., 2010). On the other hand, field studies on large-span RC culverts are limited to arch culverts (Marshall et al., 2014; McGrath et al., 2002; Zoghi and Farhey, 2006), and only two studies were reported on TSCs, which were presented in Chapter 3 and Chapter 4. Ramadan and El Naggar (2021), i.e., Chapter 4, investigated the performance of a 7.3-m-span TSC designed for a total backfill height of 3.2 m and conducted numerical analyses at serviceability and ultimate limit states. However, the field data was only available for 1.7 m of backfill at the time they developed

---

* A version of this chapter has been accepted in Journal of Structure and Infrastructure Engineering.

the numerical models. Nonetheless, their serviceability limit state analysis predicted the applied earth pressures on the culvert body and its structural performance at 3.2 m of backfill.

This chapter presents comparisons between the predicted numerical results from the preliminary analysis and the field measurements after construction completion of a 10.4-m-span TSC. Moreover, field data of a 7.3-m-span TSC up to the final backfill height (3.2 m) are presented and compared with the numerical predictions reported in Chapter 4. Finally, the results of a parametric study conducted to investigate the effect of strip footing geometry on the applied earth pressures on TSCs for the cases of yielding and non-yielding foundation soil conditions are discussed.

5.2 Projects Description

This project involved field monitoring of three precast RC TSCs designated Remembrance, Pickering, and Oshawa culverts, with spans of 7.3, 10.4, and 13.5 m, respectively. The test culverts were constructed in the Greater Toronto Area, Ontario, Canada. This chapter focusses on Pickering and Remembrance culverts.

The Pickering culvert had a span of 10.4 m and a clear rise of 1.4 m. The sidewalls and top slab had a thickness of 0.46 m, and the pavement grade elevation was 3.1 m above the top slab. The culvert was founded on a 3.8-m-wide strip footing with a thickness of 0.9 m with no pedestals. The soil profile at the Pickering culvert site was mainly composed of sandy silt till based on the conducted site investigation. The sandy silt till layer was dense to very dense below the foundation level with SPT N- values between 25 and 100 as illustrated in **Figure 5-1a**. The installation of the Pickering culvert represented the case of zero projection installation, where the natural ground surface and the top slab were almost at the same elevation.

The Remembrance culvert was a 7.3-m-span TSC with a total rise of 2.4 m. The sidewalls and top slab were 0.36-m-thick. The total backfill height was designed to be 3.2 m from the culvert top slab to the final road grade. The culvert was founded on a 0.6-m-thick and 3.6-m-wide strip footing with a 0.7-m-thick RC pedestal. The native subsurface soil at the

Remembrance culvert site consisted of silty clay to clayey silt till with occasional boulder sizes. Based on the measured SPT N-values at and below the foundation level, which increased from 26 to 55 as depicted in **Figure 5-1b**, the native soil had a stiff to hard consistency. The Remembrance culvert installation represented the case of trench installation. **Figure 5-2** displays the geometry and reinforcement details of Pickering and Remembrance culverts.

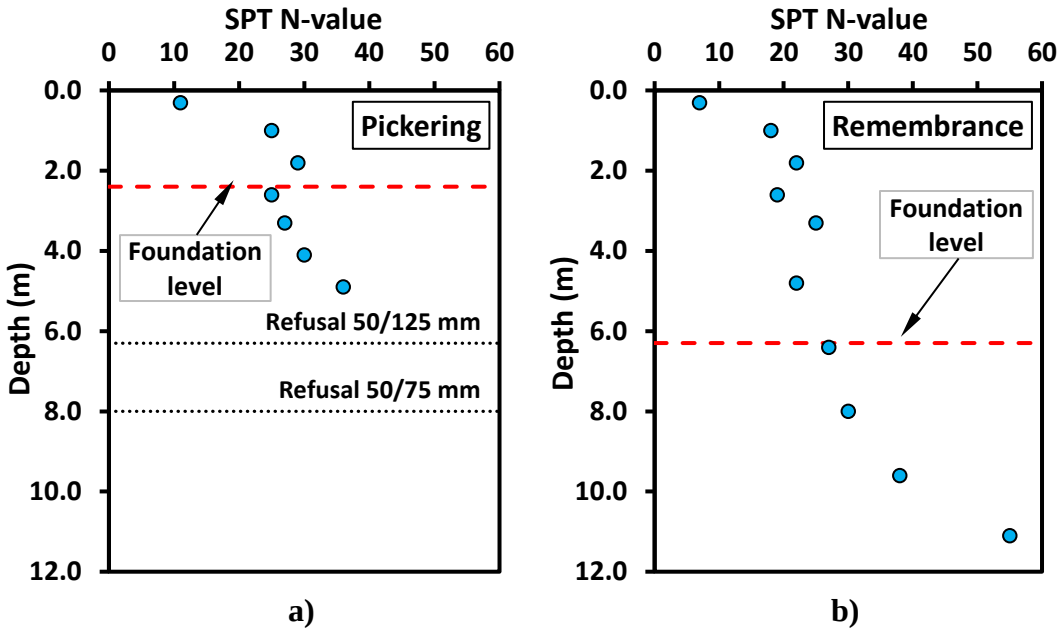

Figure 5-1 Variation of SPT N-value with depth: a) Pickering culvert; and b) Remembrance culvert.

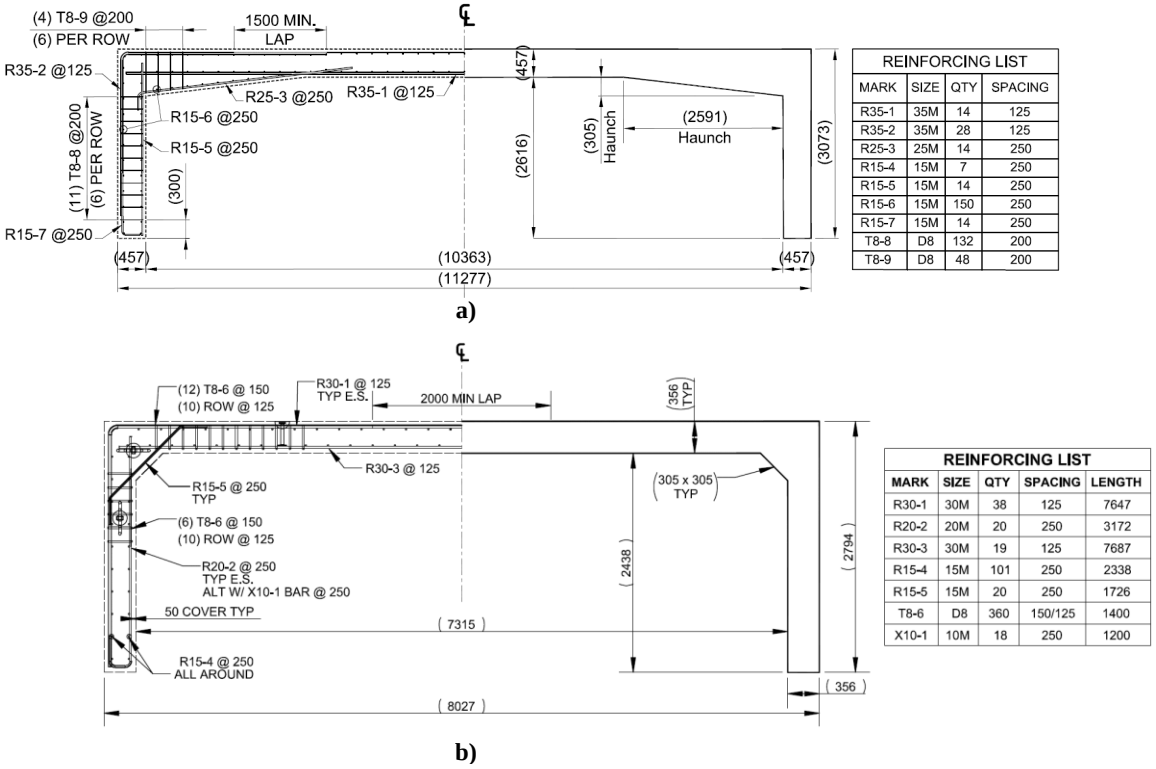

REINFORCING LIST			
MARK	SIZE	QTY	SPACING
R35-1	35M	14	125
R35-2	35M	28	125
R25-3	25M	14	250
R15-4	15M	7	250
R15-5	15M	14	250
R15-6	15M	150	250
R15-7	15M	14	250
T8-8	D8	132	200
T8-9	D8	48	200

REINFORCING LIST				
MARK	SIZE	QTY	SPACING	LENGTH
R30-1	30M	38	125	7647
R20-2	20M	20	250	3172
R30-3	30M	19	125	7687
R15-4	15M	101	250	2338
R15-5	15M	20	250	1726
T8-6	D8	360	150/125	1400
X10-1	10M	18	250	1200

Figure 5-2 Geometry and reinforcement details: a) Pickering culvert; and b) Remembrance culvert. (Not to scale)

5.3 Three-Sided Culvert System

The subject TSCs were constructed of precast RC units bearing on keyed cast-in-place strip footings as presented in Error! Reference source not found.. TSCs are characterized by their relatively large spans and absence of bottom slab compared to RC box culverts. Cast-in-place strip footings were constructed in the three projects. The RC precast units were installed along the footing keyway and were leveled and secured from lateral movement using plastic shim as depicted in Error! Reference source not found.. Once the precast units were in place, the footing keyway was filled with non-shrink grout having a compressive strength of 30 MPa. Eventually, backfilling was completed against the assembled structure in lifts no greater than 0.3 m up to the final grade level. This construction sequence was replicated in the numerical model to ensure realistic simulation of the soil-structure interaction problem.

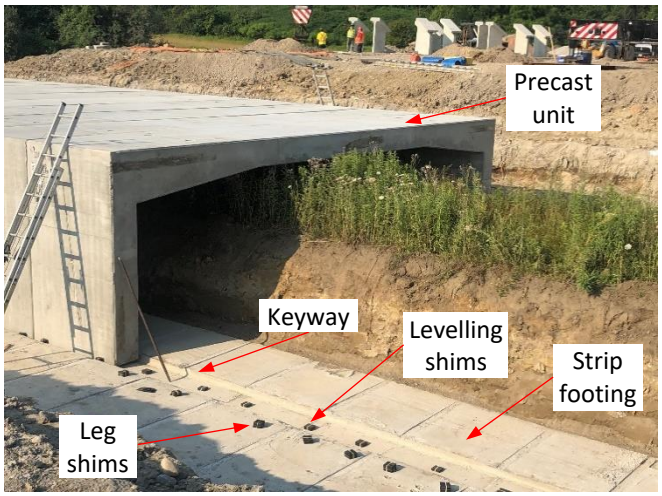

Figure 5-3. Reinforced concrete TSC system (Pickering culvert).

5.4 Preliminary Numerical Analysis (Pickering Culvert)

A preliminary numerical analysis was conducted prior to the construction and instrumentation of the three subject TSCs. The main objectives of this preliminary numerical analysis were to provide approximate magnitudes of the parameters that would be measured during the field monitoring program, predict the culverts' behavior, and optimize the instrumentation plan. Therefore, three-dimensional (3D) finite element (FE) models were developed for the three subject culverts. The 3D modeling approach was selected as the field-testing program incorporated live load testing of the culverts, which has 3D features in terms of the load transfer mechanism through the soil. The same moding approach was repeated for the three culverts. Thus, only the details of the Pickering culvert model will be presented herein.

5.4.1 Numerical Model Features

The general-purpose FE software package, ABAQUS v.6.13.3 (2013), was utilized for the analysis. The 3D model of Pickering culvert comprised two parts: the concrete culvert body and soil block as depicted in **Figure 5-4**. The width of the FE model affects the results of soil-structure models (Kim and Yoo, 2005) due to the effect of the boundary conditions. Kang et al. (2008) and Yoo et al. (2005) extended the model boundaries to 6 times the culvert width, while Ma et al. (2019) extended the model boundaries to 10 times the culvert width. Based on a conducted sensitivity analysis, the soil block was extended 5 times the

culvert span on both sides to avoid any influence of the boundaries on the culvert zone. Similarly, the depth of the foundation soil was taken 10 m, which is almost 3 times the footing width (3.8 m). The model was extended 22.0 m out-of-plane to represent the culvert length subjected to the full backfill height, which was considered 3.0 m in the preliminary analysis.

The concrete body block included the precast culvert and strip footings as one block while ignoring the sidewall-footing connection, which was not known when the preliminary 3D FE models were developed. Such approximation was considered acceptable for the purpose of the preliminary analysis. The soil block in the 3D model comprised two zones: one represented the native soil, and the second represented the backfill soil as demonstrated in **Figure 5-4b**. Based on the site stratigraphy, the culvert was founded on dense to very dense sandy silt. Thus, the native soil was divided into 4.0-m-thick dense and 6.0-m-thick very dense layers to account for the increase in stiffness and strength with depth for the cohesionless soil, reflected in the measured SPT N-values at the site. The excavation geometry was not available during the preliminary analysis; thus, embankment installation was assumed. The sidefill soil adjacent to the culvert sidewall and the backfill soil over the top slab were discretized into 23 × 0.3 m lifts, as demonstrated in **Figure 5-4b**, to simulate a realistic incremental embankment construction procedure.

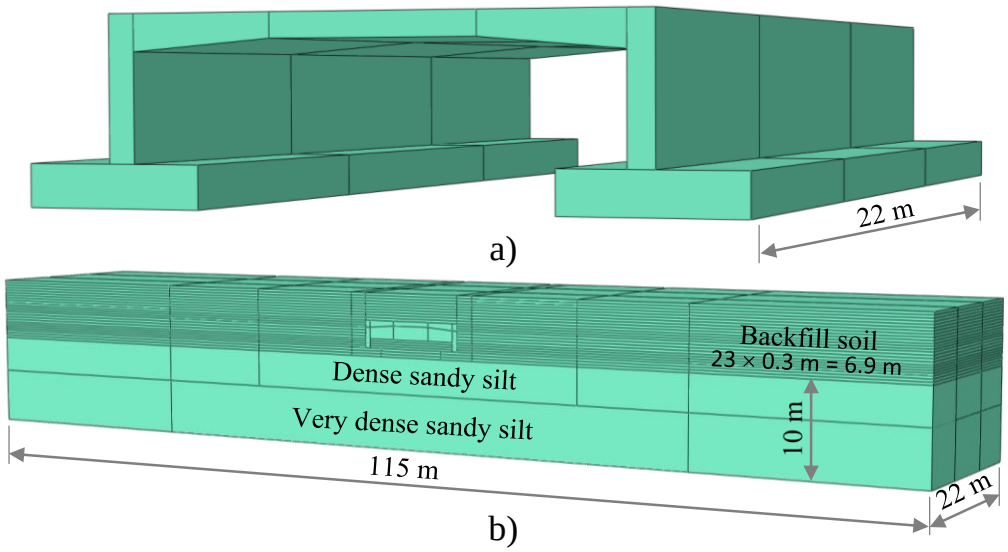

Figure 5-4 Schematic of the Pickering culvert model parts: a) culvert part; and b) soil block part.

The culvert body and soil block were discretized using 3-dimensional 8-noded, first-order (linear), reduced integration, hourglass control elements (C3D8R). The culvert mesh was refined in the middle segment, as displayed in **Figure 5-5**, to enhance the accuracy of calculations in the culvert zone, where the results will be reported. A total of 20,250 and 162,400 elements have been used to discretize the culvert and soil block parts, respectively. The boundary condition at the bottom surface of the model was fixed in all directions. On the other hand, the model side boundaries were restrained from lateral movement and only allowed to move in the vertical direction as illustrated in **Figure 5-5**.

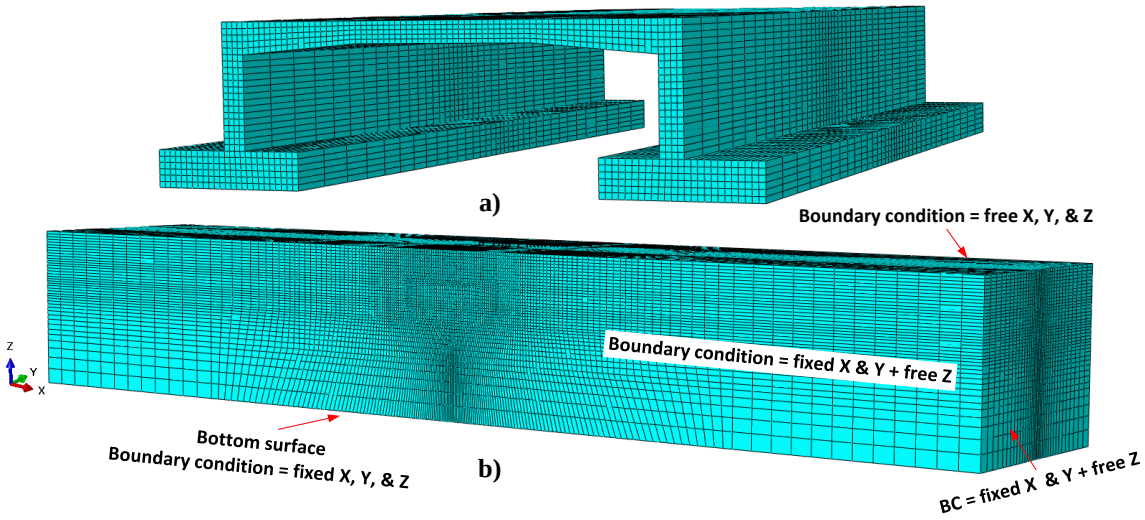

Figure 5-5 Meshing details of the Pickering culvert model parts: a) culvert part; and b) soil block part.

The average SPT N-value of the dense sandy silt till layer was 29 and increased to over 100 at a depth of 4.0 m below the foundation level. The elastic-plastic Mohr-Coulomb (MC) constitutive model was defined for both native and backfill soils. The native soil elastic modulus (E_s) was evaluated employing an empirical correlation with the measured SPT N-values, i.e., E_s = 1.33×N (Balachandran et al., 2015). The angle of internal friction (ϕ) was determined within the range provided by Manzari et al. (2014) for cohesionless till (31° to 45°). No cohesion value was given to both cohesionless till materials. Cohesionless soil compacted to 90% of its Standard Proctor density was assumed as the backfilling material to meet the CHBDC (CSA, 2014) requirements for B1 standard installation. The linear elastic model was assigned to the RC culvert part, in which equivalent stiffness (E)

and Poisson's ratio (ν) were used to represent the behavior of RC. **Table 5-1** summarizes the assigned material input parameters. It should be noted that the RC culvert compressive strength was unknown by the time the preliminary analysis was conducted. Accordingly, the RC material properties were reasonably assumed.

The surface-to-surface contact pair algorithm was used to define the contact interaction between the TSC and the surrounding backfill soil. The two surfaces in contact are denoted master and slave surfaces. The master surface is usually assigned to the stiffer body (culvert body), while the slave surface was assigned to the in-contact soil surfaces. The interface properties were defined using two distinguished behaviors: tangential and normal. Tangential behavior followed the Coulomb friction model, characterized by the friction coefficient (μ) based on the contact nature and materials in contact. A friction coefficient of 0.8 was assumed in this analysis to represent the interface of the backfill and concrete culvert surface. The normal behavior was defined as "hard" contact that ensures that both the master and slave surfaces do not penetrate each other (SIMULIA, 2013). Also, the defined normal behavior allowed for separation after contact.

Table 5-1. Summary of the material input parameters in the Pickering culvert model.

Part	Material model	Unit weight (kN/m^3)	E (MPa)	ν	ϕ (°)
Dense sandy silt	MC plasticity	20.0	25	0.25	34
V. dense sandy silt			35		38
Backfill soil			30		36
Culvert	Elastic	24.0	3×10^4	0.2	-

5.4.2 Preliminary Analysis Results

The results considered in the design of the instrumentation plan comprised the applied earth pressures on the culvert body, the contact stresses underneath the strip footing, and the induced internal strains in the culvert body. All the results are presented for the final backfill height.

Figure 5-6 presents the vertical earth pressure distribution along the top slab of the three subject culverts. The earth pressure magnitudes calculated for the Oshawa culvert were the highest compared to the Remembrance and Pickering culverts. This is attributed to the backfill height, which was 3.8 m in the case of Oshawa culvert as opposed to the 3.2 m and 3.0 m in the case of Remembrance and Pickering culverts, respectively. However, the three models exhibited non-uniform earth pressure distribution along the top slab with higher pressures concentrated at the relatively stiff edges compared to the relatively flexible midspan. Such earth pressure distribution conforms with reported results on box culverts (Bennett et al., 2005; Chen and Sun, 2014; Pimentel et al., 2009) and arch culverts (McGrath et al., 2002).

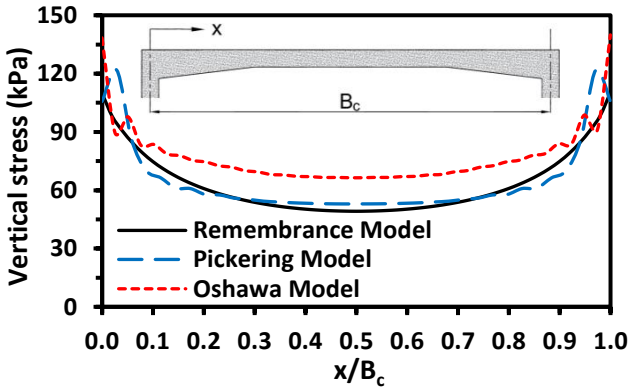

Figure 5-6 Predicted vertical earth pressure distribution along the top slab.

The predicted maximum principal strain contours in the concrete culvert body are displayed in **Figure 5-7**. Positive strain values indicate tensile strains, while negative values indicate compressive strains. The maximum values of the anticipated earth pressures on the three subject TSCs and induced strains in the culverts' bodies are summarized in **Table 5-2**. These maximum values guided the selection of the utilized sensors' full-scale ranges.

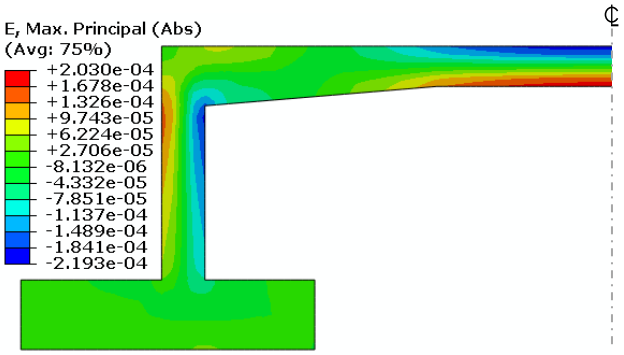

Figure 5-7 Maximum predicted principal strains in the Pickering culvert body.

Table 5-2. Summary of predicted maximum stresses and strains.

	Project		
Maximum output	Remembrance	Pickering	Oshawa
Earth pressure on top slab (kPa)	110.3	121.9	181.2
Stress below footing (kPa)	234.6	368.9	443.8
Tensile strain (με)	171.0	203.0	272.7
Compressive strain (με)	180.0	219.3	302.0

5.5 Instrumentation Plan (Pickering Culvert)

Earth pressure cells (PCs) are used to measure the imposed earth pressures on buried structures, while strain gauges (SGs) are used to monitor their structural performance by measuring the induced strains in the culvert body due to the applied loads. The most appropriate type of sensors was selected to meet the following requirements:

- Adequate accuracy within the range of magnitudes predicted from the preliminary analysis.
- Durability and stability for long-term monitoring purposes (planned to continue for three years after construction completion).
- Ability to withstand extreme seasonal temperature variations while operating within acceptable accuracy as the three culverts were to be constructed in the

Greater Toronto Area, which is characterized by warm summers and severe winters.

- Minimal influence of the signal cable length on the readings as the data acquisition system was to be located at a distance up to 40.0 m from some sensors.
- Successful experience with their use in similar applications.

Vibrating wire (VW) sensors were found to meet all the above-mentioned requirements. They are suitable for long-term static measurements (Perkins and Lapeyre, 1997). The output signal is in the form of frequency, eliminating the effect of signal cable length.

Model 4810 VW pressure cells and Model 4000 VW strain gauges (Geokon, Lebanon, New Hampshire), shown in **Figure 5-8**, were selected for measuring the applied earth pressures and the induced strains, respectively. Model 4810 VW PC has an accuracy of 0.1% of its full-scale range when using the polynomial expression for data reduction. Based on the magnitudes predicted from the preliminary analysis in **Table 5-2**, PCs with a full-scale range of 700 kPa were utilized beneath the strip footing, and those with a range of 350 kPa were installed elsewhere. Model 4000 VW SG has a full-scale range of 3000 με and an accuracy of 0.5% of this range. Both selected sensors have an operating temperature range between -20 and +80° C. Moreover, they have been successfully used for instrumenting similar buried structures (Marshall et al., 2014; Perkins and Lapeyre, 1997; Yang et al., 1999).

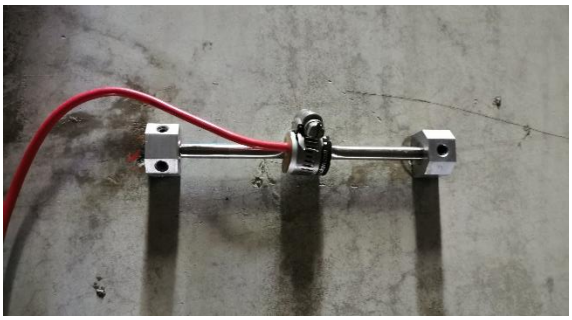

a)

b)

Figure 5-8 Samples of the installed sensors: a) VW SG; and b) VW PC.

5.5.1 Instrumentation Layout

Based on the results of the preliminary analyses, the three TSCs were instrumented with 30 VW pressure cells to measure the imposed earth pressures and 56 VW strain gauges to monitor the structural performance during and after construction completion.

The 10.4-m-span Pickering culvert was instrumented with 11 VW PCs and 18 VW SGs distributed on one precast unit as shown in **Figure 5-9**. Three PCs were installed underneath the strip footing to determine the contact stress distribution, three on the sidewalls to measure the lateral earth pressure, and five PCs distributed along the top slab. The VW SGs were installed at specific locations on the inner and outer surfaces of the culvert to measure the tensile and compressive strains at each cross-section. The symmetry of the instrumentation layout was not maintained due to budget limitations. However, the final layout ensures an acceptable level of redundancy.

All sensors were installed according to the manufacturer's recommendations. They survived the construction activities and are currently functioning properly. More details on the sensors' installation procedures are presented in Chapter 3.

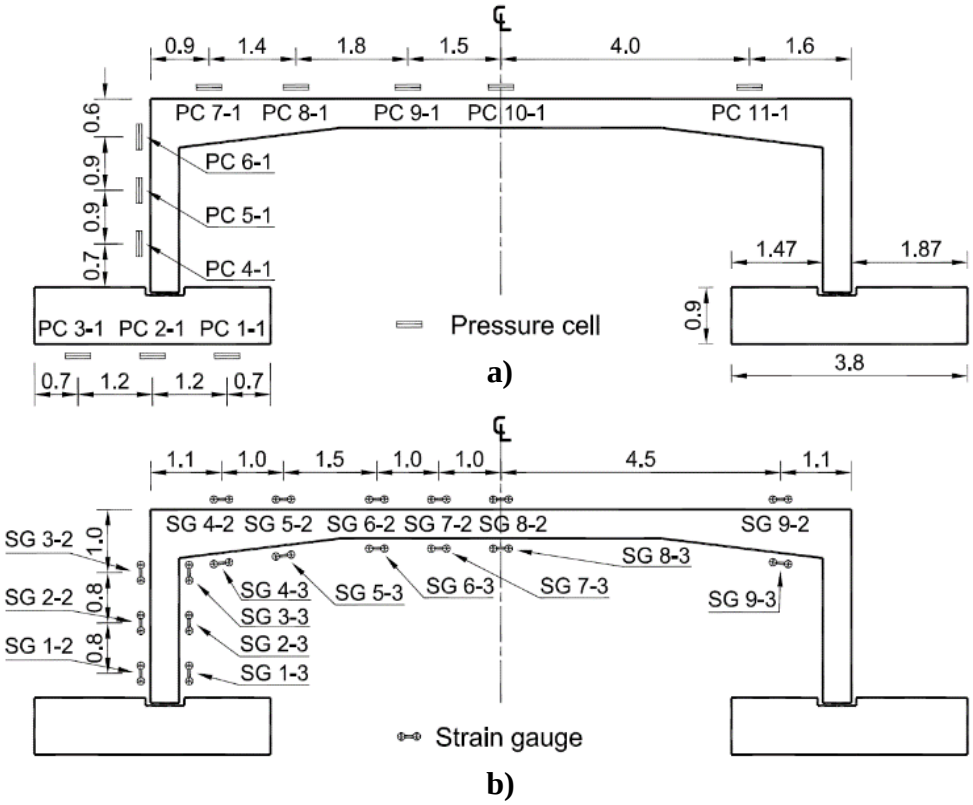

Figure 5-9. Pickering culvert instrumentation layout: a) pressure cells; and b) strain gauges. (All dimensions are in m)

5.6 Monitoring Results (Pickering Culvert)

The construction of the Pickering culvert was completed in November 2019 with a total backfill height of 3.1 m. The collected field data during and after construction completion are presented elsewhere (Chapter 6). This section presents a comparison between the results of the preliminary analysis and the field measurements at the final backfill height.

Nuclear density tests were conducted during the backfilling operations, and an average density of 22.0 kN/m^3 was measured. Moreover, the final backfill height, 3.1 m, was slightly higher than the considered backfill height in the preliminary analysis (3.0 m). Accordingly, the predicted and measured vertical earth pressures were normalized by the overburden stresses ($\gamma_s H$), giving the vertical arching factor (VAF), where γ_s is the backfill soil unit weight and H is the backfill height. **Figure 5-10** presents a comparison between the estimated VAFs from the numerical model results and the measured values along the

top slab. An excellent match can be observed between the predicted and measured values. The CHBDC (CSA, 2014) stipulates a VAF of 1.2 for B1 standard installation, which was followed in the Pickering culvert construction. **Figure 5-10** demonstrates that both the predicted and measured VAF indicate lower VAF within over 80% of the culvert span with average VAFs of 1.08 and 1.04, respectively.

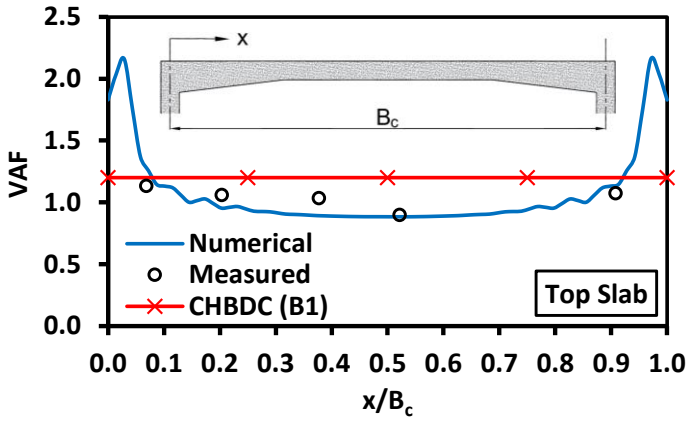

Figure 5-10. Comparison between the predicted and measured VAF distribution along the top slab of the Pickering culvert at the final backfill height.

The lateral earth pressure applied on the culvert sidewall from the preliminary analysis is compared with the field data in **Figure 5-11**. The comparison shows good agreement between the measured and predicted values except at PC 4-1, where the numerical model overestimated the soil pressure. However, the estimated lateral earth pressure from the numerical model decreased at the sidewall base, which is attributed to the flexural deflection of the sidewall near its base. The reduction in the estimated lateral earth pressure explains the low earth pressure measured by PC 4-1. The CHBDC (CSA, 2014) specifies minimum and maximum horizontal arching factors (HAFs) of 0.3 and 0.5 for the case of B1 standard installation, respectively. HAF corresponds to the lateral earth pressure coefficient used to calculate the applied lateral earth pressures on retaining walls. **Figure 5-11** shows that the measured lateral earth pressures and most of the estimated values fall within the bounds specified by the code.

Figure 5-12 presents the measured and estimated contact stresses below the strip footing. The predicted values are slightly lower than the measured ones, which can be attributed to the difference in backfill height and backfill soil density previously discussed. However,

the preliminary analysis, in agreement with the field measurements, demonstrates an almost uniform distribution along 80% of the strip footing width. Relatively high stresses were predicted by the numerical model at the footing edge on the waterside.

Generally, the presented results proved the ability of the conducted preliminary analysis to predict the applied earth loads and contact stresses underneath the footing with reasonable accuracy.

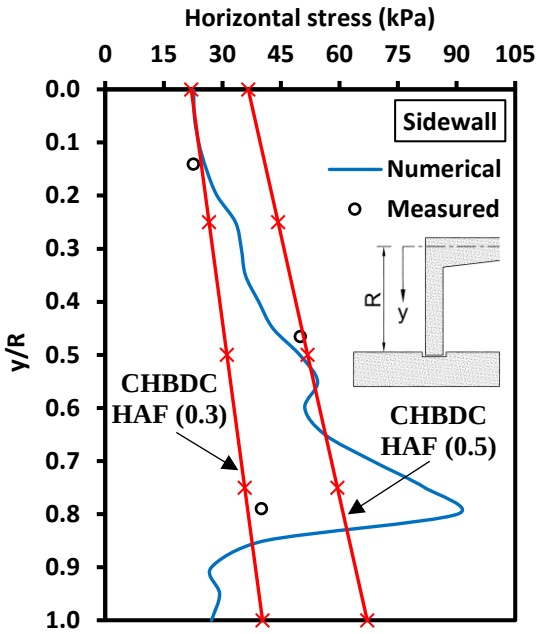

Figure 5-11. Comparison between the predicted and measured lateral earth pressure on the sidewall of the Pickering culvert at the final backfill height.

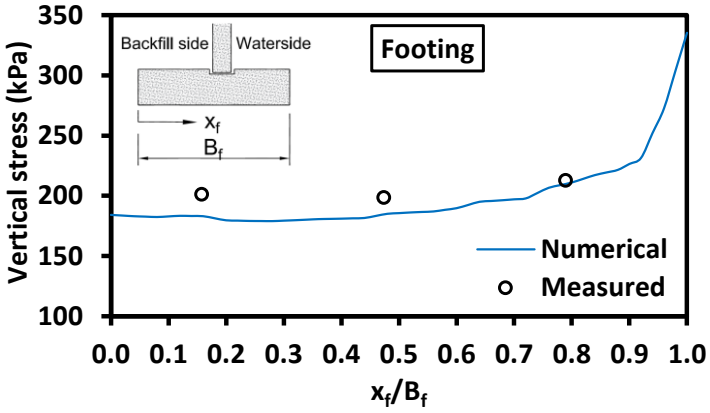

Figure 5-12. Comparison between the predicted and measured contact stresses below the strip footing of the Pickering culvert at the final backfill height.

Table 5-3 compares the predicted and measured induced strains in the RC culvert body. Although the numerical model results accurately depicted the concrete surfaces experiencing tensile and compressive strains, the estimated strains at the inner and outer surfaces were different from the measured magnitudes, especially for the tensile strains. For instance, the measured compressive strain at the midspan cross-section by SG 8-2 was 71% higher than the predicted value at the same location. On the other hand, the measured tensile strain at the same cross-section was almost 142% higher than the predicted value at the same location as clarified in **Table 5-3**. Visual inspection revealed the development of flexural cracks on the inner surface of the top slab as demonstrated in **Figure 5-13**. The cracks formation explained the significant difference between the measured and predicted tensile strains, where linear elastic behavior of the RC culvert was assumed in the 3D FE model.

The theoretical cracking strain (ε_{cr}), at which cracks start to develop in concrete, was calculated to be 133 με using (CSA, 2014):

$$\varepsilon_{cr} = \frac{f_r}{E_c} = \frac{0.6\lambda\sqrt{f_c'}}{4500\sqrt{f_c'}} \quad \textbf{(5-1)}$$

where f_r is the concrete modulus of rupture, E_c is the concrete Young's modulus, f_c' is the average 28-day concrete compressive strength, and λ is 1.0 for normal weight concrete (CSA, 2014).

The predicted tensile strain at the midspan was 203 με as listed in **Table 5-3**, which exceeds ε_{cr}. Thus, the assumption of linear elastic behavior for RC is not sufficient for strain predictions in case the estimated tensile strains exceed ε_{cr} and cracks are expected to develop. The use of a material model able to simulate the concrete nonlinear behavior and crack formation should be utilized to accurately estimate the induced strains.

Table 5-3. Predicted and measured strains comparison.

	Strain (με)			Strain (με)	
SG	Num.	Field	SG	Num.	Field
SG 1-2	72.4	118.7	SG 1-3	-112.8	-182.8
SG 2-2	106.6	162.3	SG 2-3	-145.9	-222.3
SG 3-2	149.5	270.4	SG 3-3	-181.7	-324.9
SG 4-2	59.2	56.9	SG 4-3	-66.7	-78.8
SG 5-2	-15.6	2.6	SG 5-3	-1.0	-49.1
SG 6-2	-138.7	-220.3	SG 6-3	127.1	201.2
SG 7-2	-189.4	-323.7	SG 7-3	175.7	317.6
SG 8-2	**-219.8**	**-376.8**	**SG 8-3**	**203.0**	**490.8**
SG 9-2	38.3	64.8	SG 9-3	-51.0	-74.2

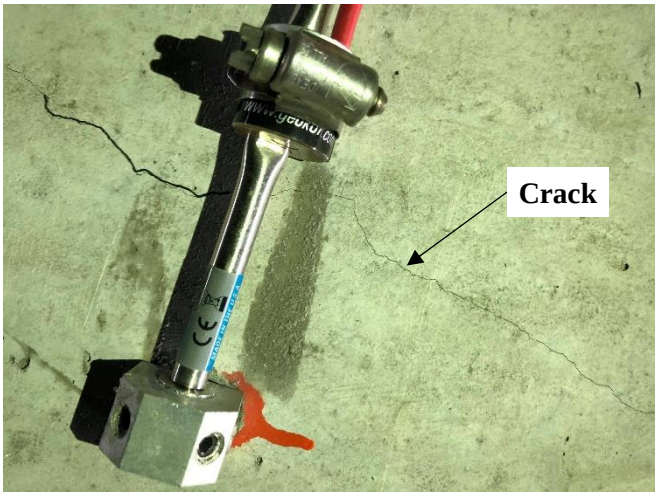

Figure 5-13. Observed cracks at the midspan of the Pickering culvert.

5.7 Class-A Prediction (Remembrance Culvert)

This section presents the Class-A prediction of the 7.3-m-span Remembrance culvert. This TSC was instrumented with 6 VW PCs and 14 VW SGs distributed on one precast unit. Two PCs were installed on the sidewall, and the remaining 4 were distributed on the top slab. Adding PCs below the strip footing of the Remembrance culvert was not possible as the strip footing was already constructed before the culvert was approved for instrumentation. The 14 SGs were mounted at 7 cross-sections along the sidewall and top

slab, on the inner and outer surfaces, to record the induced tensile and compressive strains at each cross-section. Backfilling of the Remembrance culvert took place in two consecutive construction seasons. Two-dimensional (2D) plane-strain FE models were validated against the field data at a shallow backfill height (1.7 m), and the numerical model predictions up to the final backfill height (H = 3.2 m) were presented in Chapter 4. With the culvert construction completion to the final road grade level, field data are presented to date, and the predicted values from the 2D models are compared with the field measurements at 3.2 m of backfill.

5.7.1 Field Data

The Remembrance culvert was part of a new subdivision extension project. Backfilling of the TSC was conducted in 0.3 m lifts of well-graded sand (SW) compacted to 90-100% Standard Proctor. Compaction took place using a hand-operated vibrating plate compactor up to 0.6 m of backfill on the top slab, after which compaction took place using heavy compaction equipment. The backfilling process took place in two consecutive construction seasons. The final backfill height of 3.2 m was reached only recently.

Figure 5-14 displays the PC measurements to date. During the first construction season, the culvert was backfilled to a height of 1.7 m, which was reached on day 105 of construction. The backfill was increased to approximately 3.0 m on day 167, just before the winter season. With the start of the second construction season on day 277, the top 0.5 m of backfill was removed because it was exposed to frost during the cold winter. Backfill was then completed to the final grade level on day 415. The four wing walls of the culvert were cast-in-place, and their construction took place during the backfilling activities. In addition, construction activities in the subdivision did not stop throughout the backfilling duration, even when no backfill activities were taking place. The transient loads from the construction activities of the wing walls and in the subdivision resulted in the observed spikes in the PC measurements presented in **Figure 5-14**. However, stability of the pressure readings can be recognized at constant backfill heights, e.g., after reaching 1.7 m and 3.2 m of backfill on days 105 and 277, respectively.

The lateral earth pressures on the sidewall measured using PC 1-1 and PC 2-1 are displayed in **Figure 5-14a**. PC 1-1, located near the bottom of the sidewall, exhibited higher lateral earth pressure than PC 2-1, located at a higher level near the haunch, due to the increase in effective overburden stress with depth. During the winter season (days 167 to 277), a significant increase in the measured total pressures by PC 1-1, unlike PC 2-1, which almost showed constant value. The increase in measured pressures during that period is attributed to the seasonal precipitations and snow loads that increase the total pressures on the top slab. The deformed shape of the sidewall under the increased applied loads, as described in Chapter 4, explains the significant increase in PC 1-1 measurement relative to PC 2-1. Outward deformation towards the sidefill was evaluated within the zone of PC 1-1. Thus, the lateral earth pressure approached the passive lateral earth pressure condition. On the other hand, no to inward deformation away from the sidefill occurred within the upper part of the sidewall, within the zone of PC 2-1, resulting in at-rest to active lateral earth pressure state.

The vertical earth pressures on the top slab, presented in **Figure 5-14b** and **c**, show that the highest pressure at the final backfill height was measured by PC 6-1, located near the far edge. This agrees with the field and numerical results of the same culvert at 1.7 m of backfill (Chapter 4) as well as field and numerical results of a 10.4-m-span TSC under 3.1 m of backfill (Chapter 6).

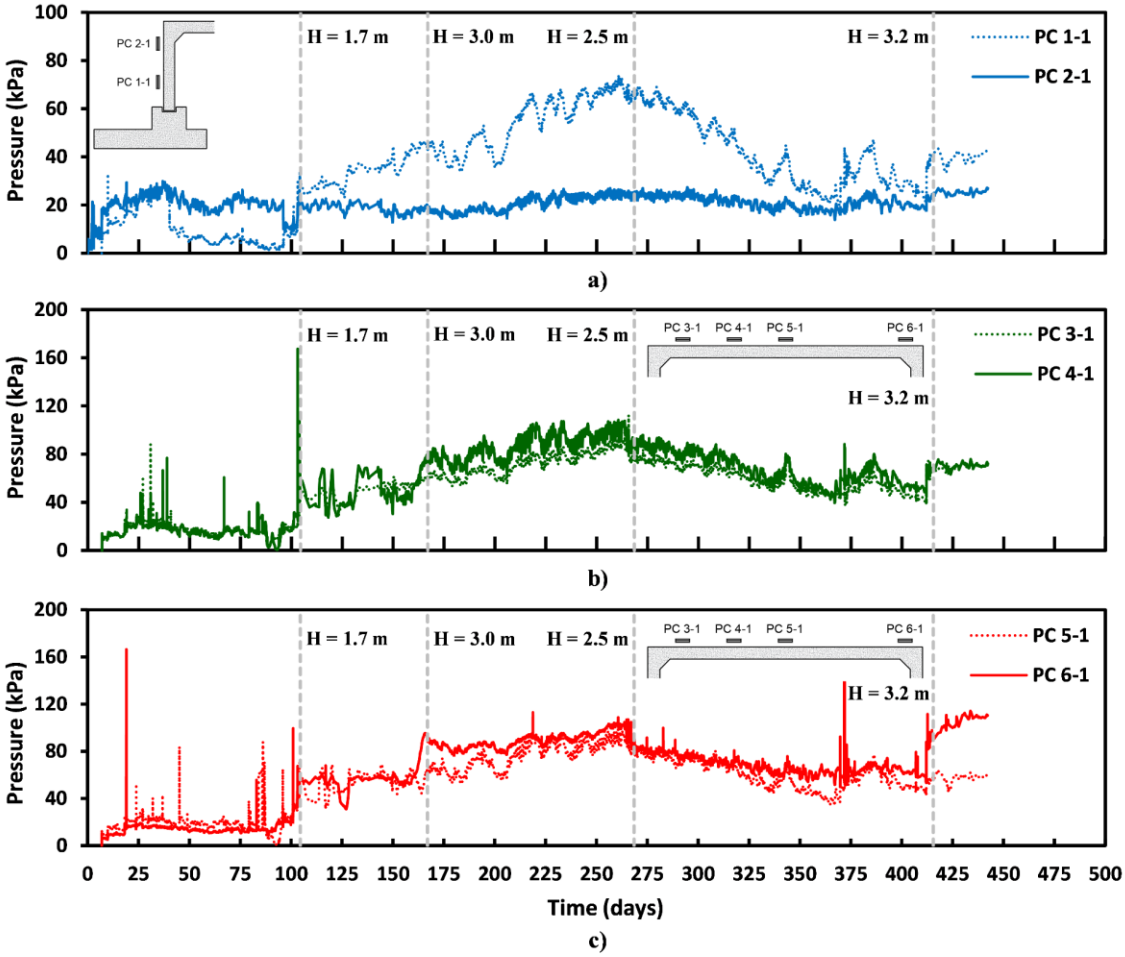

Figure 5-14. Pressure cell measurements to date: a) pressures on the sidewall; b) pressures on the top slab (PC 3-1 & PC 4-1); and pressures on the top slab (PC 5-1 & 6-1).

Figure 5-15 shows the strain gauge measurements up to the final backfill height. Compressive (negative values) and tensile (positive values) strains were measured at each cross-section. The theoretical cracking strain (ε_{cr}) was calculated to be 133 με. SG 2-2 (placed at the outer surface of the sidewall just below the haunch) and SG 11-2 and SG 12-2 (placed at the bottom of the top slab within the midspan) measured tensile strains greater than ε_{cr}, which indicated cracks have developed at these locations.

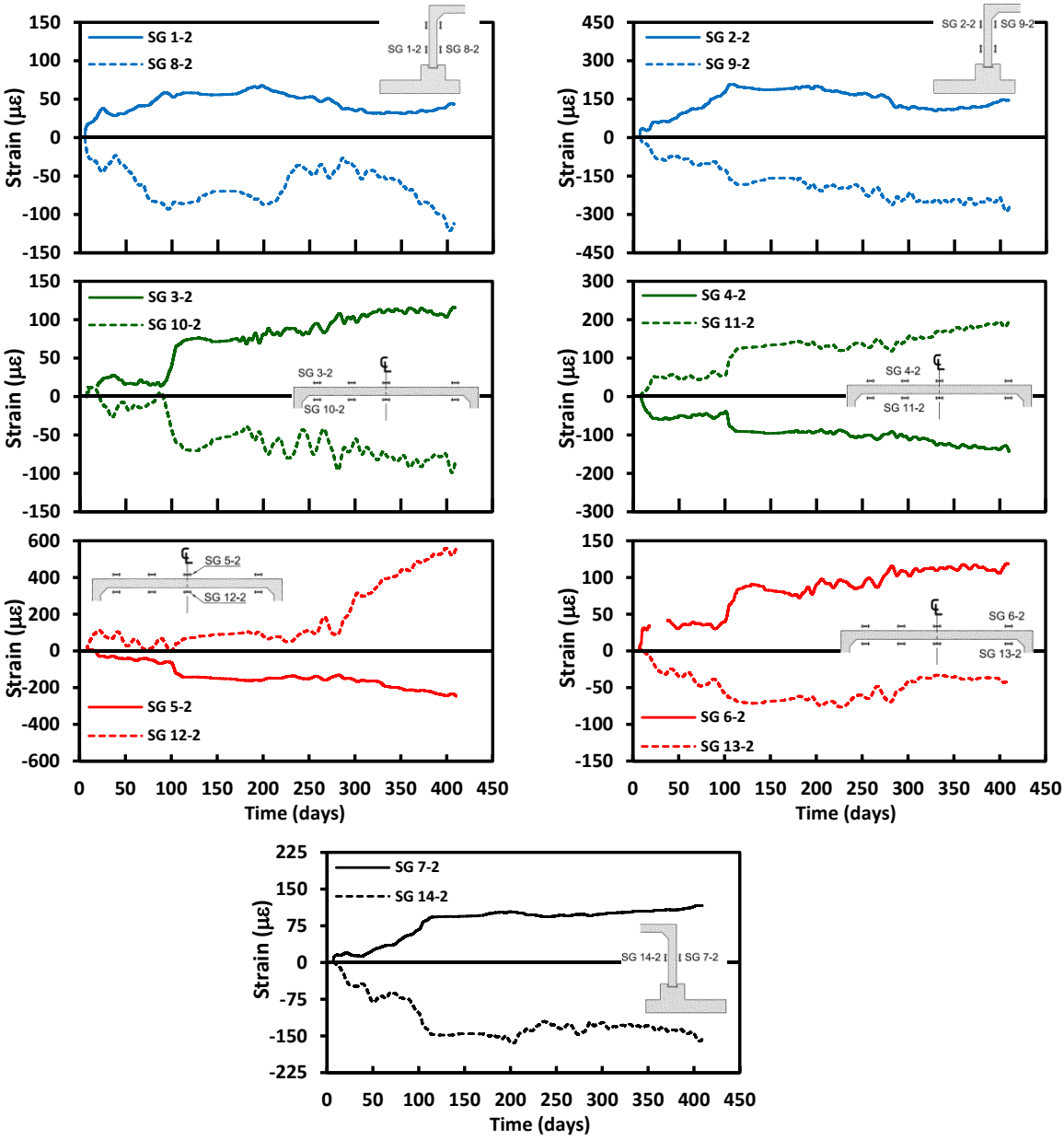

Figure 5-15. Strain gauge measurements to date.

5.7.2 Validated Model

Live load tests were not conducted on Remembrance culvert, eliminating the need for 3D modeling. Accordingly, 2D plane-strain FE models were developed for the Remembrance culvert using DIANA 10.1 (TNO Diana BV, 2016) FE software as detailed in Chapter 4. The developed models were validated against the field data at the reached 1.7 m of backfill. The predictions for earth pressure and culvert strains at the final backfill height (3.2 m)

were also presented. A brief description of the 2D FE models and a comparison between the predicted values and field measurements at 3.2 m of backfill are presented herein.

Two different 2D models were developed for the Remembrance culvert to assess the influence of RC nonlinearity on the model results: linear elastic model (LEA), in which the RC culvert body was simulated using a linear elastic material model; and nonlinear model (NLA), in which the RC culvert was simulated using the total strain-based smeared crack model to consider the material nonlinearity and cracks formation. The strip footing was assumed to behave in the linear elastic zone in both models. The nonlinear behavior of the sidefill and backfill soils (SW) was considered in both models using the Duncan and Chang (1970) material model. On the other hand, the native silty clay till layer was simulated using the Mohr-Coulomb material model. Steel reinforcement of the culvert was simulated in the NLA model using embedded bar elements, fully bonded to the concrete body. The von Mises plasticity model was used to simulate the steel reinforcement with no hardening behavior. Interface elements were defined at the soil-footing, soil-culvert, and culvert-footing interfaces to reasonably simulate the soil-culvert interaction problem. Finally, staged construction analysis was adopted, in which the sidefill and backfill soils were divided into layers to mimic the incremental phases of construction. More details on the developed FE models can be found in Chapter 4.

Figure 5-16 presents a comparison between the measured and estimated earth pressures on the culvert body at 1.7 and 3.2 m of backfill. **Figure 5-16a** shows the good agreement between the estimated earth pressures from the LEA and NLA models and the available field data by the time the models were developed (H = 1.7 m). For the vertical earth pressure on the top slab, **Figure 5-16a** indicates non-uniform earth pressure on the top slab from both field and numerical results. The vertical earth pressures are higher at the edges compared to the midspan. This can be attributed to the flexibility of the top slab at the midspan relative to the edges, resulting in the attraction of the earth loads to the more rigid zone, known as the soil arching phenomenon. **Figure 5-16a** also shows the measured and estimated lateral earth pressure on the culvert sidewall. The numerical results indicate parabolic distribution of the lateral pressure along the sidewall. Three PCs were planned for the sidewall to determine the lateral earth pressure distribution from the field

measurements. However, only two PCs were installed due to the limited space on the sidewall. In general, the field measurements indicate good agreement with the parabolic distribution predicted by the 2D models.

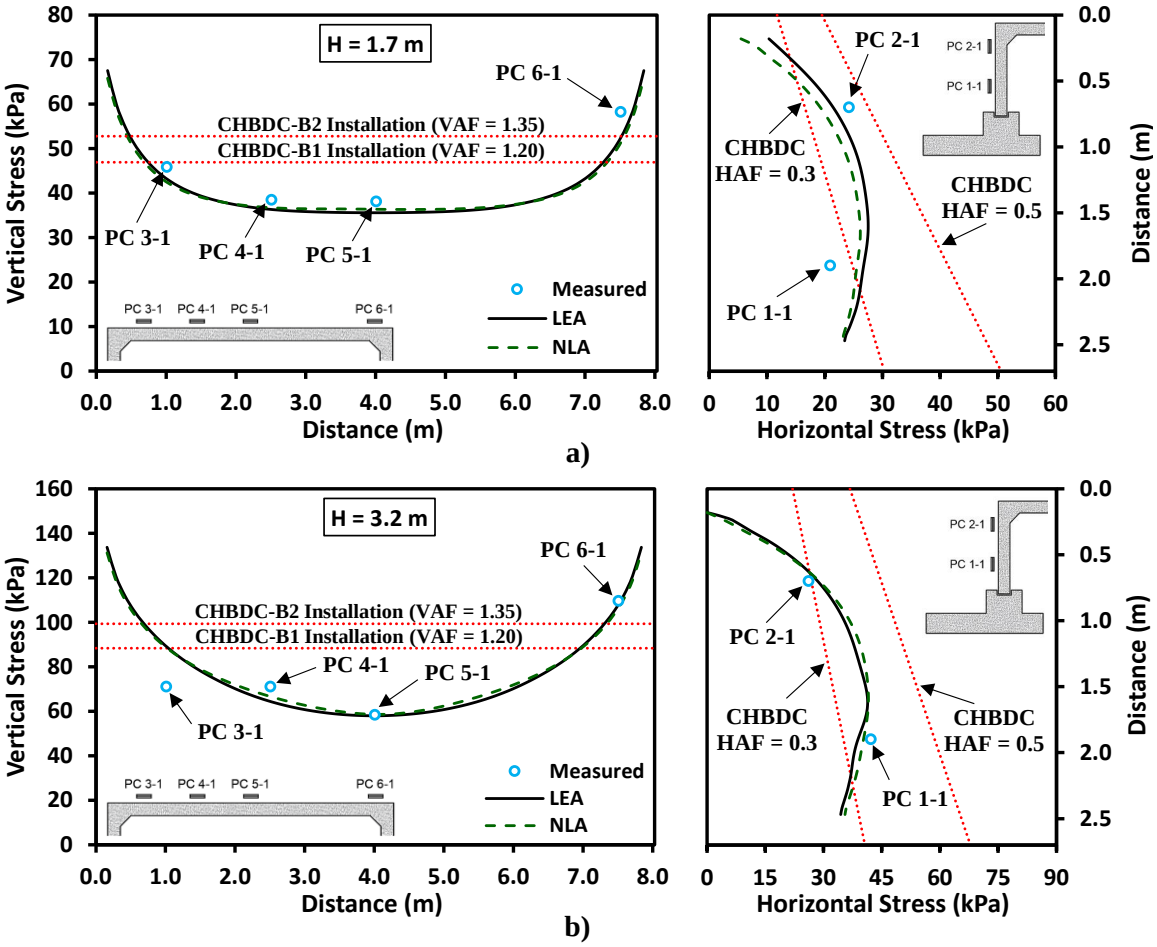

Figure 5-16. Comparison between the measured and estimated earth pressures on the culvert body at different backfill heights: a) H = 1.7 m; and b) H = 3.2 m.

Figure 5-16b compares the measured earth pressures on the culvert body and those calculated from the numerical models at the final backfill height. The comparison indicates excellent agreement between the measured and estimated vertical earth pressures, except for PC 3-1, which exhibited lower pressure compared to the numerical model results. This difference is attributed to the inability of the numerical model to consider the exact field conditions as well as the soil properties variability and uncertainty, which would significantly affect the FE model predictions (Phoon and Kulhawy, 1999; Uzielli et al., 2006; Viviescas et al., 2020). The lateral earth pressures from both models at 3.2 m of

backfill show parabolic distribution, similar to that observed at 1.7 m of backfill. The models also reflect very low lateral pressures at the upper part of the sidewall, which is attributed to the deformed shape of the culvert as depicted in **Figure 5-17**. Excellent agreement between the measured and calculated lateral earth pressures is observed; however, the lateral earth pressure distribution cannot be determined accurately from the data of only two PCs. It should be noted that the presented PC measurements at 1.7 and 3.2 m of backfill are the average values of the readings once they stabilize under constant loads.

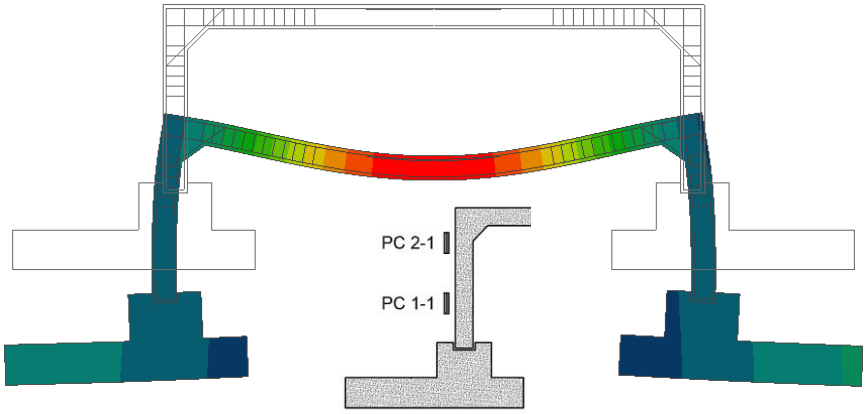

Figure 5-17 Deformed shape of the Remembrance culvert at 3.2 m of backfill.

The numerical results presented in **Figure 5-16** show almost no difference between the estimated earth pressures from the LEA and NLA models. This indicates that simplifying the numerical model by assigning linear elastic behavior to the RC culvert would still lead to reasonable estimation of the applied earth pressures on the buried TSC at service loading conditions.

The CHBDC (CSA, 2014) specifies VAF = 1.2 for B1 standard installation and 1.35 for B2 standard installation. B2 standard installation represents lower compaction level of the sidefill compared to B1 standard installation for the same type of sidefill material. The Remembrance culvert construction followed the requirements of the CHBDC (CSA, 2014) for B1 standard installation. **Figure 5-16** presents a comparison between the field and numerical results with the CHBDC values. The results indicate lower vertical earth pressure from the measured and estimated values within almost 80% of the culvert span compared to the code value at both backfill heights (1.7 and 3.2 m). Based on the field

measurements, the average VAF = 1.15 and 1.05 at 1.7 and 3.2 m backfill, respectively, while an average VAF = 1.05 is estimated at both backfill heights from the numerical models. These values coincide with the estimated average VAF of 1.04 for the Pickering culvert at 3.1 m of backfill based on field measurements (Chapter 5). The measured lateral earth pressures and the estimated values almost lie within the upper and lower bounds stipulated by the code as shown in **Figure 5-16**.

The smeared crack model used in the NLA model enabled the prediction of crack formation. **Figure 5-18** displays the predicted crack pattern at 3.2 m of backfill, which agrees well with the SG measurements in terms of crack formation. Cracks were predicted at the locations of SG 2-2, SG 11-2, and SG 12-2 as the measured strains exceeded the cracking strain. Moreover, visual inspection confirmed the formation of cracks on the bottom surface of the top slab, extending 1.5 m from the midspan on both sides, which is where SG 11-2 is installed as shown in the image in **Figure 5-18**.

The presented results demonstrate the ability of the developed 2D models, which were validated against the field data at 1.7 m of backfill, to accurately estimate the applied earth pressures on the culvert body and predict the crack pattern at a higher backfill height (3.2 m).

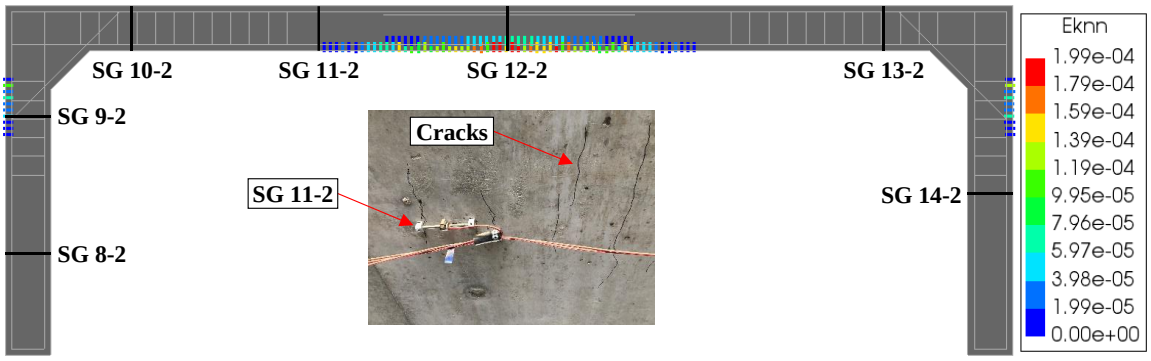

Figure 5-18. Predicted crack pattern from NLA model and observed cracks (image) at 3.2 m of backfill.

5.7.3 Effect of Shallow Foundation Geometry

The foundation of the Remembrance culvert consisted of a 1.3-m-thick strip footing, which included a 0.7-m-thick pedestal. Pedestals are mainly used to deepen the foundation level from the streambed elevation to exceed the frost depth without the need to increase the sidewall height. The frost depth is 1.2 m at the Remembrance culvert site location (OPSD, 2010). The LEA model produced reasonable results at the service loading condition. Accordingly, a parametric study has been conducted using the LEA model to investigate the influence of the strip footing geometry on the applied earth pressures on the culvert body, the stress distribution underneath the footing, and the induced bending moments along the culvert sidewall. The analysis was conducted considering two foundation soil conditions: a) yielding foundation, which represents the case of the Remembrance culvert supported on the native silty clay till layer, referred to herein as LEA-Y; and b) non-yielding foundation, which represents the case of the culvert constructed directly on rock and installed in a trench cut in rock, referred to herein as LEA-NY. The rock behavior was simulated using the Mohr-Coulomb material model with properties adopted from (Yoo et al., 2005), i.e., E_s = 34.3 GPa, ν = 0.25, ϕ = 0°, and c = 6.9 MPa.

In order to assess the influence of the strip footing shape and stiffness on the culvert behavior, FE models were developed considering different foundation geometries for both cases of yielding and non-yielding foundations. The strip footing pedestal was removed, and strip footing thicknesses of 0.6, 0.8, and 1.0 m were simulated. The following notation is used for the developed models: LEA-Y-0.6m model represents a 0.6 m thick strip footing constructed on a yielding foundation, and LEA-NY-0.6m model represents a 0.6 m thick strip footing constructed on a non-yielding foundation. The analysis was conducted at the final backfill height (3.2 m).

The effect of both footing shape and rigidity on the computed earth pressures acting on the culvert surfaces are almost negligible in both cases of yielding and non-yielding foundation soils as depicted in **Figure 5-19**. **Figure 5-19a** shows no influence of either the footing geometry or the foundation soil condition (yielding or non-yielding) on the estimated vertical earth pressure on the top slab. Similarly, the footing geometry had insignificant influence on the lateral earth pressure on the sidewall. However, higher lateral earth

pressures were estimated for the case of non-yielding foundation due to the higher confinement of the sidefill material in a trench cut in rock compared to a trench cut in the native soil.

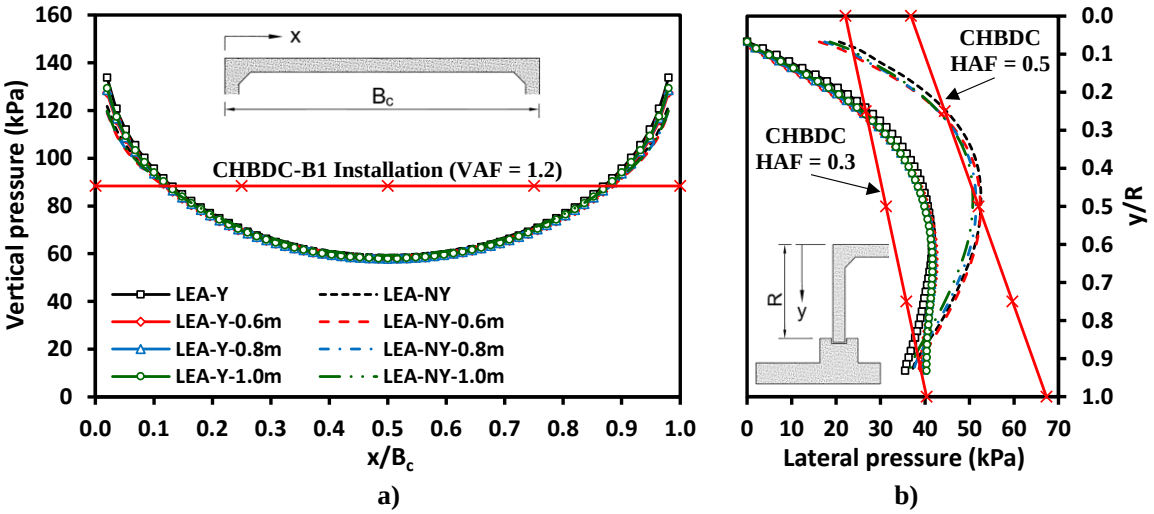

Figure 5-19. Effect of shallow foundation geometry at 3.2 m of backfill: a) vertical earth pressure on the top slab; and b) lateral earth pressure on the sidewall.

Figure 5-20a displays the influence of the footing geometry on the stresses underneath the strip footing for both cases of yielding and non-yielding foundation soils. The results indicate that the effect of footing geometry is more pronounced underneath the footing edge on the backfill side and almost diminished beyond 70% of the footing width from the backfill side. The stress distribution underneath the strip footing becomes more non-uniform as the footing thickness decreases. For instance, the stress underneath the footing edge on the backfill side decreased from 191 kPa in the LEA-Y-1.0m model to 159 kPa in the LEA-Y-0.6m for the case of yielding foundation soil and decreased from 178 kPa in the LEA-NY-1.0m to 142 kPa in the LEA-NY-0.6m for the case of non-yielding foundation soil. These results reflect a reduction of 16.8% and 20.2% in the calculated stresses below the footing edge on the backfill side, respectively. These findings agree with the experimental results reported by Lemmen et al. (2016) on strip foundations on dense sand tested at a centrifugal acceleration of 30g.

The bending moment (*BM*) distributions along the sidewall for the considered cases are presented in **Figure 5-20b**. The results demonstrate that the *BM* magnitude at the base of

the sidewall decreased as the rigidity of the strip footing increased for the case of yielding foundation soil, and the opposite is observed for the case of non-yielding foundation soil. In Chapter 4, the development of *BM* at the sidewall of TSCs was attributed to the combined effect of the footing rotation and the restraint provided by the sidewall-footing connection. The results presented in **Figure 5-20b** support this explanation, where relatively high *BMs* could be observed for the case of yielding foundation condition, in which the footing could rotate. On the other hand, relatively negligible *BMs* were calculated at the sidewall base for the case of non-yielding foundation soil, in which the footing rotation was restrained. Jawdhari et al. (2020) stated that for an arch RC culvert, the arch-footing connection represents somewhere between fixed and hinged connection. Finally, the results presented in **Figure 5-19** and **Figure 5-20** suggest that at the considered backfill height (3.2 m), the thicker the strip footing, the closer the results to the original condition with pedestal. More studies are still required to investigate such findings based on field or experimental tests.

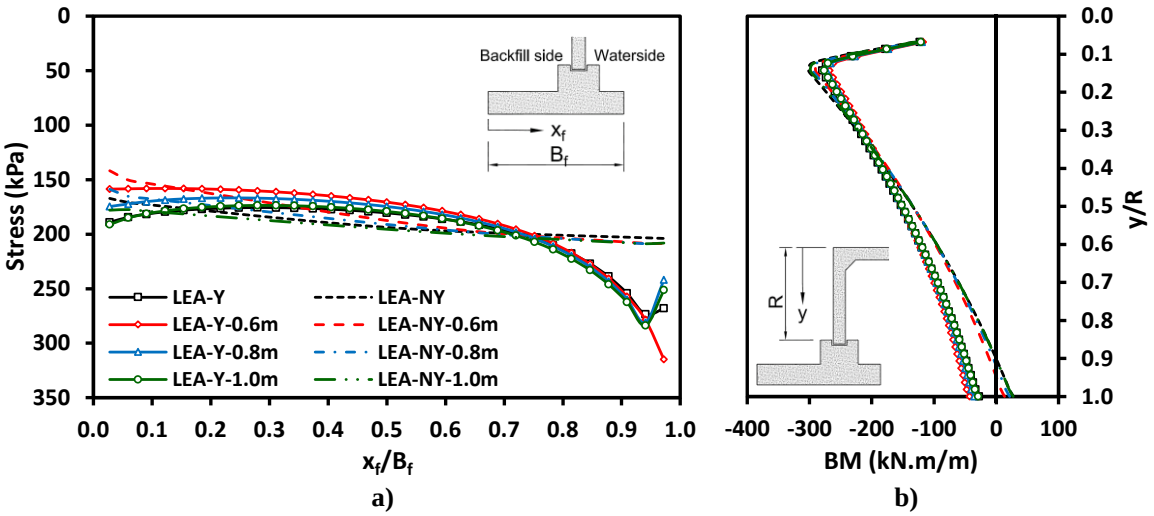

Figure 5-20. Effect of shallow foundation geometry at 3.2 m of backfill: a) stresses underneath the shallow foundation; and b) bending moment along the sidewall.

5.8 Summary and Conclusions

This chapter presents details of the preliminary finite element analyses conducted prior to the construction and instrumentation of 3 TSCs to optimize their field monitoring plans, focusing on a 10.4-m-span culvert called Pickering culvert. In addition, the Class-A

predictions of a 7.3-m-span TSC were compared with the field monitoring results obtained later. The culverts were instrumented with vibrating wire pressure cells to measure the earth pressures applied on the culvert and vibrating wire strain gauges to monitor the structural performance of the culvert during and after construction completion. The preliminary numerical model results of the Pickering culvert demonstrated the effectiveness of the conducted preliminary analysis in quantifying the target measurements to select the appropriate instruments' ranges.

The good agreement between the predicted and measured earth pressures on the culvert body and contact stresses underneath the footing after construction completion of the Pickering culvert verified the suitability of the developed numerical model, although linear elastic behavior of the RC material was assumed, which is considered acceptable for the purpose of the preliminary analysis. However, the FE model underestimated the induced strains in the culvert body, especially the tensile strains. This was attributed to the development of flexural cracks at some cross-sections, where the tensile strains exceeded the theoretical cracking strain. Thus, the assumption of linear elastic behavior of RC is not suitable for accurate estimation of the induced strains in case cracks are expected to develop in the culvert body.

Class-A prediction of the Remembrance culvert performance at the final backfill height (3.2 m) was conducted employing the 2D numerical model that was validated against the field data at 1.7 m of backfill (Chapter 4). Backfilling of the culvert to the final elevation was recently completed. Thus, field data were presented to the final backfill height, and the measurements were compared with the calculated results from the previously validated numerical models. The field measurements at the final backfill height demonstrated the reliability of the predicted values from the model. In addition, visual inspection confirmed the development of cracks on the bottom surface of the top slab, which were predicted by the nonlinear model and were determined from the final strain gauge measurements.

The validated model was employed to conduct a parametric study to investigate the effect of strip footing geometry for the cases of yielding and non-yielding foundation soil

conditions. Footings without pedestals and with thickness between 0.6 and 1.0 m were considered in the parametric study.

Based on the results of the validated numerical models and the conducted parametric study, the following conclusions can be drawn for the geometries and material properties considered:

1. Based on field measurements, the vertical earth pressure was non-uniformly distributed on the top slab at 1.7 and 3.2 m of backfill with average VAFs of 1.15 and 1.05, respectively. The calculated average VAF from the numerical model results was 1.05 at both backfill heights. These findings indicate that the specified VAF of 1.20 for B1 standard installation in CHBDC (CSA, 2014) overestimates the vertical earth pressures on large-span TSCs. Meanwhile, the measured and estimated lateral earth pressures on the culvert sidewall fell within the bounds stipulated by the code.

2. The applied earth pressures on the culvert body can be reasonably predicted assuming linear elastic behavior of the RC at service loading condition. However, this assumption leads to inaccurate prediction of the induced strains in the culvert due to crack formation.

3. The foundation soil condition, either yielding or non-yielding, does not affect the vertical earth pressure on the top slab. However, higher lateral earth pressures were estimated on the sidewall in the case of non-yielding foundation soil compared to the case of yielding foundation soil.

4. The geometry of the strip footing does not affect the applied pressures on the culvert body and the induced bending moments along the sidewall. However, the stress distribution underneath the strip footing becomes more non-uniform as the footing thickness decreases. Also, the stress underneath the footing edge on the backfill side decreases as the footing thickness decreases. More studies are still required to investigate these findings based on field or experimental tests.

These conclusions were drawn from the analysis at backfill height of 3.2 m. Thus, they might change at different backfill heights.

5.9 References

1. Balachandran, K., Liu, J., Cao, L., and Peaker, S. (2015). Statistical correlations between pressuremeter modulus and SPT N-value for glacial tills. In *Proc., 68th Canadian Geotechnical Conf. and 7th Canadian Permafrost Conf*. Richmond, BC, Canada: Canadian Geotechnical Society.

2. Bennett, R. M., Wood, S.M., Drumm, E. C., and Rainwater, N.R. (2005). Vertical loads on concrete box culverts under high embankments. *Journal of Bridge Engineering*, 10 (6), 643-649. 10.1061/(ASCE)1084-0702(2005)10:6(643).

3. Chen, B., and Sun, L. (2014). Performance of a reinforced concrete box culvert installed in trapezoidal trenches. *Journal of Bridge Engineering*, 19 (1), 120–130. https://doi.org/10.1061/(ASCE)BE.1943-5592.0000494.

4. Chen, B. C., Zheng, J., and Han, J. (2010). Experimental study and numerical simulation on concrete box culverts in trenches. *Journal of Performance of Constructed Facilities*, 24 (3), 223–234. https://doi.org/10.1061/(ASCE)CF.1943-5509.0000098.

5. CSA (Canadian Standards Association). 2014. *Canadian highway bridge design code*. CAN/CSA-S6-14. Mississauga, ON, Canada: CSA.

6. CSA (Canadian Standards Association). 2014. *Design of concrete structures (A23.3-14)*. CSA Group, Mississauga, Ontario.

7. Dassault Systems Simulia. 2013. *Abaqus-Version 6.13 Documentation*. Providence, RI: Dassault Systems Simulia Corp.

8. Duncan, J. M., and Chang. C. Y. (1970). Nonlinear analysis of stress and strain in soils. Journal of Soil Mechanics and Foundations Division, 96 (5),1629–1653.

9. Jawdhari, A., Peiris, A., and Harik, I. (2020). Load rating of bridge-size reinforced concrete arch culverts. *Structure and Infrastructure Engineering*, https://doi.org/10.1080/15732479.2020.1850803

10. Lemmen, H. E., Kearsley, E. P., and Jacobsz, S. W. (2016). The influence of foundation stiffness on the load distribution below strip foundations. In *Proc., 1st Southern African Geotechnical Conference*, Sun City, South Africa: Geotechnical Division of the South African Institution of Civil Engineering.

11. Ma, Q., Ku, Z., Xiao, H., and Hu, B. (2019). Calculation of earth pressure on culvert underlying flexible subgrade. *Results in Physics Journal*, 12, 535-542. https://doi.org/10.1016/j.rinp.2018.11.100

12. Manzari, M., Drevininkas, A., Olshansky, D., and Galaa, A. (2014). Behavioral modeling of Toronto glacial soils and implementation in numerical modeling. In *Proc., 67th Canadian Geotechnical Conf*. Richmond, BC, Canada: Canadian Geotechnical Society.

13. Marshall, J. D., Anderson, J. B., Meadows, R. L., and Jensen, T. J. (2014). Full-scale testing of three-sided precast concrete arch sections. *Journal of Bridge Engineering*, 19 (12), 04014051. 10.1061/(ASCE)BE.1943-5592.0000630.

14. McGrath, T. J., Moore, I. D., Selig, E. T., Webb, M. C., and Taleb, B. (2002). *Recommend specifications for large-span culverts.* Report No. 473. Washington, DC: Transportation Research Board.

15. MTO (Ministry of Transportation of Ontario). 2010. *Frost Penetration Depths for Southern Ontario*. Ontario Provincial Standard Drawing OPSD 3090. ON, Canada: MTO.

16. Phoon, K. -K., and Kulhawy, F. H. (1999). Evaluation of geotechnical property variability. *Canadian Geotechnical Journal*, 36, 625-639.

17. Pimentel, M., Costa, P., Félix, C., and Figueiras, J. (2009). Behavior of reinforced concrete box culverts under high embankments. *Journal of Structural Engineering*, 135 (4), 366-375. 10.1061/(ASCE)0733-9445(2009)135:4(366), 366–375

18. Ramadan, S. H., and El Naggar, M. H. (2021). Structural performance of a medium-span RC three-sided culvert based on field measurements and numerical analyses. *Canadian Geotechnical Journal.* https://doi.org/10.1139/cgj-2020-0574.

19. TNO Diana BV. 2016. *DIANA—User's manual: Material library*. Delft, Netherlands: TNO Diana BV.

20. Uzielli, M., Lacasse, S., Nadim, F., and Phoon, K. -K. 2006. Soil variability analysis for geotechnical practice. In *Proc., 2nd International Workshop on Characterization and Engineering Properties of Natural Soils*. Singapore. Taylor and Francis, The Netherlands.

21. Viviescas, J. C., Mattos, A. J., and Osorio, J. P. (2020). Uncertainty quantification in the bearing capacity estimation for shallow foundations in sandy soils. *Georisk: Assessment and Management of Risk for Engineered Systems and Geohazards*. https://doi.org/10.1080/17499518.2020.1753782

22. Yang, M. Z., Drumm, E. C., Bennett, R. M., and Mauldon, M. (1999). Measurement of earth pressures on concrete box culverts under highway embankments. *Field Instrumentation for Soil and Rock,* Durham G. and Marr W., American Society for Testing and Materials, 87-100. 10.1520/STP14215S

23. Yoo, C. H., Parker, F., and Kang, J. (2005). *Bedding and fill heights for concrete roadway pipe and box culverts*. Final Report, ALDOT Project No. 930-592, Highway Research Center, Auburn Uni., AL.

24. Zoghi, M., and Farhey, D. N. (2006). Performance assessment of a precast concrete, buried, small arch bridge. *Journal of Performance of Constructed Facilities*, 20 (3), 244–252. 10.1061/(ASCE)0887 3828(2006)20:3(244).

Chapter 6

* Field Monitoring and Numerical Analysis of a Large-Span Three-Sided RC Culvert

6.1 Introduction

Precast reinforced concrete (RC) culverts are used for passage of water, utilities, pedestrians, and even road traffic through embankments. Precast RC culverts are manufactured in different shapes, including pipe, box, and three-sided (bottomless) culverts. Three-sided culverts (TSCs) provide large hydraulic capacity at sites with limited vertical clearance to handle heavy flows. Therefore, they are typically produced in large spans and low-rise profiles. Furthermore, they provide an economical alternative for replacement of short-span bridges with clear spans below 18.3 m (Marshall et al., 2014). They also eliminate the hydraulic, environmental, and economical drawbacks of using multi-barrel box culverts (Von Handorf, 2004). Bottomless culverts can be categorized according to their shapes, i.e., arch, arched top (arched TSC), and flat top. Bottomless culverts with flat top slab are the subject of this study, hereafter referred to as TSCs.

Nowadays, TSCs are becoming more popular and are currently produced in spans up to 16.0 m. The current Canadian Highway Bridge Design Code, CHBDC, (CSA, 2014) does not provide design guidelines specific to large-span TSCs, and hence they are designed employing the same guidelines adopted for short-span box culverts. However, TSCs salient features underscore the need for specific design guidelines, including 1) typical TSCs spans fall outside the span range of conventional box culverts; 2) the absence of the bottom slab that restrains the lateral movement of the sidewall; and 3) the potential of differential settlement between the supporting strip footings. Meanwhile, studies on performance of TSCs are very scarce in the literature. Hence, this study aims to cover the current knowledge gap with regard to the structural performance of TSCs and their interaction with the surrounding soil mass. The present study involves an extensive monitoring program of

---

* A version of this chapter has been accepted for publication in Journal of Geotechnical and Geoenvironmental Engineering.

a full-scale TSC to evaluate the imposed earth pressures on the buried structure and to investigate its structural performance during and after construction. Moreover, finite element analyses (FEAs) were conducted to assess the structural performance of the buried TSC under service limit state (SLS) and ultimate limit state (ULS) conditions.

6.2 Previous Studies

Full-scale field monitoring on three-sided culverts is limited to either arch culverts, e.g., McGrath et al. (2002) and Oswald (1996), or arched TSCs, e.g., Marshall et al. (2014), Zoghi and Farhey (2006), and Beach (1988). McGrath et al. (2002) conducted a field monitoring program on a 9.1-m-span precast RC arch culvert. The backfill on top of the culvert was 1.5 m at the final stage. Field data were used to calibrate two-dimensional (2D) finite element models (FEMs). Based on field observations and numerical models, they proposed that large span arched culverts should be designed considering a nonuniform soil pressure distribution on the top slab with a vertical arching factor (VAF) of 1.0 at the midspan and 1.2 at the stiffer edges. Oswald (1996) conducted a field study on an instrumented 12.3-m-span arch culvert covered by 7.3 m of silty clay backfill. The measured soil pressure near the culvert crown was approximately 1.03 times the free-field stresses after construction completion. However, the number of installed earth pressure cells was not sufficient to reveal the pressure distribution along the culvert span. Oswald (1996) also conducted numerical analysis considering the nonlinear behavior of both concrete and backfill soil and suggested that concrete creep and shrinkage have important effects on the long-term behavior of RC buried structures.

Zoghi and Farhey (2006) investigated the ultimate load capacity of a 10.97-m-span arched TSC through a field test and a FEA. The applied loading scheme imitated two truck axles positioned side-by-side at the culvert midspan. Although failure of the culvert was not reached, it was concluded that the confinement provided by the surrounding soil mass enhanced the load-carrying capacity of the buried structure over a free-standing one. Additionally, Zoghi and Farhey (2006) pointed out that the measured horizontal displacements at the base of the sidewall were trivial at all load levels, justifying the assumption of hinged support at the base of the sidewall.

Fredrick and Tarhini (2000) conducted structural analysis of TSCs with spans between 4.2 and 11.0 m and considered two different approaches for their analysis and design. They initially used three-dimensional (3D) FEAs to evaluate straining actions in both the longitudinal and transverse directions and concluded that the straining actions in the transverse direction were minimal, and the typical shrinkage crack reinforcement would be sufficient to withstand the computed bending moments and shear forces. Consequently, they conducted 2D plane frame analyses, and their results agreed well with testing data on 1/6-size scale models. Fredrick and Tarhini (2000) suggested that TSCs can be accurately analyzed using the 2D plane frame analysis. However, their study did neither address the soil-culvert interaction and structural performance of TSCs nor the connection condition between the sidewall and the supporting strip footing. Accordingly, the present study aims to enhance the current knowledge on these subjects through field monitoring of a full-scale TSC and corresponding numerical analyses.

6.3 Culvert Construction

The subject TSC culvert has a 10.4-m-span and was constructed as part of an infrastructure project in Pickering, Ontario. The culvert consisted of 25 precast RC segments, forming a total length of 45.97 m. Each segment was 1.83-m-wide with a clear vertical hydraulic opening of 1.5 m at its midspan after construction completion. The top slab and sidewalls were 460 mm thick. **Figure 6-1** presents the geometry and reinforcement details of each precast RC segment. The precast reinforced concrete segments were erected on keyed cast-in-place strip footings. This section presents details of the followed construction procedures.

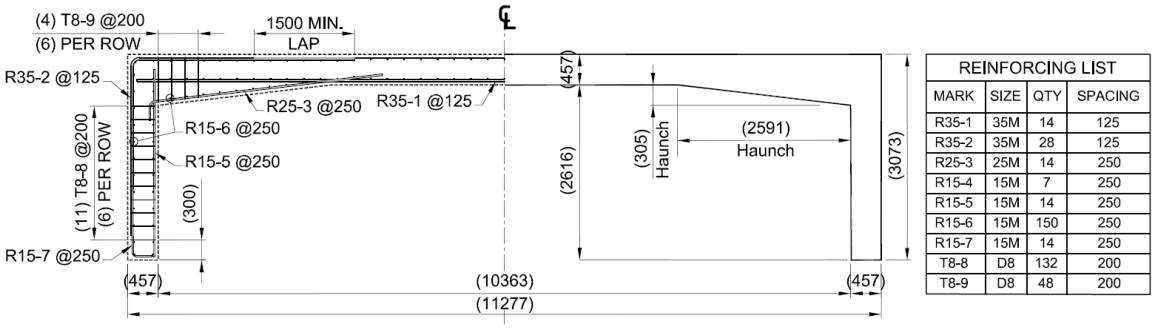

REINFORCING LIST			
MARK	SIZE	QTY	SPACING
R35-1	35M	14	125
R35-2	35M	28	125
R25-3	25M	14	250
R15-4	15M	7	250
R15-5	15M	14	250
R15-6	15M	150	250
R15-7	15M	14	250
T8-8	D8	132	200
T8-9	D8	48	200

Figure 6-1. Geometry and reinforcement details of the Pickering culvert. (All dimensions are in mm)

The construction of the precast concrete TSC commenced with the watercourse diversion and dewatering activities to facilitate construction work in dry conditions. The excavation work then started in preparation for installing the strip footings and culvert trench. When excavation reached the foundation level (FL), a concrete levelling slab (mud slab), approximately 0.1 m thick, was poured. The concrete mud slab served two functions, i.e., it provided a level bedding surface and offered a working platform for erecting the footing form and reinforcement. Afterwards, the two strip footings supporting the culvert were casted in-place. Prior to the installation of the precast segments, levelling pads (plastic shims) were placed along the keyway of the footing to guarantee the correct seating of the culvert segments. Once the segment was in its pre-specified position, plastic shims were placed between the keyway and the culvert leg to secure the segment in place and avoid any lateral spreading. The steps were repeated for the remaining segments with an acceptable 10 mm gap between the adjacent units. Sequentially, the keyway was filled with non-shrink grout.

The CHBDC (CSA, 2014) specifies two standard installation methods, namely B1 and B2 for either embankment or trench installations. The difference between the two standard installations can be summarized in the soil type and level of compaction in the sidefill and bedding zones. For the same allowed type of backfill material in the sidefill and bedding zones, the compaction requirements for B1 standard installation are higher than that for B2 standard installation, e.g., if well graded sand (SW) is used, it should be compacted to 90% and 80% of its Standard Proctor density for B1 and B2 standard installations, respectively.

Once all the precast segments were installed, backfilling against the structure was completed in lifts no greater than 300 mm and compacted to 90-100% Standard Proctor in compliance with the construction requirements stipulated by the CHBDC (CSA, 2014) for B1 standard installation. The backfilling commenced adjacent to the sidewalls simultaneously on both sides, such that the difference did not exceed 0.6 m in opposite fill layers at any stage of backfilling. Such construction approach prevents subjecting the TSC to excessive lateral deflection. The backfill soil density and moisture content were checked at each lift through nuclear density tests to assure reaching the desired compaction level. In order to avoid applying excessive loads to the culvert body, a hand-operated vibrating

plate compactor was used to compact the backfill material adjacent to the culvert body and on the top slab until reaching 0.6 m (2 ft) of soil cover. Upon reaching the 0.6 m of backfill on the culvert top slab, the compaction process was significantly accelerated as heavy-duty rollers were permitted for the subsequent lifts.

6.4 Field Monitoring

The 10.4-m-span TSC was instrumented to monitor its structural performance and quantify the imposed soil pressures against its surfaces during and after construction. One section located approximately in the middle of a road lane was instrumented with earth pressure cells (PCs) and strain gauges (SGs). For long-term monitoring purposes, the culvert was instrumented with vibrating wire (VW) sensors; 11 Model 4810 VW-PCs and 18 Model 4000 VW-SGs, distributed as shown in **Figure 6-2**. The VW-PCs were installed underneath the strip footing, on one sidewall, and on the top slab. Two VW-SGs were installed on the inner and outer surfaces of the culvert at each cross-section to measure both tensile (+ve values) and compressive (-ve values) strains. The combination of these sensors would guarantee that the structural behavior of the TSC is monitored under quantified loads. Vibrating wire sensors were selected for many reasons, i.e., 1) their stability and durability for long term measurements, as monitoring is planned to continue for three years after construction; 2) their ability to withstand harsh seasonal temperature variations, which is the case in Southern Ontario where the culvert is constructed, while operating within the manufacturer's specified accuracy; 3) the minimal effect of signal cable length on the measurements, especially that the signal cable length exceeded 40 m for some sensors; and 4) Successful previous use of the selected sensors in similar applications. The polynomial expression was used for the data reduction of Model 4810 VW-PC measurements, exhibiting an accuracy of 0.1% of its full-scale range, i.e., 0.35 kPa for the PC with 350 kPa range. The accuracy of Model 4000 VW-SG is 0.5% of its full-scale range (3000 με). All the sensors were installed according to the manufacturer's recommendations. More details on the sensors selection criteria and instruments installation are presented in Chapter 3.

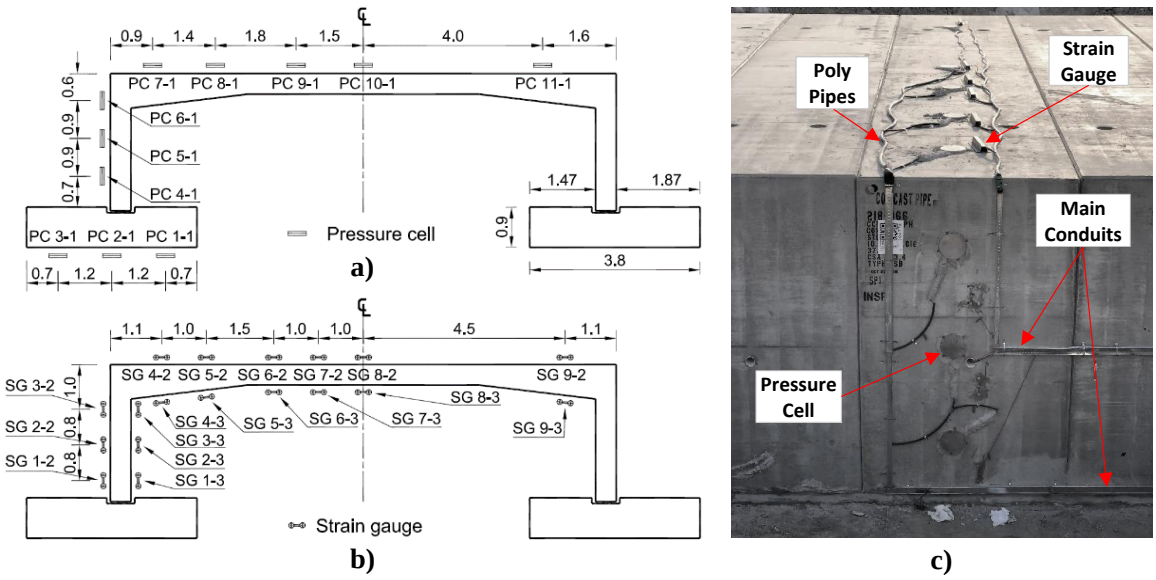

Figure 6-2. Pickering culvert instrumentation layout: a) pressure cells; b) strain gauges; and c) instrumented segment. (All dimensions are in m)

The soil profile in the vicinity of the culvert consisted mainly of sandy silt till up to 8.0 m below the ground surface. Dense sandy silt till layer extended from the ground surface up to 4.0 m below the FL. The average SPT N-value of the dense till layer was 28.7 and increased to over 100 at a depth of 4.0 m below the FL, which reflects a very dense sandy silt till layer. Accordingly, the culvert segments were founded on a 3.8-m-wide keyed strip footing with a thickness of 0.9 m as depicted in **Figure 6-2a**.

6.4.1 Monitoring Data and Analysis

Field monitoring commenced once the instruments were installed to record the induced stresses on the structure and developed strains in the RC culvert body during construction. All the installed sensors survived the construction stage and are currently functioning properly. **Figure 6-3** and **Figure 6-4** present the measured earth pressures and strains from selected sensors at different phases of construction up to date, respectively. The notations used to represent the construction phases in **Figure 6-3** are illustrated in **Table 6-1**.

Figure 6-3a demonstrates that the measured stresses below the center of the strip footing were lower than those measured closer to the edges throughout all construction stages. However, the difference diminished as the backfill height increased, reaching the final cover depth (3.1 m). Initially, before commencing with the sidefill (SF1), the difference

was 50%, then became approximately 7% after construction completion. The measured variation of stresses underneath the footing at the final backfill height reinforces the adopted design practice of assuming uniform stresses below strip footings supporting TSCs.

The lateral earth pressures (LEPs) on the sidewall shown in **Figure 6-3b** indicate higher pressures at the mid-height of the sidewall (PC 5-1) compared to that closer to the bottom (PC 4-1). This may be attributed to the higher flexibility of the sidewall at the middle compared to the top corner, where it is connected to the top slab, and the base, where it is secured in the footing keyway. Thus, the applied construction and earth loads cause more lateral deflection at the mid-height towards the sidefill, resulting in higher LEP compared to other locations. Similar observations were reported from an instrumented 2.4 × 2.4 m box culvert by James et al. (1986) and the 7.3-m-span Remembrance culvert in Chapter 4 and Chapter 5. Another explanation for the observed higher pressures at the mid-height could be the compaction-induced stresses. According to the field measurements on non-yielding and relatively flexible retaining walls reported by Carder et al. (1977), the measured lateral earth pressure was parabolic, regardless of the retaining wall flexibility. In addition, Carder et al. (1977) observed that the compaction-influenced zone rose with the rise of the compaction surface, leading to higher compaction-induced LEP at shallow depths, which decreases below the compaction-influenced zone. Similar observations were reported by Chen and Fang (2008), who studied the LEP against a non-yielding retaining wall under soil filling and vibratory compaction loads. Chen and Fang (2008) reported that below the compaction-influenced zone, the measured LEP converged to the Jaky at-rest state of stress, which means that the LEP below the compaction-influenced zone was the same as would occur without compaction. However, the latter explanation is less likely for two reasons: 1) a hand-operated vibrating plate compactor was used to compact the sidefill material adjacent to the culvert. Elshimi and Moore (2013) concluded that the compaction-induced stresses are insignificant and can be ignored in case a vibratory plate compactor was used, which represents the case in this study; and 2) the compaction effort of the sidefill soil adjacent to the instrumented sidewall was reduced to prevent damage to the monitoring sensors that may occur due to excessive compaction loads.

Figure 6-3b also shows that some relaxation of the measured LEPs occurred after each backfilling phase on the top slab. This behavior is attributed to combined effects of the relaxation of the compaction induced locked-in-stresses in the sidefill material and the unloading of construction equipment loads. Both actions reduced the wall lateral deformation and, hence reduced the LEP. The PC located at the mid-height of the sidewall (PC 5-1) exhibited the highest relaxation after each backfilling phase, which suggests that the unloading of construction equipment loads might be the main contributor to the observed response.

Figure 6-3c presents the measured vertical earth pressures (VEPs) on the top slab at the edges and midspan. It is noted from the figure that higher pressures were measured at the top slab edges compared to the relatively flexible midspan of the slab, which is in agreement with field measurements of a smaller span TSC as discussed in Chapter 5, arch culverts (McGrath et al., 2002), and box culverts (Chen and Sun, 2014; Yang, 2000). Average values of the measured VEPs at 3.1 m of backfill are summarized in **Table 6-2**. The measured pressures along the top slab (PC 7-1 to PC11-1) suggest an average VAF of 1.04, which is calculated as the average of the measured VEPs normalized by the free-field stress ($\gamma_s H$), where γ_s is the backfill soil unit weight, and H is the backfill height.

Table 6-1. Construction phases description for the Pickering culvert.

Construction phase	Status	Construction phase	Status
CI	The culvert precast units were installed	BF1	Backfill of 0.3 m over the top slab
SF1	Start of sidefill adjacent to the sidewalls	BF2	Backfill of 2.0 m over the top slab
SF2	Sidefill reached the top slab	BF3	Backfill of 3.1 m over the top slab

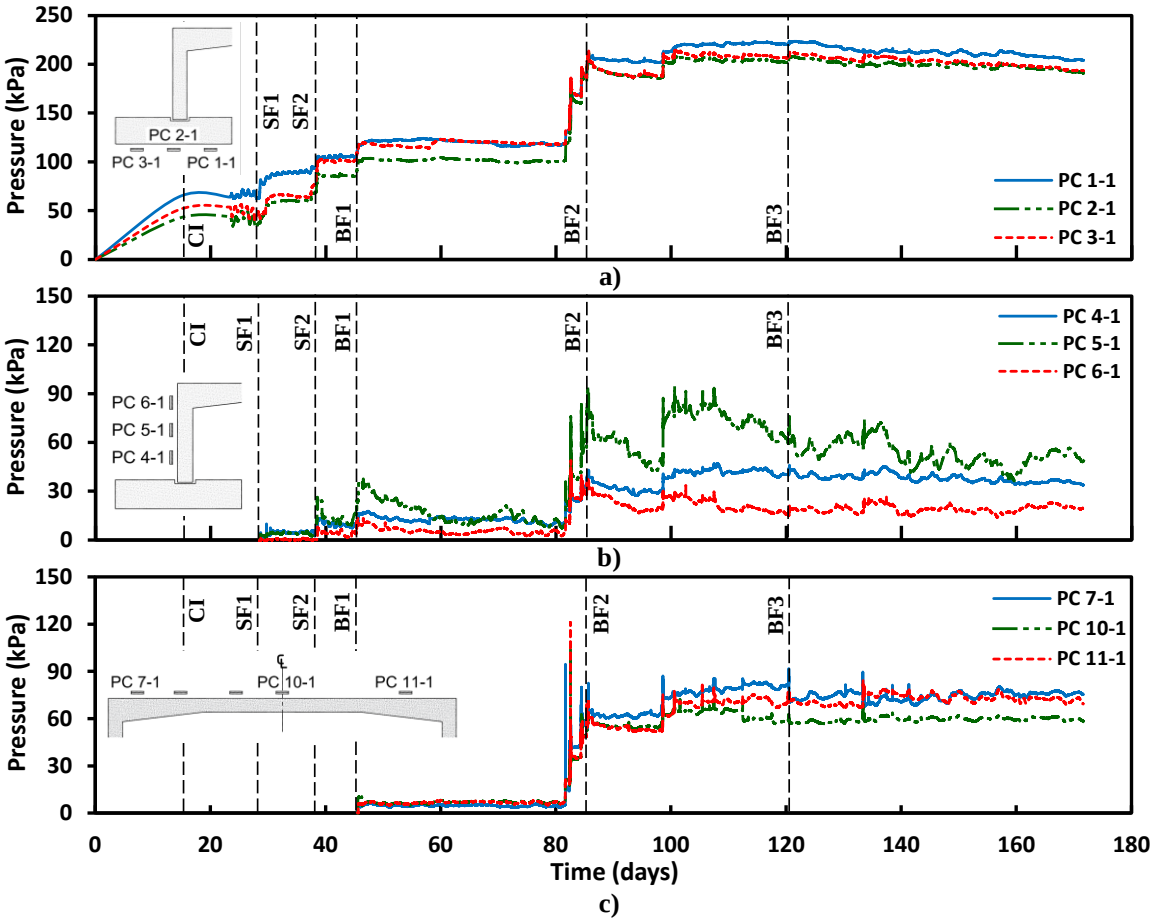

Figure 6-3. Sample pressure cell measurements: a) pressures below the footing; b) pressures on the sidewall; and c) pressures on the top slab.

Figure 6-4 shows samples of the SG measurements, and the average strains at the final backfill height are summarized in **Table 6-2**. The measured compressive strains were higher than the corresponding tensile strains at each cross-section apart from the midspan cross-section, which exhibited the highest tensile strain (490.8 με).

The average 28-day concrete compressive strength (f_c') was approximately 65 MPa for the precast culvert. According to CSA A23.3-14 (CSA, 2014), the theoretical cracking strain (ε_{cr}) can be calculated from f_c' using **Equation (6-1)**,

$$\varepsilon_{cr} = \frac{f_r}{E_c} = \frac{0.6\lambda\sqrt{f_c'}}{4500\sqrt{f_c'}} = 133\ \mu\varepsilon \qquad \textbf{(6-1)}$$

where f_r is the concrete modulus of rupture, E_c is the concrete Young's modulus, and λ is the modification factor to account for the reduced mechanical properties of lightweight concrete relative to normal weight concrete of the same f_c' (λ = 1.0 for normal weight concrete (CSA, 2014), which reflects the case in the present study). Cracks occur once the tensile strain exceeds ε_{cr} (133 με). Thus, cracks are expected at the 5 instrumented cross-sections bolded in red in **Table 6-2**. It should be noted that no sudden jumps in the strain measurements occurred due to the cracks' formation and the measured tensile strains at the cross-sections bolded in red in **Table 6-2** gradually increased with the advancement of backfilling, exceeding the estimated ε_{cr}.

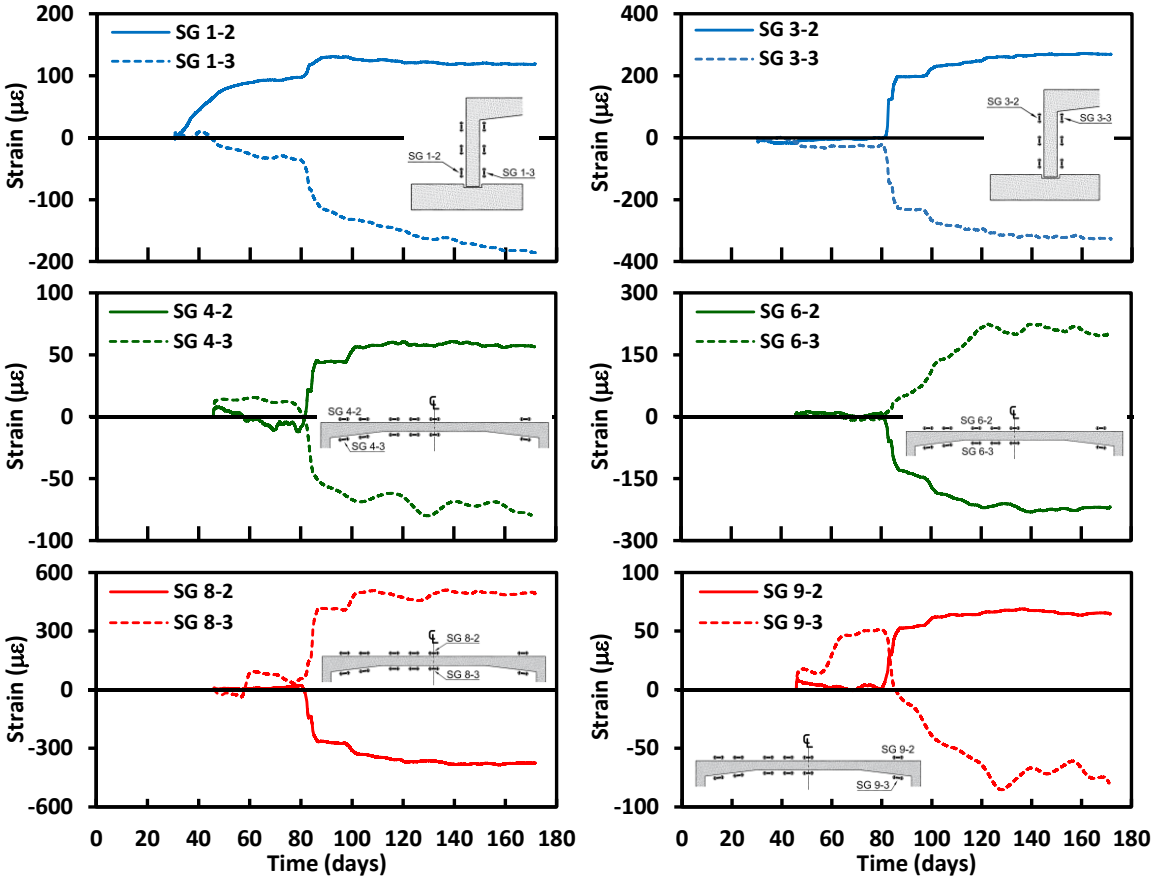

Figure 6-4. Sample strain gauge measurements of the Pickering culvert.

Table 6-2. Summary of the measured average stresses and strains at 3.1 m of backfill.

Average stresses					
Sensor	Average stress (kPa)	Sensor	Average stress (kPa)	Sensor	Average stress (kPa)
PC 1-1	212.6	PC 5-1	50.0	PC 9-1	70.5
PC 2-1	198.4	PC 6-1	22.6	PC 10-1	61.2
PC 3-1	201.2	PC 7-1	77.3	PC 11-1	73.1
PC 4-1	40.0	PC 8-1	72.2		
Average strains					
Sensor	Average strain (με)	Sensor	Average strain (με)	Sensor	Average strain (με)
SG 1-2	118.7	SG 7-2	-323.7	SG 4-3	-78.8
SG 2-2	**162.3**	SG 8-2	-376.8	SG 5-3	-49.1
SG 3-2	**270.4**	SG 9-2	64.8	SG 6-3	**201.2**
SG 4-2	56.9	SG 1-3	-182.8	SG 7-3	**317.6**
SG 5-2	2.6	SG 2-3	-222.3	SG 8-3	**490.8**
SG 6-2	-220.3	SG 3-3	-324.9	SG 9-3	-74.2

6.5 Numerical Model (SLS)

The field monitoring data was utilized to validate 2D FEMs established using the computer software DIANA 10.1 (2016). Eight-node quadrilateral plane-stress elements were used to discretize the culvert body to account for the presence of transversal joints between the culvert segments (Pimentel et al., 2009), while 8-node quadrilateral plane-strain elements were used for the strip footing and soils. The model was extended 5.5 times the culvert span on either side of the culvert to eliminate the boundaries influence. The model bottom boundary was restrained from vertical and horizontal movements, and the side boundaries were restrained from horizontal movement. **Figure 6-5** presents the geometry, boundary conditions, and mesh of the developed model. It should be noted that only half the model is displayed in **Figure 6-5**. The native soil was discretized into two layers as depicted in **Figure 6-5**, dense sandy silt till from the ground surface up to 4.0 m below the FL followed by 4.0 m of very dense silty till to account for the noticeable increase in the measured SPT N-value at 4.0 m below the FL. The mesh was refined within the zone surrounding the culvert to enhance the accuracy within the studied area. The model comprised 24,475

plane-strain elements and 3,307 plane-stress elements. The sidefill and backfill soils were divided into 13 layers, six of which are over the TSC. Construction phased analysis was adopted to simulate the incremental nature of culvert backfilling. The geostatic stresses of a new sidefill/backfill layer were introduced in each phase. The solution of each loading increment was reached iteratively using the Quasi-Newton (Secant) iteration method. Convergence of each loading increment was achieved once the estimated out-of-balance force norm and displacement norm ratios were below 0.01. The compaction induced stresses were not considered in the analysis due to the difficulty of quantifying the compaction equipment loads and their movement pattern. Moreover, Elshimi and Moore (2013) numerically investigated the behavior of five pipe culverts, i.e., two concrete pipes, two corrugated steel pipes, and one high density polyethylene (HDPE) pipe, all with an inner diameter of 2.0 m. Elshimi and Moore (2013) studied the effect of compaction forces on the behavior of the different concrete pipes. Based on the measured values reported by McGrath et al. (1999) and the results of the numerical models developed by Elshimi and Moore (2013), they concluded that the effect of compaction-induced stresses can be ignored in case a vibratory plate compactor was used, which represents the case in the present study as described in the "Culvert Construction" section.

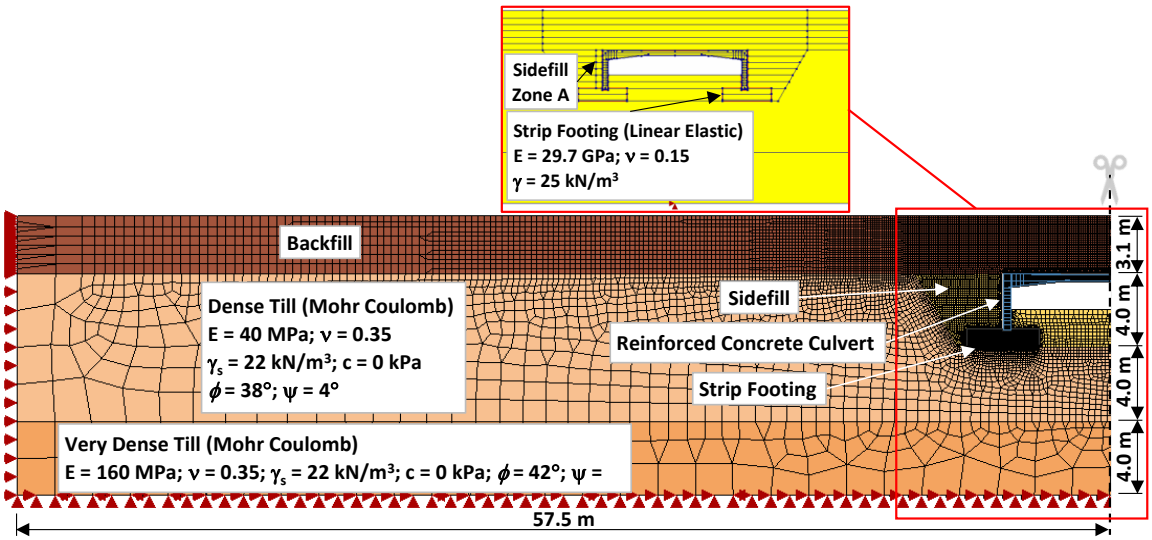

Figure 6-5. Geometry and meshing details of the Pickering culvert 2D FE model.

Two sets of models were conducted to highlight the influence of the nonlinear behavior of RC: linear elastic analysis (LEA) and nonlinear analysis (NLA) models. Nonlinear material

model was considered for sidefill and backfill soils in both models; however, linear-elastic behavior was assumed for RC in LEA model, while nonlinear concrete behavior was assumed in NLA model as will be detailed in the following subsections.

6.5.1 Native Soil

The elastic-plastic Mohr-Coulomb material model was used to simulate the behavior of the native sandy silt till. The native soil consisted of cohesionless till deposit comprising 55% silt, 33% sand, and scattered gravel and cobbles. The soil elastic modulus (E_s) was evaluated employing an empirical correlation with the measured SPT N-values, i.e., E_s = 1.33×N (Balachandran et al., 2015). The estimated E_s values are 40 and 160 MPa for the dense and very dense sandy silt till, respectively. Manzari et al. (2014) conducted a series of sixteen triaxial tests on undisturbed cohesionless till materials extracted from different locations across Toronto, Ontario, Canada. They reported that the internal friction angle (ϕ) of the tested cohesionless till ranged from 31° to 45° and the cohesion (c) ranged from 0 to 50 kPa. Based on the ranges provided by Manzari et al. (2014) and values reported in factual geotechnical reports on the till material of Ontario, the cohesion of both cohesionless till layers was set to 0 kPa and an angle of internal friction of 38° was assigned for the dense layer as opposed to the 42° for the very dense one as illustrated in **Figure 6-5**. According to Pimentel et al. (2009), the value of angle of dilation (ψ) between 0° and 15° did not influence the obtained results. Similarly, a sensitivity analysis was conducted in this study within the same range of ψ (0° and 15°) and the same conclusion as that of Pimentel et al. (2009) was drawn from this sensitivity analysis. Thus, the angle of dilation for the native till soils was assumed to be 0° for both till layers.

6.5.2 Backfill Soil

Well-graded sand (SW) was used as backfill along the sides of the culvert and up to 0.5 m on top of the culvert. The remainder of the embankment was backfilled with sandy silt (ML) from a nearby cut area. Both sidefill and backfill materials were compacted up to 90-100% of the Standard Proctor density in compliance with the compaction requirements of B1 standard installation in the CHBDC (CSA, 2014).

The applied earth pressure acting on buried structures is governed by the stiffness of the surrounding granular fill, which is stress-dependent. Accordingly, the hyperbolic Duncan-Chang constitutive model (Duncan and Chang, 1970) was assigned for the sidefill and backfill materials for realistic simulation of the soil-structure interaction problem. Boscardin et al. (1990) conducted laboratory testing on well-graded sand (SW), sandy silt (ML), and silty clay soils (CL), which are typically used as backfilling materials for buried structures, covering a wide range of densities representing different compaction levels. The grain size distributions of the SW and ML used in constructing the studied culvert were compared with those of the SW and ML soils tested by Boscardin et al. (1990). The grain size distribution curves of the soil tested by Boscardin et al. (1990) were obtained from Yang (1987). The comparison demonstrated the similarity between the particle size distributions of the soils used in the culvert construction and those tested by Boscardin et al. (1990) as shown in **Figure 6-6**, justifying the use of the properties reported by Boscardin et al. (1990) to simulate the behavior of the sidefill and backfill materials of this study. Based on the conducted nuclear density tests during the backfill operations, the average degrees of compaction for the sidefill and backfill materials were specified as 91.7% and 96.2%, respectively. Accordingly, the sidefill was considered well-graded sand (SW) compacted to 90% of the Standard Proctor density (SW-90), while the backfill soil was considered low plasticity silt compacted to 95% of its Standard Proctor density (ML-95). Moreover, an average density of 22.0 kN/m^3 was specified as per the nuclear density tests conducted on-site. The assigned properties for the sidefill and backfill materials are illustrated in **Table 6-3**.

Table 6-3. Material properties for the sidefill and backfill soils. (After Boscardin et al., 1990)

Soil Type	% Standard Proctor	ν	c (kPa)	ϕ (°)	K	R_f	N
SW	90	0.30	0	42	640	0.75	0.43
	80	0.30	0	36	320	0.83	0.35
ML	95	0.35	28	34	440	0.95	0.40

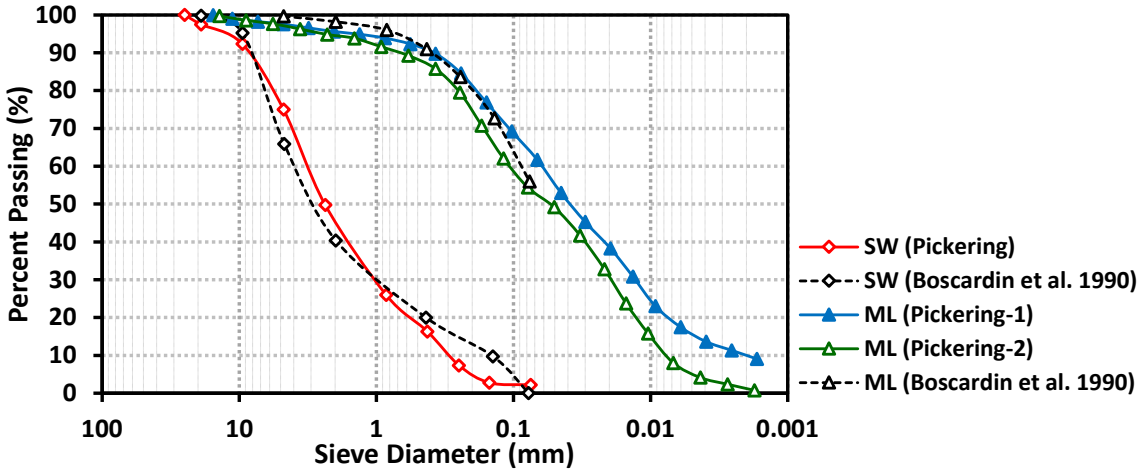

Figure 6-6. Comparison between the gradation of the sidefill and backfill soils used in this study and the soils tested by Boscardin et al. (1990).

6.5.3 Reinforced Concrete

The average 28-day compressive strength (f_c') of the precast culvert was 65 MPa. In LEA model, the culvert behavior was represented by an equivalent Young's modulus (E_c = 37.9 GPa) and Poisson's ratio (ν = 0.15).

For NLA model, the total strain-based smeared crack model was used, which simulates the nonlinear behavior of concrete with sufficient accuracy (Pimentel et al., 2009). The smeared crack model is based on the Modified Compression-Field Theory, which assumes that cracks are formed normal to the direction of the principal tensile strain (Vecchio and Collins, 1986). The fixed crack concept was adopted for the formulation of the smeared crack model, where the orientation of the crack is kept fixed throughout the computational process. The crack bandwidth was estimated as a function of the element size, i.e., $\sqrt{2}$ element size = 7 mm (Rots and Blaauwendraad, 1989). The Thorenfeldt model was implemented to represent the strain-softening behavior of concrete under compression loading (Thorenfeldt et al., 1987), while the tension softening behavior was simulated following the Hordijk nonlinear model (Hordijk, 1991). All the smeared crack model parameters were correlated to f_c' (65 MPa) of normal weight concrete as per the guidelines of fib Model Code 2010 (2013) and are exhibited in **Table 6-4**. The lower E_c assigned for concrete in LEA model in comparison with NLA model is to account for the initial plastic strain when elastic behavior is assumed for RC (fib Model Code, 2013). The strip footing

was modeled using the linear-elastic model in both models with E_c of 29.7 GPa as illustrated in **Figure 6-5** for f_c' of 40 MPa.

In NLA model, the steel reinforcement was modeled as embedded bar elements, fully bonded to the host elements (concrete). The embedded bar elements have no degrees of freedom of their own; instead, the stresses and strains are fully coupled to the degrees of freedom of the adjacent nodes of the host elements (TNO Diana BV, 2016). The von Mises plasticity model was employed for the reinforcing steel without considering the hardening behavior. Yielding stress (f_y) of 450 MPa and Young's modulus (E_{st}) of 200 GPa were assigned for the reinforcing bars.

Table 6-4. Input parameters for the concrete smeared crack model.

Compressive strength f_c' (MPa)	Young's Modulus E_c (MPa)	Tensile strength f_{ct} (MPa)	Fracture energy G_f (Nmm/mm^2)	Poisson's ratio ν -
65.0	41707	6.4	0.2332	0.15

6.5.4 Interfaces

Two sets of interfaces existed in the current soil-structure interaction problem; the soil-culvert interface and the culvert-footing interface. Both sets were modeled using 2D line interface elements with frictional behavior defined with the Mohr-Coulomb yielding criterion. The normal and shear relative displacements across the interfaces are governed by their normal and tangential stiffnesses, D_{nn} and D_{tt}, respectively, which were estimated using the recommended formulae (TNO Diana BV, 2016):

$$D_{tt} = \frac{A^2}{t} G = \frac{A^2}{t} \frac{E_s}{2(1+\nu_s)}$$
$$D_{nn} = f \times D_{tt} \qquad \textbf{(6-2)}$$

where A is a reduction factor (0.67), f is a multiplication factor (50), t is the virtual thickness of the interface (10 mm), G is the soil shear stiffness, E_s is the soil Young's

modulus, ν_s is the soil Poisson's ratio. The interface friction angle and cohesion were estimated by multiplying the soil values, illustrated in **Table 6-3**, times the reduction factor (A).

The culvert sidewall was embedded 100 mm into the strip footing when constructed. The segments were secured in-place using plastic shims, and the keyway was filled with cementitious non-shrink grout having a compressive strength of 30 MPa. Correspondingly, the grout mechanical properties proposed by Samaiklang and Fuenkajorn (2013) for a cement grout with 27.64 MPa compressive strength (E = 3.56 GPa, ϕ = 40°, and c = 5.42 MPa) were implemented in calculating the culvert-footing interface properties. Modeling the culvert-footing interface, which has never been considered in numerical modeling of TSC thus far, was necessary to evaluate the influence of this contact condition on the culvert soil-structure interaction.

6.5.5 Composed Line Elements

Composed line elements were used to estimate the bending moment (BM) along the culvert span and sidewall as BM is not a direct output of plane-stress elements. They are non-structural elements without any mechanical properties. BMs are calculated within a specified cross-section by integrating the internal stresses in the plane-stress elements over the cross-section plane perpendicular to the composed line element. The specified cross-section was 1.0 m thick for the subject culvert to ensure accounting for internal stresses within the nonuniform sections of the culvert at the haunch zones for accurate estimation of the BM. Thus, in short, composed line elements are only applied by the software in post-processing of analysis results. For NLA model, the reinforcement contributes to the estimated BM in composed line elements (TNO Diana BV, 2016).

6.5.6 Model Validation

The field measurements after construction completion, presented in **Table 6-2**, were employed to validate the developed numerical models. Two different scenarios were considered for LEA model, designated LEA-1 and LEA-2 based on the compaction condition of the sidefill near the instrumented sidewall. In LEA-1 model, the sidefill

material was assigned the properties of SW-90 provided in **Table 6-3**. **Figure 6-7** shows good agreement between the results of LEA-1 model and the field measurements in terms of the vertical earth pressure (VEP) on the top slab and the stresses underneath the strip footing. However, LEA-1 model overpredicts the lateral earth pressure (LEP) along the sidewall as shown in **Figure 6-7c**. As previously mentioned, the compaction effort of the sidefill soil adjacent to the instrumented sidewall was reduced to prevent damage to the monitoring sensors that may occur due to excessive compaction loads. Therefore, the 0.5 m sidefill adjacent to one sidewall, denoted as "Zone A" in **Figure 6-5**, was assumed to be compacted to 80% of its Standard Proctor density as nuclear density tests were not performed in this zone. Thus, the sidefill material in Zone A was assigned the properties listed in **Table 6-3** for SW-80 in LEA-2 model to account for the observed reduced compaction effort. The computed LEP from LEA-2 model exhibited excellent agreement with the field data as shown in **Figure 6-7c**. It was also observed that weakening the sidefill in Zone A had no effect on the computed pressures on the top slab or stresses underneath the footing. Consequently, the defined sidefill materials in LEA-2 model were adopted in NLA model.

Both LEA-2 and NLA models yielded approximately the same pressure values on the culvert body and below the footing as depicted in **Figure 6-7**. This suggests the adequacy of simulating RC culvert with linear-elastic behavior at service load levels to accurately predict earth pressures on the buried structure.

The obtained results from the FEMs revealed nonuniform earth pressure distribution on the top slab, with higher pressures at the top slab edges and lower pressure at the midspan. Previous studies on box culverts (Cristelo et al., 2019; Chen et al., 2016), arched culverts (McGrath et al., 2002), and TSCs (Chapters 4 and 5) reported similar observations. However, the current design practice of TSCs in the CHBDC (CSA, 2014) stipulates uniform soil pressure distribution on the top slab with a VAF of 1.2 for B1 standard installation, which represents the accomplished construction for the subject TSC. Both the measured and calculated earth pressures demonstrate that the CHBDC (CSA, 2014) overestimates the earth pressure on the top slab by considering a VAF of 1.2 for B1 installation. A similar conclusion was reported in Chapters 4 and 5 based on field

measurements on a similar TSC with smaller span. In order to simplify the loading configuration, it is proposed to consider uniform earth pressure distribution with a VAF of 1.05 to represent the applied pressures on the subject culvert more realistically (**Figure 6-7a**). This reflects a reduction of 12.5% in VAF compared to the value proposed in the current code for closed box culverts. For large spans TSCs with deep cover depths, such reduction would result in a more cost-effective, yet reliable design. However, more studies are still required to accredit the prevalence of such findings.

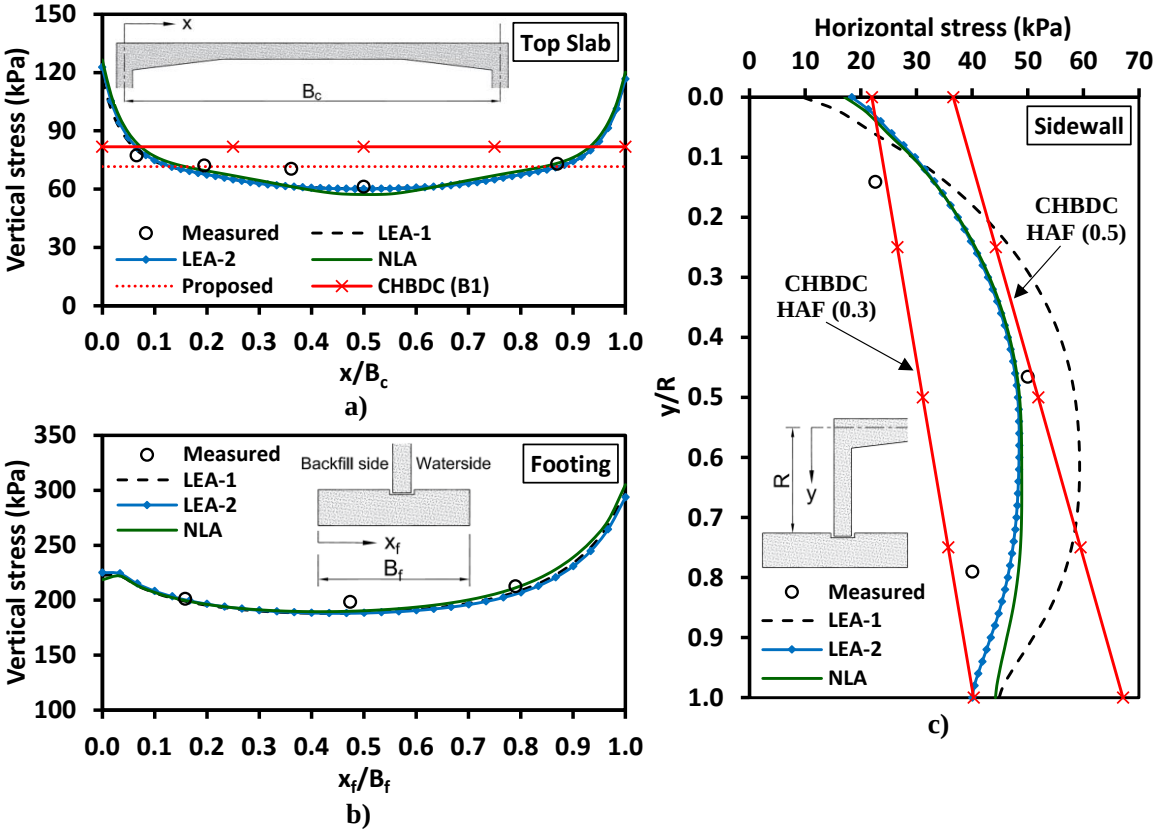

Figure 6-7. Comparison between measured and estimated pressures at 3.1 m of backfill: a) vertical pressure on the top slab; b) stresses below the strip footing; and c) lateral pressure on the sidewall.

The measured stresses at three locations underneath the footing exhibited a maximum difference of 7% at the end of construction, indicating almost uniform stress distribution below the strip footing. **Figure 6-7b** indicates excellent agreement between the measured and computed values. However, the calculated stresses were high at the edges, especially near the waterside. In general, the predicted stress distribution below the footing is almost

uniform along 70% of the footing width, indicating the adequacy of uniform stress assumption for the design of the strip footings supporting TSCs.

Figure 6-7c compares the measured LEP along the sidewall with the computed values from the numerical models. The comparison shows good agreement, with parabolic distribution of the LEP along the sidewall. Dasgupta and Sengupta (1991) and Oshati et al. (2012) reported the same parabolic LEP distribution. The current CHBDC (CSA, 2014) specifies a linear increase of LEP along the sidewall with upper and lower bounds. According to the code, separate analyses should be conducted using the design VEP combined with the upper and lower bounds of the LEP, and the governing loading combination should be considered for the design of each structural element of the culvert. The specified maximum and minimum horizontal arching factors (HAFs) for B1 standard installation are 0.3 and 0.5, respectively. The data presented in **Figure 6-7c** indicate that both field measurements and numerical results mostly fall within the lower and upper bounds of the code. It is therefore recommended to continue with the code provisions regarding the estimation of LEP on the sidewalls of TSCs.

Figure 6-8 displays the crack pattern and crack strain contours obtained from NLA model. The predicted cracked zone on the top slab coincides with that observed in the field. The numerical simulation indicated flexural cracks formation on the upper top corner of the sidewalls as shown in **Figure 6-8**. These cracks could not be visually inspected; however, the SGs measurements, i.e., SGs 2-2 and 3-2 summarized in **Table 6-2**, demonstrated that cracks occurred at these locations. Such consistency reflects the reliability of field measurements and the developed numerical simulation. As previously discussed, the collected SGs data indicated that the cracking strain (ε_{cr} = 133 με) was exceeded at 5 cross-sections, i.e., SGs 2-2; SGs 3-2; SGs 6-3; SGs 7-3; and SGs 8-3. In comparison, the marked locations of the SG groups in **Figure 6-8** indicate cracks at 4 cross-sections, the exception being the location of SG 2-2. It should be noted that the measured tensile strain by SG 2-2 was the lowest amongst the 5 cross-sections (162 με), with a value slightly higher than the theoretical ε_{cr}. The predicted maximum crack width from the validated nonlinear model was 0.17 mm, which is lower than the maximum allowable crack width of 0.25 mm (0.1″) specified by the CHBDC (CSA, 2014) excluding the influence of live load. Thus, the

numerical results demonstrate that the test culvert meets the code serviceability crack limits under the current applied loads.

Visual inspection of the interior surfaces of the TSC was undertaken after the road completion. Flexural cracks were observed on the bottom surface of the top slab within the middle 5.2 m, where the slab thickness is 457 mm (as shown in **Figure 6-1)**. The minimum and maximum spacing between two successive cracks were 70 and 190 mm, respectively, with an average spacing of 140 mm. The insert in **Figure 6-8** provides an image of the crack pattern in the vicinity of SG 8-3 located at the midspan. The crack widths were too small to be directly measured in the absence of a measuring tool with adequate tolerance. These observations further confirm the reliability of the numerical model in predicting the structural behavior of the TSC.

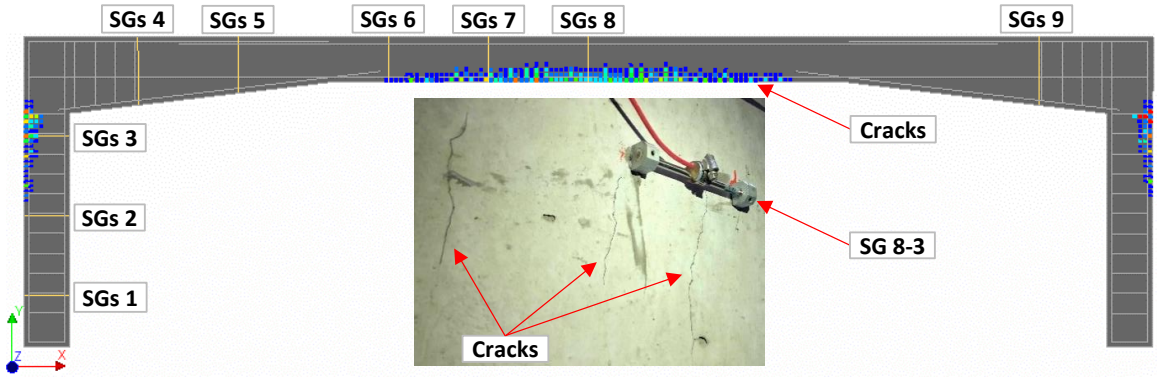

Figure 6-8. Predicted crack pattern (model) and observed cracks at the midspan (image) at 3.1 m of backfill.

The pairs of SGs installed on the inner and outer surfaces of each cross-section enabled the measurement of tensile and compressive strains, from which the bending moment (BM) could be estimated. The moment-curvature relationship of each cross-section was determined for accurate representation of the nonlinear behavior and cracks formation. The BM at each cross-section was determined from the moment-curvature curve using the corresponding curvature value (κ) evaluated as follows:

$$\kappa = \frac{(\varepsilon_i - \varepsilon_e)}{d} \qquad \textbf{(6-3)}$$

where ε_i is the strain measured on the inner surface, ε_e is the strain measured on the outer surface, and d is the section depth. The BM is deemed positive when the tensile strain exists on the inner surface of the culvert. **Figure 6-9** presents the BM distribution interpreted from the SG measurements and FEMs. **Figure 6-9** shows lower BMs computed at the cracked zones of the sidewall and top slab by NLA model compared to LEA-2 model. The lower BM magnitudes are attributed to the degradation of the flexural stiffness of the cross-section once cracks occurred, which was not accounted for in LEA-2 model. Overall, the BMs obtained from NLA model are in better agreement with the estimated values using the SGs measurements.

The current design practice of TSCs assumes the sidewall base is pinned (hinged) at the foundation and such condition was suggested in previous studies on arched TSCs (Zoghi and Farhey, 2006; Beach, 1988). However, the BM distribution on the sidewall displayed in **Figure 6-9b** clearly exhibits BM at the sidewall base. This BM may be attributed to the rotation of the footing combined with the connection condition at the base. Rotation of the footing would induce additional stresses to the enclosed portion of the sidewall in the footing causing sufficient rotational restraint, and consequently the development of BM. The footing rotation calculated from NLA model was 2.18×10^{-4} radian. The rotational stiffness (K_F) could be employed to calculate the rotation-induced BM at the base. For a smooth strip footing, K_F can be theoretically calculated as per the following expression (Muskhelishvili, 1963):

$$K_F = \frac{BM}{\theta} = \frac{2\pi\mu {B_f}^2}{(\chi+1)} = 517\ MN.m/rad$$
$$\chi = \frac{\lambda+3\mu}{\lambda+\mu} = 1.6 \qquad \textbf{(6-4)}$$

where θ is the footing rotation in radian, B_f is the footing width (3.8 m), and λ, μ are Lame's parameters. The theoretically computed BM at the base of the sidewall using Eq. 4 is -112.9 kN.m/m, which is comparable with the value evaluated from NLA model (-128.7 kN.m/m). These results indicate that the connection condition between the sidewall

and the supporting footing as described in the present study is not truly pinned, and it is prudent to calculate the developed BM at the base once rotation of the footing is predicted.

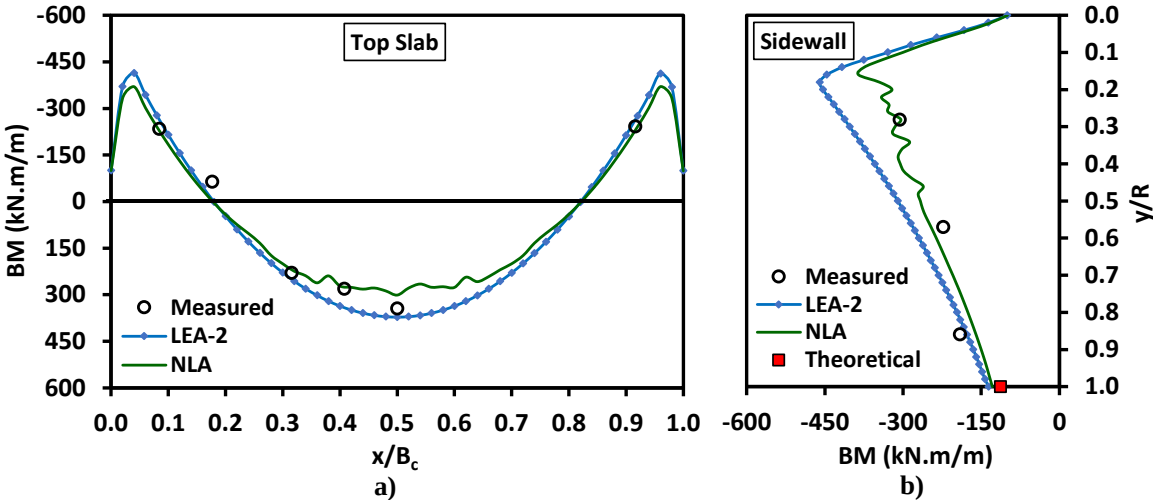

Figure 6-9. Comparison between estimated bending moments from the SG measurements and numerical models at the end of construction: a) top slab: and b) sidewall.

6.6 Numerical Model (ULS)

This section presents the results of the finite element analyses conducted to quantify the ultimate capacity of the subject TSC and the influence of the lateral confinement provided by the surrounding soil on the culvert performance. In addition, the effect of the concrete model, either linear-elastic or nonlinear, on the interaction mechanism at the ultimate limit state (ULS) is addressed.

6.6.1 Model Validation

Marshall et al. (2014) investigated the ultimate capacity of precast RC arched TSCs in an experimental study. They loaded two precast segments of arched TSCs to failure in a laboratory setting. The spans of the two tested segments were 6.1 m and 11.0 m. The test data of the 11.0-m-span segment was employed to validate the developed numerical model. The tested segment was 1.2-m-wide and had a clear midspan height of 2.7 m.

The segment was directly placed on the rigid laboratory floor and was laterally restrained at the base using HSS steel beams. Vertical loads were applied incrementally through three

W8×35 beams spanning the width of the segment. Each increment was 17.8 kN per beam. One loading beam was positioned at the midspan, and the other two were placed 1.2 m on either side as shown in **Figure 6-10a**. The precast concrete strength was f_c' = 48.5 MPa and elastic modulus, E_c = 28.3 GPa. The steel reinforcement had yield strength, f_y = 507 and 642 MPa for the small and large bars, respectively, and elastic modulus, E_{st} = 182.7 GPa (Marshall et al., 2014).

A nonlinear 3D FEA was conducted to simulate the experimental loading test. The culvert geometry and reinforcement layout reported by Marshall et al. (2014) were simulated with the same reported geometrical and material properties. Twenty-node solid brick elements with quadratic interpolation were used to model the culvert, while embedded elements were used for the reinforcing bars. The culvert body comprised 23,263 brick elements with a maximum size of 50 mm. The concrete nonlinear behavior was modeled using the smeared crack model, and the von Mises plasticity model without hardening behavior was employed to simulate the behavior of the reinforcing steel. The boundary condition at the bottom surface of the sidewall was assumed fixed in the vertical direction (Z-axis), while the outer edge at the bottom of the sidewall was fixed in the lateral direction (X-axis) as detailed in **Figure 6-10a**. The analysis procedure included incremental loading that replicated the implemented loading sequence during the experimental test. In each loading increment, a vertical stress of 71.65 kPa was applied over an area equal to the contact surface of the W8×35 beam with the culvert (1.2 m x 0.207 m) at each location of the three loading beams.

The same analysis assumptions and procedures were used to evaluate the ULS behavior of the TSC of the present study considering the geometry and reinforcement details presented in **Figure 6-1**. The same material properties used for concrete and reinforcing steel in NLA model were defined in the 3D TSC model. Features of the TSC model are presented in **Figure 6-10b**.

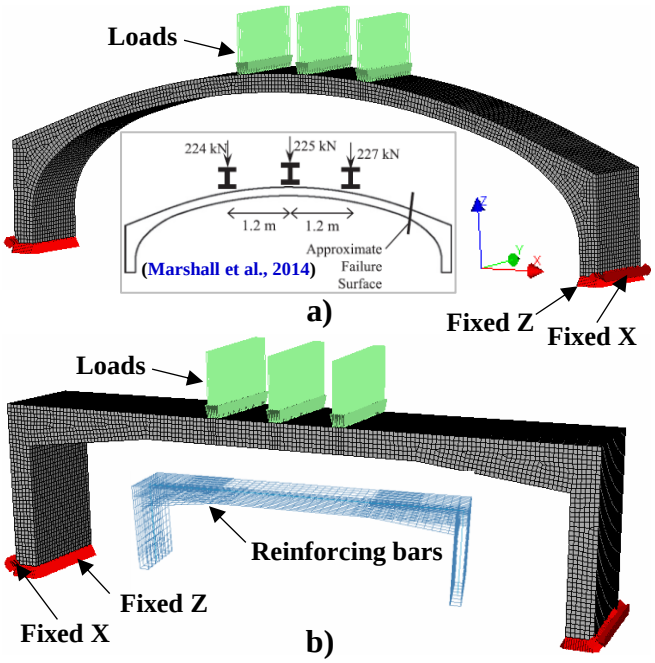

Figure 6-10. Overview of the 3D FE models: a) TSC with arched top slab; and b) Pickering TSC.

Figure 6-11a compares the load-deflection curves at different locations obtained from the FEA and the reported experimental results. The comparison demonstrates that the model predicted the ultimate load-carrying capacity accurately; the computed ultimate load was 673 kN, while the measured capacity was 675.7 kN. However, the numerical model underpredicted the vertical deflection at the midspan, indicating relatively stiffer behavior compared to the experimental observations. The calculated stiffer behavior may be attributed to: 1) the assumption of full bond between the concrete and reinforcing steel; 2) the inability of the smeared crack model to account for the discontinuity nature of cracks; and 3) stress-locking behavior which accompanies displacement-based FEAs with smeared softening approaches (Rots and Blaauwendraad, 1989). The load-deflection curves at the midspan of the culvert obtained from the numerical model and experimental data indicate ductile failure mechanism. Marshall et al. (2014) stated that failure occurred through the anchors used to lift the segment near the corner, where 17% of the reinforcement was removed to place the anchors during manufacturing. They reported the rupture of the tension steel at the failure surface before the concrete crushed. The developed 3D model exhibited a large increase in vertical deflection at the midspan with little load gain prior to failure, which reflected yielding of the steel and formation of plastic hinges. At failure, the

computed reinforcement stresses from the numerical model indicated yielding of the steel at three separate locations: the midspan and two corners, labeled plastic hinge-A to C in **Figure 6-11b**. The observed failure surface in the experiment was approximately at the location of plastic hinge-C. **Figure 6-11a** also shows that the calculated and measured lateral deflections at the top corner of the culvert sidewall agree well. Lateral deflection is assumed positive when the sidewall flexes outwards. **Figure 6-11b** displays the developed cracks and deformed shape of the culvert at failure as predicted by the 3D model.

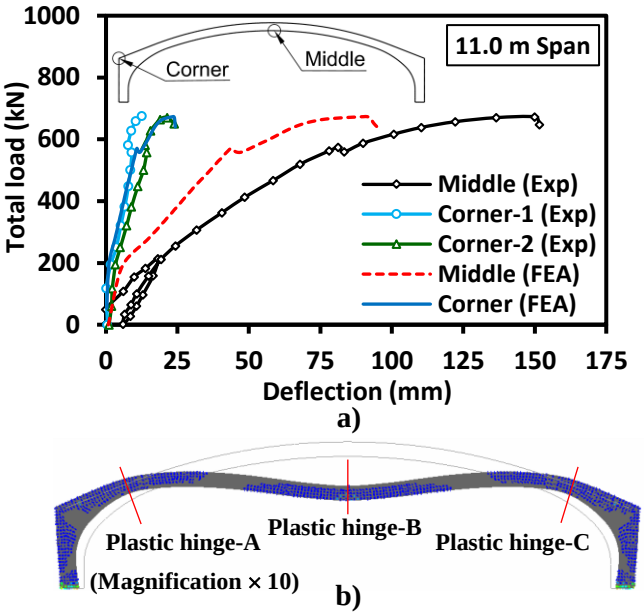

Figure 6-11. Arched TSC results: a) load-deflection curves; and b) deformed shape and crack pattern.

The load-displacement curve for the TSC displayed in **Figure 6-12a** shows an ultimate load capacity of 1214 kN. It should be noted that the arched TSC was designed for a total backfill cover of 1.5 m as opposed to the 3.1 m in the case of the subject TSC. The load-displacement curve in **Figure 6-12a** shows linear behavior up to an applied load of 717 kN. Afterwards, stiffness degradation occurred until failure was reached. The failure mechanism of the considered TSC was brittle and yielding of the reinforcing steel did not occur prior to failure. The vertical deflection at the midspan of the TSC at failure was 20.5 mm, which is much lower than the 91.3 mm predicted for the arched TSC. The failure surface of the present TSC is predicted to be at the top corner of the sidewall, where the highest concrete crack strain existed as presented in **Figure 6-12b**. Pimentel et al. (2009)

predicted failure of a RC box culvert under high embankment at the same location (top corner of the sidewall). The computed lateral deflection at the top corner of the TSC is negligible compared to the case of arched TSC and occurred in the opposite direction, i.e., inward deflection of the sidewall at the top corner and outward deflection at the mid-height, as demonstrated in **Figure 6-12b**.

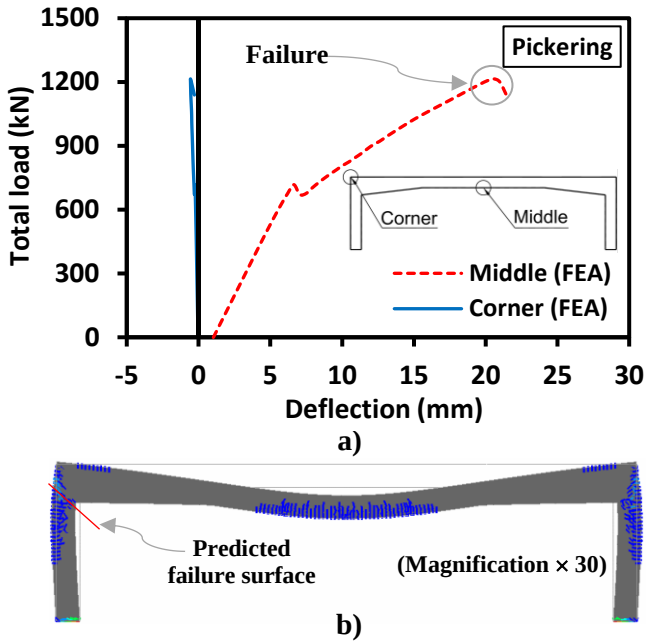

Figure 6-12. Pickering TSC results: a) load-deflection curves; and b) deformed shape and crack pattern.

6.6.2 Three-Sided Culvert 2D Models

The validated 2D numerical models were used to predict the maximum backfill height at which the investigated TSC would fail. Two different models were developed: one assuming linear-elastic behavior of the RC (LEA-U), and one assuming smeared crack behavior (NLA-U). Normal compaction effort was considered near the instrumented sidewall in both models, and the sidefill was defined as SW-90. More backfill layers were added in the modified models such that the embankment height reached 10.0 m above the top slab instead of the actual 3.1 m in the field.

Figure 6-13 compares the computed deflection of the culvert at different backfill heights from LEA-U and NLA-U models. As expected, the load-deflection curves calculated from LEA-U model exhibited linear load-deflection relationship up to the maximum backfill

height of 10 m. The load-deflection curve obtained from NLA-U model is comparable to that obtained from LEA-U model up to 3.2 m of backfill, after which NLA-U model exhibited higher vertical deflection computed at the midspan due to the development of cracks and degradation of concrete stiffness. The NLA-U model predicted failure of the existing culvert as backfill height reached 6.5 m, which is more than twice the design backfill height. **Figure 6-13** also shows the variation of the lateral deflection at the top corner of the sidewall as the backfill height increased. The results indicated minimal inward deflection of the top corner away from the sidefill, which would result in the reduction of the LEP at the upper part of the sidewall. Meanwhile, the mid-height of the sidewall experienced outward deflection towards the sidefill soil, which explains the small LEP measured at the top of the sidewall by PC 6-1 and the high pressure measured at the mid-height by PC 5-1. The maximum lateral deflection occurred at point "A" located approximately 2.2 m from the top corner of the sidewall. Furthermore, **Figure 6-13** shows the variation in lateral deflection at point A with the backfill height. The calculated responses from the LEA-U and NLA-U models agree well up to backfill height of 3.2 m (i.e., SLS condition), then the NLA-U model predicted higher lateral deflection up to failure (6.5 m). The calculated responses diverge even more as the backfill height increased beyond 6.5 m, which clearly indicates that the predictions of LEA-U model can be grossly inaccurate as failure is approached. It should be noted, however, that the predicted maximum height at failure (6.5 m) may not be accurate due to the decreased accuracy of the numerical model near failure.

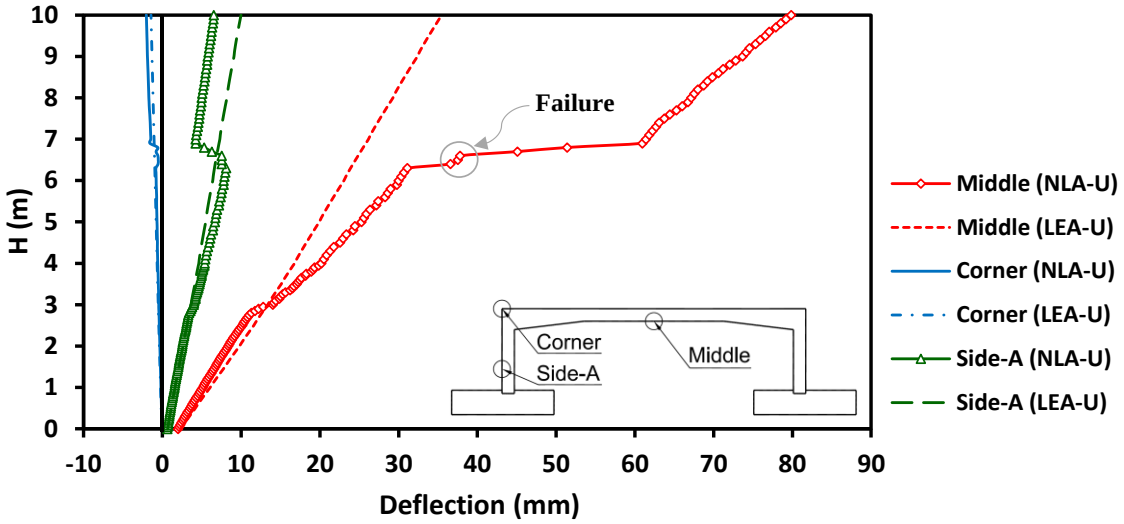

Figure 6-13. Deflection of the Pickering culvert at different backfill heights.

Figure 6-14a shows the predicted deformed shape of the culvert and the crack pattern at failure. It is noted from **Figure 6-14a** that failure is anticipated to occur at the top corner of the sidewall, same as the 3D model prediction for the loading of the TSC segment. However, the failure mechanism is ductile, and the steel reinforcement experienced yielding before failure occurred as shown in **Figure 6-14b**; the estimated stresses reached the yielding stress (450 MPa) in the horizontal stirrup through which the failure surface is predicted. The ductile behavior is also observed in the load-deflection curve at the midspan displayed in **Figure 6-13**, as the culvert sustained large vertical deflection before failure. The calculated vertical deflection at failure from NLA-U model is 37.5 mm, which is 83% higher than that obtained from the 3D model of the TSC segment with no soil confinement. Accordingly, it can be deduced that the soil confinement substantially enhanced the structural performance of the culvert and altered its failure mechanism. The enhancement of the RC culvert load-carrying capacity due to soil confinement was discussed in Chapter 4 for the Remembrance culvert, it was also reported by Moradi et al. (2016), Marshall et al. (2014), and Zoghi and Farhey (2006).

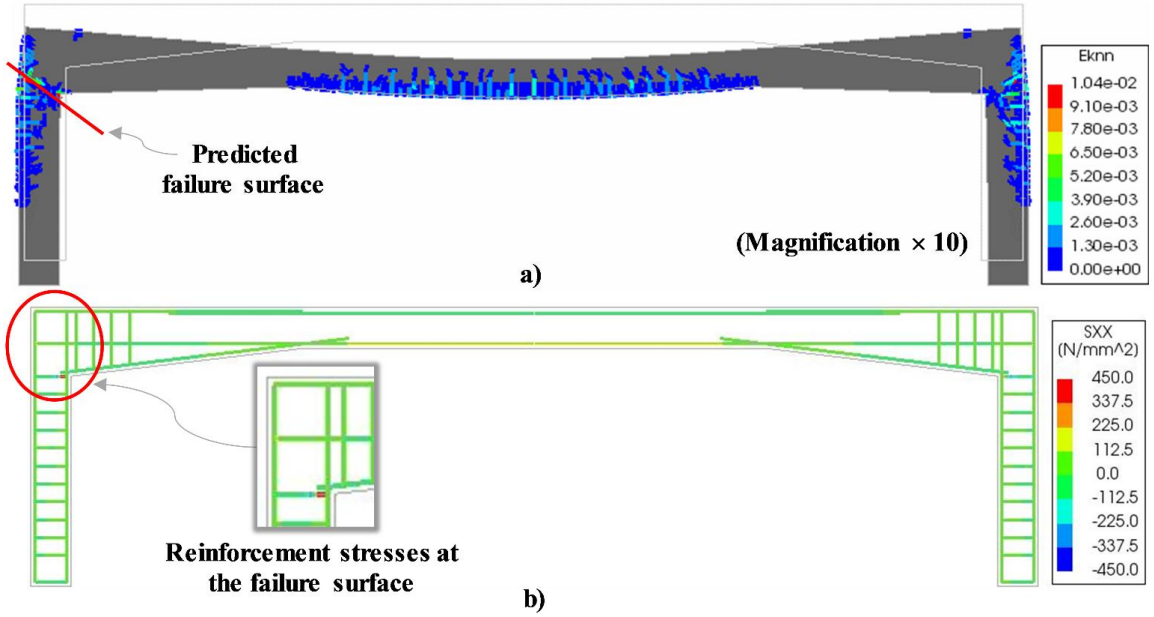

Figure 6-14. Results of the 2D model at failure (H = 6.5 m): a) predicted deformed shape and crack pattern; and b) reinforcement stresses.

Figure 6-15 presents the variation of the soil earth pressure at different locations along the culvert top slab with the backfill height obtained from both LEA-U and NLA-U models. Comparing the results in **Figure 6-15** can elucidate the influence of RC nonlinearity on the predicted earth pressures. Vertical earth pressures have been determined at the edge (x/B_c = 0.0), quarter-span (x/B_c = 0.25), and midspan (x/B_c = 0.5). The results show that the estimated VEPs from the two models almost coincided up to a backfill height of 3.2 m. For backfill heights greater than 3.2 m, the estimated VEPs from LEA-U model remained linear; however, NLA-U model shows redistribution of the earth pressures. The reduction of the cross-section stiffness is insignificant at x/B_c = 0.25, which explains the good fit between the calculated VEPs at this location from both models up to failure. On the other hand, the midspan experienced substantial degradation of the stiffness as the backfill height increased, resulting in lower VEP compared to the values calculated from the linear-elastic model, and the soil pressure was redistributed to the stiffer edges of the culvert. Unlike the linear increase in soil pressure prediction of LEA-U model, the predicted VEP from NLA model at the midspan decreased substantially while the VEP at the edges increased significantly. Also shown in **Figure 6-15** is the free-field stresses at different backfill heights. The results indicate that the computed pressures from both models at x/B_c = 0.25 and x/B_c = 0. 5 are equal to or less than the free-field stresses for all backfill heights, while

the predicted VEPs at the edge are much higher than the free-field stress. These results demonstrate the role of the soil arching action in redistributing the applied pressures to the stiffer parts of the culvert. Eventually, it may be concluded that the simplified linear-elastic model can simulate the behavior of RC at SLS, but it cannot accurately predict the culvert deformation and applied earth pressures on the culvert at ULS.

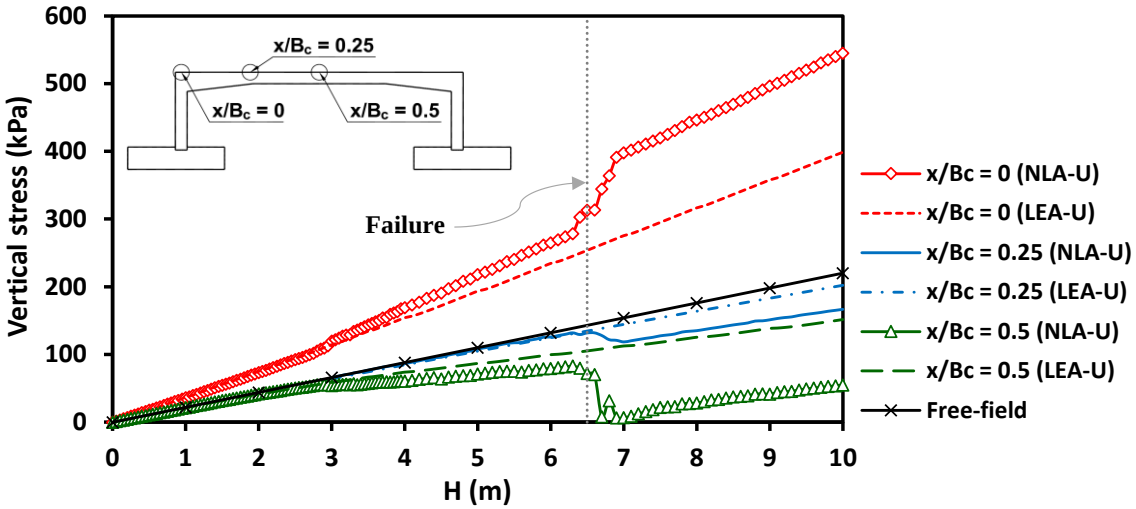

Figure 6-15. Computed earth pressure progression with backfill at different locations along the culvert span.

6.7 Conclusions

The soil-structure interaction mechanism and structural performance of a full-scale precast concrete TSC under service and ultimate load levels were investigated in this study. A 10.4-m-span culvert buried under 3.1 m of backfill was instrumented for real-time monitoring. The collected field data were implemented to validate 2D numerical models, which were used to evaluate the influence of RC nonlinearity on the TSC performance. At SLS conditions, a close match between the numerical and field results was demonstrated at the final backfill height, and the following conclusions may be drawn:

1. The measured stress underneath the footing was approximately uniform. Thus, the current design practice that assumes uniform stress distribution underneath strip footings of TSCs is appropriate.

2. The field monitoring data and numerical results demonstrated that the lateral earth pressure along the TSC sidewall has a parabolic distribution and not linearly increasing with depth as adopted in the CHBDC (CSA, 2014). However, the measured and calculated LEP values mostly fall within the upper and lower bounds stipulated by the code. Thus, the current code provisions can be used for conservative design of TSCs.

3. As expected, the quality of construction and compaction effort near the sidewall influence the measured and computed lateral earth pressure on the sidewall of the culvert.

4. The vertical earth pressure distribution along the top slab is not uniform and is overestimated by the CHBDC (CSA, 2014) provision for box culverts, which stipulates a VAF of 1.2 for B1 installation. It is proposed to use an average VAF of 1.05 to represent the applied pressures on the top slab of large span TSCs. However, further studies on TSCs are still required to validate the prevalence of such finding.

5. For the sidewall-foundation connection described in this chapter, the connection is not fully hinged. Rather, the base of the sidewall experienced some bending moment due to the combined effect of the footing rotation and the restraint provided by the connection between the sidewall base and the strip footing. The bending moment at the base may be evaluated using the computed rotation from the numerical model and the rotational stiffness for smooth strip footing proposed by Muskhelishvili (1963) and should be considered in the reinforcement design of the culvert sidewalls.

6. It is adequate to assume linear-elastic behavior of RC for predicting the imposed earth pressures on the TSCs at SLS conditions.

The analysis at the ultimate limit state of TSCs was conducted using 3D nonlinear finite element model validated using the experimental data available in the literature of an arched TSC loaded to failure. The validated model was then used to analyze the response of a segment of the studied TSC assuming the same loading and boundary conditions of the

experimental setup. Moreover, the 2D numerical models validated using the field monitoring data were used to consider situations of higher soil cover to evaluate the TSCs performance and soil-structure interaction characteristics at ULS. The following conclusions may be established from the ULS analysis:

1. The TSC segment, without soil confinement, exhibited brittle failure without yielding of the steel reinforcement and failure would occur at the top corner of the sidewall.

2. Failure of the TSC under soil confinement condition would be ductile and would occur at a maximum backfill height of 6.5 m, almost twice the design height.

3. The RC material nonlinearity should be considered for realistic prediction of the TSC deformation and applied earth pressures at ULS.

6.8 References

1. Balachandran, K., Liu, J., Cao, L., and Peaker, S. (2015). Statistical correlations between pressuremeter modulus and SPT N-value for glacial tills. In *Proc., 68th Canadian Geotechnical Conf. and 7th Canadian Permafrost Conf*. Richmond, BC, Canada: Canadian Geotechnical Society.

2. Beach, T. J. (1988). *Load test report and evaluation of a precast concrete arch culvert*. Transportation Research Record 1191, Transportation Research Board, Washington, DC, 12–21.

3. Boscardin, M. D., Selig, E. T., Lin, R. S., and Yang, G. R. (1990). Hyperbolic parameters for compacted soils. *Journal of Geotechnical Engineering*, 116 (1), 88-104.

4. Carder, D. R., Pocock, R. G., and Murray, R. T. (1977). *Experimental retaining wall facility-lateral stress measurements with sand backfill*. Trans. and Road Research Lab. Rep. No. LR 766.

5. Chen, B., Song, D., Mao, X., Chen, E.J., and Zhang, J. (2016). Model test and numerical simulation on rigid load shedding culvert backfilled with sand. *Computers and Geotechnics Journal*, 79, 31–40. 10.1016/j.compgeo.2016.05.026

6. Chen, B., and Sun, L. (2014). Performance of a reinforced concrete box culvert installed in trapezoidal trenches. *Journal of Bridge Engineering*, 19 (1), 120–130. https://doi.org/10.1061/(ASCE)BE.1943-5592.0000494.

7. Chen, T. J., and Fang, Y. S. (2008). Earth pressure due to vibratory compaction. *Journal of Geotechnical and Geoenvironmental Engineering*, 134 (4), 437–444. DOI:10.1061/(ASCE)1090-0241(2008)134:4(437)

8. Cristelo N., Félix C., Figueiras J. (2019). Experimental behaviour of concrete box culverts – comparison with current codes of practice. *Canadian Geotechnical Journal*, 56 (7), 970–982.

9. CSA (Canadian Standards Association). 2014. *Canadian highway bridge design code*. CAN/CSA-S6-14. Mississauga, ON, Canada: CSA.

10. CSA (Canadian Standards Association). 2014. *Design of concrete structures (A23.3-14)*. CSA Group, Mississauga, Ontario.

11. Dasgupta, A., and Sengupta, B. (1991). Large scale model test on square box culvert backfilled with sand. *Journal of Geotechnical and Geoenvironmental Engineering*, 117 (1), 156–161. 10.1061/(ASCE)0733-9410 (1991) 117:1(156)

12. Duncan, J. M., and Chang. C. Y. (1970). Nonlinear analysis of stress and strain in soils. *Journal of Soil Mechanics and Foundations Division*, 96 (5),1629–1653.

13. Elshimi, T. M., and Moore, I. D. (2013). Modeling the effects of backfilling and soil compaction beside shallow buried pipes. *Journal of Pipeline Systems Engineering and Practice*, 4 (4), 04013004.

14. Frederick, G. R., and Tarhini, K. M. (2000). *Structural evaluation of three-sided concrete culverts. Concrete piper for the new millenium*. ASTM STP 1368, I.I

Kaspar and J. I. Enyart, Eds., American Society of Testing and Materials, West Conshohocken, PA.

15. Hordijk, D. A. (1991). Local approach to fatigue of concrete. Doctor of Philosophy, Ph.D. dissertation, Delft University of Technology, Delft, The Netherlands.

16. International Federation for Structural Concrete. (2013). *Fib model code for concrete structures 2010*. Berlin: Verlag Ernst and Sohn.

17. James, R. W., Brown, D. E., Bartoskewitz, R. E. and Cole, H. M. (1986). *Earth pressures on reinforced concrete box culvert*. Research Rep. 294-2F, Texas Trans. Ins., The Texas A&M Uni. Sys. College Station, TX.

18. Manzari, M., Drevininkas, A., Olshansky, D., and Galaa, A. (2014). Behavioral modeling of Toronto glacial soils and implementation in numerical modeling. In *Proc., 67th Canadian Geotechnical Conf*. Richmond, BC, Canada: Canadian Geotechnical Society.

19. Marshall, J. D., Anderson, J. B., Meadows, R. L., and Jensen, T. J. (2014). Full-scale testing of three-sided precast concrete arch sections. *Journal of Bridge Engineering*, 19 (12), 04014051. 10.1061/(ASCE)BE.1943-5592.0000630.

20. McGrath, T. J., Moore, I. D., Selig, E. T., Webb, M. C., and Taleb, B. (2002). *Recommend specifications for large-span culverts.* Report No. 473. Washington, DC: Transportation Research Board.

21. McGrath, T. J., Selig, E. T., Webb, M. C., and Zoladz, G. V. (1999). *Pipe interaction with the backfill envelope*. FHWA-RD-98-191.

22. Moradi, M., Valipour, H., and Foster, S. (2016). Reserve of strength in inverted u-shaped RC culverts: effect of backfill on ultimate load capacity and fatigue life. *Journal of Bridge Engineering*, 21 (2), 04015051. 10.1061/(ASCE)BE.1943-5592.0000800

23. Muskhelishvili, N.I., (1963). *Some basic problems of the mathematical theory of elasticity*. P. Noordhoff, Groningen, The Netherlands.

24. Oshati, O.S., Valsangkar, A.J., and Schriver, A.B. (2012). Performance of two cast-in-place box culverts under high embankments. *Canadian Geotechnical Journal*, 49 (12), 1331–1346. 10.1139/t2012-094

25. Oswald, C. J. (1996). Analysis of reinforced concrete culvert considering concrete creep and shrinkage. *Transportation Research Record 1541*, TRB. National Research Council. Washington, DC, 120–126.

26. Pimentel, M., Costa, P., Félix, C., and Figueiras, J. (2009). Behavior of reinforced concrete box culverts under high embankments. *Journal of Structural Engineering*, 135 (4), 366-375. 10.1061/(ASCE)0733-9445(2009)135:4(366), 366–375

27. Rots, J. G., Blaauwendraad, J. (1989). Crack models for concrete: discrete or smeared? Fixed, multi-directional or rotating? *Heron*, 34 (1), 5–55.

28. Samaiklang, W., and Fuenkajorn, K. (2013). Mechanical and hydraulic performance of cement grouts from 5 suppliers in Thailand. In *Proc., of the Second Thailand Symposium on Rock Mechanics* (ThaiRock 2013), Im Poo Hill Resort, Nakhonratchasima, 333–342.

29. Thorenfeldt, E., Thomaszewic, A., and Jensen, J. J. (1987). 'Mechanical properties of high-strength concrete and applications in design. In *Proc., Symp. on Utilization of High-Strength Concrete*, Tapir Publishers, Stavanger, Norway, 149–159.

30. TNO Diana BV. 2016. *DIANA—User's manual: Material library*. Delft, Netherlands: TNO Diana BV.

31. Vecchio, F. J., and Collins, M. P. (1986). The modified compression-field theory for reinforced concrete elements subjected to shear. *ACI Journal*, 22, 219–231.

32. Von Handorf, J. J. (2004). Clear-span culverts: Economical designs. Better Roads, Feb. 2004.

33. Yang, G. W. (1987). Hyperbolic Young's modulus parameters for compacted soils. Master's Project Rep. No. ACP87-342P, Uni. of Massachusetts, Amherst, Mass.

34. Yang, M. Z. (2000). Evaluation of factors affecting earth pressures on buried box culverts. PhD dissertation, Uni. of Tennessee, Knoxville, TN.

35. Zoghi, M., and Farhey, D. N. (2006). Performance assessment of a precast concrete, buried, small arch bridge. *Journal of Performance of Constructed Facilities*, 20 (3), 244–252. 10.1061/(ASCE)0887 3828(2006)20:3(244).

Chapter 7

* Effect of Large-Span Three-Sided Culvert Configuration on its Performance at Service and Ultimate Loading Conditions

7.1 Introduction

Reinforced concrete (RC) three-sided culverts (TSCs) with flat top slab are widely used to handle heavy flows at sites with limited vertical clearance. The absence of the bottom slab and flow of water in its natural course makes TSCs an environmentally attractive system. Precast construction of RC TSCs offers desirable advantages in terms of quality control, reduced cost and construction time, and required road closure duration. The geometry of TSCs generally available in the market is characterized by large spans, reaching up to 16.0 m, and relatively short rises. TSCs can be supported on shallow strip footings or deep foundations depending on the loads applied on the culvert and the site subsurface conditions.

The Canadian Highway Bridge Design Code, CHBDC, (CSA, 2014) includes design guidelines for RC box culverts. These guidelines are based on field and numerical studies on box culverts; however, they are also used for the design of large-span TSCs in the current design practice. Many studies focused on the performance of RC box culverts under static and seismic loads through full-scale field tests, centrifuge tests, and numerical investigations (Yang, 2000; Bennett et al., 2005; Chen and Sun, 2014; Abuhajar et al., 2015a; Abuhajar et al., 2015b; Kheradi et al., 2017). On the other hand, studies on TSCs are limited to the work done by Ramadan and El Naggar (2021a, b), i.e., Chapter 6 and Chapter 4, repectively. These studies suggest that the CHBDC (CSA, 2014) overestimates the vertical earth pressure on the top slab of large-spans TSCs.

The configuration of the culvert precast unit is usually designed to meet certain site conditions and/or waterway span and hydraulic demand. Under certain conditions, footing

---

* A version of this chapter is under review in Tunnelling and Underground Space Technology.

pedestals are used to achieve sufficient footing embedment depth to rest on competent foundation soil, or to satisfy frost depth requirements without increasing the culvert sidewall height, especially for large-span TSCs. Thus, the sidewall height, R, and the footing pedestal height, P, may be selected according to the project demands, and could impact the performance and structural capacity of the culvert. For example, Ramadan and El Naggar (2021a) in Chapter 6 studied the soil-culvert-interaction of a 10.4-m-span TSC that had a relatively long sidewall height of 3.07 m and was supported on a strip footing with no pedestal. They reported that the sidewall-footing connection was not fully hinged as typically assumed in the current practice. Rotation of the strip footing resulted in the development of bending moment at the sidewall base. They predicted ductile failure of the TSC at almost twice the design backfill height with the formation of plastic hinges at the top corners of the sidewalls, below the haunches.

Meanwhile, Ramadan and El Naggar (2021b) in Chapter 4 investigated the structural performance of an instrumented 7.3-m-span TSC with a total sidewall height of 2.79 m, which was supported on a strip footing with a 0.7-m-high pedestal. The field data was utilized to validate a two-dimensional (2D) finite element model (FEM), which was then employed to investigate the influence of foundation soil condition, either native soil or rock on the culvert capacity. They concluded that the foundation soil condition had negligible effect on the vertical earth pressures on the top slab; but the lateral earth pressure on the sidewall was much higher for nonyielding foundation soil condition (rock). Interestingly, they reported footing rotation for the case of native soil caused by the bending moment that developed at the sidewall base. For footing supported by rock, no rotation and negligible bending moment was calculated at the sidewall base. Accordingly, it was concluded in Chapter 4 that assuming hinged connection at the footing-sidewall connection is only suitable for the case of nonyielding foundation. These important observations motivated the current study to investigate the effects of the TSC configuration on its geo-structural performance.

7.2 Objectives and Scope of Work

The main objective of this study is to investigate the effect of TSC configuration, more specifically the sidewall and pedestal heights, on its performance characteristics. To

achieve this objective, the field data of an instrumented 13.5-m-span TSC with 3.0 m of backfill on its top slab were recorded during and after construction. The earth pressures acting on the culvert body and the contact pressure underneath the footing were evaluated at service loading conditions from the field measurements. In addition, 2D FEMs were developed and validated utilizing the data collected from the instrumented culvert. The validated models were employed to conduct a comprehensive parametric study that elucidated the effects of the TSC sidewall height on its geo-structural performance at serviceability limit state (SLS) and ultimate limit state (ULS) loading conditions. Finally, three-dimensional (3D) FEMs were developed and validated employing published results of laboratory loading tests conducted on full scale TSC units with arched top slab. The validated 3D FEMs were then used to evaluate the effect of the sidewall height of the subject TSC on its ultimate capacity.

7.3 Project Details

As part of the Courtice Trunk Sanitary Sewer Extension in the city of the Oshawa, Canada, a 13.5-m-span RC TSC was constructed as a watercourse crossing for Harmony Creek. It is referred to herein as “Oshawa culvert”. The final embankment height would be 3.8 m above the culvert top slab. The culvert was instrumented to collect data on its performance during and after construction. The details of the culvert geometry, construction, and instrumentation are presented in this section.

7.3.1 Culvert Geometry and Reinforcement

The Oshawa culvert had a clear span of 13.5 m, making it the largest RC culvert with flat top slab to be instrumented to date. The geometry of the Oshawa culvert was designed to accommodate the high hydraulic demand of the Harmony Creek, with limited vertical clearance. **Figure 7-1** illustrates the geometry and reinforcement details of the Oshawa culvert. The culvert sidewall height was relatively short (2.06 m). The sidewalls and top slab were 0.66 and 0.61 m thick, respectively, with a 4.27 × 0.31 m haunch at the sidewall-top slab joint as indicated in **Figure 7-1**. The average 28-day compressive strength (f'_c) of the culvert concrete was 65 MPa, and the yield strength (f_y) and Young’s modulus (E_{st}) were 400 MPa and 200 GPa, respectively.

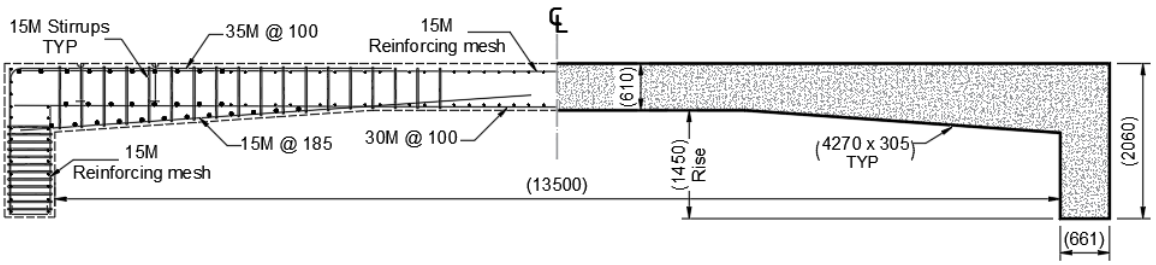

Figure 7-1. Geometry and Reinforcement details of the Oshawa culvert. (All dimensions are in mm)

7.3.2 Subsurface Conditions and Culvert Construction

The soil profile in the vicinity of the Oshawa culvert was composed predominantly of silty sand and sandy silt tills from the ground surface up to 8.0 m, where the boreholes were terminated. The native till deposits consisted of a random mixture of particle sizes ranging from clay to gravel, with silt and sand being the predominant fractions. Dense silty sand till layer extended from the ground surface to a depth of 2.5 m, with an average SPT N-value of 27. At the foundation level (FL), 2.7 m below ground surface, N-value was 63 and refusal was recorded below FL up to 8.0 m. The high SPT N-values at FL and refusal below that elevation indicate very stiff to hard soil. Thus, the culvert was constructed on strip footings.

The frost depth at the site location is 1.2 m (OPSD, 2010). Oshawa culvert was supported on 0.7-m-thick strip footings with 1.9-m-thick pedestals as depicted in **Figure 7-2**. Long footing pedestals (P = 1.9 m) were used to satisfy frost depth requirement without increasing the culvert sidewall height. The strip footing was 3.8-m-wide, extending 1.0 m from the pedestal edge on the waterside and 1.4 m on the backfill side. The footing pedestal crest was almost at the ground surface; thus, Oshawa culvert was constructed following embankment installation method.

Oshawa culvert was constructed of 38 RC precast units with a total length of 49.4 m. Each precast unit had a width of 1.3 m and weighed around 390 kN. The RC precast units were supported on keyed cast-in-place strip footings. The strip footings were casted on a 0.1-m-thick concrete mud slab. Plastic shims were installed along the footing keyway to adjust the precast units' elevations. After each precast unit was correctly positioned with almost 0.16 m of the sidewall embedded in the keyway, plastic shims were placed between the

keyway and culvert sidewall to prevent the unit lateral movement. Once all the precast units were installed, the keyway was filled with non-shrink grout with compressive strength (f'_c) of 30 MPa.

Well-graded sand (SW) compacted to 90-95% Standard Proctor was used as the backfill material for the Oshawa culvert, meeting the code specifications for B1 standard installation. The backfill was compacted using a hand-operated vibrating plate compactor within 2.0 m of the culvert body until reaching 0.6 m of soil cover on the top slab to avoid excessive compaction loads on the culvert. Vibratory rollers were used elsewhere. Backfilling was completed in 0.3 m lifts, and nuclear density tests were conducted to verify reaching the required compaction level. The average wet unit weight obtained from the nuclear density tests was 20.0 kN/m^3. The culvert is currently covered with 3.0 m backfill, and the final grade level (3.8 m) of the backfill is not yet reached.

7.3.3 Culvert Instrumentation

The culvert was instrumented with 13 pressure cells (PCs) to monitor the applied earth pressures and 24 strain gauges (SGs) to monitor the strains in one precast unit of the TSC during and after construction completion. **Figure 7-2** displays the instrumentation layout. Seven PCs were distributed on the top slab to measure the vertical earth pressure and 3 PCs were installed under the strip footing to determine the contact pressure below the footing. In addition, 2 PCs were installed on the footing pedestal and one on the sidewall to measure the lateral earth pressure. Furthermore, 24 SGs were installed in pairs at 12 different cross-sections on the outer and inner surfaces of the precast unit and footing pedestal to measure the tensile and compressive strains. **Figure 7-2a** displays the layout for the PCs, and **Figure 7-2b** presents the locations of the SG.

Model 4810 PC (Geokon, Lebanon, New Hampshire) vibrating wire (VW) pressure cells were used because of their durable long-term performance and ability to withstand construction activities (Perkins and Lapeyre, 1997). The 3 PCs underneath the footing had a pressure range of 700 kPa, while the other PCs had a pressure range of 350 kPa, which were suitable for the anticipated pressure values. The accuracy of Model 4810 PCs is 0.1% of its range when using polynomial expression. Model 4000 VW SGs (Geokon, Lebanon,

New Hampshire) with 150 mm active gauge length, 3000 με full-scale range, and accuracy of 0.5% were used. **Figure 7-3** shows an overview of the Oshawa culvert after sensors installation.

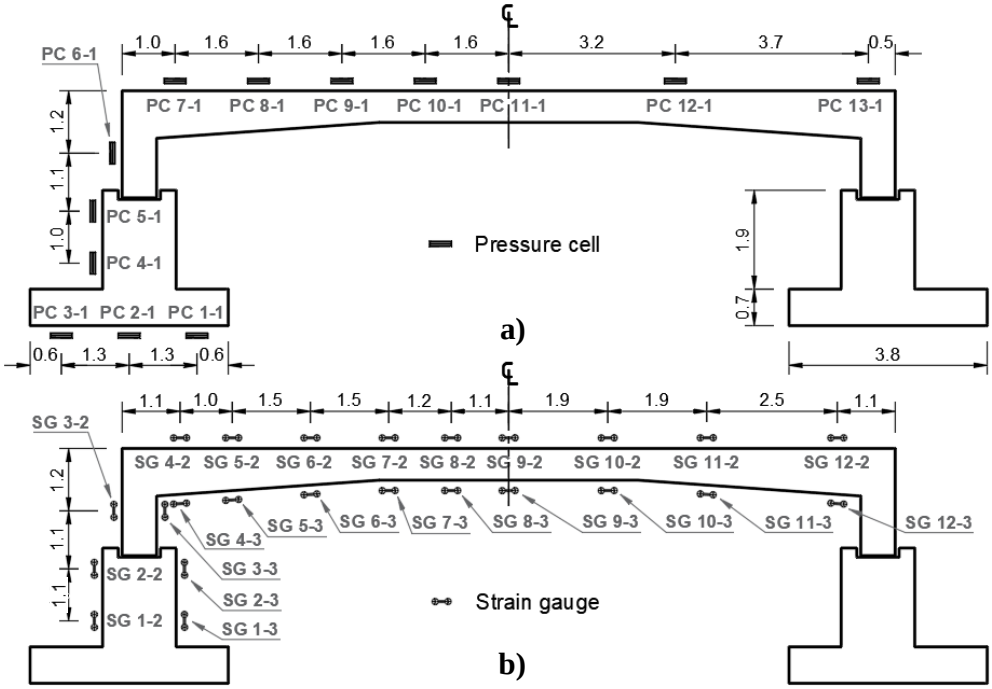

Figure 7-2. Oshawa culvert instrumentation layout: a) pressure cells; and b) strain gauges. (All dimensions are in m)

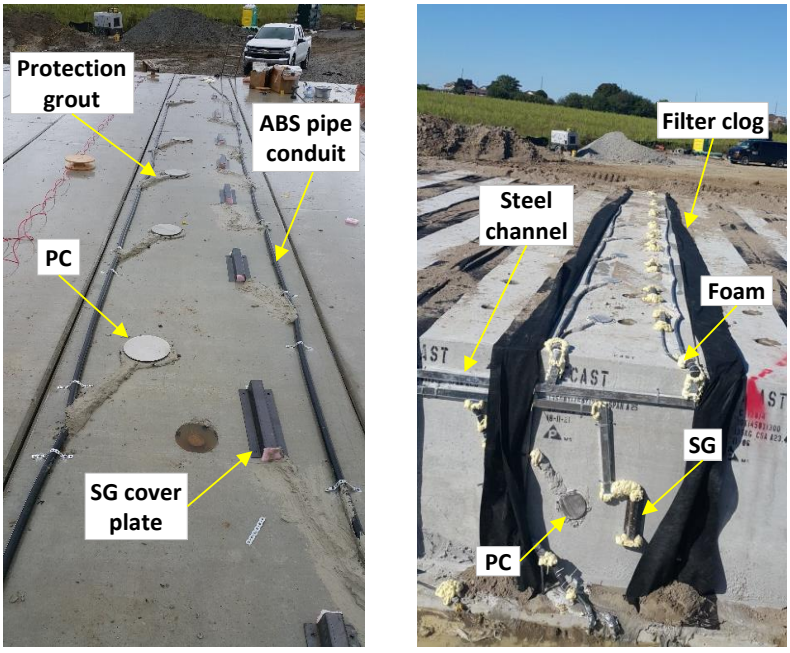

Figure 7-3. Overview of the Oshawa culvert final instrumentation.

7.4 Field Monitoring Data

Oshawa culvert was backfilled in stages over two construction seasons, and the current backfill height is 3.0 m. All the sensors survived the construction activities except PC 10-1 installed on the top slab, which recorded unrealistic measurements. **Figure 7-4** to **Figure 7-6** present the recorded field data since the construction commenced up to date.

Figure 7-4 shows the measured pressures with the variation of backfill height (H). After 54 days from culvert installation, it was covered unevenly with approximately 0.6 m of backfill on the top slab. On day 355 of construction, the backfill height reached 1.2 m and was increased to 3.0 m on day 389. The measured pressures varied between H = 0.6 m and H = 1.2 m due to the seasonal snow and rain precipitation as well as transient loads from the construction activities related to other elements of the project. The transient loads are manifested by the spikes in readings of PCs 11-1 to 13-1 between days 120 and 240 of construction as shown in **Figure 7-4d**. The measured pressures indicated that the PCs on the sidewall, pedestal, and top slab experienced relaxation of the field measurements after reaching 3.0 m backfill, except PCs 6-1 and 13-1. All the PC readings stabilized after day 515 of construction. Thus, the average values after the measurements stabilized are considered as the earth pressure values at H = 3.0 m.

Figure 7-4a shows that the measured contact pressures underneath the strip footing at the middle and near the edge of the backfill side (PCs 2-1 and 3-1) after reaching a backfill height of 1.2 m were almost identical, while the measured stresses near the footing edge on the waterside (PC 1-1) were slightly lower. The average measured stresses at 3.0 m backfill were 221.4, 236.5, 244 kPa for PCs 1-1, 2-1, and 3-1, respectively. The small variation of measured stresses (< 9%) indicates that the contact pressure underneath the strip footing was uniform. **Figure 7-4b** shows the measured lateral earth pressure on the footing pedestal and culvert sidewall. PC 6-1 installed near the haunch on the sidewall exhibited the lowest lateral pressure, while PC 5-1 (located near the crest of the footing pedestal) recorded higher pressure than that measured by PC 4-1 (located at the bottom), which indicates that the lateral earth pressure does not increase linearly with depth as postulated in the current design practice. Moreover, the measured pressure by PC 6-1

increased slightly as the backfill height increased, which is related to the deformed shape of the footing-culvert system as will be discussed later.

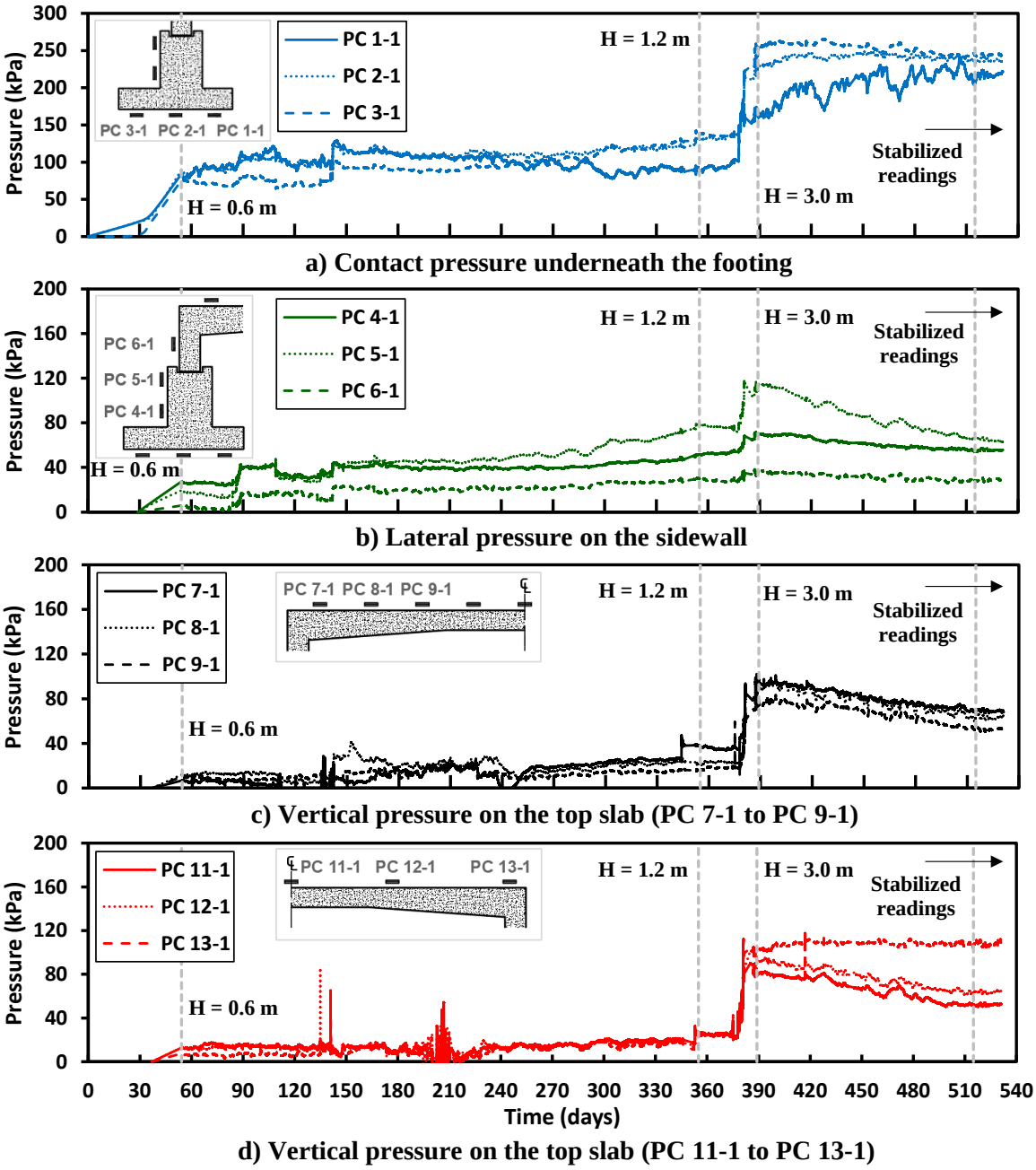

Figure 7-4. Pressure cell measurements of the Oshawa culvert.

Figure 7-4c and **d** display the measured vertical earth pressures on the top slab. The measured pressures by all PCs increased as the backfill height increased but decreased slightly after reaching the 3.0 m backfill (except for PC 13-1 close to the slab edge). The

reduction in the measured vertical pressures is attributed to the redistribution of earth pressures due to soil arching, which stabilized after day 515 of construction. At 3.0 m backfill, PC 13-1 (at the edge) measured the highest vertical pressure (109.6 kPa) and PC 11-1 (at the mid-span) measured the lowest vertical pressure (52.8 kPa), i.e., non-uniform distribution with the pressure at the edge more than double that at the mid-span. Considering the free-field stress, $\gamma_s H$, (where γ_s and H and are the soil unit weight and backfill height, respectively), the measured pressure at the culvert edge was 83% higher than the free-field stress and the mid-span pressure was 12% lower than the free-field stress.

Figure 7-5 and **Figure 7-6** present the measured strains at each instrumented cross-section, in which -ve values represent compressive strains and +ve values represent tensile strains. The theoretical crack strain (ε_{cr}) beyond which tensile cracks occur in concrete is calculated by (CSA, 2014):

$$\varepsilon_{cr} = \frac{0.6\sqrt{f_c'}}{4500\sqrt{f_c'}} \quad \textbf{(7-1)}$$

where f_c' is the concrete compressive strength. The calculated crack strain for f_c' = 65 MPa is 133 με. The tensile strains measured by SGs 7-3, 8-3, 9-3, and 10-3 located on the bottom surface of top slab between the two haunches well exceeded ε_{cr}, which indicates that cracks have occurred in this region.

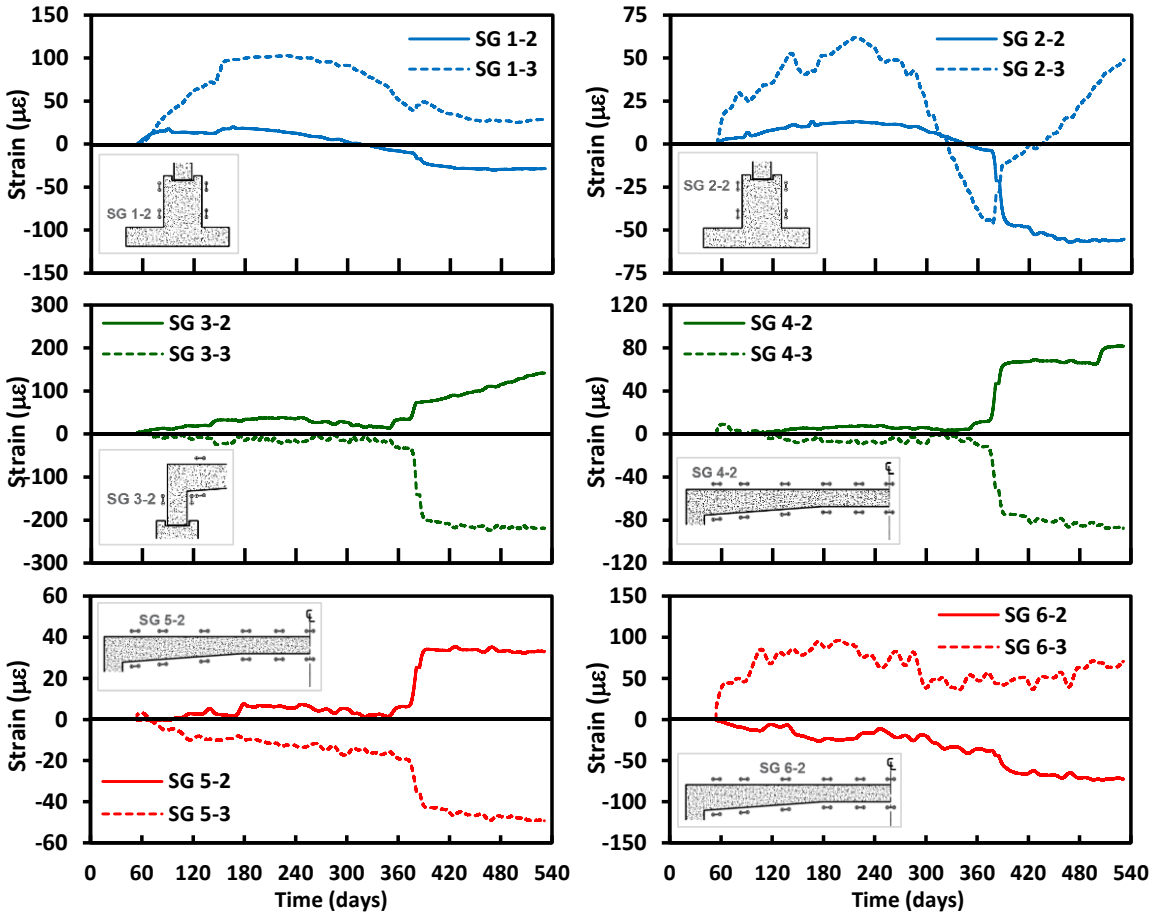

Figure 7-5. Strain gauge measurements of the Oshawa culvert (SG 1-2 to SG 6-2)

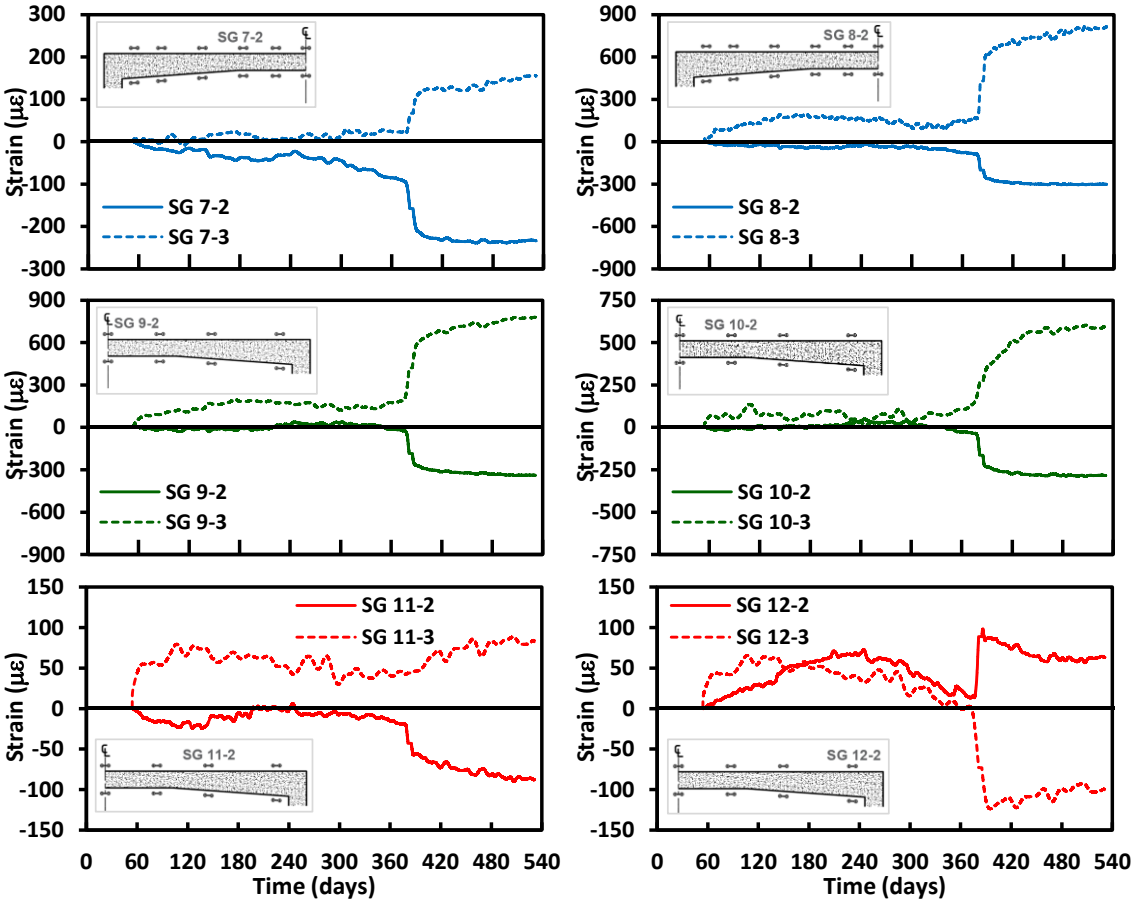

Figure 7-6. Strain gauge measurements of the Oshawa culvert (SG 7-2 to SG 12-2).

7.5 Numerical Model (2D)

Two-dimensional plane-strain FEMs were developed using the FE software DIANA 10.1 (2016), and the results were validated against the measured field data at backfill height, *H* = 3.0 m. It was reported in Chapter 4 and Chapter 6 that modeling RC behavior as linear-elastic is appropriate for estimating the imposed earth pressures on TSCs at SLS; however, the nonlinear behavior of RC should be considered for proper evaluation of the induced strains when cracks are expected. Accordingly, two identical FEMs were established (except for the material models employed to simulate reinforced concrete and the simulation of steel reinforcement): LEA model in which the RC behavior was assumed linear-elastic and NLA model in which RC nonlinearity and crack formation were considered.

7.5.1 Model Features

Each model consisted of five clusters: native very dense till layer, native dense till layer, backfill layers, strip footing, and culvert body. All clusters were discretized using 8-node plane-strain elements (51,154 elements), except the culvert body, which was discretized using 8-node plane-stress elements (4,861 elements) to consider the transversal joints between the precast units (Pimentel et al., 2009). The model mesh was refined adjacent to the culvert to increase the calculation accuracy as shown in **Figure 7-7**. Vertical and horizontal movements were restrained at the bottom boundaries of the model, while horizontal movement was restrained at the side boundaries. The model width was 11 times the culvert span to eliminate the boundaries influence. Backfill was extended up to the final backfill height (3.8 m). The sidefill and backfill were divided into layers with thickness varying between 0.4 and 0.7 m (0.5 m is the predominant thickness). Phased construction analysis was employed to account for the incremental nature of the backfill construction. The self-weight of a new backfill layer was introduced in each construction phase while neglecting the compaction-induced stresses due to the use of vibratory plate compactor (McGrath et al., 1999; Elshimi and Moore, 2013).

The behavior of the native till layers was simulated using the conventional Mohr-Coulomb material model. The Young's modulus (E_s) was evaluated using the empirical correlation with N-values proposed by Balachandran et al. (2015) for cohesionless till in the Greater Toronto Area, i.e., E_s = 1.33×N (MPa), which yielded E_s = 36 MPa and 166 MPa for the dense and very dense till layers, respectively. The angle of internal friction (ϕ) = 38° and 45° were assigned for the dense and very dense till layers, which fall within the range specified by Manzari et al. (2014) for cohesionless till materials from the Greater Toronto Area (31° to 45°), while their cohesion (c) was set to zero.

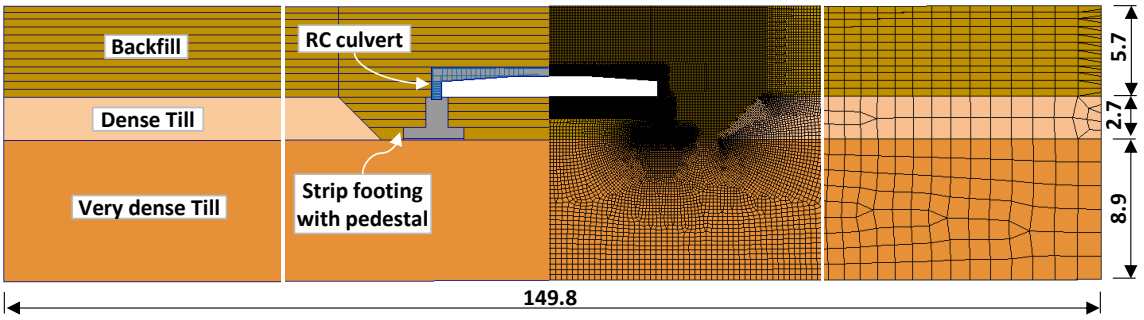

Figure 7-7. Geometry and meshing details of the Oshawa culvert 2D FE model. (All dimensions are in m)

The hyperbolic Duncan-Chang constitutive model (Duncan and Chang, 1970), which can account for the stress dependency and nonlinear behavior of backfill materials is used herein to simulate the behavior of the backfill and sidefill. The grain size distribution of the well-graded sand (SW) used in backfilling Oshawa culvert was comparable to the SW backfill tested by Boscardin et al. (1990). Accordingly, the Duncan-Chang material parameters reported by Boscardin et al. (1990) for SW compacted to 90% of its Standard Proctor (SW-90) were employed for the backfill material as summarized in **Table 7-1**.

The RC strip footing was assumed to have linear-elastic behavior in both LEA and NLA models. Its concrete had f_c' of 40 MPa and its E_c was estimated to be 29.7 GPa (fib Model Code, 2013). Similarly, the RC culvert was simulated as linear elastic material in LEA model with f_c' of 65 MPa and an equivalent E_c of 37.9 GPa. In the NLA model, the total strain-based smeared crack model was used to simulate the nonlinear behavior of the culvert concrete and to predict the crack formation. The employed smeared crack model formulation was based on the fixed crack concept (Rots and Blaauwendraad, 1989). The strain-softening behavior of concrete under compression was simulated using the Thorenfeldt model (Thorenfeldt et al., 1987), and the tension softening behavior was simulated using the Hordijk model (Hordijk, 1991). The smeared crack model input parameters summarized in **Table 7-1** were estimated from the concrete f_c' following the fib Model Code 2010 (2013). Poisson's ratio (ν) = 0.15 was assigned for all the concrete materials in both models. The culvert steel reinforcement was simulated in NLA model as embedded bar elements with von Mises plasticity behavior with yield stress (f_y) of 400 MPa and Young's modulus (E_{st}) of 200 GPa, and no strain hardening.

Line interface elements were introduced at the culvert-footing, soil-footing, and soil-culvert interfaces to realistically simulate the soil-structure interaction. Normal and tangential stiffnesses were defined for the interface elements to simulate the displacement across the interface. The Mohr-Coulomb yielding criterion was used to simulate the interface frictional behavior. The approach used to estimate the interface properties is detailed in Chapter 6.

Table 7-1. Input parameters of the backfill and concrete materials.

Backfill material							
Material model	% Standard Proctor	n	c (kPa)	ϕ (°)	Modulus No. K	Failure ratio R_f	Modulus exponent N
Duncan-Chang	90	0.30	0	42	640	0.75	0.43

Concrete (NLA model)				
Material model	Compressive strength f_c' (MPa)	Young's modulus E_c (MPa)	Tensile strength f_{ct} (MPa)	Fracture energy G_f (Nmm/mm^2)
Smeared crack	65.0	41707	6.4	0.2332

7.5.2 Model Validation (SLS)

Figure 7-8 compares the measured and calculated earth pressures from LEA and NLA models for backfill height of 3.0 m. The results demonstrate excellent agreement between the measured and calculated values, with negligible differences between the pressures calculated from the LEA and NLA models. This is in agreement with the findings reported in Chapter 6 regarding the adequacy of simulating the RC as a linear-elastic material for estimating the applied earth pressures on TSCs.

In addition, as observed from the field measurements, the distribution of the calculated earth pressure on the top slab is non-uniform. The vertical earth pressures were low and almost uniform within the middle 70% of the culvert span, but the pressure values at the slab edges were more than double the values at the mid-span. Similar earth pressure

distributions were reported in Chapter 4 and Chapter 6 for TSCs of 7.3 and 10.4 m spans under comparable backfill heights as discussed. The measured and calculated vertical earth pressures suggest an average vertical arching factor (VAF = vertical pressure/free-field stress) of 1.05, which is lower than the 1.2 value specified in the CHBDC (CSA, 2014) for B1 standard installation as demonstrated in **Figure 7-8a**.

The measured and calculated footing contact pressures were generally uniform underneath most of the footing area as shown in **Figure 7-8b**. The numerical results indicate slightly higher stresses at the footing edges, especially near the backfill side. However, the assumption of uniform stress distribution underneath the strip footing, commonly used in design, is acceptable for footings with similar geometry and subsurface conditions. The measured and calculated lateral earth pressure distributions along the footing pedestal and culvert sidewall agree well as shown in **Figure 7-8c**.

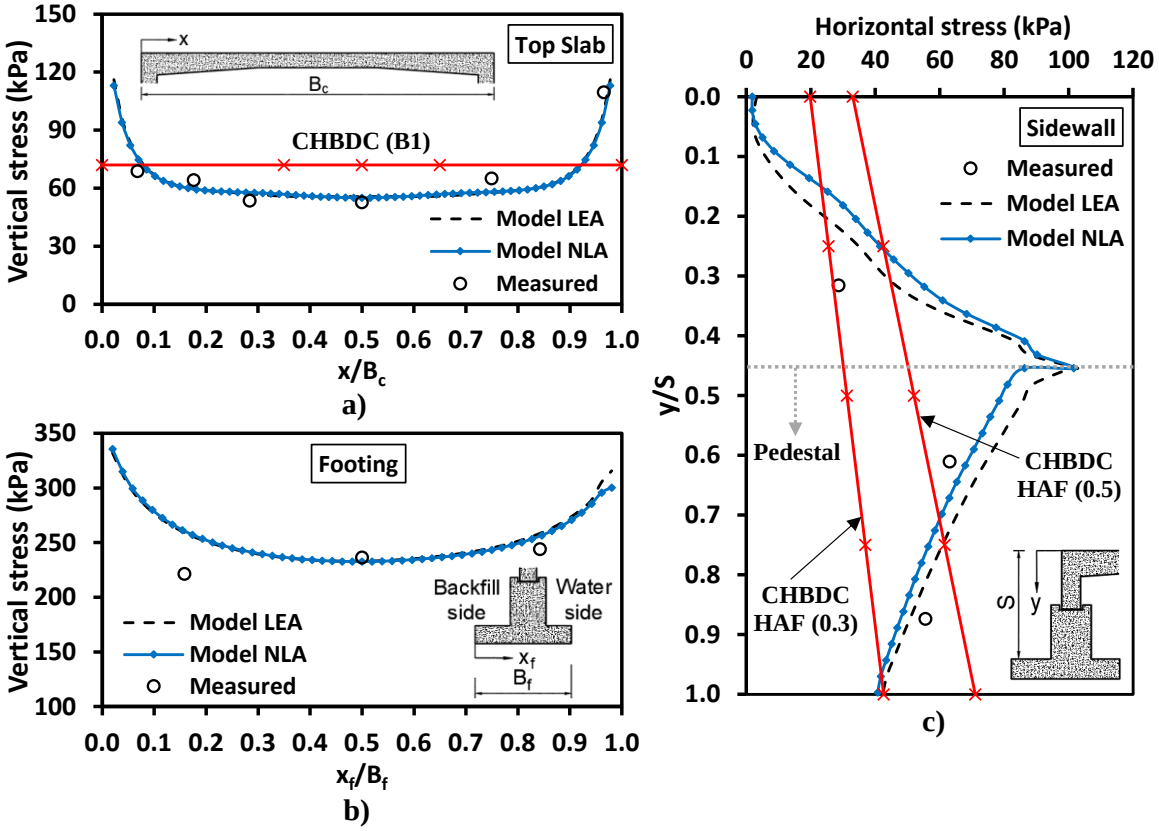

Figure 7-8. Comparison between measured and estimated pressures at 3.0 m of backfill: a) vertical earth pressure on the top slab; b) contact pressure underneath the footing; and c) lateral earth pressure on the sidewall and footing pedestal.

7.5.3 Effect of TSC Configuration on its Performance at SLS

The numerical results presented in **Figure 7-8c** indicates negligible lateral earth pressure at the sidewall upper portion, then it increased linearly with depth up to the sidewall base, then decreased linearly with depth along the footing pedestal. The lateral earth pressure distribution was influenced by the deformed shape of the footing-culvert system depicted in **Figure 7-9a**. As the mid-span of the culvert deflected downward, the upper part of the sidewall rotated away from the sidefill, which reduced the lateral earth pressure to almost zero at the top of sidewall. Meanwhile, the lower part of the sidewall rotated towards the sidefill approaching the passive state; consequently, the lateral earth pressure increased gradually up to the sidewall base. **Figure 7-9a** also demonstrates that the footing rotated in the opposite direction, i.e., the footing pedestal rotated towards the sidefill and the footing rotated away from the sidefill. This resulted in the decrease of the lateral earth pressure on the pedestal with depth. The footing rotation also explains the high stresses underneath the strip footing on the backfill side as presented in **Figure 7-8b**.

The CHBDC (CSA, 2014) specifies minimum and maximum horizontal arching factors of 0.3 and 0.5 for lateral earth pressure calculations in B1 standard installation. **Figure 7-8c** indicates that the calculated lateral earth pressure at the lower part of the sidewall and upper part of the footing pedestal exceeds the upper bound of the code. In addition, the lateral earth pressure on the footing pedestal decreases linearly with depth as previously discussed.

Figure 7-9a displays the predicted crack pattern for backfill height, H = 3.0 m. The calculated crack pattern corresponded well with the measured high tensile strains, which indicate cracks at SGs 7-3, 8-3, 9-3, and 10-3 located on the bottom surface of the slab between the two haunches.

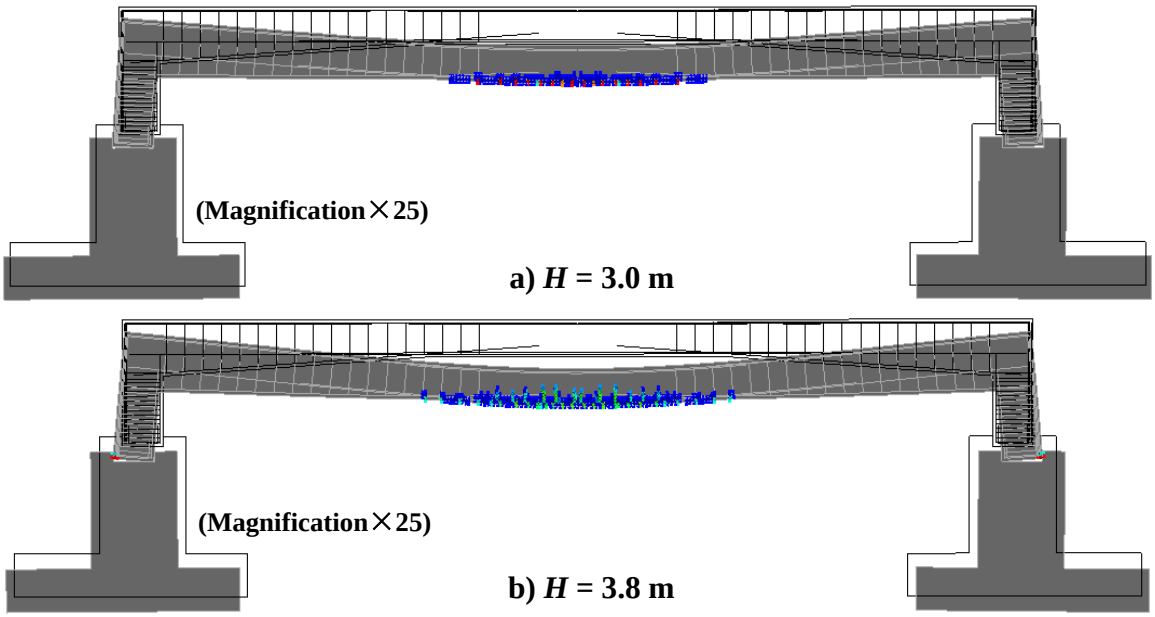

Figure 7-9. Deformed shape and crack pattern from NLA model.

The estimated bending moments (BMs) from the SG measurements are compared with the calculated values from LEA and NLA models in **Figure 7-10**. BMs from the SG measurements were estimated assuming uncracked sections where the measured tensile strains were lower than ε_{cr} employing **Equation (7-2)**:

$$BM = \frac{E_c . I_g . (\varepsilon_i - \varepsilon_e)}{d} \quad \textbf{(7-2)}$$

where I_g is the gross moment of inertia; ε_i and ε_e are the strains measured on the culvert's inner and outer surfaces, respectively; and d is the cross-section depth. For the cross-sections where the measured tensile strains exceeded ε_{cr} (SGs 7-3, 8-3, 9-3, and 10-3), the moment-curvature relationship was determined accounting for the nonlinear behavior of concrete and stiffness degradation due to the formed cracks. The curvature value (κ) at each cross-section was estimated by:

$$\kappa = \frac{(\varepsilon_i - \varepsilon_e)}{d} \quad \textbf{(7-3)}$$

The *BMs* were calculated from the FEMs by integrating the internal stresses in the plane-stress/plane-strain elements over the cross-section plane. **Figure 7-10** compares the

calculated *BM* values from LEA and NLA models with those obtained from the measured strains. Inspecting **Figure 7-10** reveals that the *BMs* estimated from NLA model agree well with the measured values, especially at the mid-span where cracks developed. The observed fluctuations in the estimated *BMs* from NLA model at the midspan are attributed to cracks formation, which reduces the cross-section stiffness. It is also noted from **Figure 7-10** that the *BMs* calculated from the LEA model results were generally higher than the measured values.

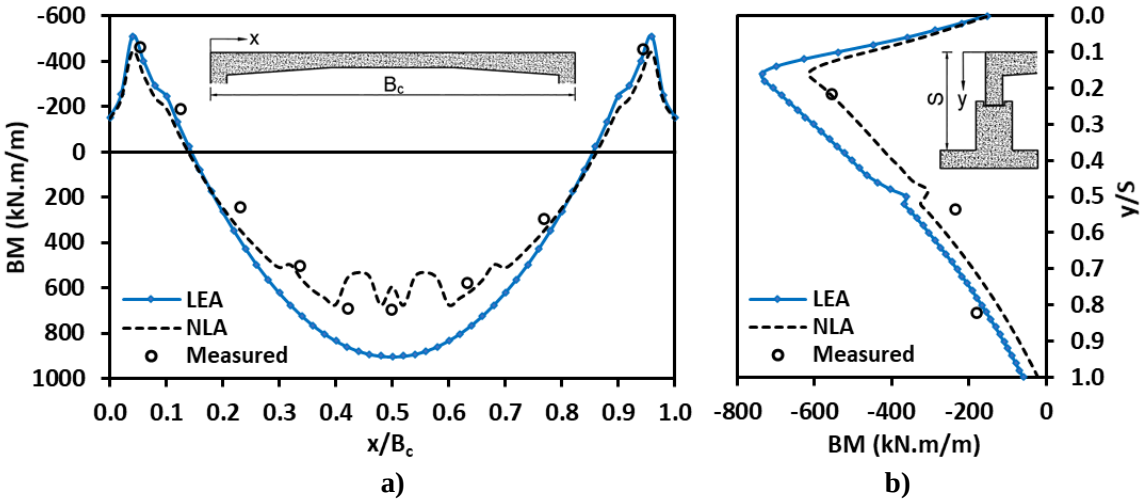

Figure 7-10. Comparison between bending moments from SG measurements and numerical models at H = 3.0 m: a) on the top slab; and b) along the sidewall.

Figure 7-11 compares the earth pressures on the slab and sidewalls as well contact pressures underneath the footing calculated from the LEA and NLA FEMs for the final backfill height, H = 3.8 m. Both LEA and NLA models yielded almost the same distributions of vertical pressures on the slab and underneath the footing, and the lateral earth pressure distribution on the sidewall differed slightly. The vertical earth pressure calculated at the mid-span from the NLA model was slightly lower than that obtained from the LEA model as shown in **Figure 7-11a**. This is due to the initiation of cracks at the mid-span as the backfill height increased, which reduced the cross-section stiffness at the mid-span and hence the earth pressure was redistributed to the stiffer cross-sections.

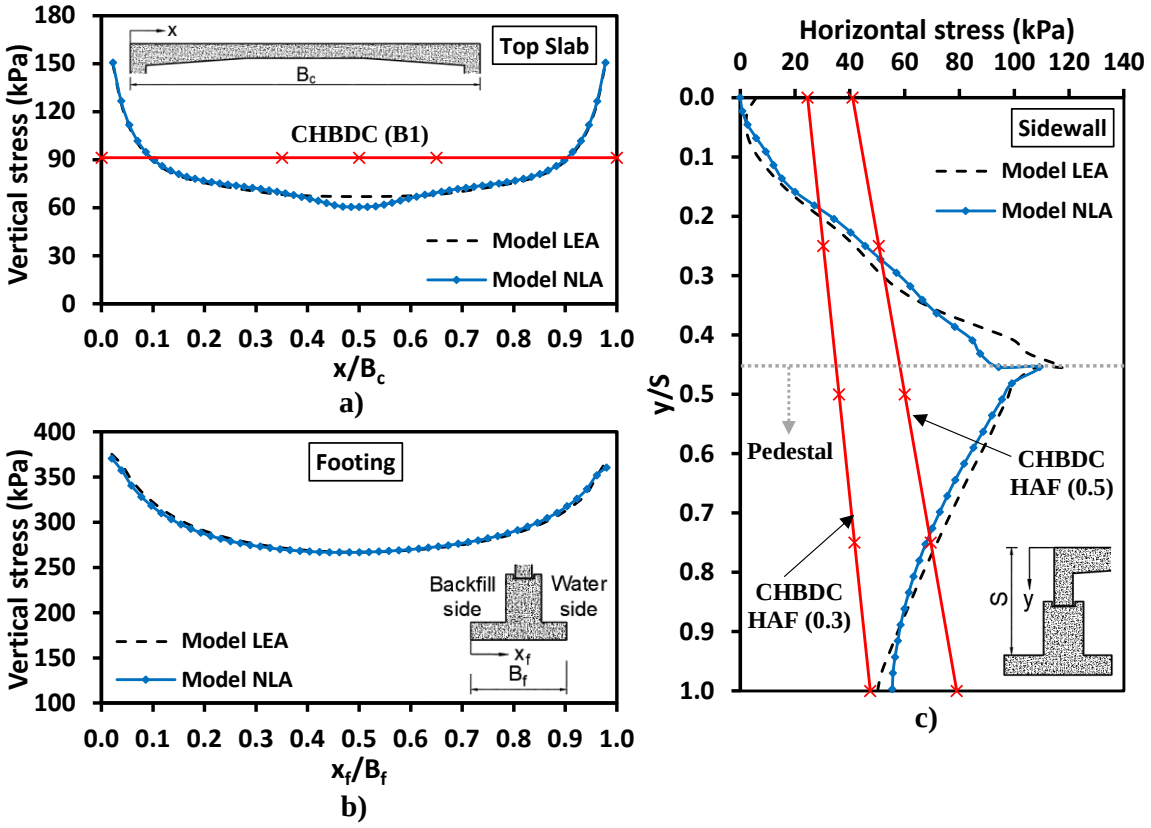

Figure 7-11. Predicted earth pressures at 3.8 m of backfill: a) vertical earth pressure on the top slab; b) contact pressure underneath the footing; and c) lateral earth pressure on the sidewall and footing pedestal.

7.5.4 Effect of Sidewall and Pedestal Heights on the Applied Earth Pressures (SLS)

A parametric study was conducted employing the NLA model to evaluate the influence of the sidewall height, *R*, and correspondingly footing pedestal height, *P*, on the earth pressures acting on the TSC and the contact pressure underneath the strip footing. The total height of the pedestal and sidewall (excluding 0.16 m embedded in the footing keyway), *S*, in the NLA model was 3.8 m (*P* = *R* = 1.9 m). Four additional culvert configurations were analyzed, considering *R* = 2.3, 2.8, 3.3, and 3.8 m, while keeping the total height constant at *S* = 3.8 m. The models were thus denoted *R*-1.9m to *R*-3.8m.

The earth pressures acting on the TSC and contact pressures underneath the strip footing at the final backfill height (*H* = 3.8 m) for the considered configurations are presented in **Figure 7-12**. It is observed from **Figure 7-12a** that R had a negligible effect on the vertical

earth pressure on the top slab, i.e., a slight increase at the mid-span along with a slight decrease at the edges as *R* increased. On the other hand, *R* (or more precisely *P*) had a considerable effect of on the contact pressure underneath the strip footing as shown in **Figure 7-12b**. As the pedestal height, *P*, decreased, the contact pressure became non-uniform as the pressure at the footing edge on the backfill side increased and that at the water side decreased. This is attributed to the change in footing relative flexibility associated with the reduction of the pedestal height.

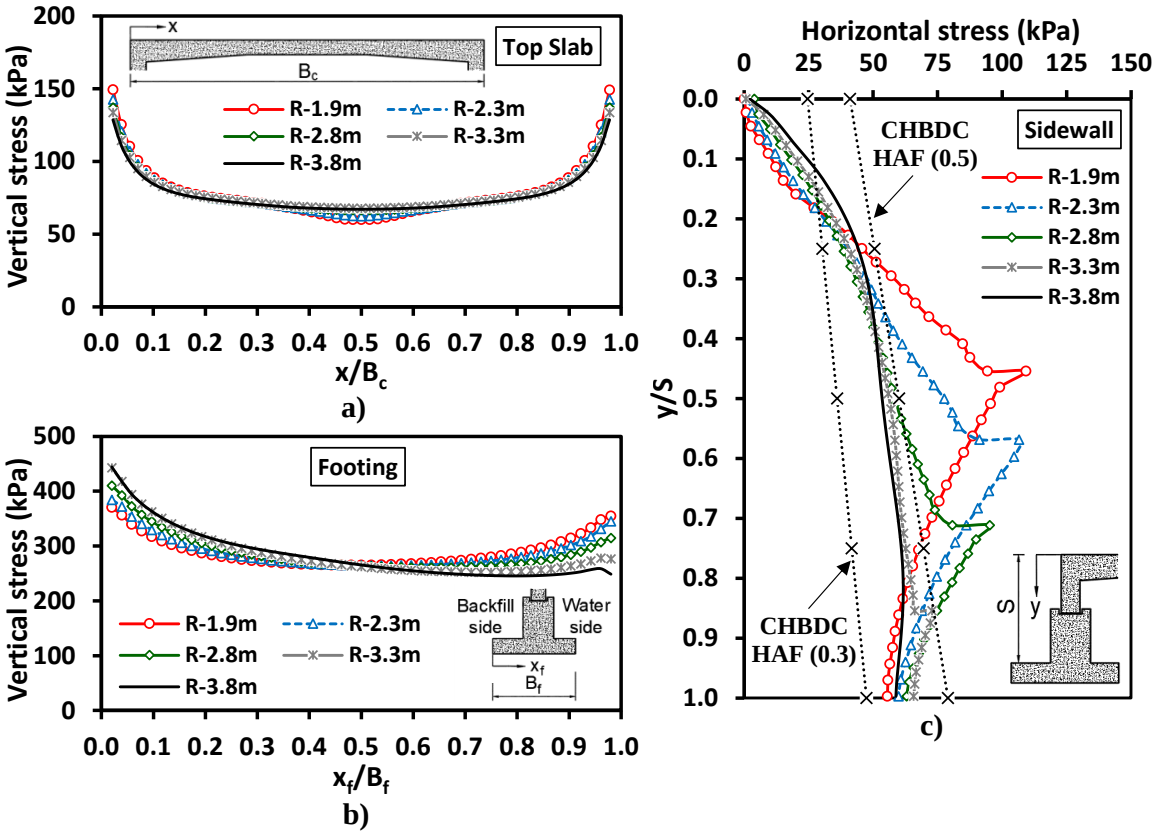

Figure 7-12. Effect of sidewall and footing pedestal heights on the earth pressures at 3.8 m of backfill (SLS): a) vertical earth pressure on the top slab; b) contact pressure underneath the footing; and c) lateral earth pressure on the sidewall and footing pedestal.

The effect of *R* on the lateral earth pressure along the sidewall and footing pedestal was also significant. As shown in **Figure 7-12c**, the lateral earth pressure on the sidewall upper part was null in all cases due to the inward deflection of sidewall away from the sidefill. For cases with footing pedestal (*R*-1.9m to *R*-3.3m), the lateral earth pressure linearly with depth up to the sidewall base, then it decreased linearly with depth along the pedestal,

which is attributed to the rotation of the sidewall lower part towards the sidefill and the rotation of the footing in the opposite direction. **Figure 7-12c** also shows that the maximum lateral earth pressure at the sidewall base decreased as *R* increased due to the larger rotation of the sidewall associated with the increase the sidewall rigidity as its height decreased. For footing without pedestal (*R*-3.8m), the lateral earth pressure distribution was trapezoidal; it increased to 50 kPa near the sidewall upper third then remained almost constant with depth. Finally, **Figure 7-12c** reveals that the calculated lateral earth pressures for footings with short or no pedestal (*R*-3.3m and *R*-3.8m) fell within the maximum and minimum values suggested by the CHBDC (CSA, 2014), while higher lateral pressures were calculated for long pedestals (*R*-1.9m to *R*-2.8m).

7.5.5 Maximum Backfill Height Prediction (ULS)

The validated NLA model was employed to predict the backfill height that could cause failure of the Oshawa culvert and to investigate the failure mechanism at ULS. The modified model is denoted NLA-U, in which backfill layers were added on the top slab up to H = 12.0 m.

Figure 7-13a displays the vertical deflection at the mid-span and lateral deflection at the sidewall top corner and base for different backfill heights. Negative sign indicates outward lateral deflection towards the sidefill. The load-deflection curve at the mid-span increased linearly with backfill height up to 3.2 m, after which cracks developed and the stiffness of cross-section decreased, and the deflection continued to increase linearly with H but with lower stiffness up to H = 10.6 m. Failure occurred at H = 10.6 m (which was 2.8 times the design backfill height, 3.8 m), as manifested by sudden increase in the vertical deflection. The backfill height at failure (H_{max} = 10.6 m) was almost 2.8 times the design backfill height (3.8 m). **Figure 7-13a** also shows some inward deflection of the sidewall top corner, which reduced the lateral earth pressure at the sidewall top part. On the other hand, the sidewall base displaced laterally outward as the backfill height increased, reaching 16.5 mm at failure causing significant increase in the lateral earth pressure at the pedestal top and sidewall base.

The evolution of the vertical earth pressures with the backfill height at the slab edge ($x/B_c = 0.0$), quarter-span ($x/B_c = 0.25$), and mid-span ($x/B_c = 0.5$) are displayed in **Figure 7-13b**. The vertical earth pressures were highest on the slab edge, while almost equal earth pressures were calculated at the quarter-span and mid-span up to H = 3.2 m (on set of cracks). Afterwards, the earth pressure at the mid-span continued to increase with H but a much slower rate. Similarly, the earth pressure at the quarter-span increased at a slower rate for H > 7.0 m. **Figure 7-13b** also shows that the earth pressures at the mid-span were comparable with the free-field stresses up to H = 3.2 m, but then decreased due to the crack formation, while the earth pressures at the quarter-span were close to the free-field stress for all backfill heights. On the other hand, the earth pressures at the slab edge were much higher than the free-field stress at all backfill heights. These changes of earth pressures at the slab mid-span and edges are due to soil arching, which underscore the important effects of RC nonlinearity due to crack formation at the ULS.

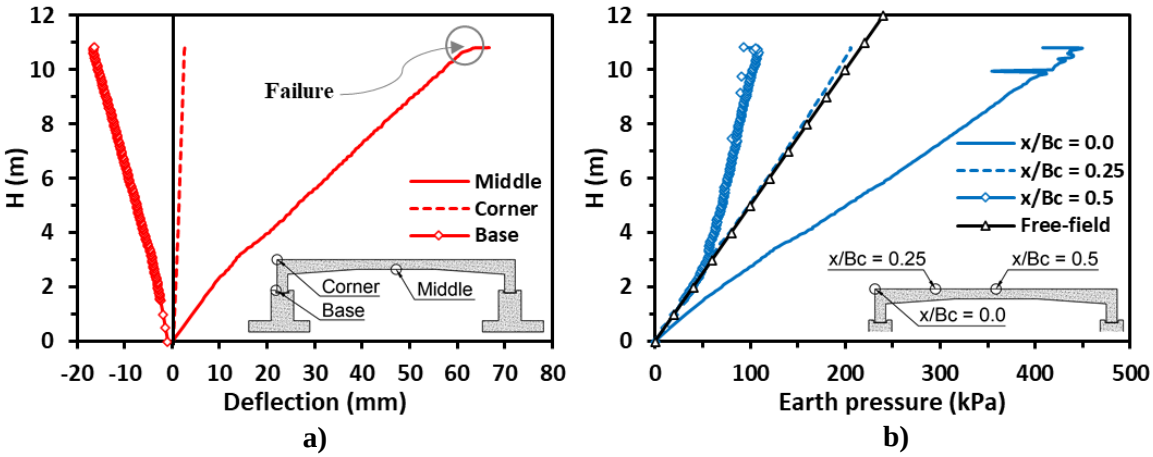

Figure 7-13. The NLA-U model results at different backfill heights up to failure: a) vertical and lateral deflections; and b) vertical earth pressures on the top slab.

7.5.6 Effect of Culvert Configuration on its Failure Mechanism

Figure 7-14a displays the deformed shape of the footing-culvert system and the predicted crack pattern at H_{max} (10.6 m). The deformed shape indicates large vertical deflection at the mid-span. The sidewall rotated as a rigid body in the footing keyway resulting in the development of additional stresses at the sidewall-keyway contact surfaces (elaborated in **Figure 7-14b**). These stresses would induce additional straining actions (shear forces and

bending moments) on the sidewall base and footing keyway, as well as the rotation of strip footing towards the backfill side as depicted in **Figure 7-14a**. Cracks are expected to develop on the bottom surface in the middle of the slab and on the outer surface along most of the sidewall height. The local cracks at the sidewall-keyway contact surfaces indicate crushing of the concrete due to the concentrated stresses resulting from the sidewall rotation. **Figure 7-14b** displays the steel reinforcement yield points (i.e., the reinforcement stresses reached its yield stress, 400 MPa). The yield points are concentrated at the mid-span, which indicates the formation of a plastic hinge and explains the load-deflection yielding plateau. Local yield points occurred at the sidewall base due to the developed stress concentration at the sidewall-keyway contact surfaces when the sidewall rotated as a rigid body. Collectively, the NLA-U model results indicate flexural failure of the Oshawa culvert at 10.6 m backfill and the formation of a plastic hinge at the mid-span.

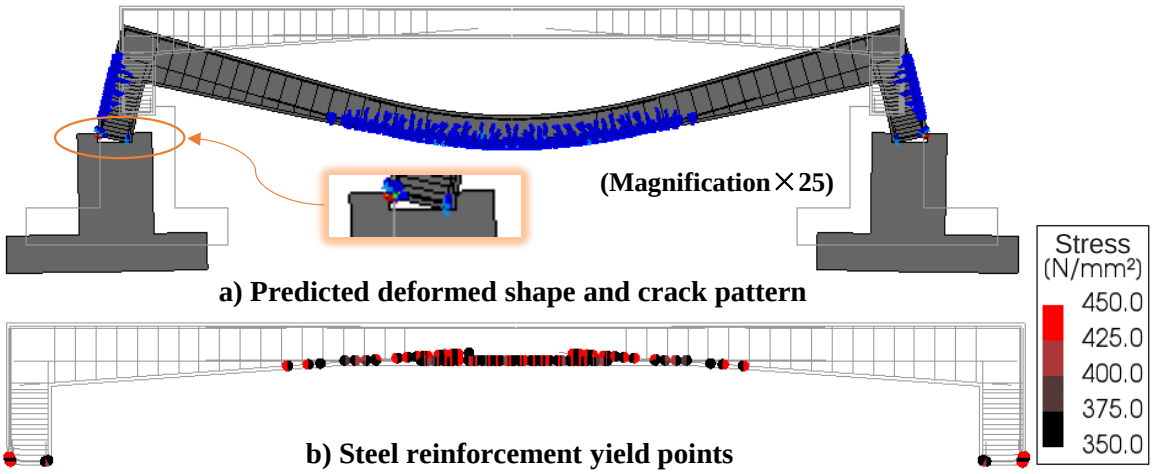

Figure 7-14. Structural performance of the Oshawa culvert at the maximum backfill height (H_{max} = 10.6 m).

7.5.7 Effect of Sidewall and Pedestal Heights on Capacity (ULS)

The nonlinear FEMs (*R*-1.9m to *R*-3.8m) were employed to investigate the effect of pedestal and side wall heights on the predicted backfill height that could cause failure of the Oshawa culvert and its failure mechanism. The backfill height on the top slab was increased up to H = 12.0 m.

Figure 7-15 displays the load-deflection curves up to failure for all models. The maximum backfill height at failure, H_{max}, decreased from 10.6 m for *R*-1.9m to 9.5 m, 8.9 m, 8.5, and 8.3 m as *R* increased from 1.9 to 2.3, 2.8, 3.3, and 3.8 m, respectively. **Figure 7-15** also shows that the mid-span vertical deflection at failure decreased as *R* increased, e.g., it was 63.3 mm and 36.9 mm for *R*-1.9m and *R*-3.8m.

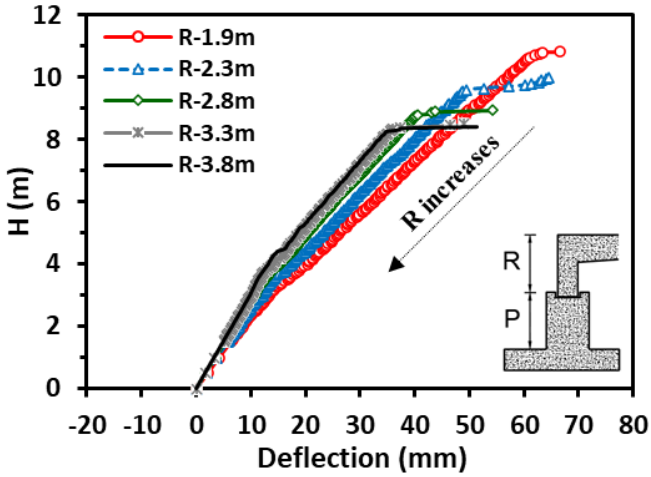

Figure 7-15. Effect of sidewall and pedestal heights on the mid-span vertical deflection up to H_{max}.

The decrease in vertical displacement at failure is attributed to the change in deformation mechanism, as revealed by the deformed shapes shown in **Figure 7-16**. The sidewall rotated as a rigid body for *R* = 1.9 m, and its rotation contributed to the vertical deflection of the slab. Mid-span However, for *R* = 2.8 and 3.8 m, the sidewall became flexible and its rotation inside the footing keyway, and consequently, the mid-span vertical deflection decreased, as well as the stresses induced at the sidewall-keyway contact surfaces.

Figure 7-17 displays the yield points of steel reinforcement for the different culvert configurations. For *R* = 1.9 and 2.3 m, yield points were concentrated at the culvert mid-span, and some at the sidewall base due to concentrated stresses caused by the sidewall rotation inside the footing keyway. For *R* > 2.3 m, yield points (i.e., plastic hinges) occurred at the mid-span and at the sidewalls' top corners just below the haunches. Ramadan and El Naggar (2021a, b) also reported plastic hinges at the sidewall top corners for TSCs with spans of 10.4 m and 7.3 m, and sidewall heights of 3.07 m and 2.79 m, as elaborated in Chapter 6 and Chapter 4, respectively. **Figure 7-17** also demonstrates that no yield points

developed at the sidewall base for $R \geq 2.8$ m due to the decrease in sidewall rotation and associated stress concentrations at the sidewall-footing contact surfaces.

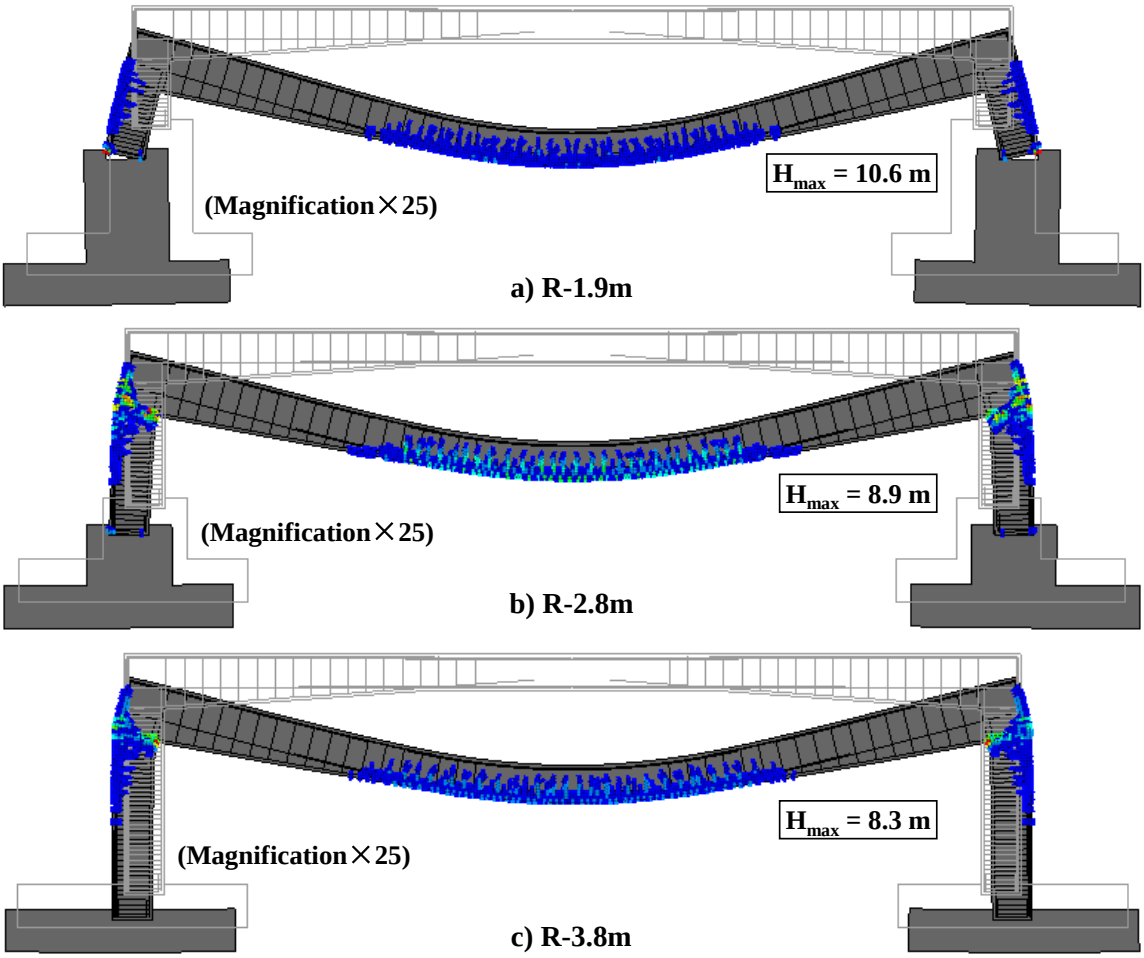

Figure 7-16. Effect of sidewall and pedestal heights on the deformed shape and crack pattern at H_{max}.

Figure 7-18 elaborates the effects of R on the earth pressures applied on the culvert and contact pressure underneath the strip footing for H = 8.0 m (i.e., < H_{max} of all cases). **Figure 7-18a** shows that, same as the case for SLS, the vertical earth pressure at the mid-span increased slightly and the earth pressures at the slab edges decreased slightly as R increased. Similarly, **Figure 7-18b** reveals that P had a considerable effect on the contact pressure underneath the strip footing. As the pedestal height, P, decreased, the contact pressure distribution became non-uniform with higher pressure at the footing edge on the backfill side. For instance, the calculated contact pressures at the footing edges on the backfill and water sides for R-1.9m were 581.4 kPa and 617.8 kPa, while they were 674.2

kPa and 509.7 kPa for *R*-3.8m. The different contact pressure distributions are attributed to the change in footing flexibility associated with the reduction of the pedestal height.

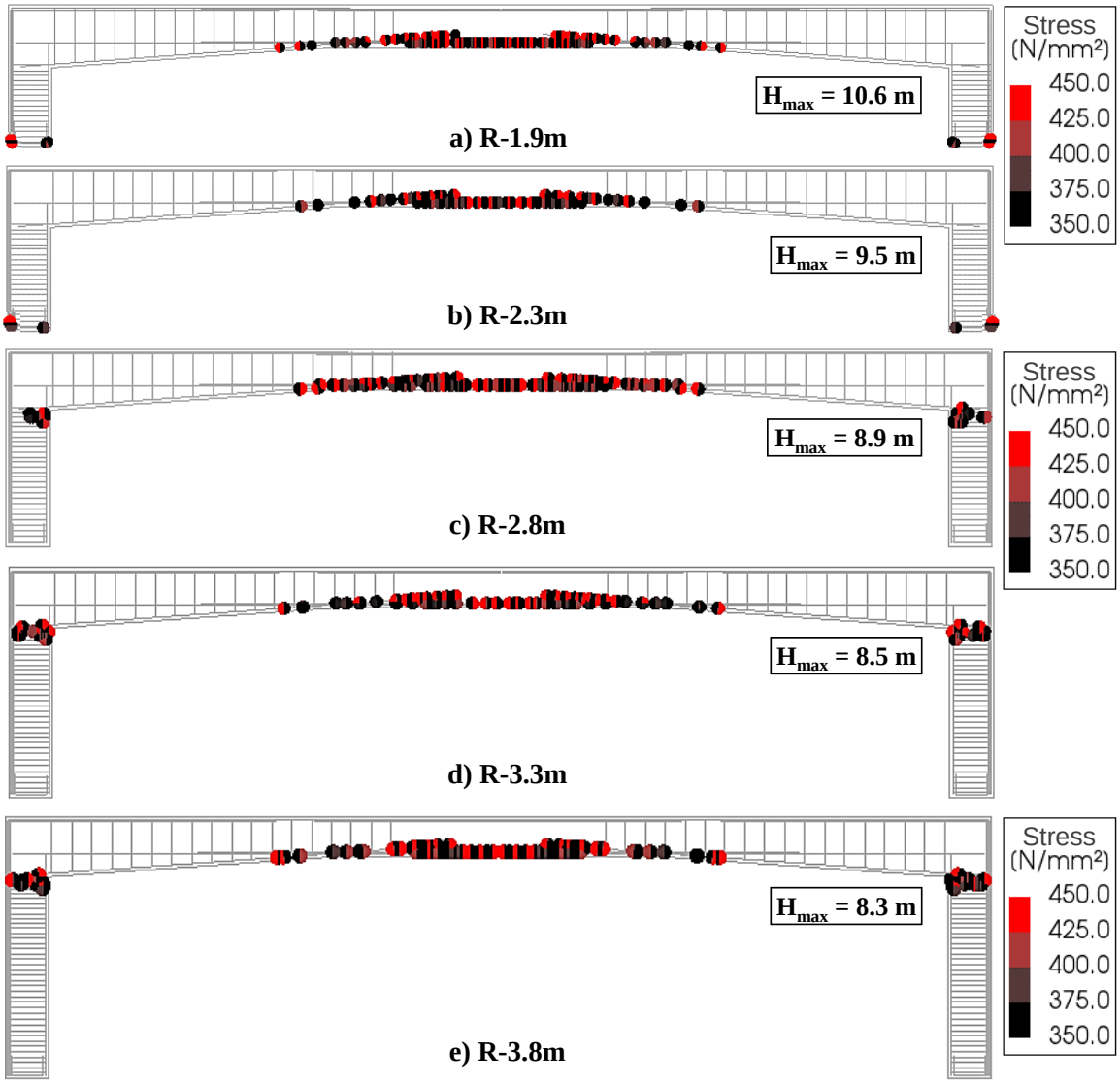

Figure 7-17. Effect of sidewall and pedestal heights on the reinforcement yield points at H_{max}.

The effect of *R* on the lateral earth pressure along the sidewall and pedestal is presented in **Figure 7-18c**. The lateral earth pressure on the upper part of the sidewall was null owing to the inward deformation of the culvert away from the sidefill material in all cases. For *R*-1.9m to *R*-3.3m, the lateral earth pressure increased linearly up to the sidewall base, then decreased linearly with depth along the pedestal. For the footing without pedestal (i.e., *R*-3.8m), the lateral earth pressure distribution was trapezoidal; it increased to approximately

105 kPa at the sidewall's upper third and remained almost constant on the middle and lower thirds. The variation of the lateral earth pressure distribution is evidently affected by sidewall and pedestal heights, which is attributed to their influence on the deformed shape of the footing-culvert system.

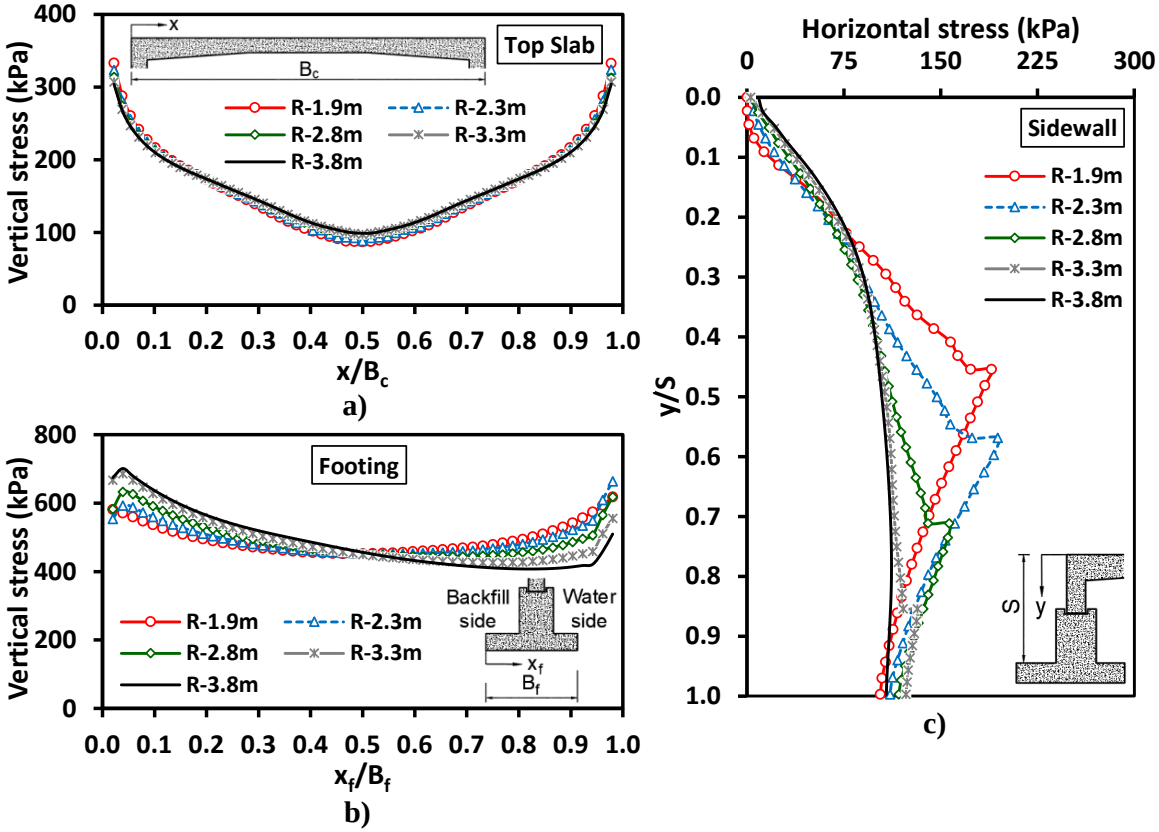

Figure 7-18. Effect of sidewall and pedestal heights on the earth pressures at 8.0 m of backfill (ULS): a) vertical earth pressure on the top slab; b) contact pressure underneath the footing; and c) lateral earth pressure on the sidewall and footing pedestal.

7.6 Ultimate Capacity of Precast Units

The ultimate capacity of an RC arched TSC precast unit with 11.0-m-span was evaluated from a laboratory load testing program (Marshall et al., 2014). The arched TSC precast unit was 1.2-m-wide with a clear mid-span height of 2.7 m. The unit was loaded to failure by placing it on a rigid floor, restrained from lateral movement at the base using steel beams, and applying the load through three W8×35 loading beams spanning the precast unit width and 1.2 m apart. The middle loading beam was positioned at the mid-span. Loads were applied simultaneously on each beam in 17.8 kN increments. In Chapter 6, a 3D FEM was

developed to simulate the loading test and validated it against the experimental data. The same modeling approach was employed in this study to investigate the structural performance of the subject TSC precast unit under the same laboratory loading conditions considering the influence of the sidewall height.

A 3D FEM was developed for one 1.3-m-wide Oshawa culvert precast unit with the same geometry and reinforcement details provided in **Figure 7-19**. The total sidewall height was 2.06 m; however, the model will continue to be referred to as *R*-1.9m. As shown in **Figure 7-19**, the precast unit was discretized using 25,304 twenty-node solid brick elements with an average element size of 85 mm. The steel reinforcing bars were simulated using embedded beam elements. The same material properties for concrete (smeared crack model) and steel reinforcement (von Mises plasticity model with no hardening behavior) used in the 2D NLA model were adopted in the 3D model. The bottom surface of the sidewall was restrained from movement in the vertical and lateral directions (Z and X-axes). Loads were applied incrementally as vertical stresses on the contact surfaces of the three loading beams spanning the width of the culvert (3 × 1.3 m × 0.204 m). The vertical stress increment at each loading beam location was 67.12 kPa, corresponding to the 17.8 kN applied during the experimental test (Marshall et al., 2014). Four additional 3D models were developed to simulate the TSC with varying sidewall heights, i.e., *R*-1.9m to *R*-3.8m.

Figure 7-20 compares the load-deflection curves at the mid-span of the investigated precast units. All the load-deflection curves reflect a linear relationship up to a total load between 1000 and 1250 kN, beyond which the culvert stiffness decreased because of the formed cracks until the ultimate load (P_{ult}) was reached. The load then decreased significantly, and the vertical deflection increased markedly, indicating brittle failure behavior without yielding plateau, unlike the soil loading condition (shown in **Figure 7-15**). This is because the soil confinement enhances the TSCs structural performance at ULS, and results in ductile failure. Zoghi and Farhey (2006), Marshall et al. (2014), and Moradi et al. (2016) reported similar effect of soil confinement on the load-carrying capacity of RC culverts.

Figure 7-20 clearly demonstrates stiffer behavior of the TSC with shorter sidewall. Lower vertical deflections at the mid-span were calculated at all load levels as the sidewall height decreased. In addition, the ultimate capacity of the precast unit decreased as the sidewall height increased as depicted in **Figure 7-20**. **Table 7-2** summarizes the calculated ultimate capacity, P_{ult}, for different R values and percentage reduction in P_{ult} relative to the reference case (R-1.9m). A reduction of 18% in P_{ult} was estimated as the sidewall height increased from 1.9 to 3.8 m. On the other hand, the vertical deflection at the mid-span at the ultimate load increased as the sidewall height increased as depicted in **Figure 7-20** and **Table 7-2** due to the increased flexibility.

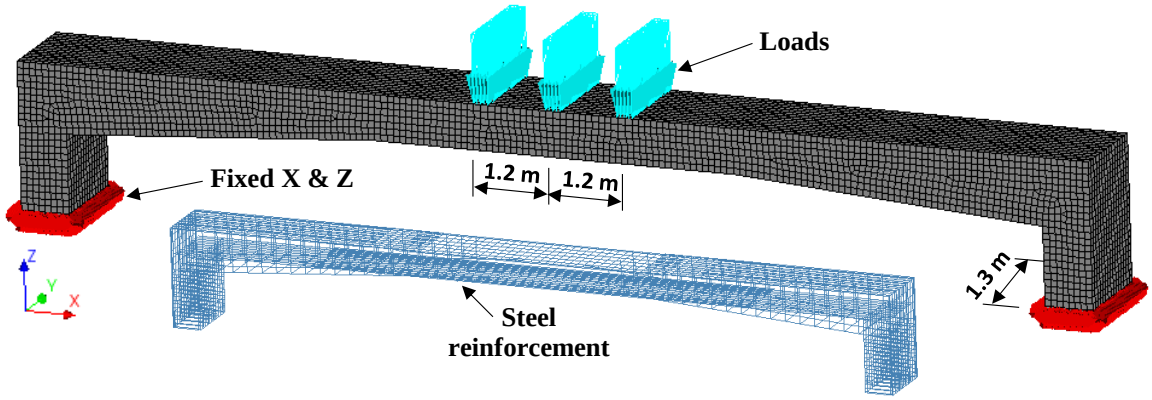

Figure 7-19. Overview of the 3D FE model (loads, mesh, boundary conditions, and steel reinforcement).

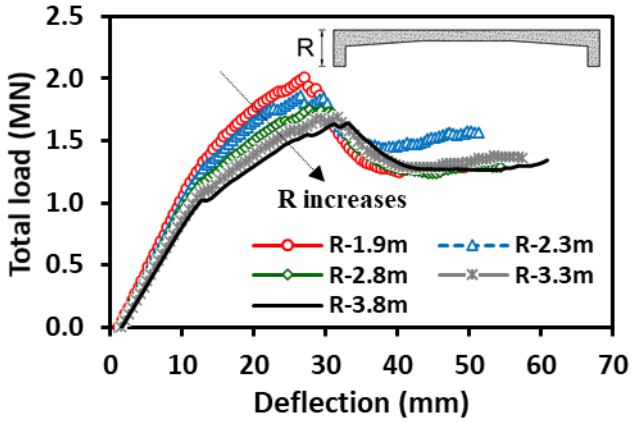

Figure 7-20. Effect of sidewall height on the load-deflection curve at the mid-span.

Figure 7-21 displays the deformed shapes of the precast units and crack patterns at the ultimate load. R-3.8m exhibited higher deflection at the top slab at lower load, compared

to *R*-1.9m and *R*-2.8m. This reflects more rigid behavior of the TSC precast unit as the height of its sidewall decreased. Comparable crack patterns were predicted for all cases, i.e., cracks on the slab bottom surface at the mid-span and on the outer surface of the sidewalls at the joint between the sidewall and top slab. Unlike the crack patterns predicted under soil loading conditions at H_{max} in **Figure 7-16**, cracks were predicted on the slab top surface within the haunch zones near the edges. These cracks indicate high negative bending moment at the top slab edges, resulting in tensile strains exceeding ε_{cr}, and thus, the formation of cracks. Moreover, cracks are expected to develop at the sidewall base in all cases, attributed to the high normal forces and the assigned fixity condition at the sidewall bases.

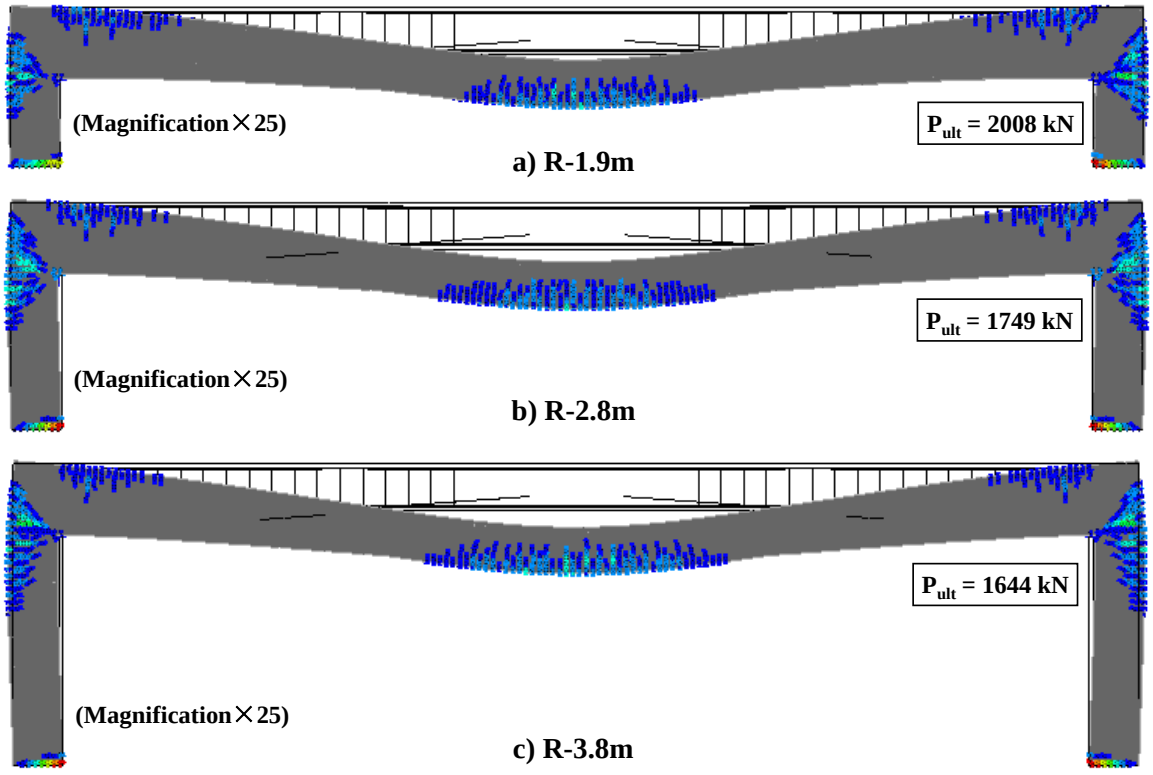

Figure 7-21. Effect of sidewall height on the precast unit deformed shape and crack pattern at the ultimate load.

Table 7-2. Summary of the 3D models' results.

Case	P_{ult} (kN)	Reduction in P_{ult} (%)	Mid-span deflection at P_{ult} (mm)	Precast segment weight (kN/1.3 m)
R-1.9m	2008	0.0	27.1	390
R-2.3m	1864	7.2	29.2	407
R-2.8m	1749	12.9	30.5	428
R-3.3m	1686	16.0	32.2	449
R-3.8m	1644	18.1	33.2	470

The steel reinforcement yield points for the five precast units are presented in **Figure 7-22**. High stresses were calculated in the reinforcing bars within the zones where significant crack formations were predicted. However, these stresses did not, in general, reach yielding. Only local yielding of the reinforcing bars at the sidewall base was observed, which is attributed to the high normal force and the assigned fixity condition at the sidewall bases. Generally, the failure mechanism of the precast unit of the subject 13.5-m-span TSC was predicted to be brittle. Crashing of the concrete is expected to occur without yielding of the reinforcing steel prior to failure. Moreover, the culvert sidewall height did not show any influence on the failure mechanism.

Finally, increasing the culvert sidewall height would increase the weight of the precast unit as listed in **Table 7-2**. For instance, increasing *R* from 1.9 to 3.8 m would increase the precast unit weight from 390 kN to 470 kN, reflecting 20.5% increase in weight. Such increase in the precast unit weight would increase the induced straining actions while lifting and handling the precast units, and would cause some challenges for transporting the precast units. Therefore, shortening the culvert sidewall height and using footing pedestal have important advantages over increasing the sidewall height and eliminating the footing pedestal.

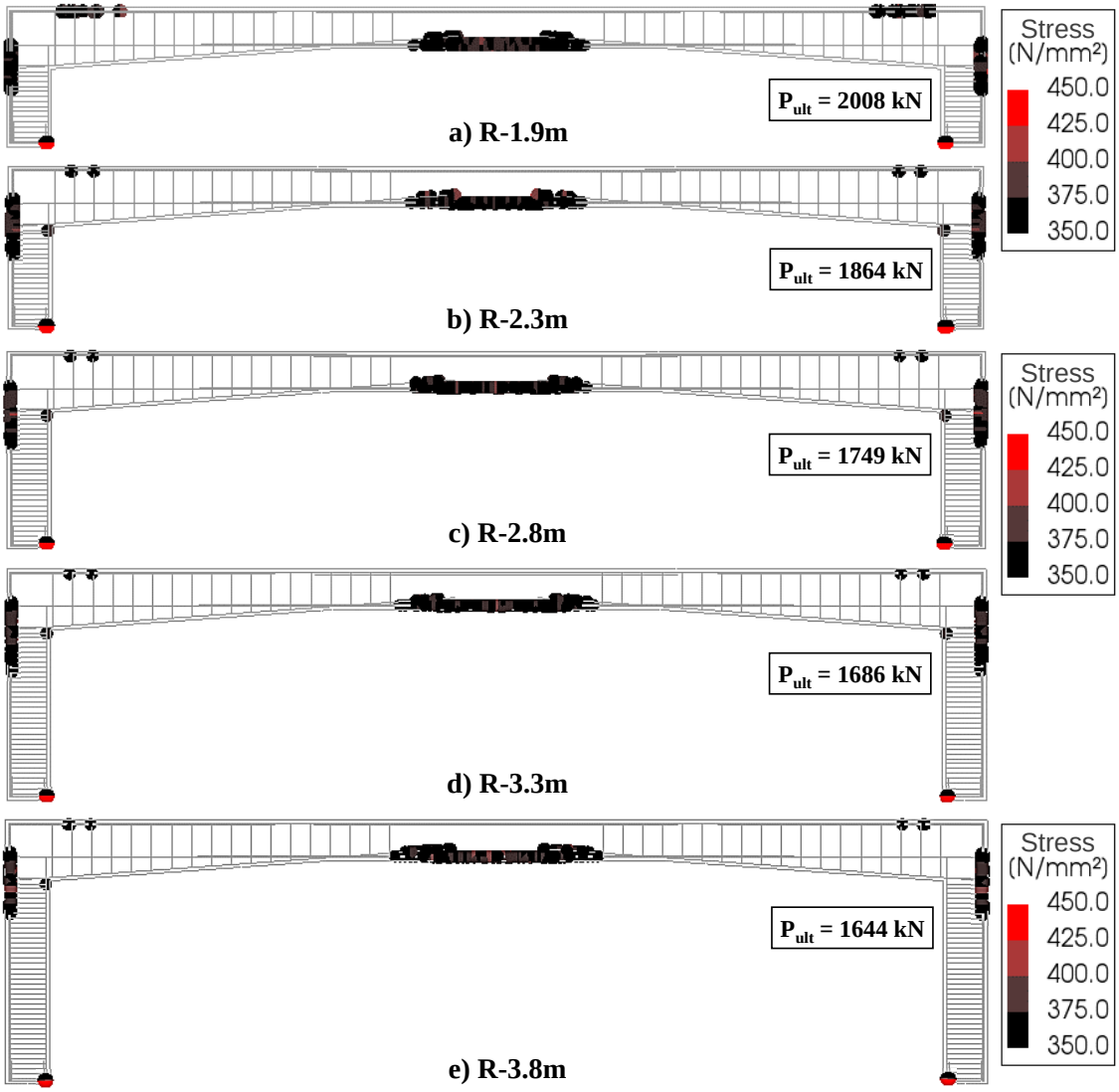

Figure 7-22. Effect of sidewall height on the steel reinforcement yield points at ultimate load.

7.7 Conclusions

A 13.5-m-span TSC was instrumented with PCs and SGs for real-time monitoring during and after construction. The TSC has a relatively short sidewall (2.06 m) and was constructed on a strip footing with a 1.9-m-thick pedestal. Field data collected during the culvert construction was presented and discussed to elucidate the effect of the culvert configuration on earth pressure distributions. In addition, two 2D finite element models of the TSC were validated using the field data and employed to further evaluate the culvert

configuration on its soil-structural interaction mechanism. The following conclusions may be drawn:

1. As per Chapters 4 and 6, the vertical earth pressure distribution on the slab was non-uniform, high at the edges and low at the mid-span. The average VAF from the numerical model results was 1.05, which was lower than the VAF = 1.2 stipulated in the CHBDC (CSA, 2014) for B1 standard installation.

2. The assumption of uniform contact pressure underneath strip footings with geometry and subsurface conditions comparable to that in this study is realistic for footing design purposes.

3. The deformed shape of the footing-culvert system resulted in lateral earth pressure linearly increasing with depth on the sidewall and linearly decreasing with depth on the footing pedestal.

4. The assumption of linear elastic behavior of RC is adequate for estimating earth pressures on the buried large-span TSC. However, it results in overestimation of the bending moment when cracks form in the RC culvert.

The sidewall height was varied between 1.9 and 3.8 m to examine its effects on the TSCs behavior. The following conclusions can be drawn:

1. The vertical earth pressure distribution on the top slab was non-uniform up to H_{max}, with high magnitudes at the edges and low magnitudes at the mid-span.

2. Increasing the sidewall height and reducing the pedestal height had insignificant effect on the slab vertical earth pressures. However, the contact pressure distribution underneath the footing became increasingly nonuniform. It also affected the culvert deformed shape and the lateral earth pressure distribution on the sidewall and footing pedestal.

3. The maximum backfill height at failure decreases as the sidewall height increases.

4. The sidewall height has no effect on the failure mechanism, but the locations of the failure surfaces and plastic hinges are affected by the sidewall height. For TSCs with relatively short sidewalls, plastic hinges are predicted only at the mid-span. For long sidewalls, plastic hinges are predicted at the mid-span and at the top corners of sidewalls.

5. Short sidewalls rotated as a rigid body as the backfill height increased, which resulted in additional straining actions (shear forces and bending moments) on the sidewall base and footing keyway. Long sidewalls resulted in relatively flexible behavior and exhibited bending deflection but no rotation within the keyway.

6. Short culvert sidewall height and footing with pedestal offer favorable performance as well as logistical and constructional advantages.

The effect of culvert sidewall height on its structural capacity was evaluated employing 3D nonlinear FEMs. A laboratory loading experiment setup reported in the literature was simulated to examine the ultimate capacity of the TSC unit, and the following conclusions are drawn:

1. The sidewall height had no influence on the failure mechanism; all investigated configurations exhibited brittle failure, with no reinforcement yielding at the ultimate load.

2. Increasing the sidewall height from 1.9 to 3.8 m decreased the ultimate capacity by 18% and increased the mid-span vertical deflection at the ultimate load.

3. As expected, short sidewall height results in stiffer behavior at all load levels.

7.8 References

1. Abuhajar, O., El Naggar, H., Newson, T., (2015a). Seismic soil-culvert interaction. *Canadian Geotechnical Journ*al, 52, 1649-1667. dx.doi.org/10.1139/cgj-2014-0494

2. Abuhajar, O., El Naggar, H., and Newson, T. (2015b). Static soil culvert interaction the effect of box culvert geometric configuration and soil properties. *Computers and Geotechnics Journal*, 69, 219-235. 10.1016/j.compgeo.2015.05.005

3. Balachandran, K., Liu, J., Cao, L., and Peaker, S. (2015). Statistical correlations between pressuremeter modulus and SPT N-value for glacial tills. In *Proc., 68th Canadian Geotechnical Conf. and 7th Canadian Permafrost Conf*. Richmond, BC, Canada: Canadian Geotechnical Society.

4. Bennett, R. M., Wood, S.M., Drumm, E. C., and Rainwater, N.R. (2005). Vertical loads on concrete box culverts under high embankments. *Journal of Bridge Engineering*, 10 (6), 643-649. 10.1061/(ASCE)1084-0702(2005)10:6(643).

5. Boscardin, M. D., Selig, E. T., Lin, R. S., and Yang, G. R. (1990). Hyperbolic parameters for compacted soils. *Journal of Geotechnical Engineering*, 116 (1), 88-104.

6. Chen, B., and Sun, L. (2014). Performance of a reinforced concrete box culvert installed in trapezoidal trenches. *Journal of Bridge Engineering*, 19 (1), 120–130. https://doi.org/10.1061/(ASCE)BE.1943-5592.0000494.

7. CSA (Canadian Standards Association). 2014. *Canadian highway bridge design code*. CAN/CSA-S6-14. Mississauga, ON, Canada: CSA.

8. CSA (Canadian Standards Association). 2014. *Design of concrete structures (A23.3-14)*. CSA Group, Mississauga, Ontario.

9. Duncan, J. M., and Chang. C. Y. (1970). Nonlinear analysis of stress and strain in soils. *Journal of Soil Mechanics and Foundations Division*, 96 (5),1629–1653.

10. Elshimi, T. M., and Moore, I. D. (2013). Modeling the effects of backfilling and soil compaction beside shallow buried pipes. *Journal of Pipeline Systems Engineering and Practice*, 4 (4), 04013004.

11. Hordijk, D. A. (1991). Local approach to fatigue of concrete. Doctor of Philosophy, Ph.D. dissertation, Delft University of Technology, Delft, The Netherlands.

12. International Federation for Structural Concrete. (2013). *Fib model code for concrete structures 2010*. Berlin: Verlag Ernst & Sohn.

13. Kheradi, H., Ye, B., Nishi, H., Oka, R., Zhang, F., (2017). Optimum pattern of ground improvement for enhancing seismic resistance of existing box culvert buried in soft ground. *Tunnelling and Underground Space Technology*, 69, 187-202. http://dx.doi.org/10.1016/j.tust.2017.06.022

14. Manzari, M., Drevininkas, A., Olshansky, D., and Galaa, A. (2014). Behavioral modeling of Toronto glacial soils and implementation in numerical modeling. In *Proc., 67th Canadian Geotechnical Conf*. Richmond, BC, Canada: Canadian Geotechnical Society.

15. Marshall, J. D., Anderson, J. B., Meadows, R. L., and Jensen, T. J. (2014). Full-scale testing of three-sided precast concrete arch sections. *Journal of Bridge Engineering*, 19 (12), 04014051. 10.1061/(ASCE)BE.1943-5592.0000630.

16. McGrath, T. J., Selig, E. T., Webb, M. C., and Zoladz, G. V. (1999). *Pipe interaction with the backfill envelope*. FHWA-RD-98-191.

17. Moradi, M., Valipour, H., and Foster, S. (2016). Reserve of strength in inverted u-shaped RC culverts: effect of backfill on ultimate load capacity and fatigue life. *Journal of Bridge Engineering*, 21 (2), 04015051. 10.1061/(ASCE)BE.1943-5592.0000800

18. MTO (Ministry of Transportation of Ontario). 2010. *Frost Penetration Depths for Southern Ontario*. Ontario Provincial Standard Drawing OPSD 3090. ON, Canada: MTO.

19. Perkins, S. W., and Lapeyre, J. A. (1997). *Instrumentation of a geosynthetic-reinforced flexible pavement system*. Report No. 1596. Washington, DC: Transportation Research Board. https://doi.org/10.3141%2F1596-05.

20. Pimentel, M., Costa, P., Félix, C., and Figueiras, J. (2009). Behavior of reinforced concrete box culverts under high embankments. *Journal of Structural Engineering*, 135 (4), 366-375. 10.1061/(ASCE)0733-9445(2009)135:4(366), 366–375

21. Ramadan, S. H., and El Naggar, M. H. (2021a). Field monitoring and numerical analysis of a large-span three-sided reinforced concrete culvert. *Journal of Geotechnical and Geoenvironmental Engineering*, 147 (4), 04021008. 10.1061/(ASCE)GT.1943-5606.000248

22. Ramadan, S. H., and El Naggar, M. H. (2021b). Structural performance of a medium-span RC three-sided culvert based on field measurements and numerical analyses. *Canadian Geotechnical Journal.* https://doi.org/10.1139/cgj-2020-0574.

23. Rots, J. G., Blaauwendraad, J. (1989). Crack models for concrete: discrete or smeared? Fixed, multi-directional or rotating? *Heron*, 34 (1), 5–55.

24. Sama, M., Sykora, D. W., and Vytiniotis, A. (2015). Vertical pressures produced by controlled low strength material (CLSM) poured into pipe trenches. *IsnowEE*, ASCE, 429-441. https://doi.org/10.1061/9780784479087.043.

25. Seed, R. B., Duncan, J. M., and Ou, C. Y. (1991). Finite element analysis of compaction problems. *Advanced Geotechnical Analysis-Development in Soil Mechanics and Foundation Engineering-4, Ed*. Banerjee, P. K. and Butterfield, R. Elsevier Applied Science.

26. Thorenfeldt, E., Thomaszewic, A., and Jensen, J. J. (1987). 'Mechanical properties of high-strength concrete and applications in design. In *Proc., Symp. on Utilization of High-Strength Concrete*, Tapir Publishers, Stavanger, Norway, 149–159.

27. TNO Diana BV. 2016. *DIANA—User's manual: Material library*. Delft, Netherlands: TNO Diana BV.

28. Wood, S. M. (2000). Internal forces in a reinforced concrete box culvert. Master's dissertation, Dep. of Civil Engineering. Uni. of Tennessee.

29. Yang, M. Z. (2000). Evaluation of factors affecting earth pressures on buried box culverts. PhD dissertation, Uni. of Tennessee, Knoxville, TN.

30. Zoghi, M., and Farhey, D. N. (2006). Performance assessment of a precast concrete, buried, small arch bridge. *Journal of Performance of Constructed Facilities*, 20 (3), 244–252. 10.1061/(ASCE)0887 3828(2006)20:3(244).

Chapter 8

Design Guidelines for Reinforced Concrete Three-Sided Culverts

8.1 Introduction

The Canadian Highway Bridge Design Code, CHBDC, (CSA, 2014) provides design guidelines for reinforced concrete (RC) box culverts. In these guidelines, the backfill soils are categorized into three different groups (soil group I to III): sand and gravel, sandy silt (ML), and silty clay (CL) as listed in **Table 8-1**. The code does not distinguish between embankment and trench installations; instead, it defines two standard installations, namely, B1 and B2. The differences between B1 and B2 installations relate to the backfill soil type and compaction level in the sidefill and bedding zones as summarized in **Table 8-2**.

Table 8-1. Soil groups classification in the CHBDC (CSA, 2014).

Soil group	Description	Unified Soil Classification symbols
I	Sand and Gravel	SW, SP, GW, GP
II	Sandy Silt	GM, SM, ML, GC, and SC with less than 20% passing #200 sieve
III	Silty clay	CL, MH, GC, and SC with more than 20% passing #200 sieve

Table 8-2. Soils and compaction requirements for B1 and B2 standard installations. (CSA, 2014)

Installation type	Soil group	Equivalent minimum Standard Proctor compaction in sidefill and outer bedding zones
B1	I	90%
	II	95%
	III	Not permitted
B2	I	80%
	II	85%
	III	95%

Many studies addressed the earth loads and soil arching effect on RC box culverts, and different equations were proposed to estimate the vertical arching factors (VAFs) (Tadros et al., 1989; Bennett et al., 2005; Kim and Yoo, 2005; Kang et al., 2008). They reported that the primary factors, which influence the VAF are the backfill height (H), the compaction condition of the sidefill material, the soil type of the sidefill material, and the culvert span.

Based on typical practice and limited soil-structure interaction finite element analyses (FEAs), the code stipulates VAFs to estimate the vertical earth pressure on the top slab and horizontal arching factors (HAFs) to estimate the lateral earth pressure on the sidewall as summarized in **Table 8-3**. Higher VAF is specified for the case of B2 installation, which represents the case of moderately compacted sidefill. The higher VAF value accounts for the anticipated higher passive soil arching in case of loosely compacted sidefill material surrounding the RC box culvert. The code stipulates that both the minimum and maximum HAFs should be considered in design to estimate the maximum negative and positive bending moments induced in the sidewalls.

Table 8-3. Arching factors for box culverts in standard installations. (CSA, 2014)

Installation Type	Vertical Arching Factor, (VAF)	Horizontal Arching Factor, (HAF)	
		Minimum	Maximum
B1	1.20	0.30	0.50
B2	1.35	0.25	0.50

The American Association of State and Highway Transportation, AASHTO, (AASHTO LRFD, 2014) differentiates between embankment and trench installations when determining the vertical earth pressure on the top slab of RC box culverts. The AASHTO specifications include equations to estimate the soil-structure interaction factors (equivalent to the VAF) for embankment and trench installations based on the Marston-Spangler theory (Marston, 1930; Spangler, 1950). The soil-structure interaction factor for embankment installation (F_e) is given by:

$$F_e = \text{VAF} = 1 + 0.20\frac{H}{B_c} \quad \textbf{(8-1)}$$

where H is the backfill height over the top slab of the box culvert, and B_c is the outside width of the culvert. To account for the compaction condition of the sidefill material, the value of F_e shall not exceed 1.15 for compacted sidefill and 1.40 for uncompacted sidefill (AASHTO LRFD, 2014). However, the compaction requirements to classify the soil as compacted or uncompacted are not defined. The soil-structure interaction factor for trench installation (F_t) is given by:

$$F_t = \text{VAF} = \frac{C_d\, {B_d}^2}{H\, B_c} \leq F_e \quad \textbf{(8-2)}$$

where C_d is a load coefficient to account for the type of backfill soil, and the box culvert and embankment geometric properties, and B_d is the trench width. The earth loads in trench installation shall not exceed those in embankment installation (AASHTO LRFD, 2014), which implies that embankment installation is relatively more critical for design purposes.

RC three-sided culverts (TSCs) with flat top slab are widely used nowadays to provide large hydraulic capacity at sites with limited vertical clearance. TSCs are produced in spans relatively larger than box culverts, reaching up to 16.0 m. Based on field measurements and numerical analyses, McGrath et al. (2002) proposed non-uniform vertical earth pressure distribution on the top slab of large-span RC arch culverts with earth pressure magnitudes lower than that stipulated in the CHBDC (CSA, 2014). In addition, studies on RC box culverts demonstrated the influence of culvert span on the applied vertical earth pressures on the top slab (Bennett et al., 2005; Kang et al., 2008). However, the current design practice does not distinguish between large-span TSCs and relatively small-span box culverts. Therefore, TSCs are designed following the same guidelines stipulated for small-span box culverts.

Limited field and numerical studies on RC TSCs with spans of 7.3 to 10.4 m in Chapter 4 to Chapter 6 suggested VAF = 1.05 for estimating the vertical earth pressure on the top slab of TSCs in the case of B1 standard installation, which is lower than the 1.2 VAF specified in the CHBDC (CSA, 2014). However, the results of these studies are limited to

specific conditions and do not cover the influence of many parameters expected to affect the applied earth loads on TSCs.

Therefore, this chapter presents a detailed numerical study on the influence of backfill height and soil type, installation method and compaction level, as well as the concrete compressive strength on the applied earth pressures and the structural performance of TSCs. The numerical study was conducted employing finite element (FE) models of TSCs validated with full-scale field measurements. VAFs and HAFs were estimated for different cases representing B1 and B2 installations. The estimated values were compared with the CHBDC (CSA, 2014) and AASHTO (AASHTO LRFD, 2014) provisions. Finally, equations are proposed for efficient, yet conservative, estimation of the applied earth pressures on large-span TSCs.

8.2 Culverts Details

The field monitoring program involved three TSCs constructed in the Greater Toronto Area (GTA), Ontario, Canada, to convey creek water through new road embankments. Three culverts, designated Remembrance, Pickering, and Oshawa were constructed using RC precast units supported on RC cast-in-place strip footings. The culverts' construction complied with the CHBDC (CSA, 2014) specifications for B1 standard installation. The culverts were instrumented with vibrating wire pressure cells (PCs) and vibrating wire strain gauges (SGs) to measure the applied contact earth pressures and their structural performance during and after construction completion. The studied TSCs had spans of 7.3, 10.4, and 13.5 m as displayed in **Figure 8-1**. Different installation methods were used in the culverts' construction, i.e., trench, zero-projection, and embankment installations as depicted schematically in **Figure 8-2**. For all three culverts, the sidewalls were secured in the strip footing key using plastic shims then the footing keyway was filled with nonshrink grout. A brief description of the culverts' geometry, subsurface conditions, foundation, and instrumentation details is presented herein.

8.2.1 Remembrance Culvert

The span of the Remembrance culvert was 7.3 m and its total sidewall height was 2.8 m as depicted in **Figure 8-1a**. The subsurface soil consisted of silty clay to clayey silt till with

very stiff to hard consistency below the foundation level (FL). The very stiff till layer extended from the ground surface to 4.0 m below the FL, followed by hard till layer up to 8.0 m below the FL, where the boreholes were terminated. The culvert foundation was 3.6-m-wide × 0.6-m-thick keyed strip footing with a 0.7-m-thick pedestal as shown in **Figure 8-1a**. The footing pedestal allowed placing the footing below frost depth at 1.2 m below FL (OPSD, 2010). The culvert was constructed in a trench with edges sloped at 45° as presented in **Figure 8-2a**, and was backfilled with well-graded sand (SW) compacted to 90-100% Standard Proctor up to a total backfill height of 3.2 m. The average wet unit weight of the backfill material was measured using nuclear density tests to be 23.0 kN/m^3.

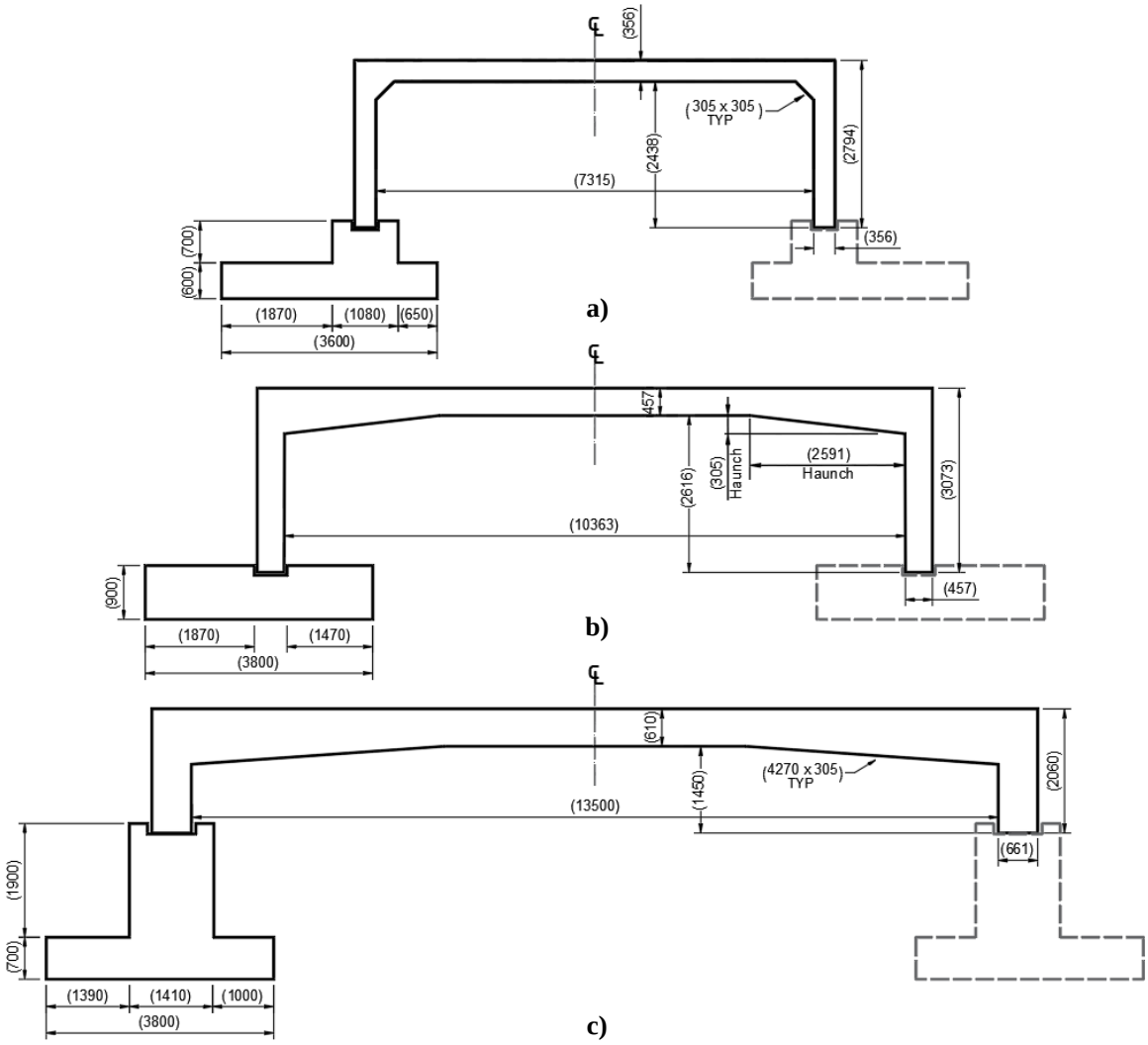

Figure 8-1. Geometry details of the studied TSCs and the supporting strip footings: a) Remembrance culvert; b) Pickering culvert; and c) Oshawa culvert. (All dimensions are in mm)

Remembrance culvert was instrumented along one section with 6 PCs and 14 SGs. Two PCs were distributed on the sidewalls and 4 on the top slab. It was not possible to install PCs underneath the footing of this culvert as they were already constructed at the time of sensors installation. The 14 SGs were installed in pairs on the inner and outer surfaces at 7 cross-sections (3 on the sidewall and 4 on the top slab). Field data of the Remembrance culvert were presented in Chapter 3 to Chapter 5.

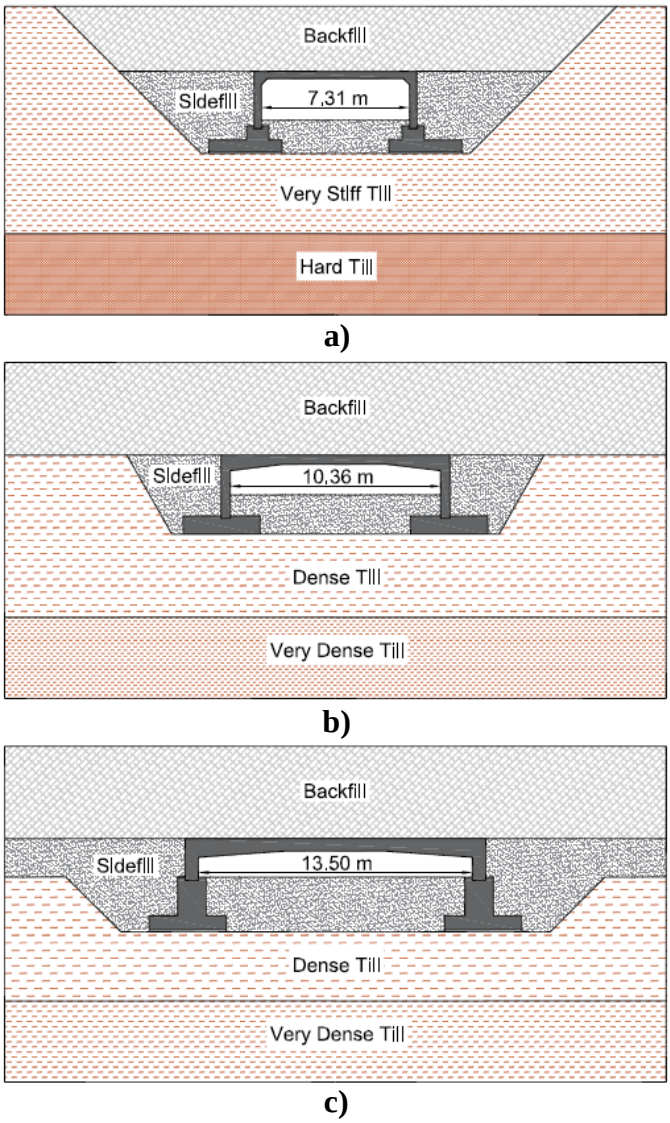

Figure 8-2. Installation method of the instrumented culverts: a) Remembrance culvert; b) Pickering culvert; and c) Oshawa culvert.

8.2.2 Pickering Culvert

Pickering culvert is a 10.4-m-span RC TSC with a total sidefill height of 3.07 m as shown in **Figure 8-1b**. The soil profile at the Pickering culvert site consisted of dense to very dense sandy silt till from the ground surface to the end of boreholes (8.0 m below ground surface). Dense sandy silt till layer extended from the ground surface to 4.0 m below the FL, followed by a 4.0-m-thick very dense till layer. The ground surface was at the same elevation as the culvert top slab, reflecting zero-projection culvert installation as depicted in **Figure 8-2b**. The culvert foundation was 3.8-m-wide × 0.9-m-thick RC strip footing as shown in **Figure 8-1b**. The culvert was backfilled up to 3.1 m on the top slab. The backfill along the culvert sides and up to 0.5 m on top of the culvert was SW compacted to 92% Standard Proctor, while sandy silt (ML) compacted to 96% Standard Proctor was used for the remainder of the embankment. Nuclear density tests conducted on the backfill indicated an average wet unit weight of 22.0 kN/m^3.

Pickering culvert was instrumented along one section with 11 PCs and 18 SGs. Three PCs were installed underneath the footing, 3 on the sidewall and 5 on the top slab. The SGs were installed in pairs at 9 cross-sections on the inner and outer surfaces (3 on the sidewall and 6 on the top slab). Field data of the Pickering culvert to the final backfill height were presented in Chapter 6.

8.2.3 Oshawa Culvert

Oshawa culvert had the largest span (13.5 m) and shortest sidewall height (2.06 m) among the monitored TSCs. The subsurface soil at the Oshawa culvert site consisted of silty sand and sandy silt tills up to 8.0 m below the ground surface. Dense silty sand till layer extended from the ground surface to the FL, followed by very dense till layer. The culvert foundation was 3.8-m-wide × 0.7-m-thick cast-in-place strip footing with a 1.9-m-thick pedestal as depicted in **Figure 8-1c**. The frost depth at the construction site was 1.2 m (OPSD, 2010). **Figure 8-2c** shows that the natural ground surface was almost at the same elevation as the footing pedestal crest, reflecting embankment installation. The culvert was backfilled with SW compacted to 90-95% Standard Proctor with an average unit weight of 20.0 kN/m^3 as per the nuclear density measurements.

Oshawa culvert was instrumented with 13 PCs and 24 SGs. Three PCs were installed underneath the footing, 2 on the footing pedestal, 1 on the sidewall, and 7 distributed on the top slab. The SGs were installed in pairs at 12 cross-sections along the inner and outer surfaces of the footing pedestal and precast culvert unit. Field data of the Oshawa culvert to 3.0 m of backfill were presented in Chapter 7.

The instrumentation plans were established based on the results of preliminary FEAs as discussed in Chapter 3. All the sensors were installed following the manufacturer's recommendation. They all survived the construction activities and are functioning properly to date, except for one PC on the top slab of the Oshawa culvert.

8.3 Validated Numerical Models

Two-dimensional (2D) nonlinear plane-strain FE models were developed for the three culverts using DIANA 10.1 (2016) FE software. The same modeling approach was followed for the three culverts as detailed in Chapter 4 and Chapter 6. The numerical model results for the three culverts showed good fit with the entire set of field measurements. The model features of the Oshawa culvert are presented herein as an example, and all assigned input parameters of the validated models are summarized in **Table 8-4** to **Table 8-6**.

The 2D FE model of the Oshawa culvert consisted of four main parts: native soil, backfill soil, strip footing, and culvert body as displayed in **Figure 8-3**. The native soil was divided into a dense till layer from the natural ground surface to the FL and a very dense till layer extending 8.9 m below the FL. Backfill was simulated up to the final backfill height (3.8 m). The sidefill and backfill materials were divided into layers with a predominant thickness of 0.5 m. Each backfill layer was introduced in a separate construction phase to account for the incremental nature of the backfilling process. The bottom boundary of the model was fixed in both vertical and horizontal directions, while the side boundaries were restrained in the horizontal direction only. Based on a sensitivity analysis, the model width was extended almost 11 times the culvert span to eliminate any influence of the model boundaries on the results. The native soil, backfill soil, and strip footing parts were discretized using 8-node plane-strain elements. The culvert body was discretized using 8-node plane-stress elements to account for the transversal joints between the installed

precast units (Pimentel et al., 2009). The steel reinforcement of the culvert was simulated using embedded bar elements, fully bonded to the surrounding concrete. **Figure 8-3** shows the model mesh, which was refined around the buried structure to ensure accuracy.

The native till layers were simulated as elastic-perfectly plastic material using the Mohr-Coulomb model. The assigned material properties were correlated to the measured SPT N-values. The hyperbolic Duncan-Chang material model (Duncan and Chang, 1970) was used to simulate the nonlinear behavior of the backfill soil and to consider the stiffness stress-dependency. The Duncan-Chang material properties used for the backfill soil were based on Boscardin et al. (1990) measurements for SW compacted to 90% Standard Proctor (SW90), as it had a comparable grain size distribution of that tested by Boscardin et al. (1990).

The RC strip footing was simulated using the linear-elastic material model, while the nonlinear behavior of the culvert concrete and crack formation were considered using the total strain-based smeared crack model with the fixed crack model formulation (Rots and Blaauwendraad, 1989). In the smeared crack model, the Thorenfeldt model (Thorenfeldt et al., 1987) was used for the strain-softening behavior under compressive loading, and the Hordijk model (Hordijk, 1991) was to simulate tensile loading condition. The linear elastic and smeared crack model parameters for the strip footing and culvert body, respectively, were correlated to the average 28-day compressive strength (f_c') following the guidelines of fib Model Code 2010 (*fib*, 2013). The culvert steel reinforcement was simulated using the von Mises plasticity model with no hardening behavior. It should be noted that Young's modulus, E = 200 GPa was used in the validated models of the three culverts. Yield stress, f_y = 450 MPa was used in the Remembrance and Pickering culvert models, while f_y = 400 MPa was used in the Oshawa culvert model.

Table 8-4. Mohr-Coulomb input parameters for the native soils in the three culvert models.

Model	Layer	ν	Cohesion c (kPa)	Friction angle ϕ (°)	E_s (MPa)	γ (kN/m^3)
Remembrance	Very stiff till	0.35	10	35	43.0	22.0
	Hard till	0.35	30	37	90.0	22.0
Pickering	Dense till	0.35	0	38	40.0	22.0
	Very dense till	0.35	0	42	160.0	22.0
Oshawa	Dense till	0.35	0	38	36.0	22.0
	Very dense till	0.35	0	45	166.0	22.0

Table 8-5. Duncan-Chang input parameters for the backfill materials in the three culvert models.

Backfill soil	ν	c (kPa)	ϕ (°)	Modulus No. K	Failure ratio R_f	Modulus exponent N
SW90	0.30	0	42	640	0.75	0.43
ML95*	0.35	28	34	440	0.95	0.40

* Only used in Pickering culvert model.

Table 8-6. Material input parameters for the RC materials in the three culvert models.

Model	Material model	f_c' (MPa)	Young's modulus E_c (GPa)	Tensile strength f_{ct} (MPa)	Fracture energy G_f (Nmm/mm^2)
Remembrance	Smeared crack	57.0	40.1	5.9	0.2020
Pickering	Smeared crack	65.0	41.7	6.4	0.2332
Oshawa	Smeared crack	65.0	41.7	6.4	0.2332
All*	Linear elastic	40.0	29.7	-	-

* Material input parameters for the RC strip footing in all models.

The interfaces at the culvert-footing, soil-footing, and soil-culvert contacts were simulated using line interface elements. The definition of these interfaces is essential to realistically simulate the soil-structure interaction behavior. The displacement across the interface is controlled by the defined normal and tangential stiffnesses, D_{nn} and D_{tt}, respectively, which were estimated by (TNO DIANA BV, 2016):

$$D_{tt} = \frac{A^2}{t}\frac{E_s}{2(1+\nu)} \quad ; \quad D_{nn} = f \times D_{tt} \qquad \textbf{(8-3)}$$

where A is a reduction factor (0.67 in this study), f is a multiplication factor (50 in this study), t is the virtual interface thickness (10 mm in this study), for soil-footing and soil-culvert interfaces, E_s is soil Young's modulus, and for the culvert-footing interface, E_s is the elastic modulus of the non-shrink grout used to fill the voids between footing keyway and culvert sidewall (f_c'= 30 MPa), and ν is the soil Poisson's ratio for soil-footing and soil-culvert interfaces, and that of grout in the culvert-footing interface.

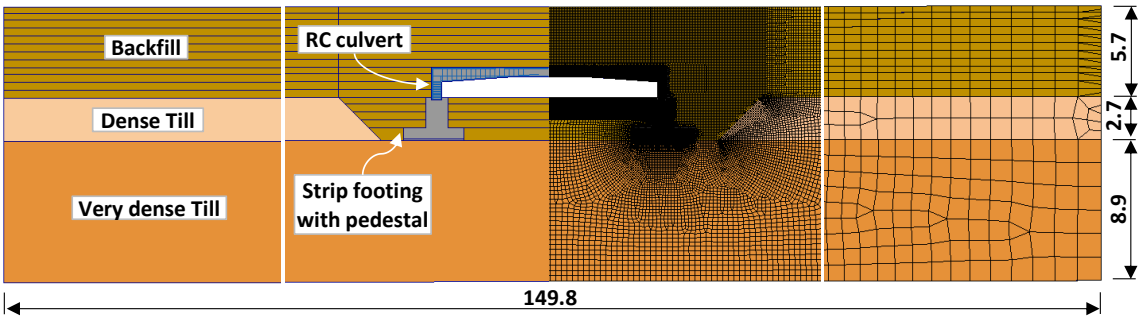

Figure 8-3. Geometry and meshing details of the Oshawa culvert 2D FE model. (All dimensions are in m)

Figure 8-4 displays the VAF distribution along the top slab for the three TSCs established based on field measurements and the 2D FE models at different backfill heights (H). The measured and calculated vertical earth pressures on the top slab are in excellent agreement. **Figure 8-4** also displays the VAF stipulated in the CHBDC (CSA, 2014) for B1 installation (VAF = 1.2). The results suggest that the CHBDC (CSA, 2014) overestimates the vertical earth loads on the top slab of all three TSCs, which gives impetus to establishing more realistic VAFs to be used in design of TSCs.

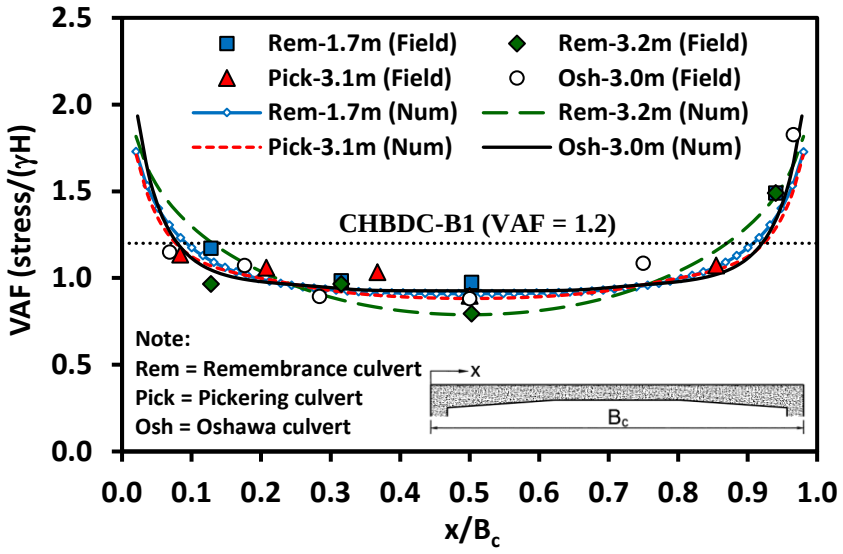

Figure 8-4. Comparison between the VAF distribution along the TSCs spans from field measurements and validated numerical models at different backfill heights.

8.4 Parametric Study Details

The effects of four main design parameters on the structural performance of TSCs and the applied earth pressures on their sidewalls and top slabs were investigated employing 62 FE models. The considered parameters were the backfill height and soil type, the installation method and compaction level, as well as the compressive strength of the RC culvert units.

The validated TSCs models were modified by extending the backfill height (H) to 16.0 m on the top slab, and the maximum backfill height at which failure might occur (H_{max}) was determined. The estimated earth pressures on the culvert body are only reported for backfill heights lower than H_{max}. For the three TSC models, f_c' = 60 MPa for the RC culvert and yield stress of 400 MPa for the steel reinforcement were assumed. Both the sidefill and backfill on the top slab were assumed to be SW90 with total unit weight, γ_s kN/m^3.

Embankment and trench installations were simulated for each of the TSCs in addition to the actual installation method to examine the influence of installation method. For the Remembrance culvert, the actual installation method was the trench installation. Thus, only the embankment installation was analyzed additionally. Embankment installation in this parametric study represents the case when the natural ground surface is at the FL. Therefore, the actual installation method of the Oshawa culvert, in which the natural

ground surface was at the elevation of the footing pedestal crest, did not fully represent embankment installation. Thus, embankment and trench installations were analyzed additionally.

The CHBDC (CSA, 2014) allows the use of two backfill soil types (SW and ML) as sidefill in B1 standard installation and three backfill soil types (SL, ML, and CL) in B2 standard installation with different compaction requirements as illustrated in **Table 8-2**. The three backfill soil types are allowed to be used as the backfill material on top of the culvert in both standard installations. Boscardin et al. (1990) conducted a series of triaxial tests on SW, ML, and CL soils, typically used as backfill materials for buried structures. The soils were tested at different densities, representing a wide range of compaction levels. Based on the tests data, Boscardin et al. (1990) reported the Duncan-Chang (DC) input parameters for the different backfill soils at different compaction levels.

To investigate the influence of backfill soil type and compaction level, the three soil types (SW, ML, and CL) were considered at different compaction levels to represent B1 and B2 standard installations as well as other installation scenarios. Different compaction levels were considered for SW and ML soils which represent the case of compacted backfill, moderately compacted backfill, and dumped backfill with no compaction. The CHBDC (CSA, 2014) does not allow using CL soil as a sidefill material in B1 standard installation, while CL95 can be used in B2 standard installation. Thus, CL95 (B2 standard installation) and CL50 (dumped backfill soil) were analyzed. The soils input parameters summarized in **Table 8-7** were adopted from ACPA (1993), which are based on the work done by Boscardin et al. (1990).

The RC culvert compressive strength (f_c') was 60 MPa in all above cases. The models representing B1 and B2 standard installations were replicated with f_c' = 40 MPa to examine the influence of f_c' on the TSCs structural performance. **Table 8-8** summarizes the assigned input parameters for the considered concrete compressive strengths.

Table 8-7. Input parameters of the considered backfill soils. (After ACPA, 1993)

Soil type	Compaction level	γ (kN/m^3)	ν	c (kPa)	ϕ (°)	K	R_f	N	K_o*
SW	SW90	21.0	0.30	0	42	640	0.75	0.43	1.1
	SW80	19.0	0.30	0	36	320	0.83	0.35	0.8
	SW65	15.0	0.25	0	29	54	0.90	0.85	0.5
ML	ML95	20.0	0.30	28	34	440	0.95	0.40	1.2
	ML85	18.0	0.30	21	30	110	0.85	0.25	0.8
	ML50	11.0	0.25	0	23	16	0.55	0.95	0.5
CL	CL95	19.0	0.30	62	15	120	1.00	0.45	0.8
	CL50	10.0	0.25	0	23	16	0.75	0.95	0.3

* At-rest earth pressure coefficient

Table 8-8. Input parameters of the considered RC culvert compressive strengths.

Material model	f_c' (MPa)	Young's modulus E_c (GPa)	Tensile strength f_{ct} (MPa)	Fracture energy G_f (Nmm/mm^2)
Smeared crack	60.0	40.7	6.11	0.2219
	40.0	36.3	4.66	0.1739

8.5 Results and Discussion

8.5.1 Effect of Backfill Height

The validated models of the three TSCs were modified to investigate the influence of backfill height for the same actual installation method. The analyses considered SW90 as the sidefill and backfill soil, concrete strength, f_c' = 60 MPa, and steel yield strength, f_y = 400 MPa. **Figure 8-5** presents the load-deflection curve at the midspan of top slab for different backfill heights (H) (H is used as proxy for load). The three culverts exhibited linear behavior at shallow backfill heights until cracks developed, at which point the load-deflection curve changed slope as marked on the load-deflection curves. The load-deflection continued almost linearly beyond the point of crack development up to the maximum backfill height at failure (H_{max}). Failure was manifested by significant increase in the midspan deflection with minimal increase in the backfill height, indicated ductile

failure. The comparison of load-deflection curves presented in **Figure 8-5** demonstrates that as expected, the midspan deflection increased and the backfill height at which cracks developed decreased as the TSC span increased due to the corresponding significant increase in bending moment.

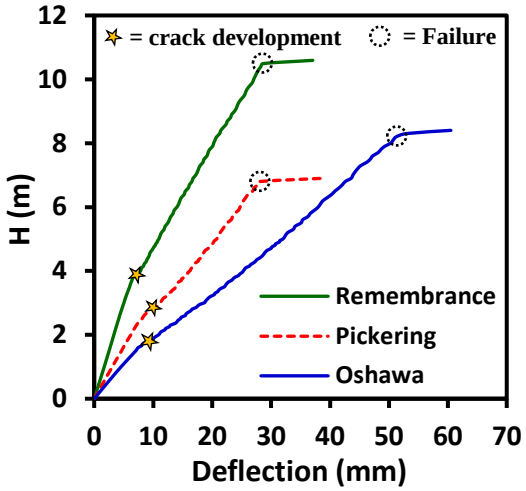

Figure 8-5. Midspan deflection of the TSCs at different backfill heights to failure.

Figure 8-6 displays the deformed shapes and crack patterns at H_{max}. The culverts experienced slight inward lateral deflection of the sidewalls' top corner (i.e., away from sidefill). The sidewalls of the Remembrance and Pickering culverts exhibited larger flexural deflection, while the short sidewalls of the Oshawa culvert rotated as a rigid body inside the footing keyway. **Figure 8-6** also shows that the culverts' footings moved laterally outward. The rotation of the Oshawa culvert sidewalls increased the vertical deflection at the midspan and the lateral displacement of its footing (due to additional loads induced by sidewall rotation at the keyway contact surfaces). Furthermore, the strip footings rotated under the applied earth loads; the Remembrance culvert footing rotated towards the waterside, while the Pickering and Oshawa culvert footings rotated towards the sidefill side.

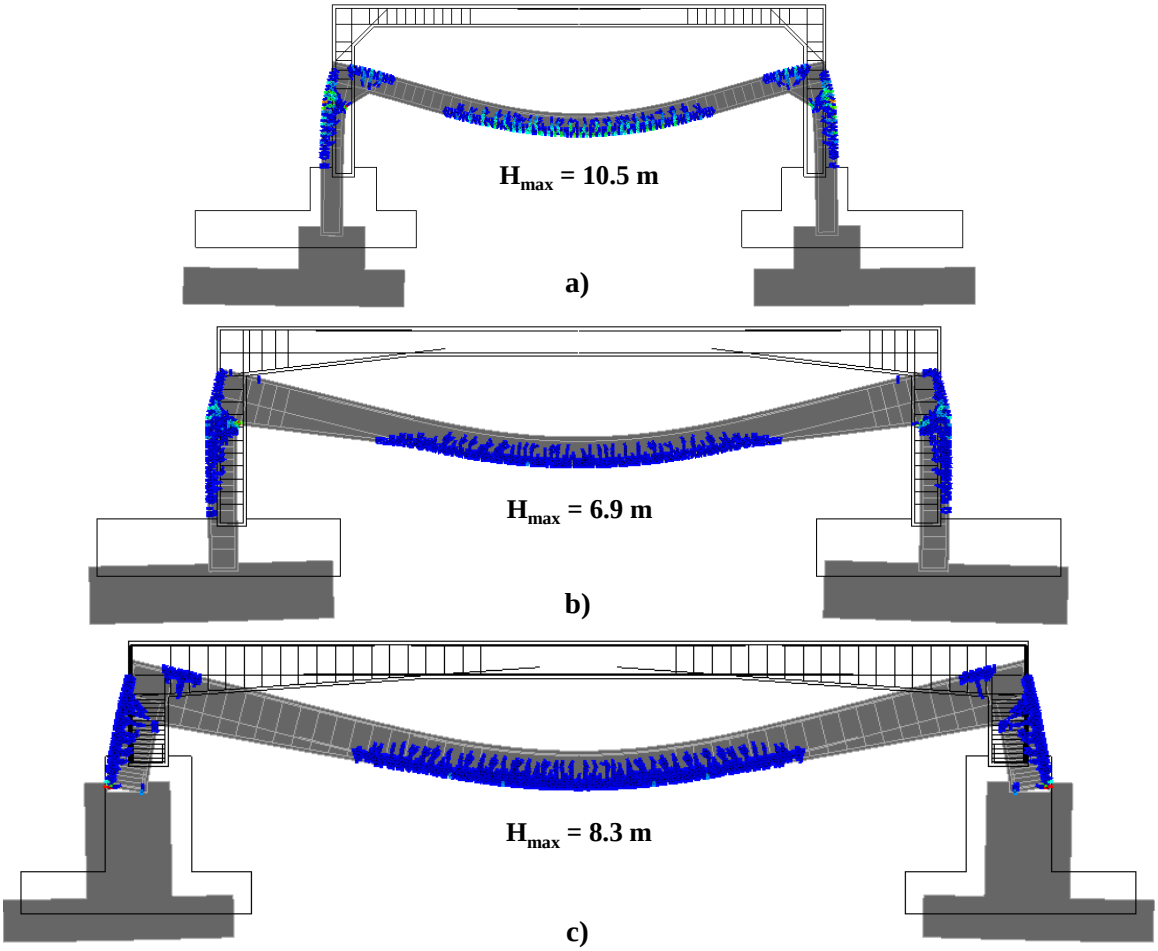

Figure 8-6. Deformed shape and crack pattern at failure: a) Remembrance culvert; b) Pickering culvert; and c) Oshawa culvert. (Magnification × 25)

Figure 8-7 displays the locations of yielding in the steel reinforcement, which indicated the formation of plastic hinges at the top corners of the sidewalls of the Remembrance and Pickering culverts and at the midspan of the Oshawa culvert. The different failure mechanism of the Oshawa culvert is attributed to its large span and short sidewall. In addition, local yield points were observed at the sidewall base of the Oshawa culvert due to the induced stresses at the keyway contact surfaces caused by sidewall rotation.

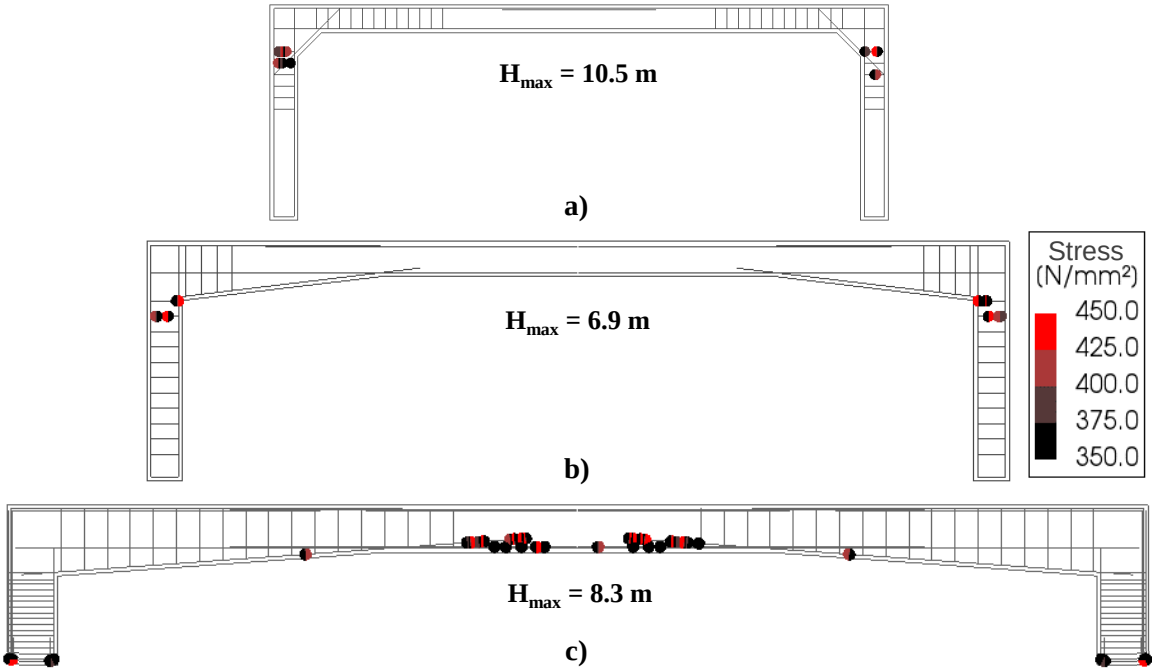

Figure 8-7. Reinforcement yield points at failure: a) Remembrance culvert; b) Pickering culvert; and c) Oshawa culvert.

Figure 8-8 presents the calculated vertical earth pressures on the culverts top slab and lateral earth pressures on their sidewalls and footing pedestals at different backfill heights. The results clearly demonstrate non-uniform vertical earth pressure distribution on the top slab with high pressure at the edges and low pressure at the midspan, and this non-uniformity increased as backfill height increased. **Figure 8-8** also shows that the lateral earth pressure on the sidewall upper part is almost null due to its inward lateral deflection away from the sidefill. The lateral earth pressure distributions on the Remembrance and Pickering culvert sidewalls were parabolic and linear with depth on the Oshawa culvert sidewall. Moreover, the rotation of the Oshawa culvert sidewall towards the sidefill at the base resulted in higher lateral earth pressures at its sidewall base compared to the other culverts. The Remembrance culvert footing (and pedestal) experienced some rotation at H_{max} (as indicated in **Figure 8-6a**), which caused higher lateral earth pressure on the pedestal crest as shown in **Figure 8-8a**. The Oshawa culvert footing rotated even more, causing higher pressure at the pedestal top and lower lateral earth pressure at the bottom as shown in **Figure 8-8c**.

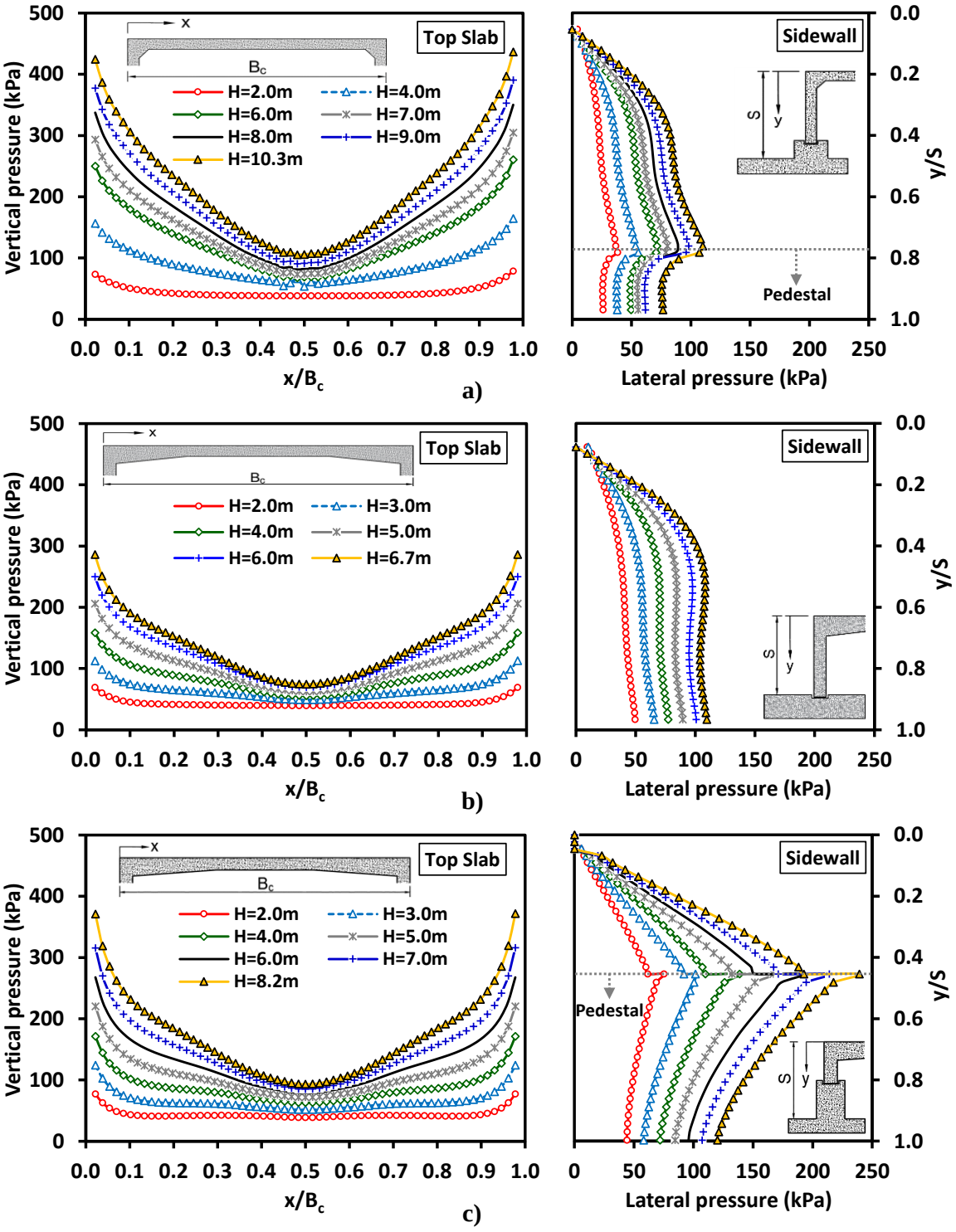

Figure 8-8. Earth pressure distribution on the top slab and sidewall at different backfill heights: a) Remembrance culvert; b) Pickering culvert; and c) Oshawa culvert.

8.5.2 Effect of Installation method

The CHBDC (CSA, 2014) does not distinguish between embankment and trench installations, unlike the AASHTO specifications (AASHTO LRFD, 2014). Alternatively, the CHBDC (CSA, 2014) specifies B1 and B2 standard installations to account for the soil type and compaction level of the sidefill material. This study aims to investigate the influence of the installation method on the structural performance and applied earth pressures on TSCs at different backfill heights considering B1 and B2 installations. Accordingly, embankment and trench installations were simulated for the studied culverts besides the actual installation method considering B1 installation, where the sidefill and backfill materials were assumed SW90. For B2 installation, the actual installations were excluded, and only embankment and trench installations were simulated. The sidefill and backfill materials were assumed SW80 in B2 installation. The models' notation scheme incorporated, in the following order: installation method, soil type, compaction level of the sidefill, and compaction level of the backfill. For instance, Tren (SW90-90) represents the case of trench installation with SW soil compacted to 90% in the sidefill and 90% in the backfill.

Figure 8-9 displays the load-deflection curves for all installation methods considered for the Remembrance, Pickering, and Oshawa culverts. For the same compaction level, the load-deflection curves showed slight to no influence of the installation method, either actual, embankment, or trench. The installation method did not influence the point of crack development or the predicted ductile failure mode. For the Remembrance and Pickering culverts, trench installation showed trivial increase in the predicted H_{max}. In general, the installation method did not influence the structural performance of the subject TSCs within the considered range of earth loads. In contrast, the compaction level appeared to have a significant influence, which will be discussed later in detail.

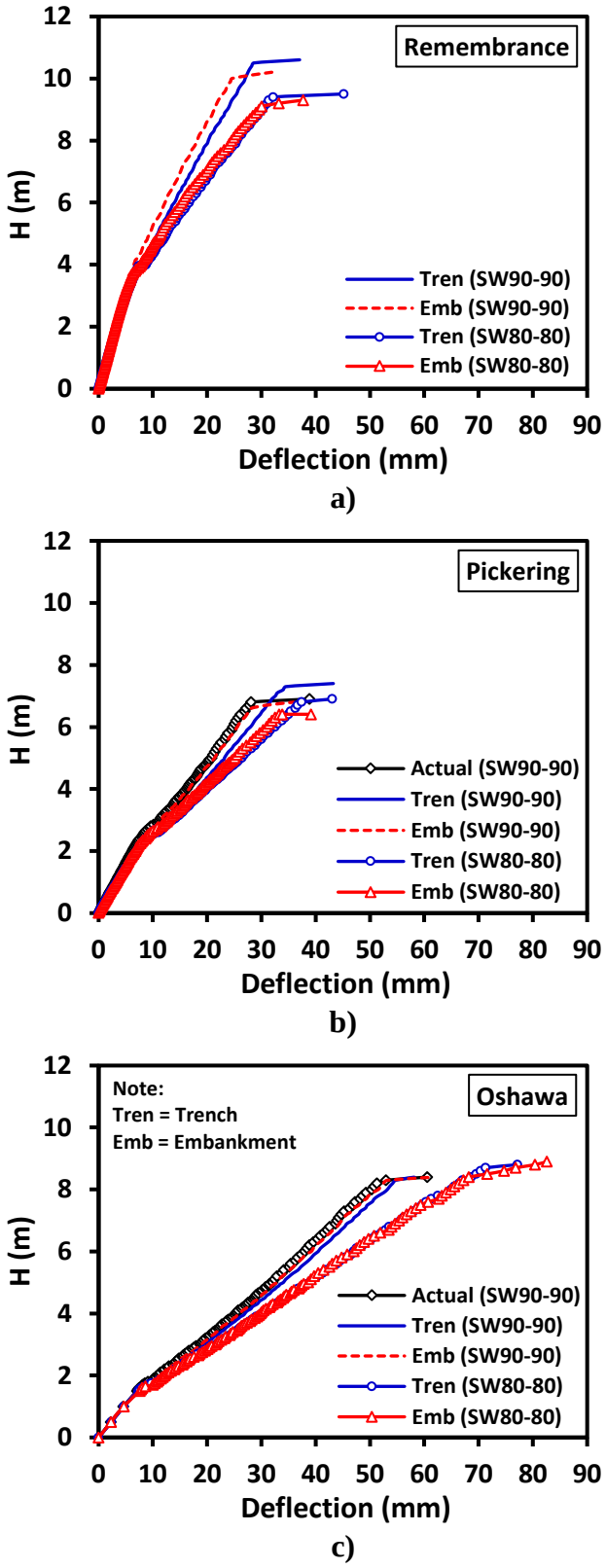

Figure 8-9. Effect of installation method on the midspan deflection at different backfill heights: a) Remembrance culvert; b) Pickering culvert; and c) Oshawa culvert.

Figure 8-10 presents the average VAFs at different backfill heights for the considered installation methods. No noticeable difference between the estimated VAFs except for the case of SW80-80 in Remembrance and Oshawa culverts, where the VAFs showed an increasing trend with backfill heights over 6.0 m in embankment installation as opposed to the decreasing trend observed in trench installation. Thus, the results agree with the CHBDC (CSA, 2014) provision in terms of not distinguishing between embankment and trench installations when estimating the vertical earth pressure on the top slab RC culverts. Yet, embankment installation is considered more critical since it yielded slightly higher VAFs than the trench installation method in some cases, which complies with the AASHTO (AASHTO LRFD, 2014) specifications previously described.

Figure 8-11 compares the estimated lateral earth pressures along the culverts' sidewalls and footing pedestals for the different installation methods at a backfill height of 6.0 m. The results indicate slightly higher lateral earth pressures in embankment installation, especially for the case of SW90-90 in Remembrance and Pickering culverts as shown in **Figure 8-11a** and **b**. The effect of installation method is less obvious in Oshawa culvert as demonstrated in **Figure 8-11c**. Overall, the comparisons provided in **Figure 8-10** and **Figure 8-11** suggest slightly higher earth pressures on TSCs in embankment installation compared to trench installation. Therefore, embankment installation is deemed the critical installation method and was considered in the following investigations.

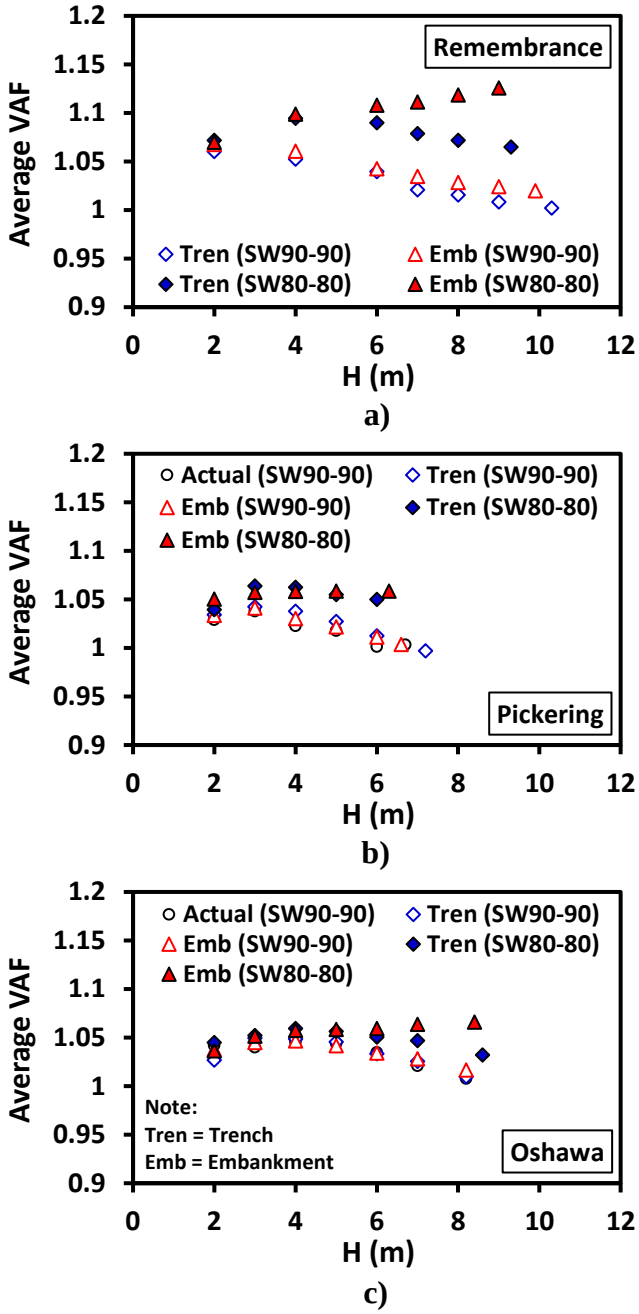

Figure 8-10. Effect of installation method on the average VAF at different backfill heights: a) Remembrance culvert; b) Pickering culvert; and c) Oshawa culvert.

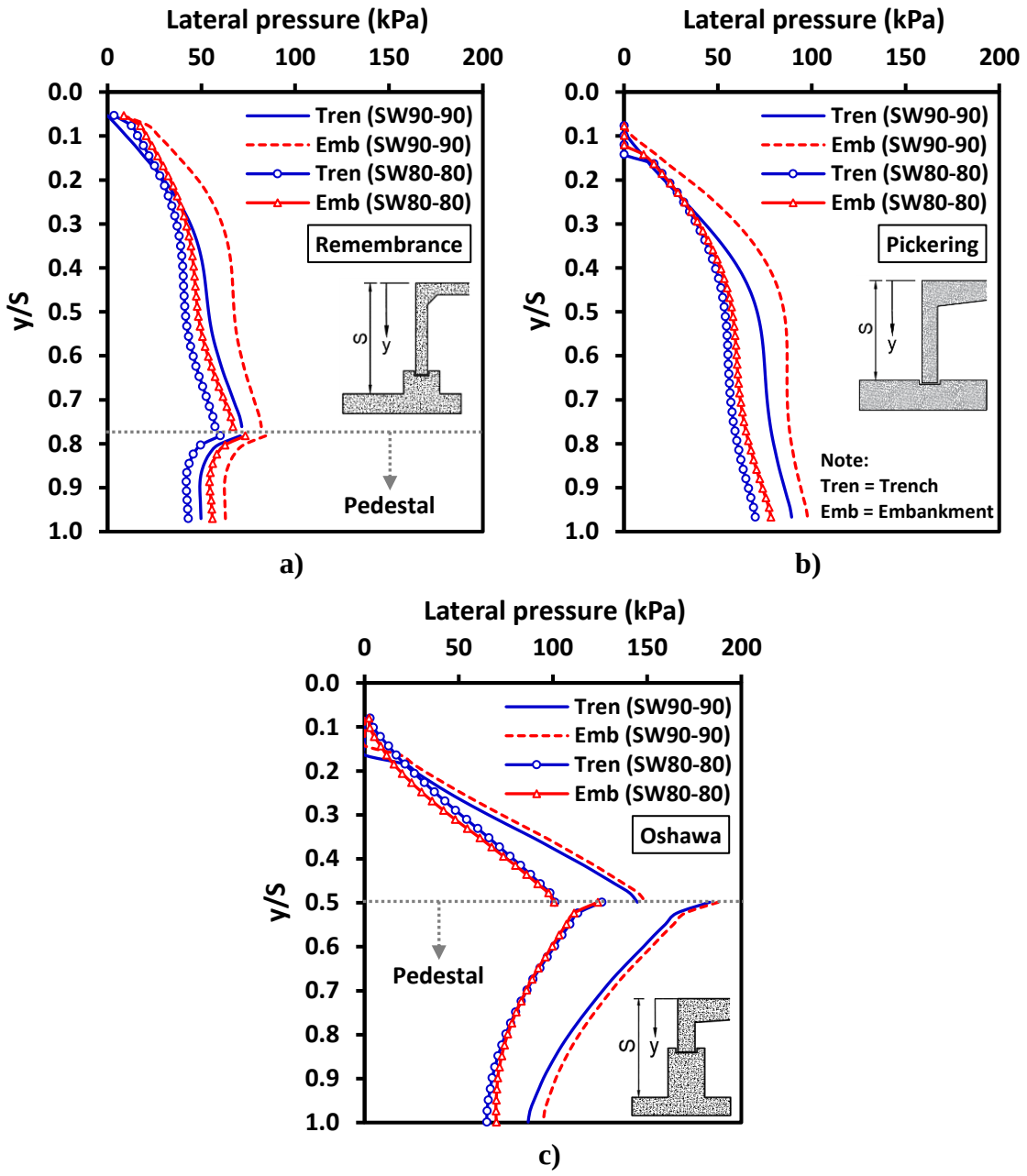

Figure 8-11. Effect of installation method on the lateral earth pressure at H = 6.0 m: a) Remembrance culvert; b) Pickering culvert; and c) Oshawa culvert.

8.5.3 Effect of Backfill Soil Type and Compaction Level

Table 8-9 provides a summary of the considered soil types for backfill and sidefill and their compaction levels, as well as the notation used for the numerical models. The material parameters of considered backfill soil types with different compaction levels are listed in **Table 8-7**. The analysis was conducted for the three culverts, which cover the practical

range of TSC span used in practice. The same soil type was assumed for the sidefill and backfill in each scenario while varying the compaction level to simulate B1 and B2 installations, as well as other installation conditions as described in **Table 8-9**.

Table 8-9. Summary of the considered soil types and compaction level scenarios.

Soil type	Model notation	Sidefill soil	Backfill soil	Installation condition
SW	SW90-90	SW90	SW90	B1 installation
	SW80-80	SW80	SW80	B2 installation
	SW90-80	SW90	SW80	Other
	SW80-90	SW80	SW90	Other
	SW65-65	SW65	SW65	Dumped soil
ML	ML95-95	ML95	ML95	B1 installation
	ML85-85	ML85	ML85	B2 installation
	ML95-85	ML95	ML85	Other
	ML85-95	ML85	ML95	Other
	ML50-50	ML50	ML50	Dumped soil
CL	CL95-95	CL95	CL95	B2 installation
	CL95-50	CL95	CL50	Other
	CL50-50	CL50	CL50	Dumped soil

The load-deflection curves for the considered SW, ML, and CL scenarios are presented in **Figure 8-12**. The load-deflection curves are presented in terms of the free-field stress (γH) to account for the difference in the backfill soil unit weight with the compaction level as summarized in **Table 8-7**. The results revealed that compacted sidefill (e.g., SW90-90) reduced the midspan deflection compared to less compacted sidefill (e.g., SW80-80 and SW65-65) due to the higher confinement to the buried structure. Reduction in γH_{max} of the Remembrance culvert was observed when comparing the cases of B1 installation with B2 installation. For example, γH_{max} of the Remembrance culvert for B1 (SW90-90) and B2 (SW80-80) installations was 212.1 kPa and 172.9 kPa; and 196.0 kPa for ML95-95 and 158.4 kPa for ML85-85, reflecting an approximate reduction of 19% in the culvert capacity. All the scenarios representing dumped soils exhibited the most flexible behavior and least capacity compared to the other scenarios as depicted in **Figure 8-12**. For example,

Figure 8-12b shows that the Oshawa culvert for ML50-50 exhibited the highest deflection and least γH_{max} (145.2 kPa). Thus, dumped soils should not be used in TSC construction.

Figure 8-13 presents the deformed shapes, crack patterns, and yield points in the steel reinforcement of the Oshawa culvert at failure for selected scenarios (ML95-95, ML85-95, and ML50-50). The deformed shape and crack pattern were the same regardless of the compaction level of the sidefill; however, its effect on the footing response was significant. **Figure 8-13a** shows that for ML95-95, the footing displaced laterally and the pedestal rotated into the sidefill. On the other hand, the lateral displacement increased but the rotation decreased for ML85-95, as shown in **Figure 8-13b,** compared to ML95-95. The increased footing displacement resulted in higher rotation of the sidewall, which increased the midspan vertical deflection as displayed in **Figure 8-13b**. For dumped sidefill and backfill soils (ML50-50), the lateral footing displacement increased significantly as shown in **Figure 8-13c** due to the low stiffness and confinement of sidefill. The increased displacement caused increasing sidewall rotation, which resulted in large midspan deflection of the top slab. Meanwhile, the footing rotation was minimal. Thus, low compaction of sidefill increases the footing lateral displacement but decreases its rotation.

Figure 8-13 shows that the sidefill soil compaction level had no influence on the predicted failure location. In all cases, the yield points are concentrated at the midspan, which indicates the formation of plastic hinges and flexural failure of the Oshawa culvert at the midspan. In addition, local yield points occurred at the sidewall base due to the rotation of the sidewall in the footing keyway.

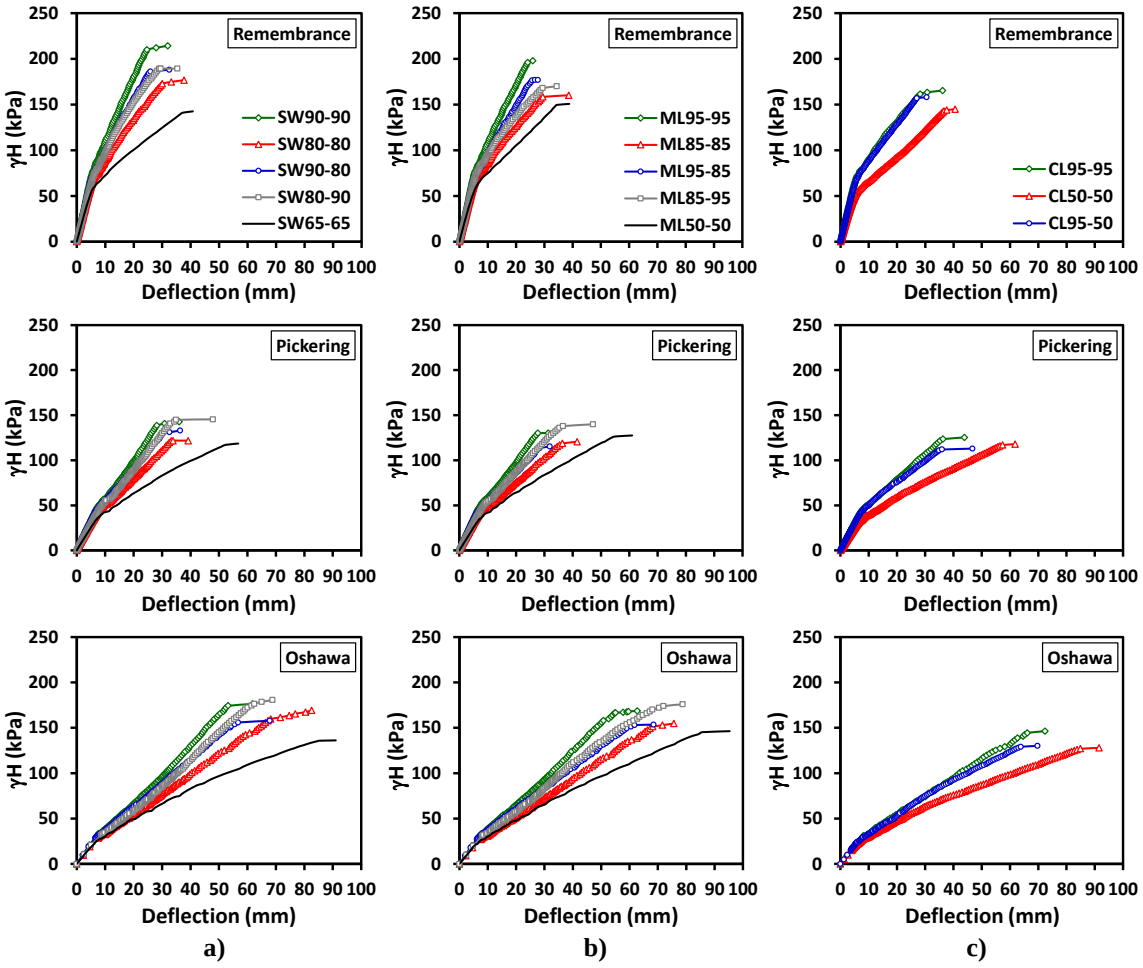

Figure 8-12. Effect of compaction level of different backfill soils on the midspan deflection at different backfill heights: a) SW soil; b) ML soil; and c) CL soil.

Figure 8-14 displays the effect of compaction level on the vertical earth pressure on the top slab of the Oshawa culvert at a backfill height of 6.0 m. In all cases, the vertical earth pressure distribution was non-uniform, i.e., high pressures at the edges and low pressures at the midspan. **Figure 8-14a** and **b** indicate that for moderately compacted sidefill and compacted backfill (SW80-90 and ML85-95), the difference between the vertical earth pressure magnitudes at the edges and midspan was larger than that for compacted sidefill and moderately compacted backfill, e.g., SW90-80 and ML95-85. **Figure 8-14c** shows that the pressure distribution was almost uniform for compacted silty clay sidefill and dumped silty clay backfill (CL95-50). Finally, as expected, the vertical earth pressures were the lowest for dumped soil case due to its low unit weight.

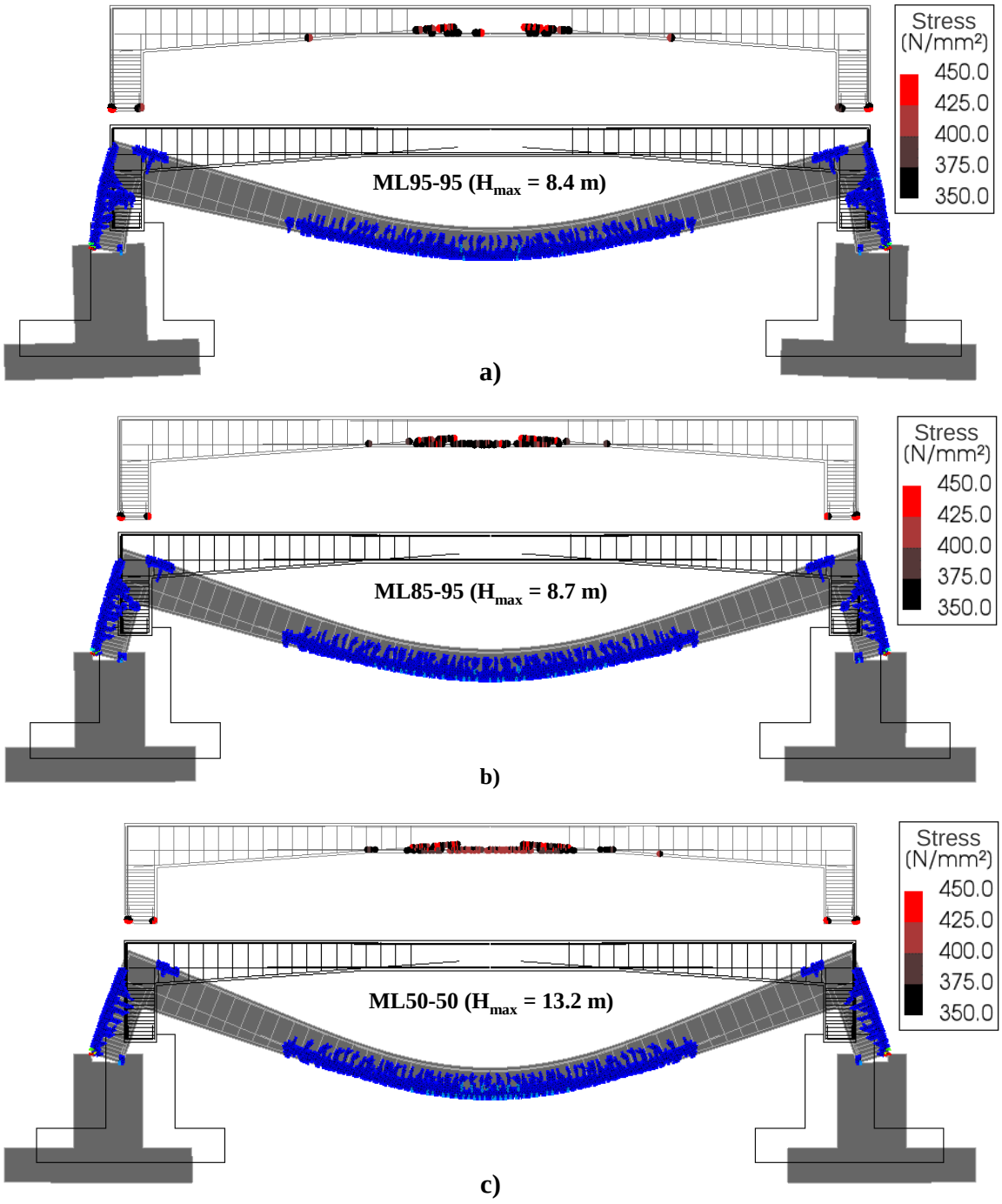

Figure 8-13. Effect of compaction level of ML backfill soils on the reinforcement yield points, deformed shape, and crack pattern of the Oshawa culvert at failure: a) ML95-95; b) ML85-95; and c) ML50-50. (Magnification × 25)

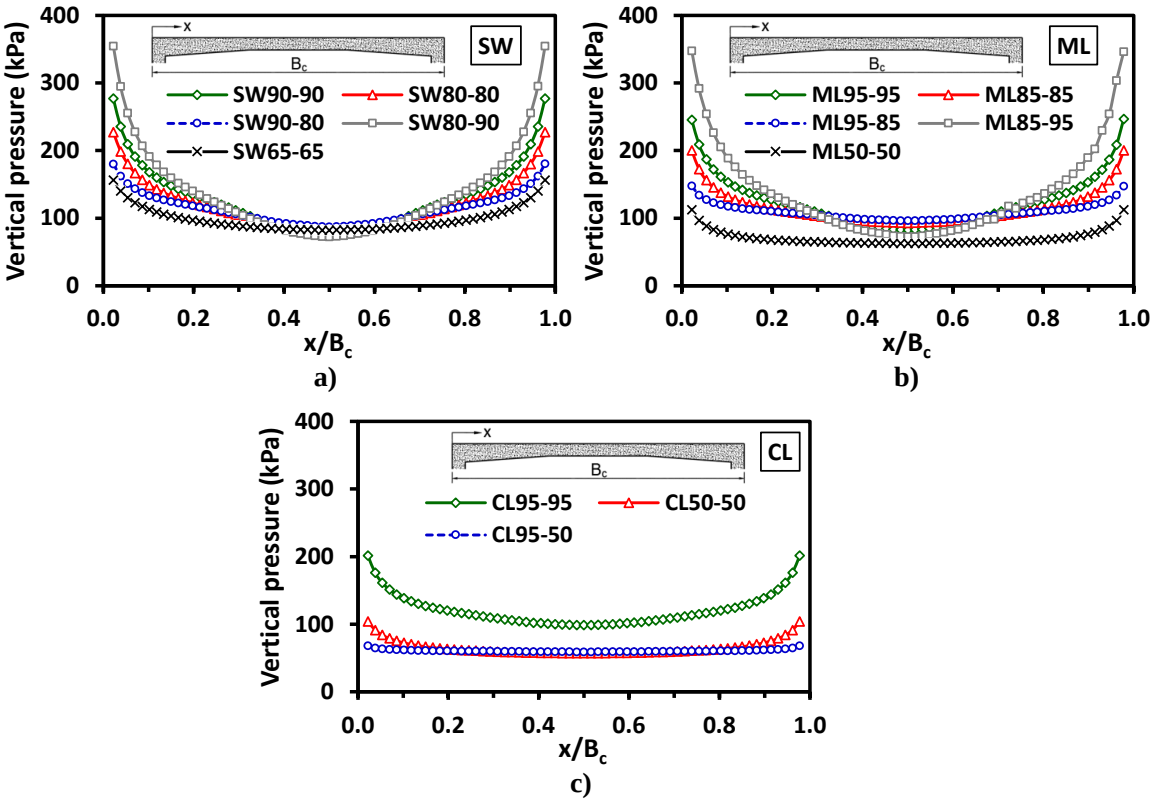

Figure 8-14. Effect of backfill soil compaction level on the vertical earth pressure distribution on the top slab of the Oshawa culvert at H = 6.0 m: a) SW soil; b) ML soil; and c) CL soil.

Figure 8-15 compares the estimated average VAFs for the different compaction scenarios at different backfill heights. The results reveal that B2 installation resulted in higher VAFs than B1 installation for backfill height, H > 4.0 m, but VAFs were comparable for H < 4.0 m. The compacted sidefill and less compacted backfill (e.g., SW90-80, ML95-85, and CL95-50) yielded the lowest VAFs. For SW soils, the dumped sidefill and backfill soils (SW65-65) resulted in high VAFs. For ML soils, moderately compacted sidefill and compacted sidefill (ML80-95) resulted in the highest VAF, which was 1.38 for the Remembrance culvert at H = 8.3 m. Therefore, it is recommended that the sidefill compaction level should be at least the same as the backfill on the top slab. **Figure 8-15** also suggest that the effect of compaction level on the estimated VAF is more pronounced for small-span TSC.

Furthermore, **Figure 8-15** demonstrates that VAF for B1 installation decreased slightly for H > 4.0 m; however, VAF for B2 installations increased as H increased. Meanwhile, VAF

for compacted sidefill and moderately compacted backfill (SW90-80, ML95-85, and CL95-50) was almost constant, near a value of 1.0 for the different backfill heights. It can be concluded that low compaction of the sidefill increases the difference in stiffness between the buried TSC and the surrounding soil. Thus, the passive soil arching effect increases, and more earth load is attracted to the culvert body and vice versa.

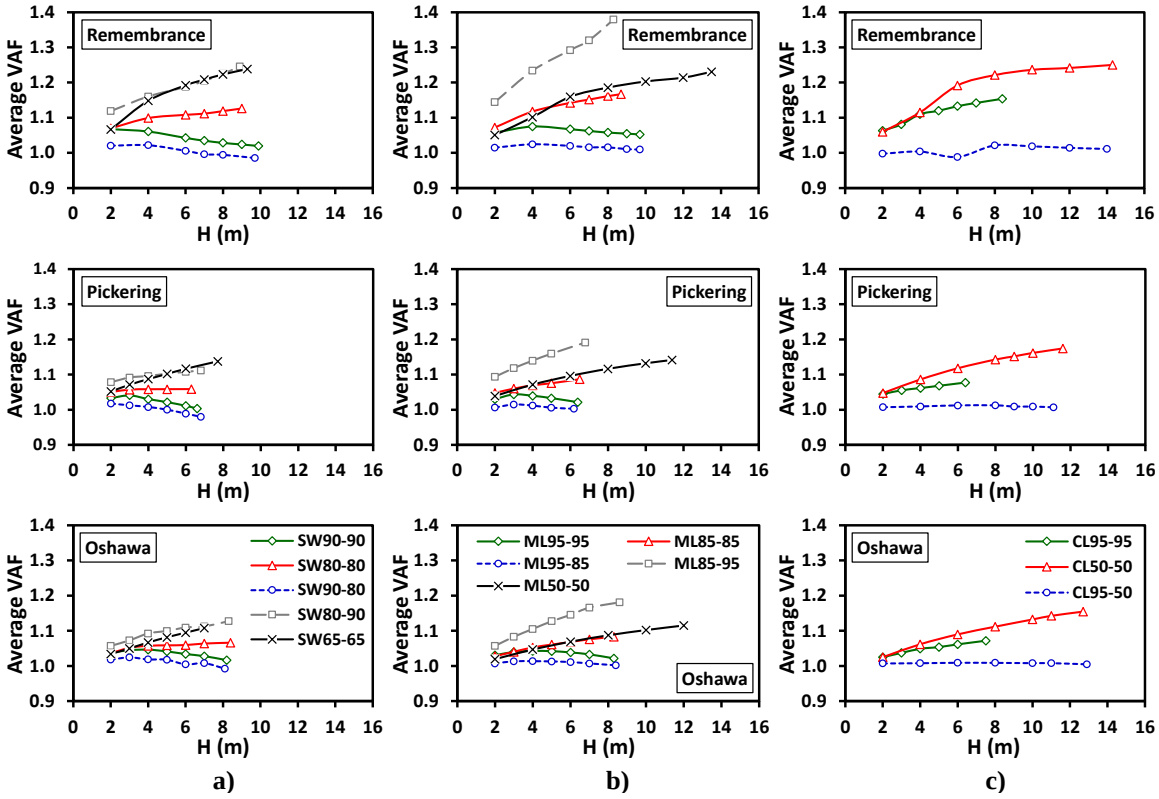

Figure 8-15. Effect of compaction level of different backfill soils on the VAF at different backfill heights: a) SW soil; b) ML soil; and c) CL soil.

Figure 8-16 to **Figure 8-18** presents the lateral earth pressure on the culverts' sidewalls and footing pedestals at H = 6.0 m considering different soil types at different compaction levels. As expected, the lateral earth pressure increased as the compaction level increased, and the pressure was highest for the Oshawa culvert due to rotation of its sidewall and footing. **Figure 8-16c** shows that the lateral earth pressure on the footing pedestal decreased linearly with depth for compacted and moderately compacted sidefill, while it remained almost uniform for dumped soil (SW65-65). It is also noted that the distribution of lateral earth pressure for the case of footing with no pedestal (Pickering culvert) is

different from that when pedestal existed, especially tall pedestals (Oshawa culvert). The high lateral earth pressure on the pedestal must be considered in its structural design.

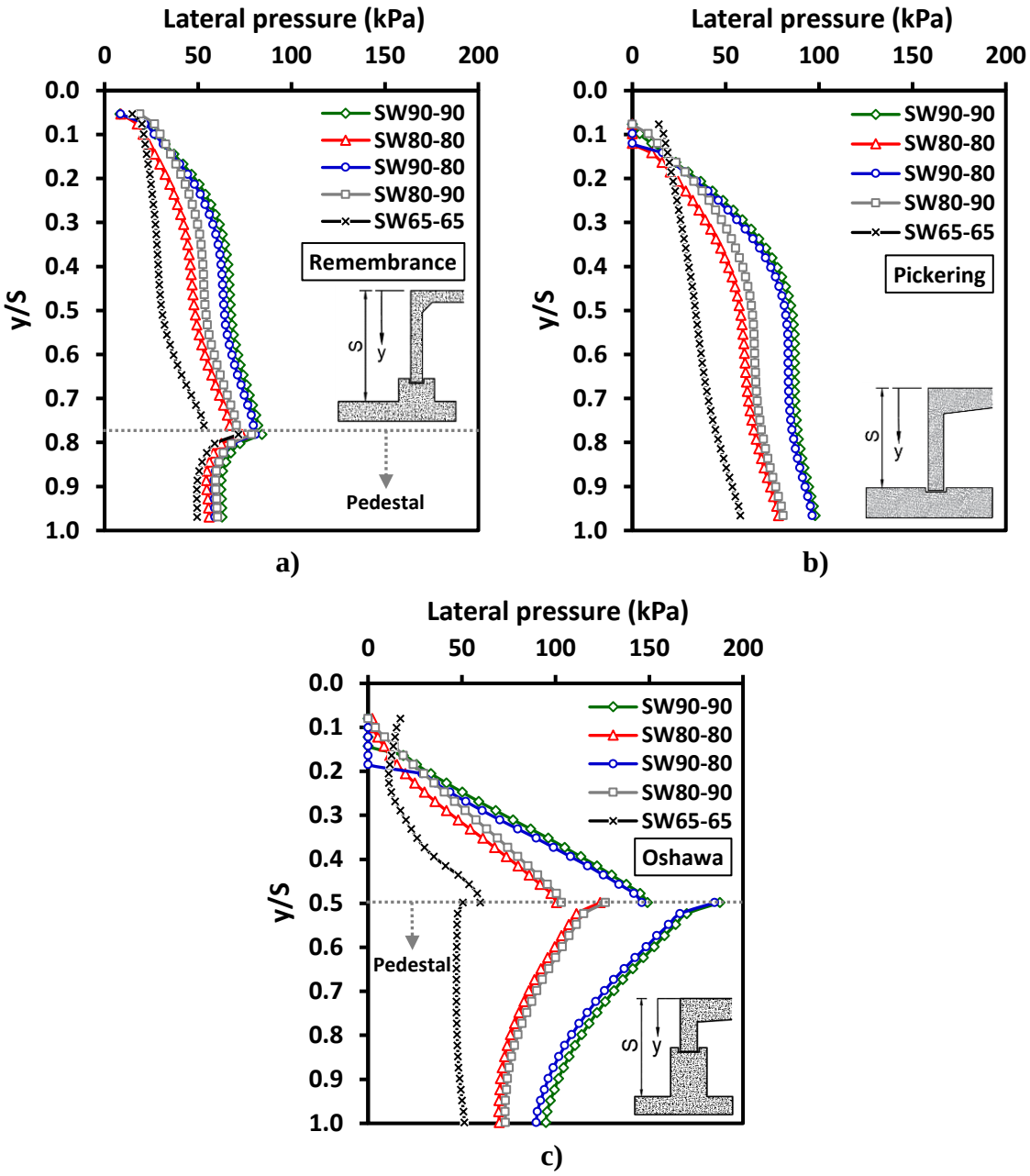

Figure 8-16. Effect of compaction level of SW backfill soils on the lateral earth pressure at H = 6.0 m: a) Remembrance culvert; b) Pickering culvert; and c) Oshawa culvert.

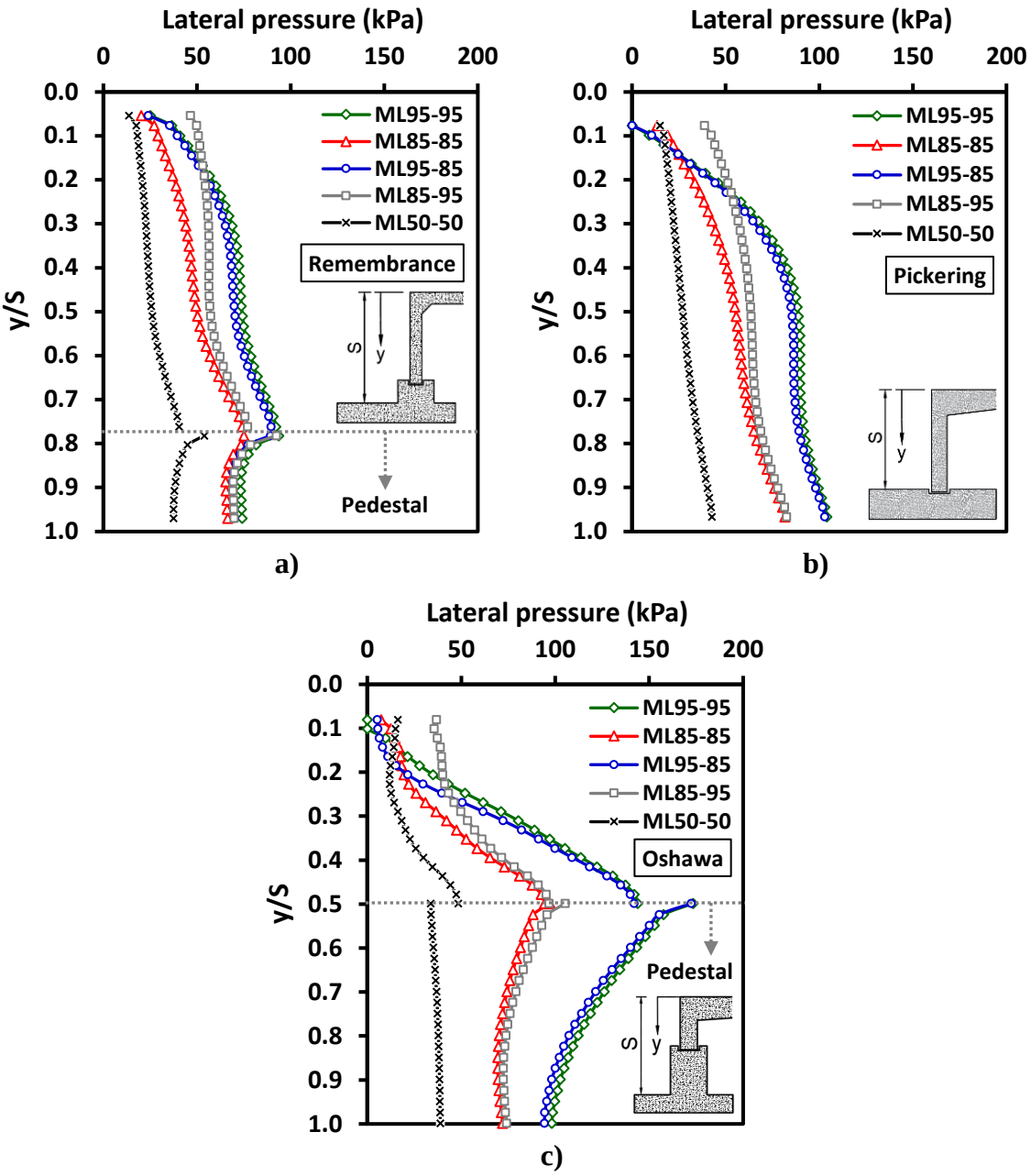

Figure 8-17. Effect of compaction level of ML backfill soils on the lateral earth pressure at H = 6.0 m: a) Remembrance culvert; b) Pickering culvert; and c) Oshawa culvert.

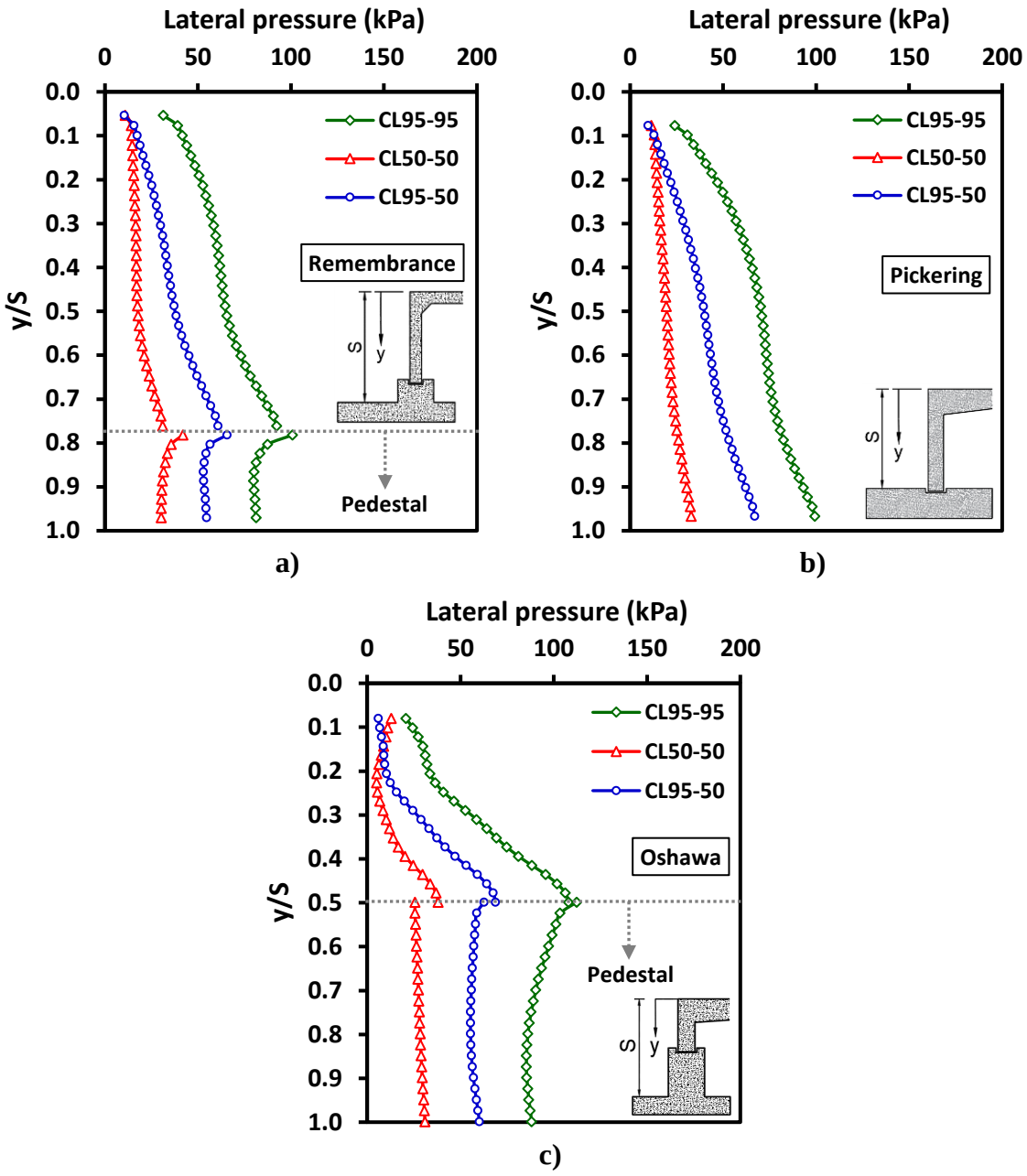

Figure 8-18. Effect of compaction level of CL backfill soils on the lateral earth pressure at H = 6.0 m: a) Remembrance culvert; b) Pickering culvert; and c) Oshawa culvert.

8.5.4 Effect of Concrete Compressive Strength

The compressive strength of precast RC culvert units, f_c' = 60 MPa, was considered in all previous analyses. The effect of concrete strength on the performance of TSCs is investigated by analyzing the response of the same models for the three culverts considering B1 and B2 standard installations and f_c' = 40 MPa.

Figure 8-19 compares the load-deflection curves for the culverts with f_c' = 40 and 60 MPa. The results indicate minor effect on the culverts response. However, cracks developed at shallower backfill heights for f_c' = 40 MPa, due to the corresponding reduction in the concrete tensile strength and fracture energy (G_F) **Figure 8-19** also indicates that f_c' has a profound effect on the maximum backfill height at failure (H_{max}), which decreased significantly (22% to 36% reduction) as f_c' decreased from 60 MPa to 40 MPa as demonstrated in **Table 8-10**. Hence, the compressive strength of the RC culvert would govern its ultimate capacity when considering the soil-culvert-interaction effect. However, the failure mode was ductile and failure location remained the same for both values of f_c'. The applied earth pressures on the top slab and the sidewalls were not influenced by the values of f_c'.

Table 8-10. Summary of the effect of the RC culvert compressive strength on the predicted H_{max}.

Culvert	Model	Installation condition	H_{max} (m)		Reduction in H_{max} (%)
			f_c' = 60 MPa	f_c' = 40 MPa	
Remembrance	SW90-90	B1 installation	10.1	7.4	26.7
	ML95-95		9.8	7.2	26.5
	SW80-80	B2 installation	9.1	6.9	24.2
	ML85-85		8.8	6.9	21.6
	CL95-95		8.5	6.4	24.7
Pickering	SW90-90	B1 installation	6.7	4.3	35.8
	ML95-95		6.5	4.3	33.8
	SW80-80	B2 installation	6.4	4.8	25.0
	ML85-85		6.6	4.8	27.3
	CL95-95		6.5	4.3	33.8
Oshawa	SW90-90	B1 installation	8.3	6.3	24.1
	ML95-95		8.4	6.2	26.2
	SW80-80	B2 installation	8.5	5.5	35.3
	ML85-85		8.4	5.5	34.5
	CL95-95		7.6	4.9	35.5

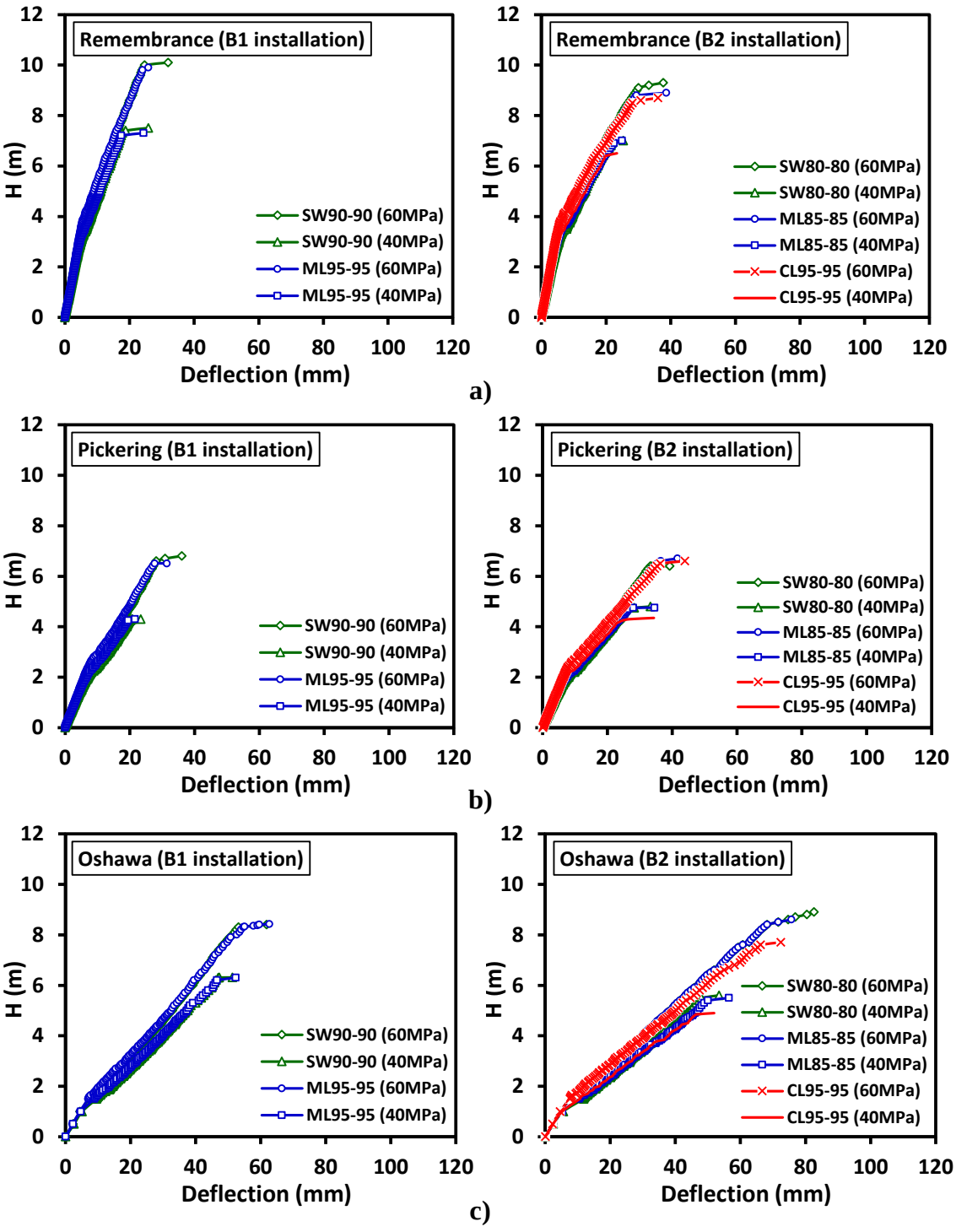

Figure 8-19. Effect of concrete compressive strength on the midspan deflection at different backfill heights considering B1 and B2 standard installation cases: a) Remembrance culvert; b) Pickering culvert; and c) Oshawa culvert.

8.6 Proposed Design Guidelines

This section presents design guidelines for TSCs established based on the results of the parametric study. Earth loads (i.e., VAF and HAF) are proposed for the design of TSCs based on the results obtained considering embankment installation method and culvert concrete strength, f_c' = 60 MPa. Moreover, midspan deflection limits are proposed for serviceability limit states based on the results considering both B1 and B2 standard installations and culvert concrete strength, f_c' = 40 and 60 MPa. To generalize the findings from the parametric study considering the range of culvert span, the results are presented in terms of the backfill height to culvert width ratio (H/B_c).

Figure 8-20 compares the calculated average VAFs for the B1 and B2 standard installations at different backfill heights with the provisions of CHBDC (CSA, 2014) and AASHTO (AASHTO LRFD, 2014). For B1 installation, **Figure 8-20a** demonstrates that VAF = 1.2 stipulated in the CHBDC (CSA, 2014) is overly conservative and consistently exceeded the calculated (and also measured) VAFs for all cases. On the other hand, the AASHTO (AASHTO LRFD, 2014) equation for embankment installation underestimated VAF at small $H/B_c \leq 0.25$ and overestimated the VAF at $H/B_c > 0.75$. Accordingly, the AASHTO equation is modified to ensure safe VAF values within the considered range of H/B_c (0 – 1.25) that represents the TSCs manufactured and used in current practice (i.e., up to 16.0-m-span), i.e.:

$$VAF\ (\text{B1 installation}) = \text{Minimum of}\begin{pmatrix} 1.0 + 0.4\dfrac{H}{B_c} \\ 1.1 \end{pmatrix} \qquad \textbf{(8-4)}$$

Figure 8-20a shows that the estimated VAFs from the proposed **Equation (8-4)** for B1 installation covered all the considered cases and yielded VAFs lower than the provisions of CHBDC (CSA, 2014) within the considered range of H/B_c.

Figure 8-20b compares the estimated VAFs from the numerical models with the codes' values for B2 installation. The results indicate that the provision of CHBDC (CSA, 2014) is conservative by specifying the 1.35 VAF, especially at H/B_c values below 0.5. On the contrary, the AASHTO equation yielded VAFs lower than the estimated values in some

cases below H/B_c of 0.5. Therefore, the AASHTO equation is modified to ensure safe VAF values for all the considered cases, i.e.:

$$VAF\ (\text{B2 installation}) = \begin{pmatrix} 1.0 + 0.4\dfrac{H}{B_c}, & \text{for } 0 < \dfrac{H}{B_c} \leq 0.25 \\ 1.06 + 0.16\dfrac{H}{B_c}, & \text{for } 0.25 < \dfrac{H}{B_c} \leq 1.25 \end{pmatrix} \quad \textbf{(8-5)}$$

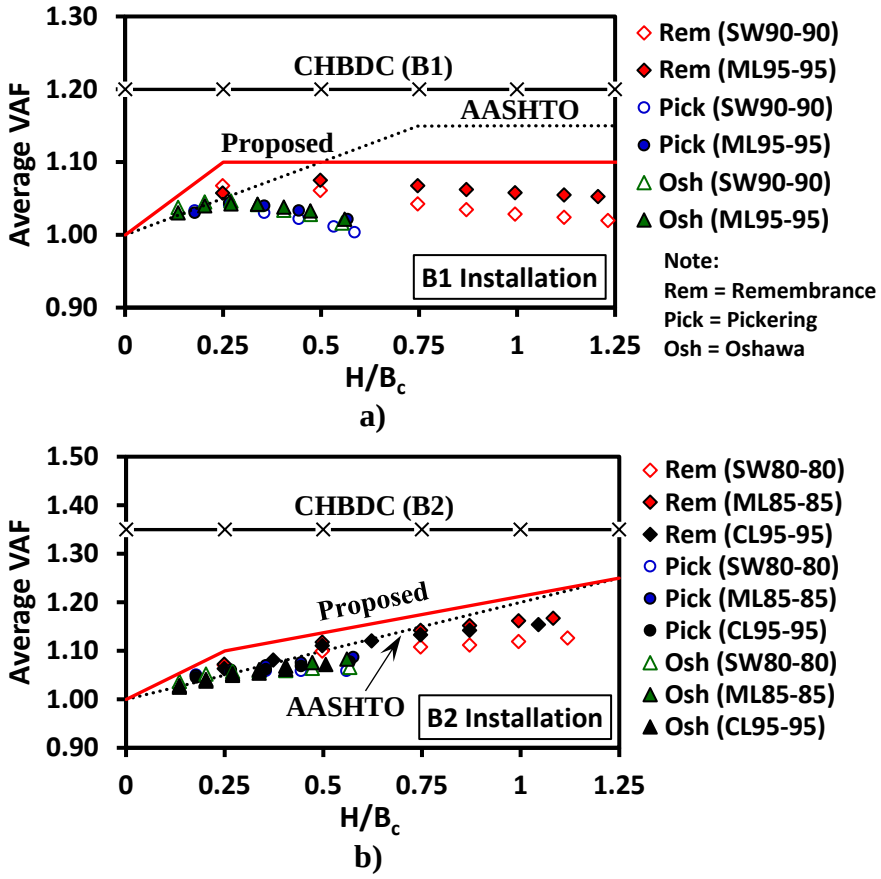

Figure 8-20. Comparison between the estimated average VAFs and the code values for the standard installations: a) B1 installation; and b) B2 installation.

To estimate the lateral earth pressure on the culvert sidewalls, the CHBDC (CSA, 2014) specifies minimum and maximum values of HAF = 0.3 and 0.5 for B1 installation, and 0.25 and 0.5 for B2 installation. **Figure 8-21** compares the distribution of the calculated HAF along the Pickering culvert sidewall at a backfill height of 6.0 m. **Figure 8-21a** shows that for B1 installation, HAF at the top quarter of the sidewall is lower than the code-specified minimum value (0.3). For SW90-90, the calculated HAFs reach 0.5 at the sidewall mid-height then remains almost constant to the sidewall base. Similar distribution

is obtained for ML95-95 with higher HAFs (due to higher at-rest earth pressure coefficient for ML95 compared to SW90). For B2 installation, **Figure 8-21b** indicates that the calculated HAFs for SW80 and ML85 lie within the code bounds, but HAFs for CL95-95 exceed the maximum value specified by CHBDC.

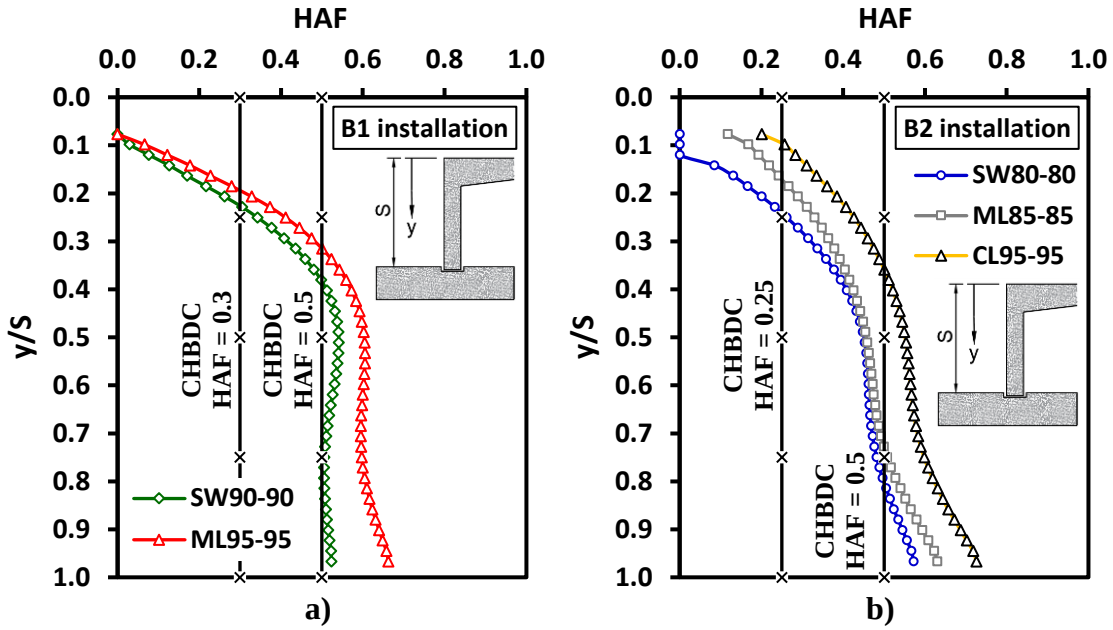

Figure 8-21. HAF distribution along the Pickering culvert sidewall at H = 6.0 m: a) B1 installation; and b) B2 installation.

Figure 8-21 demonstrates that the distribution of lateral earth pressure on the sidewalls of TSCs generally lies within the minimum and maximum values specified by the CHBDC (CSA, 2014). Thus, the average of the HAFs along the sidewall was estimated to determine an average HAF for each case. It should be noted that the average is obtained for HAF on the sidewalls only (i.e., not including lateral earth pressure on the pedestal). **Figure 8-22** compares the estimated HAFs for all cases with the CHDC (CSA, 2014) bounds at different backfill heights. In general, **Figure 8-22** demonstrates that the HAF values stipulated in the CHBDC (CSA, 2014) are adequate to estimate the lateral earth pressures applied on the sidewalls of TSCs. **Figure 8-22a** shows that for B1 installation, most of the estimated HAFs fell within the code bounds except for slightly higher HAFs in a few cases when ML95 was used as the sidefill and backfill materials. **Figure 8-22b** shows that all the estimated HAFs fell within the code bounds.

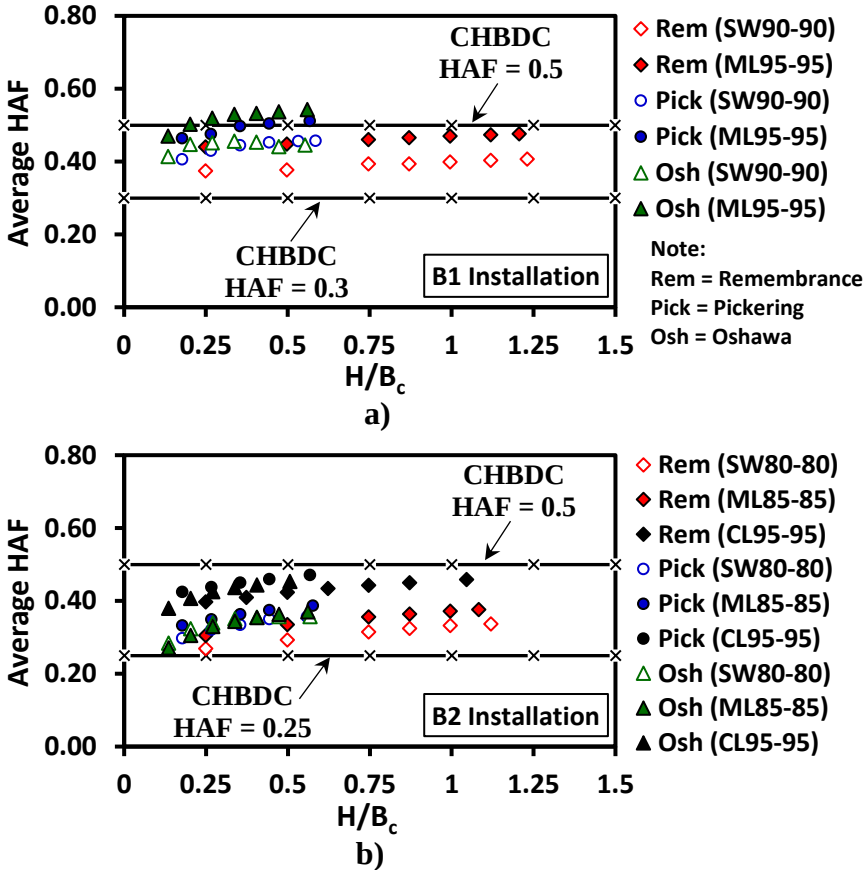

Figure 8-22. Comparison between the estimated average HAFs and the CHBDC (CSA, 2014) values for the standard installations: a) B1 installation; and b) B2 installation.

For serviceability limit states, the CHBDC (CSA, 2014) specifies limits on the crack width of non-prestressed RC structures depending on the exposure type. A maximum crack width of 0.25 mm is specified for structures exposed to de-icing chemicals, spray or surface runoff containing de-icing chemicals, marine spray, swamp, marsh, salt water, and aggressive backfill. A maximum crack width of 0.35 mm is specified for all other environmental exposures (CSA, 2014). The midspan vertical deflections (Δ) corresponding to the two maximum crack widths (0.25 and 0.35 mm) were determined from the nonlinear numerical models for B1 and B2 installations for both f_c' = 40 and 60 MPa. **Figure 8-23** presents the calculated culvert span to deflection ratios (S/Δ) for all cases analyzed. The results indicate that the estimated S/Δ values fall within a specific range for each crack width for all cases of B1 and B2 installations and f_c' = 40 and 60 MPa.

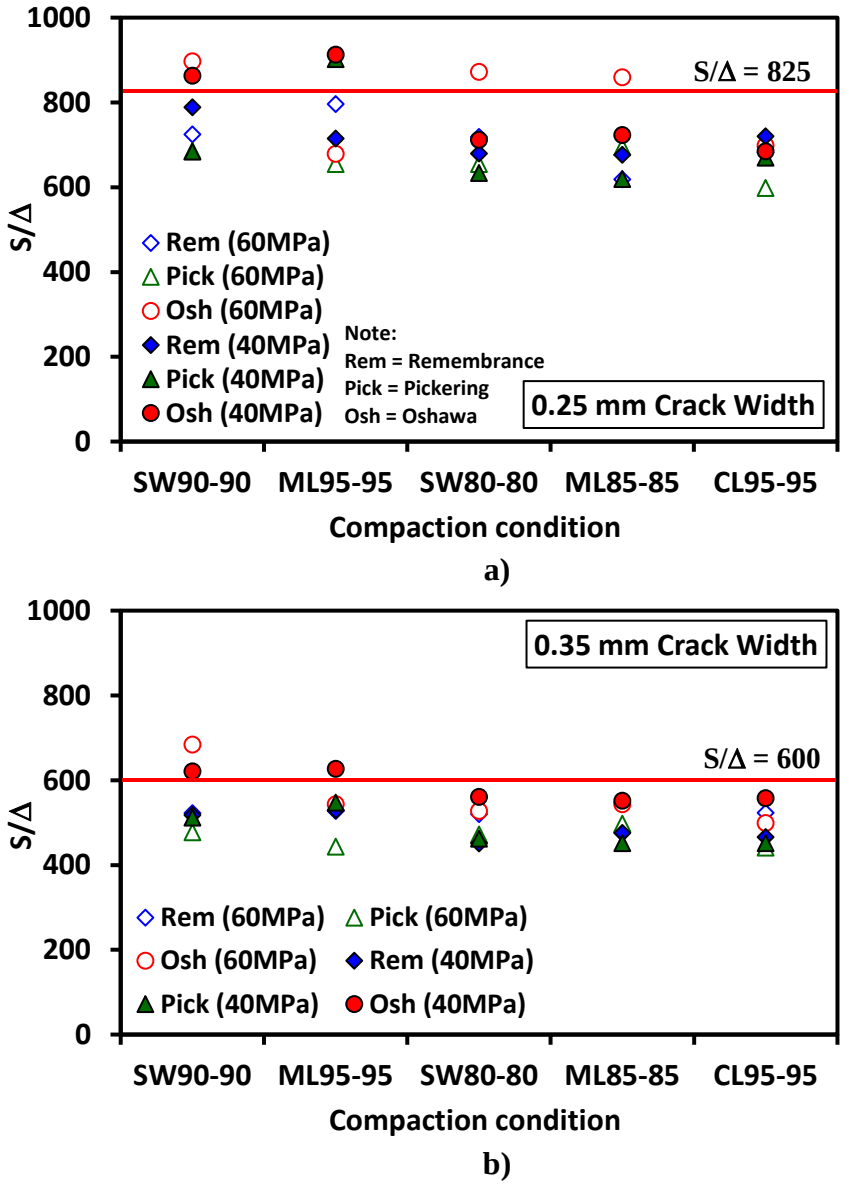

Figure 8-23. Span-deflection ratios at the allowable crack widths for the cases of B1 and B2 standard installations: a) 0.25 mm crack width; and b) 0.35 mm crack width.

Figure 8-21 displays a box-whisker plot of the dataset presented in **Figure 8-20** to better visualize its statistical variability (Tukey, 1977). Each box-whisker plot summarizes the maximum and minimum values, the median, the 1st quartile (Q_1 = 25th percentile), and the 3rd quartile (Q_3 = 75th percentile). The outliers in the box-whisker are the extreme values outside the dataset range, taken as lower than Q_1 or higher than Q_3 by 1.5 times the interquartile range (IQR), where IQR is the difference between Q_3 and Q_1. The IQR is represented by the box height and indicates the spread of the inner 50% of the dataset

(Banacos, 2011). Thus, the boxes small height for the datasets of both crack widths (0.25 and 0.35 mm) indicates small dispersion of *S*/Δ results. Moreover, only one outlier was determined for 0.35 mm crack width and no outliers for 0.25 mm crack width. For 0.25 mm crack width, the mean, standard deviation (SD), and coefficient of variation (CoV) were 727, 91, and 12.5%, respectively, and for 0.35 mm crack width, the values were 516, 57, and 11.1%, respectively. The low CoVs reflect small dispersion of the *S*/*Δ* results. The mean + SD for a dataset with no zero values represents the 84th percentile value (Sayani et al., 2011); therefore, the *S*/*Δ* 84th percentile values are 818 and 573 for crack widths 0.25 mm and 0.35 mm.

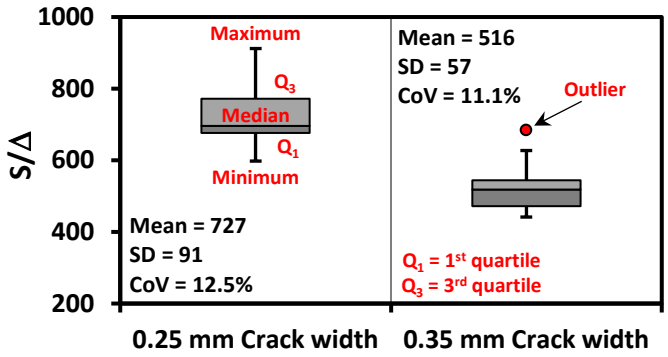

Figure 8-24. Box-whisker plot of the span-deflection ratios at the allowable crack widths for the cases of B1 and B2 standard installations.

Based on the calculated *S*/Δ values, the following limits are proposed for the midspan deflection corresponding to maximum crack widths of 0.25 and 0.35 mm:

$$\Delta \leq \begin{pmatrix} \frac{S}{825} & \text{for } 0.25\ mm\ crack\ width \\ \frac{S}{600} & \text{for } 0.35\ mm\ crack\ width \end{pmatrix} \quad \textbf{(8-6)}$$

8.7 Conclusions

A comprehensive parametric study was conducted to investigate the effects of backfill height, installation method, backfill soil type and compaction level, and culvert concrete compressive strength on the structural performance of TSCs and the applied earth pressure. The parametric study was based on 2D nonlinear finite element models validated with full-scale field data of three TSCs, with spans between 7.3, 10.4, and 13.5 m. The TSCs were

supported on strip footings with different geometries and different subsurface soil conditions. The installation of the TSCs complied with the CHBDC (CSA, 2014) requirements for B1 standard installation, and they were constructed employing different installation methods: trench, zero-projection, and embankment installations. The following conclusions can be drawn from the parametric study results:

1. The vertical earth pressure distribution on the culvert top slab is non-uniform, with increased non-uniform distribution as backfill height increases.

2. The TSCs exhibited ductile failure under earth loading conditions. The failure location (i.e., plastic hinges) is governed by the culvert span and sidewall height.

3. The TSC structural performance at service and ultimate limit states is the same for embankment and trench installations. However, VAFs and HAFs are slightly higher for embankment installation compared to trench installations. Therefore, embankment installation is considered the critical installation method for determining earth loads.

4. The mode of failure and location are not affected by the sidefill compaction level; however, the deformed shape of the footing-culvert system was significantly affected. Loosely compacted sidefill increases the footing lateral displacement but decreases its rotation, which affects the sidewalls and top slab deformations.

5. Compacted sidefill and moderately compacted backfill lead to almost constant VAF = 1.0 for all cases; therefore, this may be a construction option in case high stiffness backfill material above the RC TSC is not required (e.g., light pedestrian traffic).

6. The sidefill should be compacted to at least the same compaction level of the backfill material of the same soil type to ensure good structural performance and enhanced ultimate capacity. In addition, very loose (dumped soil) sidefill and backfill should not be used in constructing TSCs.

7. As expected, the ultimate capacity of RC culvert is governed by its concrete compressive strength; the predicted maximum backfill height at failure (i.e., factor

of safety) would increase by 50% as the concrete compressive strength increases from 40 MPa to 60 MPa.

8. The VAFs stipulated in the CHBDC (CSA, 2014) for B1 and B2 standard installations consistently exceeded the calculated values for all scenarios considered. On the other hand, The AASHTO (ASHTO LRFD, 2014) equation for embankment installation underestimated VAF for B1 installation with $H/B_c < 0.25$, and B2 installation with $H/B_c < 0.5$.

9. Two equations are proposed to provide safe estimates of VAF for B1 and B2 installations for TSCs with $0 < H/B_c \leq 1.25$.

10. The calculated HAFs for TSCs generally fall within the maximum and minimum values stipulated by the CHBDC (CSA, 2014) for B1 and B2 installations for box culverts. Therefore, these HAFs values are considered adequate to estimate the lateral earth pressures applied on the sidewalls of TSCs.

11. To satisfy serviceability limit state requirements, midspan vertical deflection should be limited to $S/825$ and $S/600$ to ensure crack width limits of 0.25 mm and 0.35 mm, respectively.

8.8 References

1. AASHTO (American Association of State Highway and Transportation Officials). (2014). *AASHTO LRFD bridge design specifications*. 7th ed. AASHTO, Washington, DC.

2. ACPA (American Concrete Pipe Association). (1993). *Concrete technology handbook: a presentation of historical and current state-of-the-art design and installation methodology*. ACPA, Irving, TX.

3. Banacos, P. C. (2011). *Box and whisker plots for local climate datasets: interpretations and creation using excel 2007/2010*. Eastern Region Technical Attachment. NOAA/NWS Burlington, Vermont.

4. Bennett, R. M., Wood, S.M., Drumm, E. C., and Rainwater, N.R. (2005). Vertical loads on concrete box culverts under high embankments. *Journal of Bridge Engineering*, 10 (6), 643-649. 10.1061/(ASCE)1084-0702(2005)10:6(643).

5. Boscardin, M. D., Selig, E. T., Lin, R. S., and Yang, G. R. (1990). Hyperbolic parameters for compacted soils. *Journal of Geotechnical Engineering*, 116 (1), 88-104.

6. CSA (Canadian Standards Association). 2014. *Canadian highway bridge design code*. CAN/CSA-S6-14. Mississauga, ON, Canada: CSA.

7. Duncan, J. M., and Chang. C. Y. (1970). Nonlinear analysis of stress and strain in soils. *Journal of Soil Mechanics and Foundations Division*, 96 (5),1629–1653.

8. Hordijk, D. A. (1991). Local approach to fatigue of concrete. Doctor of Philosophy, Ph.D. dissertation, Delft University of Technology, Delft, The Netherlands.

9. International Federation for Structural Concrete. (2013). *Fib model code for concrete structures 2010*. Berlin: Verlag Ernst & Sohn.

10. Kang, J., Parker, F., Kang, Y. J., and Yoo, C. H. (2008). Effects of frictional forces acting on sidewalls of buried box culverts. *International Journal for Numerical and Analytical Methods in Geomechanics*, 32 (3), 289-306.

11. Kim, K., and Yoo, C. H. (2005). Design loading for deeply buried box culverts. *Journal of Geotechnical and Geoenvironmental Engineering*, 131 (1), 20–27.

12. Marston, A. (1930). The theory of external loads on closed conduits in the light of the latest experiments. *Bulletin 96*, Iowa Engineering Experiment Station.

13. McGrath, T. J., Moore, I. D., Selig, E. T., Webb, M. C., and Taleb, B. (2002). *Recommend specifications for large-span culverts.* Report No. 473. Washington, DC: Transportation Research Board.

14. MTO (Ministry of Transportation of Ontario). 2010. *Frost Penetration Depths for Southern Ontario*. Ontario Provincial Standard Drawing OPSD 3090. ON, Canada: MTO.

15. Pimentel, M., Costa, P., Félix, C., and Figueiras, J. (2009). Behavior of reinforced concrete box culverts under high embankments. *Journal of Structural Engineering*, 135 (4), 366-375. 10.1061/(ASCE)0733-9445(2009)135:4(366), 366–375

16. Rots, J. G., Blaauwendraad, J. (1989). Crack models for concrete: discrete or smeared? Fixed, multi-directional or rotating? *Heron*, 34 (1), 5–55.

17. Sayani, P. J., Erduan, E., and Ryan, K. L. (2011). Comparative response assessment of minimally compliant low-rise base-isolated and conventional steel moment-resisting frame buildings. *Journal of Structural Engineering*, 137 (10), 1118-1131. 10.1061/(ASCE)ST.1943-541X.0000358

18. Spangler, M.G. (1950). A theory on loads on negative projecting conduits. *In Proc., Highway Research Board*, 30, 153-161.

19. Tadros, M. K., Benak, J. V., Abdel-Karim, A. M., and Bexten, K. A. (1989). *Field testing of a concrete box culvert*. Report No. 1231. Washington, DC: Transportation Research Board.

20. Thorenfeldt, E., Thomaszewic, A., and Jensen, J. J. (1987). 'Mechanical properties of high-strength concrete and applications in design. In *Proc., Symp. on Utilization of High-Strength Concrete*, Tapir Publishers, Stavanger, Norway, 149–159.

21. TNO Diana BV. 2016. *DIANA—User's manual: Material library*. Delft, Netherlands: TNO Diana BV.

22. Tukey, J. W. (1977). *Exploratory data analysis*. Addison-Wesley, Reading, Massachusetts.

Chapter 9

Summary, Conclusions, and Recommendations

9.1 Summary

This research effort attempts to evaluate the structural behavior and performance related to the interaction of precast RC TSCs with the surrounding soil mass and investigate the boundary conditions at the bottom of the sidewalls. A particular emphasis is placed on evaluating the applied earth pressures on these structures to enhance their design criteria. These objectives were achieved through a field-monitoring program and nonlinear finite element analyses.

Preliminary 3D FE models were developed to optimize the instrumentation plan and field tests for three TSCs. The results of the numerical models were utilized to predict the structure response, provide approximate magnitudes of parameters that would be measured during the field tests, and determine the critical locations where the instrumentation should be located for field measurements and data collection. Based on the preliminary analysis results, three TSCs were instrumented with a total of 30 pressure cells and 56 strain gauges to measure the soil-culvert interface pressures and the induced strains, which reflect the structural behavior of the buried culvert. The monitored TSCs covered intermediate to large spans with spans of 7.3 m, 10.4 m, and 13.5 m, which were designated as Remembrance, Pickering, and Oshawa culverts, respectively. Each culvert had a unique geometry and installation method. All the sensors were installed following the manufacturer's recommendation. They all survived the construction activities and are functioning properly to date, except for one PC on the top slab of the Oshawa culvert.

Field data were collected for the three culverts during and after construction completion. These field measurements were analyzed, and then utilized to validate the developed 2D FE models for the three culverts. The validated numerical models were employed to investigate the influence of many parameters on the applied earth pressures and the structural performance of TSCs at service and ultimate limit states (SLS and ULS). The

considered parameters included the subsurface soil condition (yielding vs. non-yielding), strip footing geometry, culvert configuration (sidewall and footing pedestal heights), backfill height, installation method, backfill soil type and compaction level, and culvert concrete compressive strength. Moreover, the ultimate capacity of an 11.0-m-span arched TSC has been experimentally measured through load testing one precast unit to failure by Marshall et al. (2014). The results of the load test were utilized to validate a 3D FE model, which was then used to predict the ultimate capacity of the precast units used in constructing the monitored TSCs. In addition, parametric studies were conducted to investigate the influence of the precast unit width and sidewall height on its structural performance at ULS.

9.2 Conclusions

Based on the results of this study, main conclusions can be drawn from the field monitoring program, 2D numerical analyses, and 3D numerical analyses.

9.2.1 Field Monitoring Program

The following conclusions can be drawn from the collected field data from the three monitored TSCs:

1. For the studied TSCs, the vertical earth pressure is non-uniformly distributed along the top slab. The calculated average VAF from the field measurements were lower than the value specified in the CHBDC (CSA, 2014) for B1 standard installation. These findings indicate that the specified VAF of 1.20 for B1 standard installation in CHBDC (CSA, 2014) overestimates the vertical earth pressures on large-span TSCs.

2. The measured lateral earth pressures on the sidewalls mostly fell within the upper and lower bounds stipulated by the CHBDC (CSA, 2014) for B1 installation.

3. the quality of construction and compaction effort near the sidewall influence the measured lateral earth pressure on the sidewall of the Pickering culvert.

4. The assumption of uniform contact pressure underneath strip footings with geometry and subsurface conditions comparable to that in this study is realistic for footing design purposes.

5. Strain measurements on the sidewall indicated that the strip footing might have rotated, resulting in imposing additional stresses to the sidewalls of the culvert and the development of bending moment at the base. Thus, the base connection does not behave as a pure hinge, at least for the soil conditions on which the subject culverts were constructed.

Building on the experience gained from these projects, some recommendations for future instrumentation of similar projects are as follows:

a. Results of preliminary numerical analysis can guide efficient instrumentation planning and instrument selection.

b. The location of the data logger on-site should be determined to estimate the required signal cable length for each instrument. This saves the time and effort required for splicing the cables on-site.

c. The vibrating wire strain gauge used in this study requires 6 hours on average for the initial reading to stabilize after installation.

d. The main conduit for signal cables should be sized such that the percent occupancy does not exceed 25%, especially for long cables.

e. Galvanized steel channels provide good protection for signal cables.

f. The maximum sampling rate for vibrating wire transducers is controlled by both the number of instruments and speed of the data logger. Thus, the data logger should be tested with all cables connected to determine the maximum sampling rate.

9.2.2 Two-Dimensional Numerical Analyses

Conclusions from the conducted 2D finite element analyses are categorized into conclusions at SLS and ULS.

9.2.2.1 Service Limit State

1. The applied earth pressures on the TSC body can be reasonably predicted assuming linear elastic behavior of the RC at service loading conditions. However, this assumption leads to inaccurate prediction of the induced strains in TSCs due to crack formation.

2. The foundation soil condition has negligible effect on the estimated vertical earth pressure on the top slab. However, the estimated lateral earth pressure on the sidewall was much higher for the case of non-yielding foundation soil (rock) compared to the case of yielding foundation soil (native soil).

3. For the sidewall-foundation connection described in this study, the connection is not fully hinged. Rather, the base of the sidewall experienced some bending moment due to the combined effect of the footing rotation and the restraint provided by the connection between the sidewall base and the strip footing. The bending moment at the base may be evaluated using the computed rotation from the numerical model and the rotational stiffness for smooth strip footing proposed by Muskhelishvili (1963) and should be considered in the reinforcement design of the culvert sidewalls.

4. Changing the geometry of the strip footing without varying the culvert sidewall height does not affect the applied pressures on the culvert body and the induced bending moments along the sidewall. However, the stress distribution underneath the strip footing becomes more non-uniform as the footing thickness decreases. Also, the stress underneath the footing edge on the backfill side decreases as the footing thickness decreases.

5. The assumption of uniform contact pressure underneath strip footings with geometry and subsurface conditions comparable to that in this study is realistic for footing design purposes.

For the 13.5-m-span Oshawa culvert, the sidewall height was varied between 1.9 and 3.8 m to examine its effects on the TSCs behavior. The following conclusions can be drawn:

1. The deformed shape of the footing-culvert system resulted in lateral earth pressure linearly increasing with depth on the sidewall and linearly decreasing with depth on the footing pedestal.

2. Increasing the sidewall height and reducing the pedestal height had insignificant effect on the slab vertical earth pressures. However, the contact pressure distribution underneath the footing became increasingly nonuniform. It also affected the culvert deformed shape and the lateral earth pressure distribution on the sidewall and footing pedestal.

3. Short sidewalls rotated as a rigid body as the backfill height increased, which resulted in additional straining actions (shear forces and bending moments) on the sidewall base and footing keyway. Long sidewalls resulted in relatively flexible behavior and exhibited bending deflection but no rotation within the keyway.

4. Short culvert sidewall height and footing with pedestal offer favorable performance as well as logistical and constructional advantages.

A comprehensive parametric study considering the three studied TSCs was conducted to investigate the effects of backfill height, installation method, backfill soil type and compaction level, and culvert concrete compressive strength on the structural performance of TSCs and the applied earth pressure. The following conclusions can be drawn from the parametric study results:

1. The vertical earth pressure distribution on the culvert top slab is non-uniform, with increased non-uniform distribution as backfill height increases.

2. The TSC structural performance at service and ultimate limit states is the same for embankment and trench installations. However, VAFs and HAFs are slightly higher for embankment installation compared to trench installations. Therefore, embankment installation is considered the critical installation method for determining earth loads.

3. Compacted sidefill and moderately compacted backfill lead to almost constant VAF = 1.0 for all cases; therefore, this may be a construction option in case high stiffness backfill material above the RC TSC is not required (e.g., light pedestrian traffic).

4. The sidefill should be compacted to at least the same compaction level of the backfill material of the same soil type to ensure good structural performance and enhanced ultimate capacity. In addition, very loose (dump soil) sidefill and backfill should not be used in constructing TSCs.

5. The VAFs stipulated in the CHBDC (CSA, 2014) for B1 and B2 standard installations consistently exceeded the calculated values for all scenarios considered. On the other hand, The AASHTO (AASHTO LRFD, 2014) equation for trench installation underestimated VAF for B1 installation with $H/B_c < 0.25$, and B2 installation with $H/B_c < 0.5$.

6. Two equations are proposed to provide safe estimates of VAF for B1 and B2 installations for TSCs with $0 < H/B_c \leq 1.25$.

7. The calculated HAFs for TSCs generally fall within the maximum and minimum values stipulated by the CHBDC (CSA, 2014) for B1 and B2 installations for box culverts. Therefore, these HAFs values are considered adequate to estimate the lateral earth pressures applied on the sidewalls of TSCs.

8. To satisfy serviceability limit state requirements, midspan vertical deflection should be limited to $S/825$ and $S/600$ to ensure crack width limits of 0.25 mm and 0.35 mm, respectively.

9.2.2.2 Ultimate Limit State

1. The RC material nonlinearity should be considered for realistic prediction of the TSC deformation and applied earth pressures at ULS.

2. The TSCs exhibited ductile failure under earth loading conditions. The failure location (i.e., plastic hinges) is governed by the culvert span and sidewall height.

3. The 7.3-m-span Remembrance TSC is expected to fail at a backfill height of 9.2 m in case of yielding foundation soil and backfill height of 8.6 m in case of non-yielding foundation soil. Moreover, the estimated maximum mid-span deflection at failure is higher in case of yielding foundation soil as opposed to the non-yielding foundation soil.

4. The mode of failure and location are not affected by the sidefill compaction level; however, the deformed shape of the footing-culvert system was significantly affected. Loosely compacted sidefill increases the footing lateral displacement but decreases its rotation, which affects the sidewalls and top slab deformations.

5. As expected, the ultimate capacity of RC culvert is governed by its concrete compressive strength; the predicted maximum backfill height at failure (i.e., factor of safety) would increase by 50% as the concrete compressive strength increases from 40 MPa to 60 MPa.

For the 13.5-m-span Oshawa culvert, the following conclusions can be drawn:

1. The maximum backfill height at failure decreases as the sidewall height increases.

2. The sidewall height has no effect on the failure mechanism, but the locations of the failure surfaces and plastic hinges are affected by the sidewall height. For TSCs with relatively short sidewalls, plastic hinges are predicted only at the mid-span. For long sidewalls, plastic hinges are predicted at the mid-span and at the top corners of sidewalls.

9.2.3 Three-Dimensional Numerical Analyses

Conclusions from the conducted 3D finite element analyses conducted on the TSC precast units can be drawn:

1. The TSC units, without soil confinement, exhibited brittle failure without yielding of the steel reinforcement.

2. The precast unit width has no influence on the ductility, failure mechanism, or predicted failure surface. However, the ultimate load capacity per unit width and the corresponding mid-span vertical deflection increase as the unit width decreases.

3. For the Oshawa culvert, increasing the sidewall height from 1.9 to 3.8 m decreased the ultimate capacity by 18% and increased the mid-span vertical deflection at the ultimate load.

4. The sidewall height had no influence on the failure mechanism; all investigated configurations exhibited brittle failure, with no reinforcement yielding at the ultimate load.

5. As expected, short sidewall height results in stiffer behavior at all load levels.

9.3 Recommendations for Future Work

The current research revealed that further studies on RC TSCs are still required. The following are recommendations for future research:

1. Field monitor large-span TSCs designed following the proposed equations in this study and evaluate their structural performance.

2. Field monitor RC TSCs supported on piles and investigate their structural performance and applied earth pressures.

3. Field test TSCs to failure under soil loading condition to determine the actual failure mechanism and failure location.

4. Perform full-scale live load testing using standard trucks to investigate the load transfer mechanism to large-span TSCs under different backfill heights.

5. Investigate the effect of bottomless culvert shape, i.e., arch, arched TSC, and TSC with flat top slab.

6. Examine different connection conditions between the culvert sidewall and strip footing and investigate their influence on the performance of the footing-culvert system.

7. Evaluate the applied earth loads on large-span TSCs installed using the induced trench installation method.

8. Investigate the performance of TSCs subjected to differential settlement due to the non-homogeneity of the subsurface soil condition underneath the strip footings.

9. Evaluate the seismic performance of RC TSCs while considering the effect of culvert span, backfill height, and compaction condition of the sidefill material.

9.4 References

1. AASHTO (American Association of State Highway and Transportation Officials). (2014). *AASHTO LRFD bridge design specifications*. 7th ed. AASHTO, Washington, DC.

2. CSA (Canadian Standards Association). 2014. *Canadian highway bridge design code*. CAN/CSA-S6-14. Mississauga, ON, Canada: CSA.

3. Marshall, J. D., Anderson, J. B., Meadows, R. L., and Jensen, T. J. (2014). Full-scale testing of three-sided precast concrete arch sections. *Journal of Bridge Engineering*, 19 (12), 04014051. 10.1061/(ASCE)BE.1943-5592.0000630.

4. Muskhelishvili, N.I., (1963). *Some basic problems of the mathematical theory of elasticity*. P. Noordhoff, Groningen, The Netherlands.

Curriculum Vitae

Safwat Ramadan

- ## Education

Ph.D. Candidate in Civil and Environmental Engineering Western University, London, Ontario	2016-present
M.Sc. in Civil Engineering (Geotechnical Engineering) Cairo University, Giza, Egypt	2013-2016
B.Sc. in Civil Engineering with Distinction Cairo University, Giza, Egypt	2008-2013

- ## Relevant Work Experience

Geotechnical Engineer (MHE Engineers Ltd., London, ON, Canada): Analysis and design of different geotechnical problems, e.g., shoring systems, machine foundations, buried pipes, etc.	2017-present
Teaching Assistant (Western University, London, ON, Canada): Reinforced and Prestressed Concrete; Foundations of Engineering Practice.	2016-2021
Geotechnical Engineer (Mohamed El Khouly Consulting Bureau, Cairo, Egypt): Site supervision, design of deep foundations, design of shoring systems, etc.	2013-2016
Teaching Assistant (Cairo University, Giza, Egypt): Soil Mechanics; Foundations	2013-2016

- ## Awards and Honors

Eric & Ruby Chung Award, Western University	2021
Canadian Geotechnical Society of Southern Ontario, 1st place, student competition	2020

Ontario Graduate Scholarship (OGS)	2019-2020
L.G. Soderman Award, Western University	2019
John Booker Award, Western University	2018
Milos Novak Memorial Award, Western University	2017
Western Graduate Research Scholarship, Western University	2016-2020

- Publications

  - Ramadan, S. H., and El Naggar, M. H., (2021). Structural performance of a medium-span RC three-sided culvert based on field measurements and numerical analyses. *Canadian Geotechnical Jour*nal. https://doi.org/10.1139/cgj-2020-0574

  - Ramadan, S. H., and El Naggar, M. H., (2021). Field monitoring and numerical analysis of a large span three-sided reinforced concrete culvert. *Journal of Geotechnical and Geoenvironmental Engineering*, ASCE, 147 (4), 04021008.

  - Ramadan, S. H., El Naggar, M. H., Drbe, O., and Embaby, K. (2021). Preliminary analysis and instrumentation of large-span three-sided reinforced concrete culverts. *Journal of Bridge Engineering*, ASCE. 10.1061/(ASCE)BE.1943-5592.0001798

  - Al-Asadi, A. K., and Ramadan, S. H., (2019). Effect of silica fume on the compressive strength and acid resistance of concrete. *Journal of Engineering and Applied Science*, Faculty of Engineering, Cairo University, 66 (4).

  - El-Sherbiny, R. M., Ramadan, S. H., and El-Khouly, M. A. (2018). Dynamic properties of sand-EPS geofoam beads mixtures". *Geosynthetics International*, 25 (4).

  - Shaia A. H., Al-Asadi A. K. and Ramadan S. H. (2018). Evaluation of the interface Friction between fiber-reinforced polymers and granular materials using modified shear apparatus". *International Journal of Civil Engineering and Technology*, 9 (13), 1010-1016.

  - Ramadan, S. H., El-Sherbiny, R. M. and El-Khouly, M. A. (2018). Small-strain dynamic properties of sand-EPS geofoam mixtures". *Proceedings-ICG 11th International Conference on Geosynthetics*, Seoul, Korea.